METTL7 Alkyl Thiol Methyltransferases: Implications in Drug Metabolism and Human Health

Benjamin J. Maldonato

A dissertation

submitted in partial fulfillment of the

requirements for the degree of

Doctor of Philosophy

University of Washington

2020

Reading Committee:

Rheem A. Totah, Chair

Allan Rettie

William Atkins

Program Authorized to Offer Degree:

School of Pharmacy

University of Washington

Abstract

METTL7 Alkyl Thiol Methyltransferases: Implications in Drug Metabolism and Human Health

Benjamin J. Maldonato

Chair of the Supervisory Committee:

Dr. Rheem A. Totah

Department of Medicinal Chemistry

Thiol metabolism in humans is catalyzed by two enzymes, thiopurine methyltransferase (TPMT) and thiol methyltransferase (TMT). TPMT selectively methylates thiopurine compound while TMT is selective for aliphatic thiol substrates. Both enzymes exhibit highly variable activity *in vivo* which can lead to toxicity for thiol-containing drugs that undergo methylation, such as azathioprine. While TPMT has been extensively characterized, TMT has never been purified despite prior attempts. As such, the gene and protein sequence remain unknown.

We identified methyltransferase-like protein 7A and 7B, METTL7A and METTL7B respectively, as thiol methyltransferases specific for aliphatic thiol compounds. Modulation of

their gene and protein expression in multiple human cell lines directly alters methylation of captopril, a TMT marker reaction. Purified recombinant METTL7B enzymatically catalyzes methylation of several known TMT substrates, including hydrogen sulfide, and exhibits classic Michaelis-Menten steady state kinetics.

TMT activity is highly variable (~9-fold) between single donor human liver microsomes (HLMs) and is not explained by variation in the expression of METTL7A and METTL7B protein. *METTL7A* and *METTL7B* gene expression is not correlated in single donor human liver microsomes (HLMs), however relative protein expression is highly correlated, suggesting potential post-translational co-regulation. Both genes are downregulated in human ventricular cardiomyocytes upon exposure to doxorubicin-induced oxidative stress, possibly due to their role in hydrogen sulfide catabolism.

Overall, TMT activity in humans is catalyzed, in part, by METTL7A and METTL7B. This is supported by modulating gene expression in human cell culture and using purified recombinant enzyme. Variation in TMT interindividual activity is not fully explained by protein expression of METTL7A and METTL7B and could be due to post-translational modification. Preliminary analysis suggests that both proteins are involved in oxidative stress response, however, future experiments should focus on their role in human health and disease.

Table of Contents

List of Tables

List of Figures

Acknowledgements

First and foremost, I would like to thank Dr. Rheem Totah, my advisor throughout my graduate studies. You introduced me to the world of medicinal chemistry and drug metabolism as an undergraduate. You then let me join your lab as a graduate student where you always had time to talk about science. I truly appreciate all of the mentoring you have given me throughout the years, giving me the flexibility to go visit Katie often, and for letting me try an experiment, fail, and try again until I got it right.

I would like to thank all the past and present members of the Totah lab, specifically Dr. Theresa Aliwarga, Dr. Eric Evangelista, Christi Cho, Drake Russell, Marvin Chau, Alex Wiley, Dr. Max Zeigler, Julie Denham, Dr. Yuanyuan Shi, and Dr. Byron Gallis. I have had a great time bouncing ideas around and working alongside everyone for the past couple of years. I will miss hanging out in the lab hallway and discussing random topics well into the evening when we should have gone home. Keep being awesome people and scientists. I'd also like to thank Dr. Rob Pelletier for always having a minute to talk about science and for teaching me the arts of metabolite identification and poker. I firmly believe that you are an honorary Totah lab member.

I would also like to thank Dr. William Atkins, Dr. Allan Rettie, Dr. Mike Guttman, and Dr. Champak Chatterjee for serving as my thesis committee members and giving me lots of great feedback at our meetings. I always left the meetings with a long list of really cool ideas for new experiments. I'd specifically like to thank Dr. Atkins and Dr. Rettie for reading my thesis and for helping make sure that the ideas I have in my head translate effectively to the page.

I'd also like to thank the mass spectrometry core facility staff, namely Dale Whittington, Scott Edgar, and Tauri Senn. Dale and Scott have taught me almost everything I know about

designing and troubleshooting mass spectrometric analytical methods as well as general instrument maintenance. I've enjoyed our great conversations down in the mass spec lab about science and life in general as well as our Galaga competition.

Similarly, I'd like to thank all of the administrative staff in the Department of Medicinal Chemistry. You keep the wheels turning and the lights on while we're off arguing about tiny details of individual proteins. Whoever puts Trader Joe's snacks in the break room is a saint.

I would like to thank my other graduate students, particularly my cohort John Kowalski and Mark Benhaim. You guys have made graduate school a really fun time and I will truly miss hanging out with you both. Beer is on me the next time we're at the College Inn!

Finally, I want to thank my friends and family. My parents, Tom and Jen, have been extremely supportive my entire life and have made me the person I am today. My brothers, Dean and Connor, have always been there for me. My grandparents, Jane and Joe Maldonato and Ellie and Mike Goldman, may not know what I'm talking about half the time but are always happy to hear about my research. Lastly, my lovely fiancée Katie Cieri has just been the best all throughout graduate school. Long distance is horrible but seeing you every month or two gave me the motivation to keep going and to finish my degree. Thank you for giving me your love and support, especially when I was feeling like I wanted to quit.

Dedication

To Katie, my parents, Connor, and Dean,

I could not have done any of this without your love and support.

Chapter 1: Introduction

Thiols in Biochemistry and Human Health:

Alkyl thiols play an important role in biochemistry. Not only do they enable higher order protein structure via formation of disulfide bonds, but they also help protect cellular macromolecules from soft electrophiles through the action of glutathione and glutathione *S*-transferases[1]. A large number of proteins have catalytic thiols, via active site cysteine residues, that are required for enzyme function[2]. This has been demonstrated by the wide inhibitory action of thiol-adducting reagents such as iodoacetamide or *N*-ethyl maleimide on catalytic processes[3]. Unfortunately, not all thiols are beneficial to the health of the cell. Exogenous thiol compounds, usually found in environmental toxins or pharmaceutical compounds, can cause toxic effects[4,5].

Thiols exert their toxicity through two general mechanisms[6]. In the first mechanism, two reduced thiols can form a single oxidized disulfide bond that is then reduced again, resulting in a constant redox cycle. This process is initiated by a thiyl radical formed when a deprotonated thiol donates one electron to a transition metal, usually copper or iron[7]. The thiyl radical will then react with another deprotonated thiol to form a disulfide radical anion. The disulfide radical anion is easily oxidized by molecular oxygen, resulting in the formation of highly reactive superoxide anion that can cause peroxidation of plasma membrane lipids[8]. Production of this reactive oxygen species (ROS) is maintained by the continued futile cycling of disulfide bond formation and reduction.

The second mechanism of thiol toxicity is through adduction to cellular proteins, generally on exposed cysteine residues[9]. Covalent binding to intracellular proteins, paired with

high levels of drug exposure, can cause drug-induced liver injury (DILI)[10]. Once adducted, these proteins can be metabolized via the proteasome and presented to the immune system, triggering an inflammatory response[11]. Several thiol-containing pharmaceutical compounds, including captopril and clopidogrel, are known to cause liver toxicity, however the exact mechanisms have not been elucidated[12–15]. As such, pharmaceutical companies tend to avoid thiols during drug design to limit potential toxicity. This approach is not failsafe since thiols can be exposed during subsequent rounds of oxidative metabolism, especially from thiophene rings[16–18]. Once formed, thiols can be detoxified via oxidation to sulfonic acid, methylation, or both by forming a methyl sulfone[19].

Thiol metabolism takes advantage of the fact that sulfur can exist in a number of different redox states. Thiols have a redox state of -2 and the sulfur of a disulfide bond has a redox state of -1, however sulfur can be oxidized up to a redox state of +6 as sulfate. In general, sulfates are highly water soluble and can be efficiently excreted by the kidneys[20]. Sulfur can be oxidized non-enzymatically via interaction with transition metals or enzymatically by FMOs and cytochrome P450 (CYP) enzymes[21–23]. While oxidative sulfur metabolism is important, the work in this thesis project is focused on methylation pathways[24].

Thiol Methylation in Humans:

Canonically speaking, thiol methylation in humans is catalyzed by two *S*-adenosyl-*L*-methionine (SAM)-dependent enzymes, thiopurine methyltransferase (TPMT) and a putative thiol methyltransferase (TMT)[25,26]. TPMT is a cytosolic enzyme that prefers aromatic thiols such as thiopurine compounds, like 6-mercaptopurine (6-MP) and 6-thioguanine, and is inhibited by dimethoxy-5-hydroxybenzoic acid (DMHBA)[27]. TMT is a microsomal enzyme that

methylates aliphatic thiol compounds, such as captopril and 7α-thiospironolactone, and can be inhibited by 2,3-dichloro-α-methylbenzylamine (DCMB)[28]. TPMT has been extensively characterized, mainly due to the fact that it is easier to purify, given its cytosolic subcellular localization, while the gene(s) and protein(s) responsible for aliphatic thiol methylation are unknown.

Thiol methylation in humans is a drug clearance pathway. This is best exemplified by the impact of TPMT on the methylation of azathioprine, an immunosuppressant drug commonly used during organ transplantation[29]. Azathioprine is metabolized to release 6-mercaptopurine (6-MP), which inhibits purine synthesis and induces T cell apoptosis[30]. Methylation of the purine thiol is a major route of drug clearance and detoxification for 6-MP and is catalyzed by TPMT[31]. Similarly, several clinically useful drugs contain aliphatic thiols, and their methylated metabolites have been observed *in vivo* (Figure 1.1). For example, captopril was the first approved inhibitor of angiotensin-converting enzyme (ACE), is used to treat hypertension and heart failure, and contains a crucial sulfhydryl functional group. As much as 17% of orally administered captopril undergoes methylation in monkeys, which indicates that methylation is a major route of clearance[32]. While captopril not widely used today, over 2 million patients were prescribed the drug in 1991[33]. Other thiol-containing drugs, such as clopidogrel, are currently prescribed to almost 20 million people[34].

Many of the drugs metabolized by TMT exhibit idiosyncratic toxicity, or variable efficacy, which could, in part, be attributed to an impaired methylation clearance pathway[13,14,35–37]. For example, roughly 10% of the population exhibits hyper- or hyporesponsiveness to clopidogrel treatment[38]. CYP2C19 bioactivates clopidogrel to the active metabolite and genetically induced alterations in catalytic activity have been proposed to cause much of the

observed variability in clinical response[39]. However, prasugrel is not bioactivated by CYP2C19 but still exhibits highly variable efficacy[40]. Methylated thiol metabolites of both drugs are observed in patient plasma, however the methylation pathway has not been investigated as a potential source of variation despite its potential contribution.

The rate of thiol and thiopurine methylation in humans can be highly variable. Thiopurine methylation is impacted by the presence of single nucleotide polymorphisms (SNPs) that reduce TPMT activity[41]. The presence of certain inactivating SNPs can increase levels of circulating 6-MP, causing toxicity and undesirable off-target effects[42]. As such, genetic testing for TPMT SNPs is now standard practice prior to treatment with 6-mercaptopurine[43]. While the frequency of each SNP is relatively low, observed phenotypic variation in TPMT activity ranges over 5-fold within large populations[26]. Like TPMT, enzymatic activity of TMT is also highly variable, with a 6-fold variation reported in red blood cell membranes when tested using the substrate ß-mercaptoethanol[44]. Despite the amount of variation observed at the population level, TMT activity is highly correlated within family units[45]. Therefore, it is likely that TMT activity is controlled at the gene level. Like TPMT, this implies that there may be specific populations that are at risk for either toxicity or lack of efficacy of thiol-containing drugs due to naturally low or high TMT activity respectively.

To date, very little is known about the enzymatic characteristics of TMT. In the 1970s, several efforts were made to purify the enzyme from rat liver homogenate. While these investigations showed that TMT is likely a 28 kDa protein, they failed to obtain an amino acid sequence[46,47]. Therefore, further characterization work conducted on TMT has been performed in cell lysates, microsomal fractions, or isolated membranes[48]. Interestingly, biphasic kinetics were generally observed with a number of known TMT substrates in these systems[44]. This led

researchers to propose that multiple enzymes catalyze aliphatic thiol methylation, but further confirmation required purified protein(s). Purification and characterization of the TMT enzyme(s) is the only sure way to fully understand aliphatic thiol methylation in humans.

Hydrogen Sulfide: Anabolism and Catabolism:

While TMT mostly methylates thiol-containing xenobiotics, prior work identified hydrogen sulfide (H_2S) as an additional endogenous substrate[24,49]. Hydrogen sulfide was originally thought to be an environmental toxin and a byproduct of metabolism from gut bacteria[50]. We now know that it can be produced by multiple enzymes within the body and is considered one of three gasotransmitter signaling molecules along with nitric oxide and carbon monoxide[51]. As shown in Figure 1.2, the three main enzymes responsible for the formation of hydrogen sulfide are cystathionine ß-synthase (CBS), cystathionine γ-lyase (CSE), and 3-mercaptopyruvate sulfurtransferase (3-MST)[52–54].

CBS is a cytosolic enzyme that catalyzes the formation of L-cystathionine and hydrogen sulfide from L-homocysteine and L-cysteine[55]. Interestingly, CBS contains a SAM-binding site that leads to activation and greater production of H_2S when occupied[56]. The physiological implications of SAM-mediated activation of H_2S production is unclear however this is an exciting avenue for future investigation. CBS is predominantly expressed in the central nervous system, however, other H_2S-generating enzymes exist that may contribute to H_2S pools in the brain as well[57].

CSE is a cytosolic enzyme that catalyzes the breakdown of L-cysteine to hydrogen sulfide, pyruvate, and ammonia[54]. Additionally, CSE will metabolize cystathionine, producing L-cysteine, ammonia, and α-ketobutyrate. CSE activity is modulated by intracellular calcium

concentrations[58]. As calcium levels increase, CSE activity is downregulated though the precise mechanism is currently unknown. CSE is likely the main H_2S-producing enzyme outside of the central nervous system and is found at high concentrations in the cardiovascular and respiratory systems[59].

The final enzyme responsible for the production of hydrogen sulfide is 3-MST. This mitochondrial enzyme is distinct from CBS and CSE in that it does not interact with $_L$-cysteine. In the case of 3-MST, $_L$-cysteine must first be converted to 3-mercaptopyruvate (3-MP) by cysteine aminotransferase (CAT). 3-MST then transfers a sulfur atom directly from 3-MP onto itself, forming a persulfide. Hydrogen sulfide is only released from the enzyme after being reduced to the starting state by an intracellular reductant such as thioredoxin[60]. 3-MST is also widely expressed in cardiac, liver, and kidney tissues as well as the brain, where it may compensate for downregulation or inhibition of CBS[53,61].

While hydrogen sulfide biosynthesis is well characterized, routes of metabolism are significantly poorly understood. These pathways are also very important given that high levels of hydrogen sulfide can cause toxic side effects and death[62]. Additionally, hydrogen sulfide-donating drugs are entering clinical trials as anti-inflammatory agents which require assessment of drug safety and characterization of their metabolism[63]. Currently, several methods are known for removing hydrogen sulfide from the body; namely oxidation, methylation, and expiration.

Oxidation of hydrogen sulfide to sulfate is commonly accepted as the major route of clearance in healthy individuals. Much of the sulfate formation is catalyzed by rhodanese in the mitochondria and, once produced, is rapidly excreted in urine by the kidneys[64]. The major organ responsible for hydrogen sulfide oxidation is debatable, but high rates of sulfate formation have

been observed in the colonic mucosa[65]. The same researchers investigated the extent of hydrogen sulfide oxidation in other organs and found that the activity sharply declined outside of the colonic mucosa[66]. The currently accepted view is that hydrogen sulfide catabolic processes are elevated in intestinal tissue to reduce high levels produced by the gut microbiome. This also suggests that, outside of the gastrointestinal tract, oxidation may not be the dominant pathway of hydrogen sulfide catabolism.

Methylation is the main catabolic alternative to hydrogen sulfide oxidation[67–69]. This pathway has been understudied for two main reasons. Firstly, the enzyme that catalyzes the methylation of hydrogen sulfide is unknown. Therefore, it is not possible to identify altered expression levels of H_2S-methylating enzymes in specific disease states. Secondly, measurement of methanethiol is significantly more difficult than measuring oxidized sulfur compounds. Specific gas chromatographic separation and detection methods or time-consuming derivatization prior to liquid chromatography-tandem mass spectrometric (LC-MS/MS) analysis are required [70,71]. These analytical methods are generally not compatible with measuring oxidized sulfates, therefore hydrogen sulfide methylation is usually ignored when studying specific disease states. As such, hydrogen sulfide methylation may play a larger role than previously recognized, especially outside of the colonic mucosa and in disease states that exhibit inhibited oxidative metabolism, such as the anoxic interior of solid tumors[72].

The final route of hydrogen sulfide elimination is through expiration. Since hydrogen sulfide is a gaseous molecule, it can freely diffuse into the lungs from the bloodstream[73]. This route of elimination only appears to be relevant in disease states where excess hydrogen sulfide is being created, namely septic shock or hemorrhagic shock[74]. Otherwise, this method of elimination is assumed to be minimal in healthy patients.

Physiological Effects of Hydrogen Sulfide:

Once formed, hydrogen sulfide can exert a number of physiological effects in vivo. Most signaling mediated by hydrogen sulfide appears to be exerted by formation of disulfide bonds on important cysteine residues of specific proteins[75]. Proteins that are known to be adducted by hydrogen sulfide include the potassium-ATP channel, actin, ß-tubulin, and GAPDH[75]. For some of these proteins, as much as 25% contain persulfides at physiological conditions.

At low concentrations, hydrogen sulfide appears to act as an anti-inflammatory signaling molecule which promotes cell survival and motility[76]. At high concentrations, it becomes toxic and actively promotes inflammation, apoptosis, and other destructive pathways[77]. It is unclear at which point hydrogen sulfide levels turn toxic however intracellular concentrations are held under tight control in healthy tissue[78].

Hydrogen sulfide plays a clear role in disease states that involve inflammation, including rheumatoid arthritis and many types of cancer[79,80]. In cancer, the effect of hydrogen sulfide on cell health takes on a distinct bell-shaped curve[81]. Decreased intracellular concentrations of hydrogen sulfide negatively impact cell proliferation while super-physiological concentrations trigger cell death[82]. Cancer cell proliferation is greatest at basal and slightly elevated levels of hydrogen sulfide. In fact, hydrogen sulfide-producing enzymes are upregulated at the protein level in a number of different cancers which may increase intracellular hydrogen sulfide concentrations[83,84]. Therefore, cancer cell proliferation and survival are closely tied to control over hydrogen sulfide production and metabolism.

Currently, hydrogen sulfide homeostasis is an attractive target for pharmaceutical intervention[85]. There are a number of compounds in development to inhibit CBS and therefore,

decrease the intracellular concentration of hydrogen sulfide[82]. While this may be effective at preventing tumor proliferation, it is unclear whether there would be off-target or systemic toxicity associated with dysregulating an endogenous signaling molecule. Alternatively, several compounds are being developed that are hydrogen sulfide donors[85]. These molecules degrade within the body to slowly release hydrogen sulfide, similar to the effect of overexpressing H_2S-generating enzymes[86]. Theoretically, treatment will increase intracellular hydrogen sulfide concentrations in cancer cells, resulting in toxicity and apoptosis. This approach relies on differential sensitivity to hydrogen sulfide between cancerous and healthy tissue. Therefore, a thorough understanding of hydrogen sulfide catabolism, particularly in disease states, is required for future drug development.

METTL7 Gene and Protein Expression in Humans:

This thesis project is centered on methyltransferase-like protein 7A (METTL7A) and mostly methyltransferase-like protein 7B (METTL7B). The two proteins were originally discovered in a large-scale bioinformatic screen of the human genome that identified novel proteins containing secretory and transmembrane peptide sequences[87]. Each gene encodes a 28 kDa protein that contains a conserved Rossman fold that binds the SAM methyl donor cofactor and is a common feature of DNA and small molecule methyltransferase enzymes[88]. Interestingly, while both proteins have been identified in microsomal fractions, they also may localize to lipid droplets due to a very hydrophobic *N*-terminal alpha helix signaling sequence[89]. The physiological implications of lipid droplet targeting are unclear however this process allows METTL7A and METTL7B to translocate outside of the endoplasmic reticulum to the cytosol [90]. To date, no enzymatic function has been conclusively identified conclusively for either protein, however they were originally classified as membrane-bound methyltransferases.

METTL7A and *METTL7B* appear to be involved in numerous disease states, particularly cancer, as signified by altered gene expression compared to healthy tissues[91–97]. The downstream effects of altered *METTL7A* and *METTL7B* expression remain a mystery, largely due to the lack of defined enzymatic functions. Some initial work suggested that METTL7A protein interacts with structural and chaperone proteins however this has not been further investigated[98,99]. Additionally, METTL7B has been speculated to catalyze protein methylation and be involved in Alzheimer's disease etiology, however there is no firm evidence[100]. Interestingly, gene expression of *METTL7A* and *METTL7B* appear to be related to cellular redox state. *METTL7B* expression is responsive to inflammation signaling pathways via JAK1 and gene expression changes in response to certain oxidative stress-inducing chemotherapeutics[101–103]. In this work, we will demonstrate unequivocally that METTL7B is a small-molecule thiol methyltransferase and catalyzes the methylation of hydrogen sulfide.

Hypothesis and Specific Aims:

The overarching goal of this work is to identify, purify, and characterize the enzyme or enzymes responsible for methylation of aliphatic thiols in humans.

Two main hypotheses are tested in this dissertation.

1. *METTL7A* and *METTL7B* encode enzymes, METTL7A and METTL7B, that are active in methylating aliphatic thiol compounds.
2. Expression and activity of METTL7A and METTL7B across individual human liver microsomes (HLMs) are highly variable and could be due in part to genetic factors.

Chapter 2 describes the identification and validation of *METTL7A* and *METTL7B* as potential thiol methyltransferases. We partially purify the rat thiol methyltransferase and use proteomic

and bioinformatic analysis to identify the two main human candidate proteins. We then modulate their expression in two human cell lines and correlate changes in mRNA and protein expression with changes in thiol methyltransferase activity.

Chapter 3 presents the expression, purification, and biochemical characterization of recombinant METTL7B fusion protein. We design and express affinity-tagged METTL7B and purify it using a dual-stage affinity chromatography approach. The presence of METTL7B is validated by multiple western blots and proteomic analysis. We then define substrate specificity and steady state kinetics using the purified recombinant protein.

Chapter 4 investigates the interindividual variability of thiol methylation as well as METTL7A and METTL7B gene and protein expression. We measure rates of methylation for multiple thiol substrates and correlate individual turnover rates in human liver microsomes. We also correlate gene and protein expression for METTL7A and METTL7B. Finally, we present RNA-seq data showing that both *METTL7A* and *METTL7B* gene expression is responsive to oxidative stress and correlated with redox-sensitive genes.

Chapter 5 summarizes the presented work and proposes future directions to build on the work presented in this thesis to further characterize the importance of METTL7A and METTL7B in health and disease.

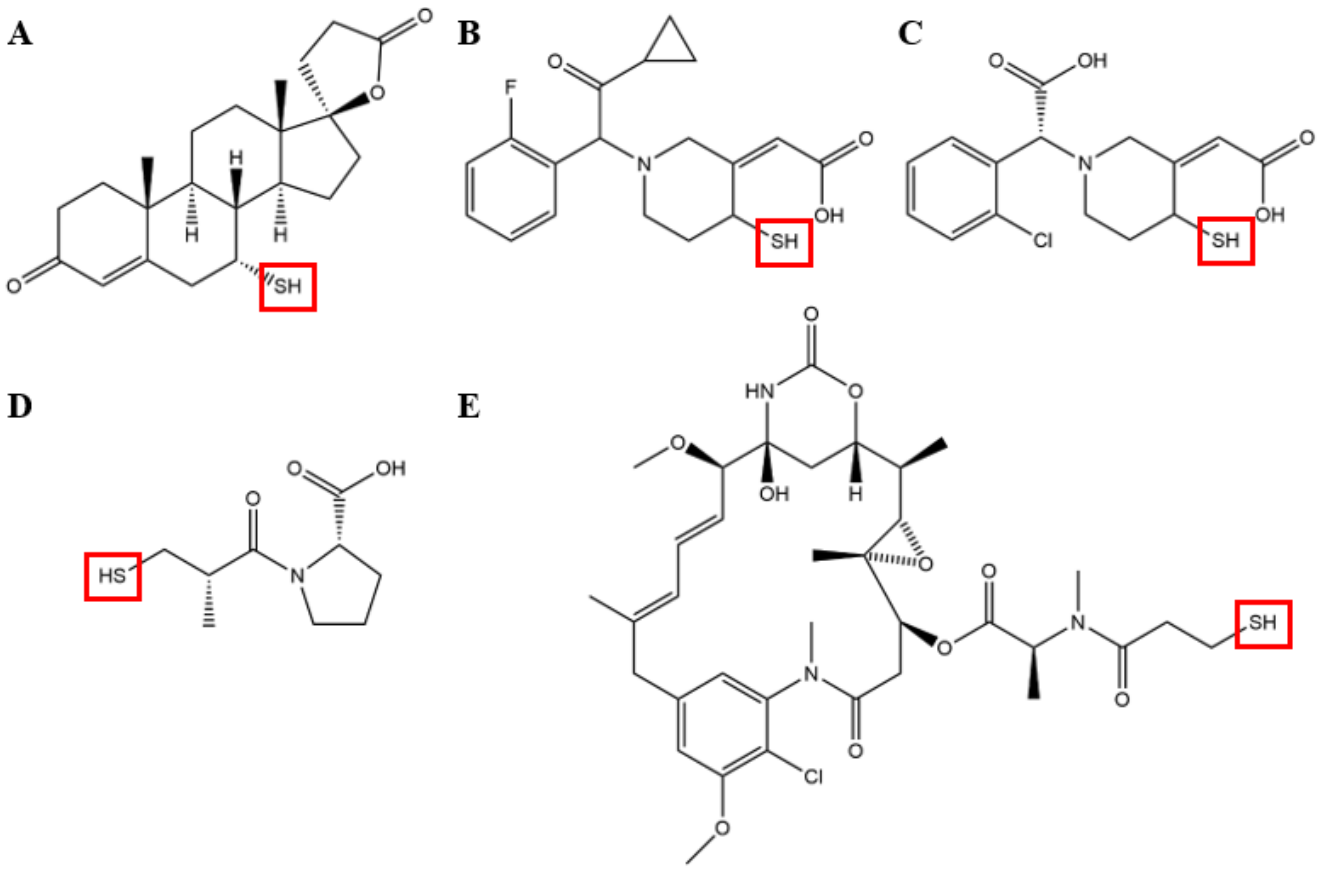

Figure 1.1. Pharmaceutical Thiol-Containing Compounds: Multiple drug compounds and active metabolites containing aliphatic thiols, boxed in red. **A)** 7α-Thiospironolactone **B)** Prasugrel active metabolite **C)** Clopidogrel active metabolite **D)** Captopril **E)** Mertansine

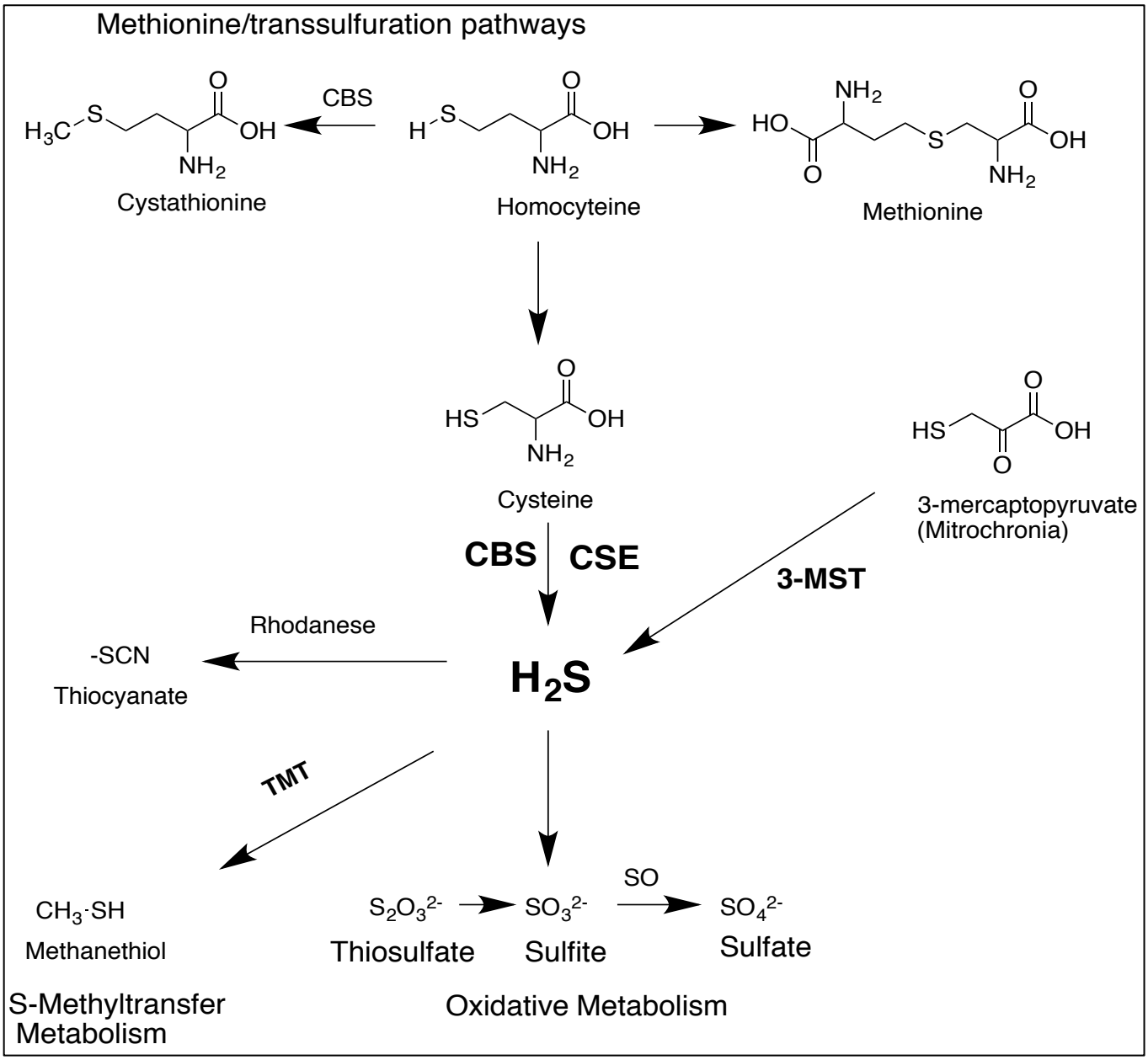

Figure 1.2. Major Routes of H_2S Synthesis and Metabolism: CBS and CSE form hydrogen sulfide from cystine whereas 3-MST uses 3-mercaptopyruvate. Hydrogen sulfide can be oxidized, converted to thiocyanate, or methylated. Figure courtesy of Dr. Totah.

Bibliography:

1. Coles, B. F. & Kadlubar, F. F. Detoxification of electrophilic compounds by glutathione S-transferase catalysis: Determinants of individual response to chemical carcinogens and chemotherapeutic drugs? *BioFactors* **17**, 115–130 (2003).

2. Nagahara, N. Catalytic site cysteines of thiol enzyme: sulfurtransferases. *J. Amino Acids* **2011**, 709404 (2011).

3. Piedrafita, F. J., Elorriaga, C., Fernández-Alvarez, E. & Nieto, O. Inhibition of Catechol-O-Methyltransferase by N-(3,4-Dihydroxyphenyl) Maleimide. *J. Enzyme Inhib.* **4**, 43–50 (1990).

4. Amrolia, P., Sullivan, S. G., Stern, A. & Munday, R. Toxicity of aromatic thiols in the human red blood cell. *J. Appl. Toxicol.* **9**, 113–118 (1989).

5. Fairchild, E. J. & Stokinger, H. E. 1. Acute Toxicity of Some Aliphatic and Aromatic Thiols (Mercaptans). *Am. Ind. Hyg. Assoc. J.* **19**, 171–189 (1958).

6. Munday, R. Toxicity of thiols and disulphides: Involvement of free-radical species. *Free Radical Biology and Medicine* **7**, 659–673 (1989).

7. Munday, R. B. T.-M. in E. [10] In vivo toxicity of thiols: Relationship to rate of one-electron oxidation by oxyhemoglobin. in *Biothiols Part A Monothiols and Dithiols, Protein Thiols, and Thiyl Radicals* **251**, 117–120 (Academic Press, 1995).

8. Held, K. D. & Biaglow, J. E. Mechanisms for the Oxygen Radical-Mediated Toxicity of Various Thiol-Containing Compounds in Cultured Mammalian Cells. *Radiat. Res.* **139**, 15–23 (1994).

9. Schöneich, C. Thiyl radicals and induction of protein degradation. *Free Radic. Res.* **50**, 143–149 (2016).

10. Gibson, J. D., Pumford, N. R., Samokyszyn, V. M. & Hinson, J. A. Mechanism of Acetaminophen-Induced Hepatotoxicity: Covalent Binding versus Oxidative Stress. *Chem. Res. Toxicol.* **9**, 580–585 (1996).

11. Ju, C. & Reilly, T. Role of immune reactions in drug-induced liver injury (DILI). *Drug Metab. Rev.* **44**, 107–115 (2012).

12. Schattner, A., Kozak, N. & Friedman, J. Captopril-Induced Jaundice: Report of 2 Cases and a Review of 13 Additional Reports in the Literature. *Am. J. Med. Sci.* **322**, 236–240 (2001).

13. Keshmiri, H., Behal, A., Shroff, S. & Berkelhammer, C. Clopidogrel-Induced Severe Hepatitis: A Case Report and Literature Review. *Case Reports Hepatol.* 8068276 (2016). doi:10.1155/2016/8068276

14. Howell, P. *et al.* Clopidogrel-induced liver failure. *J. R. Soc. Med. Short Reports* **2**, (2011).

15. Rosenbaum, J., Katz, W. A. & Schumacher, H. R. Hepatotoxicity associated with use of D-penicillamine in rheumatoid arthritis. *Ann. Rheum. Dis.* **39**, 152–154 (1980).

16. Gramec, D., Peterlin Mašič, L. & Sollner Dolenc, M. Bioactivation Potential of Thiophene-Containing Drugs. *Chem. Res. Toxicol.* **27**, 1344–1358 (2014).

17. Dansette, P. M., Libraire, J., Bertho, G. & Mansuy, D. Metabolic Oxidative Cleavage of Thioesters: Evidence for the Formation of Sulfenic Acid Intermediates in the

Bioactivation of the Antithrombotic Prodrugs Ticlopidine and Clopidogrel. *Chem. Res. Toxicol.* **22**, 369–373 (2009).

18. Mansuy, D. & Dansette, P. M. Sulfenic acids as reactive intermediates in xenobiotic metabolism. *Arch. Biochem. Biophys.* **507**, 174–185 (2011).

19. Shen, B.-Q. *et al.* Non-Clinical Disposition and Metabolism of DM1, a Component of Trastuzumab Emtansine (T-DM1), in Sprague Dawley Rats. *Drug Metabolism Letters* **9**, 119–131 (2015).

20. Kirschbaum, B. Sulfate Regulation: Native Kidney vs Dialysis. *Int. J. Artif. Organs* **22**, 591–592 (1999).

21. Mitchell, S. C. Flavin Mono-Oxygenase (FMO) - The "Other" Oxidase. *Current Drug Metabolism* **9**, 280–284

22. Rydberg, P., Ryde, U. & Olsen, L. Sulfoxide, Sulfur, and Nitrogen Oxidation and Dealkylation by Cytochrome P450. *J. Chem. Theory Comput.* **4**, 1369–1377 (2008).

23. Ortiz de Montellano, P. R. Substrate Oxidation by Cytochrome P450 Enzymes. in *Cytochrome P450: Structure, Mechanism, and Biochemistry* (ed. Ortiz de Montellano, P. R.) 111–176 (Springer International Publishing, 2015). doi:10.1007/978-3-319-12108-6_4

24. Bremer, J. & Greenberg, D. M. Enzymic methylation of foreign sulfhydryl compounds. *Biochim. Biophys. Acta* **46**, 217–224 (1961).

25. Pacifici, G. M., Santerini, S., Giuliani, L. & Rane, A. Thiol methyltransferase in humans: development and tissue distribution. *Dev. Pharmacol. Ther.* **17**, 8–15 (1991).

26. Kasirer, Y. *et al.* Thiopurine S-methyltransferase (TPMT) Activity Is Better Determined

by Biochemical Assay Versus Genotyping in the Jewish Population. *Dig. Dis. Sci.* **59**, 1207–1212 (2014).

27. Szumlanski, C. L. & Weinshilboum, R. M. Sulphasalazine inhibition of thiopurine methyltransferase: possible mechanism for interaction with 6-mercaptopurine and azathioprine. *Br. J. Clin. Pharmacol.* **39**, 456–459 (1995).

28. Glauser, T. A., Saks, E., Vasova, V. M. & Weinshilboum, R. M. Human liver microsomal thiol methyltransferase: inhibition by arylalkylamines. *Xenobiotica* **23**, 657–69 (1993).

29. Chocair, P. R., Duley, J. A., Simmonds, H. A. & Cameron, J. S. The importance of thiopurine methyltransferase activity for the use of azathioprine in transplant recipients. *Transplantation* **53**, 1051–1055 (1992).

30. Leitner, J. *et al.* The effects of Cyclosporine A and azathioprine on human T cells activated by different costimulatory signals. *Immunol. Lett.* **140**, 74–80 (2011).

31. Kröplin, T. & Iven, H. Methylation of 6-mercaptopurine and 6-thioguanine by thiopurine S-methyltransferaseA comparison of activity in red blood cell samples of 199 blood donors. *Eur. J. Clin. Pharmacol.* **56**, 343–345 (2000).

32. Migdalof, B. H. *et al.* Captopril: Pharmacology, Metabolism, and Disposition. *Drug Metab. Rev.* **15**, 841–869 (1984).

33. Hemels, M. E. H. *et al.* HOPE Study Impact on ACE Inhibitors Use. *Ann. Pharmacother.* **37**, 640–645 (2003).

34. Kane, S. ClinCalc DrugStats Database, Version 20.0 ClinCalc: https://clincalc.com/DrugStats. Accessed May 29, 2020

35. Xie, H.-G. *et al.* Individual variability in the disposition of and response to clopidogrel: Pharmacogenomics and beyond. *Pharmacol. Ther.* **129**, 267–289 (2011).

36. Farid, N. A. *et al.* The Disposition of Prasugrel, a Novel Thienopyridine, in Humans. *Drug Metab. Dispos.* **35**, 1096 LP – 1104 (2007).

37. Smith, R. L., Gillespie, T. A., Rash, T. J., Kurihara, A. & Farid, N. A. Disposition and metabolic fate of prasugrel in mice, rats, and dogs. *Xenobiotica* **37**, 884–901 (2007).

38. Serebruany, V. L. *et al.* Variability in platelet responsiveness to clopidogrel among 544 individuals. *J. Am. Coll. Cardiol.* **45**, 246 LP – 251 (2005).

39. Ancrenaz, V. *et al.* Impact of Genetic Polymorphisms and Drug-Drug Interactions on Clopidogrel and Prasugrel Response Variability. *Current Drug Metabolism* **11**, 667–677

40. Perl, L. *et al.* Variability in Response to Prasugrel and Ticagrelor Over Time in Patients with Acute Coronary Syndrome. *J. Am. Coll. Cardiol.* **63**, A23 (2014).

41. Black, A. J. *et al.* Thiopurine Methyltransferase Genotype Predicts Therapy-Limiting Severe Toxicity from Azathioprine. *Ann. Intern. Med.* **129**, 716–718 (1998).

42. Lennard, L., Van Loon, J. A. & Weinshilboum, R. M. Pharmacogenetics of acute azathioprine toxicity: Relationship to thiopurine methyltransferase genetic polymorphism. *Clin. Pharmacol. Ther.* **46**, 149–154 (1989).

43. Black, A. J. *et al.* Thiopurine methyltransferase genotype predicts therapy-limiting severe toxicity from azathioprine. *Ann. Intern. Med.* **129**, 716–718 (1998).

44. Keith, R. A., Jardine, I., Kerremans, A. & Weinshilboum, R. M. Human erythrocyte membrane thiol methyltransferase. S-methylation of captopril, N-acetylcysteine, and 7

alpha-thio-spirolactone. *Drug Metab. Dispos.* **12**, 717–24 (1984).

45. Keith, R. A., Van Loon, J., Wussow, L. F. & Weinshilboum, R. M. Thiol methylation pharmacogenetics: heritability of human erythrocyte thiol methyltransferase activity. *Clin. Pharmacol. Ther.* **34**, 521–8 (1983).

46. Weisiger, R. A. & Jakoby, W. B. Thiol S-methyltransferase from rat liver. *Arch. Biochem. Biophys.* **196**, 631–7 (1979).

47. Borchardt, R. T. & Cheng, C. F. Purification and characterization of rat liver microsomal thiol methyltransferase. *Biochim. Biophys. Acta - Enzymol.* **522**, 340–353 (1978).

48. Babidge, W. J., Millard, S. H. & Roediger, W. E. Thiol methyltransferase activity in colonocytes and erythrocyte membranes. *J. Clin. Pathol.* **48**, 641–4 (1995).

49. Weisiger, R. A., Pinkus, L. M. & Jakoby, W. B. Thiol S-methyltransferase: suggested role in detoxication of intestinal hydrogen sulfide. *Biochem. Pharmacol.* **29**, 2885–2887 (1980).

50. Tangerman, A. Measurement and biological significance of the volatile sulfur compounds hydrogen sulfide, methanethiol and dimethyl sulfide in various biological matrices. *J. Chromatogr. B* **877**, 3366–3377 (2009).

51. Yang, G., Sener, A., Ji, Y., Pei, Y. & Pluth, M. D. Gasotransmitters in Biology and Medicine: Molecular Mechanisms and Drug Targets. *Oxid. Med. Cell. Longev.* **2016**, 4627308 (2016).

52. Braunstein, A. E., Goryachenkova, E. V & Lac, N. D. Reactions catalysed by serine sulfhydrase from chicken liver. *Biochim. Biophys. Acta - Enzymol.* **171**, 366–368 (1969).

53. Shibuya, N. *et al.* 3-Mercaptopyruvate Sulfurtransferase Produces Hydrogen Sulfide and Bound Sulfane Sulfur in the Brain. *Antioxid. Redox Signal.* **11**, 703–714 (2008).

54. Chiku, T. *et al.* H2S biogenesis by human cystathionine gamma-lyase leads to the novel sulfur metabolites lanthionine and homolanthionine and is responsive to the grade of hyperhomocysteinemia. *J. Biol. Chem.* **284**, 11601–11612 (2009).

55. Braunstein, A. E., Goryachenkova, E. V, Tolosa, E. A., Willhardt, I. H. & Yefremova, L. L. Specificity and some other properties of liver serine sulphhydrase: Evidence for its identity with cystathionine β-synthase. *Biochim. Biophys. Acta - Enzymol.* **242**, 247–260 (1971).

56. Shan, X., Dunbrack Jr, R. L., Christopher, S. A. & Kruger, W. D. Mutations in the regulatory domain of cystathionine β–synthase can functionally suppress patient-derived mutations in cis. *Hum. Mol. Genet.* **10**, 635–643 (2001).

57. Abe, K. & Kimura, H. The possible role of hydrogen sulfide as an endogenous neuromodulator. *J. Neurosci.* **16**, 1066–1071 (1996).

58. Mikami, Y., Shibuya, N., Ogasawara, Y. & Kimura, H. Hydrogen sulfide is produced by cystathionine γ-lyase at the steady-state low intracellular Ca2+ concentrations. *Biochem. Biophys. Res. Commun.* **431**, 131–135 (2013).

59. Hosoki, R., Matsuki, N. & Kimura, H. The Possible Role of Hydrogen Sulfide as an Endogenous Smooth Muscle Relaxant in Synergy with Nitric Oxide. *Biochem. Biophys. Res. Commun.* **237**, 527–531 (1997).

60. Yadav, P. K., Yamada, K., Chiku, T., Koutmos, M. & Banerjee, R. Structure and kinetic

analysis of H2S production by human mercaptopyruvate sulfurtransferase. *J. Biol. Chem.* **288**, 20002–20013 (2013).

61. Shibuya, N., Mikami, Y., Kimura, Y., Nagahara, N. & Kimura, H. Vascular Endothelium Expresses 3-Mercaptopyruvate Sulfurtransferase and Produces Hydrogen Sulfide. *J. Biochem.* **146**, 623–626 (2009).

62. Truong, D. H., Eghbal, M. A., Hindmarsh, W., Roth, S. H. & O'Brien, P. J. Molecular Mechanisms of Hydrogen Sulfide Toxicity. *Drug Metab. Rev.* **38**, 733–744 (2006).

63. Wallace, J. L. & Wang, R. Hydrogen sulfide-based therapeutics: exploiting a unique but ubiquitous gasotransmitter. *Nat. Rev. Drug Discov.* **14**, 329–345 (2015).

64. Smirnov, A. *et al.* Mitochondrial enzyme rhodanese is essential for 5 S ribosomal RNA import into human mitochondria. *J. Biol. Chem.* **285**, 30792–30803 (2010).

65. Levitt, M. D., Furne, J., Springfield, J., Suarez, F. & DeMaster, E. Detoxification of hydrogen sulfide and methanethiol in the cecal mucosa. *J. Clin. Invest.* **104**, 1107–14 (1999).

66. Furne, J., Springfield, J., Koenig, T., DeMaster, E. & Levitt, M. D. Oxidation of hydrogen sulfide and methanethiol to thiosulfate by rat tissues: A specialized function of the colonic mucosa. *Biochem. Pharmacol.* **62**, 255–259 (2001).

67. Picton, R., Eggo, M. C., Langman, M. J. S. & Singh, S. Impaired detoxication of hydrogen sulfide in ulcerative colitis? *Dig. Dis. Sci.* **52**, 373–8 (2007).

68. Moore, J. W., Babidge, W. J., Millard, S. H. & Roediger, W. E. Thiolmethyltransferase activity in the human colonic mucosa: implications for ulcerative colitis. *J. Gastroenterol.*

Hepatol. **12**, 678–84 (1997).

69. Pitcher, M. C. L., Beatty, E. R., Harris, R. M., Waring, R. H. & Cummings, J. H. Sulfur metabolism in ulcerative colitis: Investigation of detoxification enzymes in peripheral blood. *Dig. Dis. Sci.* **43**, 2080–5 (1998).

70. Shen, X., Kolluru, G. K., Yuan, S. & Kevil, C. G. Measurement of H2S in vivo and in vitro by the monobromobimane method. *Methods Enzymol.* **554**, 31–45 (2015).

71. Shen, X., Peter, E. A., Bir, S., Wang, R. & Kevil, C. G. Analytical measurement of discrete hydrogen sulfide pools in biological specimens. *Free Radic. Biol. Med.* **52**, 2276–2283 (2012).

72. Stein, A. & Bailey, S. M. Redox biology of hydrogen sulfide: Implications for physiology, pathophysiology, and pharmacology. *Redox Biol.* **1**, 32–39 (2013).

73. Insko, M. A., Deckwerth, T. L., Hill, P., Toombs, C. F. & Szabo, C. Detection of exhaled hydrogen sulphide gas in rats exposed to intravenous sodium sulphide. *Br. J. Pharmacol.* **157**, 944–951 (2009).

74. Hui, Y., Du, J., Tang, C., Bin, G. & Jiang, H. Changes in arterial hydrogen sulfide content during septic shock and endotoxin shock in rats. *J. Infect.* **47**, 155–160 (2003).

75. Mustafa, A. K. *et al.* H2S Signals Through Protein S-Sulfhydration. *Sci. Signal.* **2**, (2010).

76. Bhatia, M. Role of Hydrogen Sulfide in the Pathology of Inflammation. *Sci.* **2012**, 12 (2012).

77. Li, L. *et al.* Hydrogen sulfide is a novel mediator of lipopolysaccharide-induced inflammation in the mouse. *FASEB J.* **19**, 1196–1198 (2005).

78. Libiad, M., Sakamoto, N., Fearon, E. & Banerjee, R. Hydrogen sulfide homeostasis and signaling in normal and neoplastic intestinal cells. *FASEB J.* **31**, 773.4-773.4 (2017).

79. Wu, D. *et al.* Hydrogen sulfide in cancer: Friend or foe? *Nitric Oxide* **50**, 38–45 (2015).

80. Whiteman, M. *et al.* Detection of hydrogen sulfide in plasma and knee-joint synovial fluid from rheumatoid arthritis patients: relation to clinical and laboratory measures of inflammation. *Ann. N. Y. Acad. Sci.* **1203**, 146–150 (2010).

81. Wu, D. *et al.* Hydrogen sulfide acts as a double-edged sword in human hepatocellular carcinoma cells through EGFR/ERK/MMP-2 and PTEN/AKT signaling pathways. *Sci. Rep.* **7**, 5134 (2017).

82. Hellmich, M. R., Coletta, C., Chao, C. & Szabo, C. The therapeutic potential of cystathionine β-synthetase/hydrogen sulfide inhibition in cancer. *Antioxid. Redox Signal.* **22**, 424–448 (2015).

83. Szabo, C. & Hellmich, M. R. Endogenously produced hydrogen sulfide supports tumor cell growth and proliferation. *Cell Cycle* **12**, 2915–2916 (2013).

84. Szabo, C. *et al.* Tumor-derived hydrogen sulfide, produced by cystathionine-β-synthase, stimulates bioenergetics, cell proliferation, and angiogenesis in colon cancer. *Proc. Natl. Acad. Sci. U. S. A.* **110**, 12474–12479 (2013).

85. Song, Z. J. *et al.* Hydrogen sulfide donors in research and drug development. *Medchemcomm* **5**, 557–570 (2014).

86. Xu, S. *et al.* Diallyl trisulfide, a H2S donor, inhibits cell growth of human papillary thyroid carcinoma KTC-1 cells through a positive feedback loop between H2S and

cystathionine-gamma-lyase. *Phyther. Res.* **34**, 1154–1165 (2020).

87. Clark, H. F. *et al.* The secreted protein discovery initiative (SPDI), a large-scale effort to identify novel human secreted and transmembrane proteins: a bioinformatics assessment. *Genome Res.* **13**, 2265–2270 (2003).

88. Petrossian, T. & Clarke, S. Bioinformatic Identification of Novel Methyltransferases. *Epigenomics* **1**, 163–175 (2009).

89. Zehmer, J. K., Bartz, R., Liu, P. & Anderson, R. G. W. Identification of a novel N-terminal hydrophobic sequence that targets proteins to lipid droplets. *J. Cell Sci.* **121**, 1852–1860 (2008).

90. Zehmer, J. K. *et al.* Targeting sequences of UBXD8 and AAM-B reveal that the ER has a direct role in the emergence and regression of lipid droplets. *J. Cell Sci.* **122**, 3694–3702 (2009).

91. Liu, H., Liu, Y. & Qu, J. Construction of an eight-gene signature for survival evaluation of papillary thyroid cancer patients. *Int J Clin Exp Med* **12**, 7241–7248 (2019).

92. Dong, Z. *et al.* Identification of potential key genes in esophagael adenocarcinoma using bioinformatics. *Exp. Ther. Med.* **18**, 3291–3298 (2019).

93. Ye, D. *et al.* METTL7B promotes migration and invasion in thyroid cancer through epithelial-mesenchymal transition. *J. Mol. Endocrinol.* **63**, 51–61 (2019).

94. Mckinnon, C. M. & Mellor, H. The tumor suppressor RhoBTB1 controls Golgi integrity and breast cancer cell invasion through METTL7B. *BMC Cancer* **17**, (2017).

95. Liu, D. *et al.* METTL7B Is Required for Cancer Cell Proliferation and Tumorigenesis in

Non-Small Cell Lung Cancer. *Frontiers in Pharmacology* **11**, 178 (2020).

96. Zhou, S. *et al.* DNA methylation of METTL7A gene body regulates its transcriptional level in thyroid cancer. *Oncotarget* **8**, 34652–34660 (2017).

97. Guo, T., Ma, H. & Zhou, Y. Bioinformatics analysis of microarray data to identify the candidate biomarkers of lung adenocarcinoma. *PeerJ* **7**, e7313–e7313 (2019).

98. Dall'Era, M. A., Oudes, A., Martin, D. B. & Liu, A. Y. HSP27 and HSP70 interact with CD10 in C4-2 prostate cancer cells. *Prostate* **67**, 714–721 (2007).

99. Park, E.-M., Lim, Y.-S., Ahn, B.-Y. & Hwang, S. B. AAM-B Interacts with Nonstructural 4B and Regulates Hepatitis C Virus Propagation. *PLoS One* **10**, e0132839–e0132839 (2015).

100. Franjic, D. *et al.* Molecular Diversity Among Adult Human Hippocampal and Entorhinal Cells. *bioRxiv* 2019.12.31.889139 (2020). doi:10.1101/2019.12.31.889139

101. Taylor, P. C. *et al.* Selective Inhibition of Janus Kinase 1 (JAK1) by Filgotinib Modulates the Disease-Associated Whole Blood Transcriptional Profile of Patients With Active Rheumatoid Arthritis. *Ann. Rheum. Dis.* **78**, 374–375 (2019).

102. Kashkin, K. N. *et al.* Genes potentially associated with Cisplatin resistance of lung cancer cells. *Dokl. Biochem. Biophys.* **438**, 147–150 (2011).

103. Ahmed, N. *et al.* Unique proteome signature of post-chemotherapy ovarian cancer ascites-derived tumor cells. *Sci. Rep.* **6**, 30061 (2016).

Chapter 2: Identification of METTL7A and METTL7B as Alkyl Thiol Methyltransferases

Introduction:

Mammalian thiol methyltransferase (TMT) activity was first reported in the early 1960's by Bremer and Greenberg[1] after they discovered that methyltransferase activity is enzymatic in nature and localized to the microsomal subcellular fraction in a wide variety of animals, including rat and mouse. Additionally, they showed that *S*-adenosyl-*L*-methionine (SAM) is a required cofactor and that multiple compounds could act as methyl acceptors. The only chemical requirement is that the substrate contains an aliphatic thiol functional group.

Methylation activity was measured by conducting reactions in presence of SAM labeled with a tritiated methyl group. Following liquid-liquid extraction to remove excess SAM, the radioactivity remaining in the organic layer was counted and converted to a specific activity. In a very clever set of experiments, the authors confirmed that the methyl transfer was occurring on an aliphatic thiol by using ß-mercaptoethanol and its *O*-methyl and *S*-methyl analogs as additional probe substrates. The amount of extractable radioactive product was severely reduced when using *S*-methyl-ß-mercaptoethanol as a substrate but was not inhibited when using *O*-methyl-ß-mercaptoethanol. Therefore, while the radioactive technique itself was blind to the identity of the methyl acceptor, Bremer and Greenberg conclusively identified alkyl thiol methyltransferase activity.

Since the initial landmark publication, little progress was made on the characterization of thiol methyltransferase until almost two decades later. Within a year of each other, Borchardt et al.[2] and Weisiger et al.[3] published methods attempting to purify thiol methyltransferase from rat liver, showing specific activity improvements of 10- to 1,000-fold over liver homogenate. Each paper confirmed that microsomal thiol methyltransferase utilizes SAM as a cofactor, has a wide

substrate specificity for exogenous aliphatic thiol compounds, and is most active between pH 7.5-8. The molecular weight was estimated to be either 28 kiloDaltons (kDa) or 200 kDa based on data from gel electrophoresis and size exclusion chromatography, measured against known molecular weight protein standards. Unfortunately, the candidate protein was not purified to homogeneity, was not sequenced, and the gene remained unknown. Given the conflicting reported biochemical characteristics, it is important to identify the true enzyme responsible for thiol methyltransferase activity in order to determine its overall role in drug metabolism and human disease.

The clinical relevance of thiol methyltransferase is unclear yet the observed interindividual variability in aliphatic thiol metabolism varies up to five-fold[4,5]. A similar enzyme, thiopurine methyltransferase (TPMT), whose function is critical for treating cancer patients, also exhibits a five-fold range of enzymatic activity across homogenous populations[6,7]. Patients with the lowest TPMT activity risk toxicity when treated with thiopurine drugs such as 6-mercaptopurine and azathioprine[8–10] and a genotypic test to detect TPMT deficiency is routinely used to avoid bone marrow toxicity. Therefore, it is possible that patients with TMT deficiency also may experience toxicity from aliphatic thiol-containing drugs. In fact, aliphatic thiol drugs or their metabolites that are potentially metabolized by TMT, such as clopidogrel and D-penicillamine, are known to exhibit idiosyncratic heptatotoxicity[11–13]. Once again, it is important to fully characterize thiol methyltransferase and determine if it contributes to idiosyncratic toxicities.

In this chapter, we report our initial attempts to purify thiol methyltransferase from rat liver guided by previously published protocols, proteomic analysis of the partially purified protein, and subsequent gene expression experiments using two different cell lines. We initially

attempted to repeat a similar purification protocol to that published by Borchardt and Weisiger, but could not achieve acceptable levels of purity. We turned to generic shotgun proteomics to identify as many proteins as possible in purification fractions exhibiting methyltransferase activity and this resulted in two candidate proteins, METTL7A and METTL7B. We then validated the candidate proteins' involvement in thiol methylation by modulating their mRNA expression levels and measuring the effect on methylation of an aliphatic thiol probe substrate.

Materials and Methods:

Materials:

Mammalian overexpression plasmids and siRNA were purchased from Origene (Rockville, MD). HepG2 and HeLa cells were obtained from ATCC (Manassas, VA). Liver microsomes from various species were purchased from Sekisui (Kansas City, KS). Cell culture materials and lipofection reagents were purchased from ThermoFisher (Waltham, MA). Buffer salts and ion exchange resins were acquired from Sigma-Aldrich (St. Louis, MO). 7α-Thiospironolactone was purchased from Santa Cruz Biotechnology (Dallas, TX). Zwittergent 3-14 was purchased from EMD Millipore which is now a part of Sigma Aldrich. *S*-adenosyl-*L*-methionine and molecular biology kits were obtained from New England Biolabs (Ipswich, MA). Stellar competent cells were purchased from Takara (Mountain View, CA). LOBSTR-BL21(DE3) competent cells were bought from Kerafast (Boston, MA). CHAPS detergent and UPLC-grade solvents were obtained from Fisher Scientific (Hampton, NH). Sequencing grade porcine trypsin and MTase-Glo Methyltransferase Assays were purchased from Promega (Madison, WI). 1,2-Dimyristoyl-*sn*-glycero-3-PG (DMPG) and mertansine were obtained from

Cayman Chemical (Ann Arbor, MI). The prasugrel active metabolite was a gift from Dr. Allan Rettie.

Ion Exchange Purification of Thiol Methyltransferase:

Commercially available tubes of pooled rat liver microsomes were thawed on ice and combined. Four tubes were combined, resulting in 2 mL of a 20 mg/mL solution (40mg total used for purification). The microsomes were pelleted by centrifugation at 13,000 x g for 15 minutes at 4 ^{o}C and then resuspended in solubilization buffer containing 10 mM KPi at pH 8.0, 20% (v/v) glycerol, and 0.3% (v/v) Zwittergent 3-14. The resuspended microsomes were rotated end-over-end for 30 minutes at 4 ^{o}C followed by addition of more solubilization buffer and another 30 minutes of rotation. The solubilized microsomes were centrifuged at 100,000 x g for one hour at 4 ^{o}C and the supernatant was used for further purification.

The solubilized microsome supernatant was applied to a 5 mL diethylaminoethanol (DEAE)-Sepharose anion exchange column equilibrated with solubilization buffer. The column was then washed with 10 column volumes (CV) of solubilization buffer and 5 mL fractions were collected. Protein was eluted using a stepwise gradient of solubilization buffer with an adjusted KPi ionic strength of 50, 100, 200, 350, or 500 mM. The column was washed with two CV of each elution step and 5 mL fractions were collected. Thiol methyltransferase activity was assayed using the prasugrel active metabolite activity assay detailed below. Aliquots were taken from each fraction for determination of protein concentration by BCA and overall purity by SDS-PAGE.

Fractions exhibiting thiol methyltransferase activity were pooled and loaded onto a 5 mL sulphopropyl (SP)-Sepharose cation exchange column equilibrated with solubilization buffer.

The column was washed with 10 CV of solubilization buffer while collecting 5 mL fractions. Protein was eluted using the same procedure as detailed above for DEAE-Sepharose. Thiol methyltransferase activity was assayed using the prasugrel active metabolite activity assay detailed below. Aliquots were again taken from each fraction for determination of protein concentration by BCA and overall purity by SDS-PAGE.

In vitro 7α-Thiospironolactone Methylation Assay for Tracking Thiol Methyltransferase Activity:

An aliquot (490 µL) of each purification fraction was added to a 1.5 mL Eppendorf tube on ice alone with 5 µL of 3 mM 7α-Thiospironolactone in DMSO for a final concentration of 30 µM. The reaction tubes were pre-incubated at 37 ^{o}C for 2-3 minutes and then enzymatic assays were initiated by adding 5 µL of 2.5 mM SAM for a final concentration of 25 µM and a final reaction volume of 500 µL. The final concentration of DMSO did not exceed 1% (v/v). Reactions were incubated at 37 ^{o}C for 30 minutes and enzymatic activity was quenched via 1:10 addition of aqueous 15% (w/v) $ZnSO_4$ solution. The samples were placed on ice for 10 minutes to facilitate protein precipitation followed by addition of progesterone internal standard to a final concentration of 13.5 µM. The samples were then centrifuged at 13,000 x g for 5 minutes at 4 ^{o}C and the supernatant was analyzed by HPLC-UV as detailed below.

The HPLC system used to analyze 7α-Thiospironolactone methylation was comprised of a Shimadzu SIL-HTc autosampler, Shimadzu DGU-14A in-line degasser, two Shimadzu LC-10AD pumps and a Shimadzu SPD-10A UV-Vis detector. Samples were detected using a wavelength of 254 nm and chromatographic separation of compounds was achieved using an Agilent Zorbax 4.6x250 mm, 5 µm, 300SB-C18 HPLC column. The mobile phase used consisted of 10 mM formic acid in water and neat acetonitrile for solvents A and B respectively.

Flow rate was held at 1.0 mL/min and the gradient was as follows: solvent B was set at 48% initially and held for 8.5 minutes, then increased to 75% and held for 2.5 minutes, and then returned to initial conditions and re-equilibrated for 4 additional minutes for a total run time of 15 min. No sample was diverted to waste but absorbance was only measured only for the first 12.5 min.

Prasugrel Active Metabolite Methylation Assay for Tracking Thiol Methyltransferase Activity In vitro:

Fractions eluted from the DEAE column (240 µL) were aliquoted into a 1.5 mL Eppendorf tube on ice along with 5 µL of 100 µM prasugrel active metabolite for a final concentration of 2 µM. Reaction tubes were pre-incubated at 37 ^{o}C for 2-3 minutes. Enzymatic activity was initiated via addition of 5 µL of 2.5 mM SAM for a final concentration of 50 µM and a final reaction volume of 250 µL. The samples were incubated at 37 ^{o}C for 25 min and quenched via a 1:10 addition of an aqueous 15% (w/v) $ZnSO_4$ solution and chilled on ice for 10 min. The d_3-6-mercaptopurine internal standard was added to a final concentration of 150 ng/mL. The tubes were vortexed and centrifuged at 13,000 x g for 5 min to pellet precipitated proteins. Supernatants were analyzed by liquid chromatography-tandem mass spectrometry (LC-MS/MS).

The LC-MS/MS system used for prasugrel active metabolite methylation analysis was an AB Sciex 4000 QTrap paired with a Waters Acquity LC. Compound separation was achieved using a 2.1x150 mm Acquity BEH C18 column and 0.1% formic acid in water and 0.1% formic acid in acetonitrile as solvents A and B respectively. Column temperature was held at room temperature and samples were kept at 5 ^{o}C. Chromatographic separation was obtained using the

following gradient: solvent B was set at 10% initially, then increased to 50% during the first minute, followed by a decrease to 35% over the next three minutes, and re-equilibrated to the starting conditions for another 3.5 min for a total run time of 7.5 min. Flow rate was held constant at 0.3 mL/min and flow was only diverted to the mass spectrometer between 1.8 to 5.5 min.

Prasugrel's active thiol metabolite, the corresponding *S*-methyl metabolite, and the internal standard, d_3-6-mercaptopurine, were monitored in negative mode. The monitored mass transitions m/z^- were 349.0 > 99.0 and 349.0 > 215.0 (prasugrel thiol metabolite), 362.0 > 177.0 (*S*-methyl metabolite) and 170.1 > 128.2 (internal standard). The MS conditions were as follows: collision energy -30.0, declustering potential -50.0, entrance potential -10.0, collision cell exit potential -15.0, IonSpray voltage -4500.0, desolvation temperature 350 ^oC, curtain gas 10.0, ion source gas #1 40.0, and ion source gas #2 50.0.

The same method described above was also used for microsomal activity assay screening at 0.15 mg/mL final protein concentrations.

Tryptic Digest:

Tryptic digests were conducted following a method similar to that of Shevchenko[14]. Briefly, protein aliquots were added to sterile tubes, treated with 10 mM dithiothreitol (DTT) solution, and incubated at 56 ^oC to reduce all proteins. The samples were then treated with 55 mM iodoacetamide at room temperature in the dark to alkylate all exposed cysteine side chains. Finally, the samples were incubated overnight at 37 ^oC with 13 ng/µL trypsin-containing solution. Tryptic digests were concentrated to near-dryness in a centrifugal evaporator. Concentrated peptides were analyzed using a high-resolution mass spectrometer, a

Finnigan LTQ Orbitrap in our case, and then used to identify the protein of interest via ProteinProspector.

The LC-MS system used for proteomic analysis was a Finnigan LTQ Orbitrap coupled to a Waters Acquity LC. Peptides were separated using a 1x150 mm Acquity UPLC CSH C18 column and 0.1% formic acid in water and 0.1% formic acid in acetonitrile as solvents A and B. Separation was achieved using the following gradient: solvent B was held at 5% for the first two minutes, increased to 40% over the next 90 min, increased to 90% over the next five minutes and held for an additional 8 minutes, then re-equilibrated over five minutes. The flow rate was held at 0.06 mL/min and flow as diverted to the mass spectrometer from 2 to 95 minutes.

Peptides were analyzed using a data dependent scan method in positive mode. The initial high-resolution scan from 300-2,000 m/z was conducted in the FTMS with 60,000 resolution. Four data dependent scans were completed in the ion trap to obtain fragmentation. Dynamic exclusion was enabled which excluded the top 25 most intense ions after they had been selected twice over a four second window. The following mass spectrometer settings were used: sheath gas flow rate was 12 arb, spray voltage was 3.5 kV, capillary temperature was 350 ^{o}C, capillary voltage was 22 V, and tube lens voltage was 100 V.

Proteomic Data Analysis:

Mass spectra of the tryptic digest samples were analyzed using the online ProteinProspector proteomic analysis tool. Spectra were first converted to compatible .mzXML files using MSConvert and uploaded to ProteinProspector. The spectra were searched against the most current SwissProt database, limiting the taxonomy to *Rattus norvegicus* (rat), *Escherichia coli,* or *Homo sapiens* (human), depending upon the sample. Ions were specified as

monoisotopic with a precursor charge range of 1-5. Parent tolerances were set at 20 ppm error and fragment tolerances were set at 200 ppm error. A trypsin-based digestion pattern was applied with a maximum of one missed cleavage, and a constant carbamidomethyl modification on cysteine residues to account for incubation with iodoacetamide. The pre-set list of variable modifications was used which included *N*-terminal acetylation, methionine oxidation, loss of methionine from the *N*-terminus, conversion of glutamine to pyroglutamate, and a number of combinations thereof. A maximum of two variable modifications were allowed for each peptide.

HepG2 and HeLa Cell Culture:

Cells were maintained and expanded using Dubelco's Modified Eagle Medium supplemented with 10% fetal bovine serum and 0.1% penicillin/streptomycin. All cellular captopril methylation assays were conducted in serum-free media under optimized incubation conditions. Cells used for RNA isolation were washed with 1x phosphate buffered saline (PBS) prior to aspiration and storage at -80 ^{o}C until future use.

Gene Expression Modulation:

HepG2 cells were treated with Lipofectamine RNAiMax (ThermoFisher Scientific, Waltham, MA) according to the manufacturer's protocol, optimized for transfection duration. *GAPDH* gene knockdown using the Trilencer small interfering RNA (Origene, Rockville, MD) acted as the positive control for all gene expression knockdown experiments.

Cells were transfected in 12-well plates using a reverse transfection protocol. Briefly, *METTL7B* or scrambled siRNA was mixed with Lipofectamine RNAiMax in OptiMEM at room temperature for a final siRNA concentration of 50 nM. HepG2 cells were harvested using

trypsin, pelleted, and resuspended to a final concentration of 200,000 cell/mL. Lipofectamine/siRNA stocks were added to culture plate wells, followed by 1 mL of cell mixture, for a final concentration of 10 nM siRNA. Cells were allowed to incubate in the transfection media for 72 hours followed by RNA isolation or captopril methylation assays.

HeLa cells were treated with Lipofectamine 3000 (ThermoFisher Scientific) according to the manufacturer's protocol, optimized for transfection duration. Cells were transfected in 12-well plates via reverse transfection where purified empty or FLAG-tagged *METTL7* overexpression plasmids (Origene) were mixed with P3000 reagent in OptiMEM at room temperature followed by Lipofectamine 3000. HeLa cells were harvested via trypsinization, pelleted, and resuspended to a final concentration of 200,000 cell/mL. Lipofectamine/plasmid stocks were added to culture plate wells, followed by 1 mL of cells, for a final plasmid concentration of 833 ng/mL. Cells were allowed to incubate in transfection media for 48 hours prior to RNA isolation or captopril methylation assays.

Measurement of Gene Expression Changes:

Cellular RNA was extracted using the MagMAX-96 Total RNA Isolation kit (ThermoFisher Scientific) according to the manufacturer's protocol. RNA quality (A_{260}/A_{280}) and concentration was assayed using a NanoDrop spectrophotometer. Isolated RNA was used to create cDNA using the High Capacity RNA-to-cDNA kit (ThermoFisher Scientific) according to the manufacturer protocol. Subsequently, reverse-transcription polymerase chain reaction (RT-PCR) was conducted using an Applied Biosystems StepOnePlus Real-Time PCR System with TaqMan FAM reporter primers for *METTL7B, GAPDH,* and the housekeeping gene, *GusB*.

Expression level changes upon siRNA or plasmid treatment were determined using the $\Delta\Delta C_T$ method[15]. In this method, *METTL7B* cycle threshold (C_t) values are normalized to *GusB* C_t values in all samples, yielding a ΔC_T value. Relative gene expression changes are then calculated between treated and control cells using $2^{-\Delta\Delta CT}$.

Cellular Captopril Methylation Assay:

Cells with altered *METTL7B* gene expression were created as described above. After the appropriate transfection period, cells were washed with 1x PBS and treated with serum-free media containing 500 μM captopril. Cell media aliquots were sampled after 24 hours and the S-methyl captopril metabolite was measured via liquid chromatography-tandem mass spectrometry (LC/MS-MS) and multiple reaction monitoring (MRM).

The LC-MS/MS system used for captopril methylation analysis was a Waters Xevo TQS mass spectrometer paired with a Waters Acquity LC. Compound separation was achieved using a 2.1x100 mm Ascentis Express RP Amide column and 0.1% formic acid in water and 0.1% formic acid in methanol as solvents A and B respectively. Column temperature was maintained at 50 ^{o}C at all times. Chromatographic separation was obtained using the following gradient: solvent B was held at 30% from 0 to 3 min, then held at 90% from 3 to 7 min, followed by re-equilibration to the starting conditions for another 3 min for a total run time of 10 min. Flow rate was held constant at 0.2 mL/min and flow was only diverted to the mass spectrometer between 2 to 7.5 min.

S-methyl captopril and the internal standard, d_3-*S*-methyl captopril, were monitored in positive mode. The monitored mass transitions m/z+ were 232.1 > 89 and 232.1 > 116 (S-methyl captopril) as well as 235.1 > 91.9 and 235.1 > 115.9 (internal standard). The MS

conditions were as follows: collision energy 15 V, cone voltage 30 V, capillary voltage 3.2 kV, desolvation temperature 450 ºC, desolvation gas flow 1,000 L/hr and cone gas 150 L/hr.

Protein Purity Analysis:

All SDS-PAGE silver stain analysis was conducted using NuPAGE 4-12% Bis-Tris gels in the XCell SureLock Mini-Cell Electrophoresis system using PageRuler Plus Prestained Protein Ladder as a molecular weight marker. Samples were prepared using NuPAGE LDS Sample Buffer sample buffer and 1.4 M ß-mercaptoethanol before boiling for 5 minutes. Gels were run at room temperature, at a constant 200 volts, and developed using previously published silver staining protocols[14].

All western blot analyses were conducted using the XCell SureLock Mini-Cell Electrophoresis system, PageRuler Plus Prestained Protein Ladder, and NuPAGE 10-20% Tricine gels. Samples were prepared using 4X Protein Loading Buffer (LiCor) and 0.7 M ß-mercaptoethanol before boiling for 5 minutes. After initial SDS-PAGE separation, the gel was removed from the cassette and placed with PVDF blotting membrane into the XCell II Blot Module according to the manufacturer's protocol. Blot transfer was conducted over 1 hour at a constant 30 volts on ice. The membrane was blocked using Odyssey Blocking Buffer (LiCor) for 1 hour at room temperature. A primary antibody incubation was conducted overnight using the suggested dilution factor for the rabbit anti-METTL7B (Sigma Aldrich), anti-FLAG (Cell Signaling), anti-GST (Cell Signaling), or anti-ß actin (Cell Signaling) antibodies. The secondary antibody incubation was conducted for 1 hour at room temperature using IRDye 680RD goat anti-rabbit antibody (LiCor). Western blots were scanned using an Odyssey gel scanner. Blot images were visualized using Image Studio Version 4.0 software.

Data Analysis:

All experiments were conducted with biological triplicates, and repeated at least twice on two separate days. All data are reported as the mean ± standard deviation, however individual data points from multiple experiments are presented when possible. Statistical significance was determined by a two-tailed unpaired *t* test with a threshold *P* value of 0.05. All statistical analysis was conducted using GraphPad Prism, version 8.3.1 for Windows (GraphPad Software, La Jolla, CA).

Results:

Initial Thiol Methyltransferase Activity Testing in Animal Liver Microsomes:

A variety of commercially available pooled liver microsomes exhibited thiol methyltransferase activity when probed with the prasugrel active metabolite as shown in Figure 2.1. Multiple mammalian species were tested and TMT activities were similar except for dog, where rates were relatively low. There were no statistically significant differences in TMT activity between sexes in non-human species. TMT activity was significantly greater in pooled human male liver microsomes compared to pooled human female liver microsomes, however this gender difference was not observed with other species.

Attempts to Purify Thiol Methyltransferase from Rat Liver Microsomes:

Solubilized rat liver microsomal proteins were first fractionated using DEAE Sepharose. TMT-active fractions, namely flow-through and initial washes, were then pooled and separated by SP-Sepharose. Protein purity was monitored via SDS-PAGE and silver stain as shown in

Figures 2.2 and 2.3. Thiol methyltransferase activity was monitored by UV-Vis using 7α-Thiospironolactone as a probe substrate. A representative chromatogram is shown in Figure 2.4.

Tryptic Digest and Proteomic Analysis of Collected Purification Fractions:

Fractions eluted from the SP-Sepharose column and containing thiol methyltransferase activity, measured by 7α-Thiospironolactone methylation, were subjected to in-solution tryptic digestion. Parent and daughter ion masses were obtained using an Orbitrap LTQ. The resulting mass spectra were analyzed against the SwissProt database via ProteinProspector. The only putative methyltransferase protein identified in multiple active fractions was methyltransferase-like protein 7B (METTL7B). It was identified with multiple unique peptides at high mass accuracy after DEAE Sepharose and SP Sepharose separation as shown in Figure 2.5 and 2.6. Additional proteins identified in the tryptic digest of a TMT-active DEAE Sepharose fraction are shown in Figure 2.7. Most proteins identified are known to associate with the endoplasmic reticulum and are expressed in liver tissue, such as cytochrome P450 (CYP450) and glutathione *S*-transferase (GST) enzymes.

Bioinformatic Identification of Human Orthologs:

The rat METTL7B protein sequence was compared to the known human proteome using the NCBI Basic Local Alignment Search Tool (BLAST). Two main human orthologs were identified, methyltransferase-like protein 7A (METTL7A) and methyltransferase-like protein 7B (METTL7B). Rat and human METTL7B proteins share 83% sequence identity while rat METTL7B and human METTL7A share 56% sequence identity. Human METTL7A and METTL7B share 58% sequence identity. Homology models for each protein were generated in collaboration with Dr. Abhi Nath. The protein sequences contain a conserved *S*-adenosyl-*L*-

methionine (SAM) binding sequence and allow a seven-beta strand fold tertiary structure, which are common features of small molecule and DNA methyltransferases[16]. Additionally, both proteins contain a hydrophobic *N*-terminal alpha helix that is predicted to insert into plasma membranes (Appendix II). Dr. Nath also computationally docked *S*-adenosyl-*L*-homocysteine (SAH) into each homology model as shown below in Figure 2.8.

siRNA Gene Knockdown in Mammalian HepG2 Cells:

Treating HepG2 cells with *METTL7B* specific small interfering RNA (siRNA) caused an average 60% decrease in *METTL7B* mRNA expression compared to cells treated with a scrambled negative siRNA control (Figure 2.9). Treatment with *METTL7A* specific siRNA caused and average 80% decrease in *METTL7A* mRNA expression but also caused a 100% increase in *METTL7B* mRNA expression. Concomitant treatment with both siRNA caused both gene mRNA levels to decrease at least 50%. Treatment with the *GAPDH* positive control siRNA caused mRNA levels to decrease over 90%.

Effect of Gene Knockdown on Captopril Methylation in Mammalian HepG2 Cell Culture:

Captopril methylation was significantly decreased (~30%) in cells pre-treated with *METTL7A* or *METTL7B* siRNA. More extensive reduction (~50%) in captopril methylation was observed in cells treated with both siRNA at the same time (Figure 2.10).

Western Blot Confirmation of Decreased Protein Expression in HepG2 Cell Culture:

HepG2 cell lysate treated with METTL7B or control siRNA was analyzed for reduced expression of METTL7B by western blot. METTL7B was visualized using an anti-METTL7B primary antibody and loading controls were conducted using an anti-ß-actin primary antibody.

METTL7B band intensity was slightly reduced in cell lysate from cells with reduced *METTL7B* gene expression compared to control lysate (Figure 2.11).

Constitutive Gene Overexpression in Mammalian HeLa Cells:

METTL7A and *METTL7B* genes were overexpressed in HeLa cells via transient transfection with a constitutive overexpression plasmid (Figure 2.12). For each gene, mRNA levels were increased over 1,000-fold compared to cells treated with an empty control plasmid as measured by RT-PCR (Figure 2.13). Similar levels of upregulation were observed upon single or co-transfection. Additionally, *METTL7A* gene expression was not altered by upregulation of *METTL7B* gene expression and vice versa.

Effect of Gene Overexpression on Captopril Methylation in Mammalian HeLa Cell Culture:

HeLa cells overexpressing *METTL7A* and/or *METTTL7B* exhibited a much higher rate of captopril methylation compared to control cells (Figure 2.14). Overexpression of *METTL7B* increased captopril methylation more than overexpression of *METTL7A*. Overexpression of both genes increased captopril methylation to the same level observed in cells overexpressing *METTL7B* alone.

Western Blot Confirmation of Protein Overexpression in HeLa Cell Culture:

Overexpressing HeLa cell lysate was analyzed for overexpression of FLAG-tagged METTL7B protein by western blot. METTL7B was visualized using an anti-FLAG primary antibody and loading controls were conducted using an anti-ß-actin primary antibody. Cell lysate from cells treated with the *METTL7B* overexpression plasmid clearly showed expression of a FLAG-tagged METTL7B protein, which was absent in control cell lysate (Figure 2.15).

Discussion:

In 1961 Bremer and Greenberg first reported that mammalian liver microsomal fractions could catalyze the methylation of several aliphatic thiol substrates in the presence of SAM. Thiol methyltransferase activity was roughly similar across many species tested, including rat, mouse, and rabbit. Interestingly, chicken liver microsomes exhibited very low activity compared to other mammalian species. It is possible that this enzymatic activity is generally lower in non-mammalian species, however more species need to be tested beyond chicken liver microsomes to confirm this observation. We were able to recapitulate these results in a larger screen of mammalian liver microsomes that were also stratified by sex (Figure 2.1). For the most part, TMT activity was similar across the tested species and no significant sex differences were observed. However, dog TMT activity was lower compared to other animals and this should be confirmed with additional substrates and multiple lots of dog liver microsomal preparations. Additionally, in commercially purchased human liver microsomes, TMT activity was significantly higher in males than females. However, this finding is not in accord with previously published works[5,17] and is not supported using other human liver microsomal fractions that were prepared in-house.

In order to characterize thiol methyltransferase substrate specificity and steady state reaction kinetics, we attempted to purify the enzyme from rat liver microsomes using ion exchange chromatography. However, pure thiol methyltransferase was unattainable due to difficulties in separation from other proteins using ion exchange resins. Therefore, partially purified fractions were subjected to tryptic digest and proteomic analysis in order to identify potential candidate proteins. Our search parameters were restricted to the SwissProt database;

therefore, we could only identify previously known proteins and were blind to novel ones. That said, many microsomal proteins and one potential methyltransferase were identified (Figure 2.7). This protein, rat methyltransferase-like protein 7B, contains a SAM binding domain and has a molecular weight similar to that reported previously for TMT[3]. Bioinformatic comparison to the human proteome identified human methyltransferase-like protein 7A (METTL7A) and methyltransferase-like protein 7B (METTL7B) as potential orthologs. Rat METTL7A has been observed in liver fractions[18] as well but was not identified in our proteomic analysis due likely to low abundance.

METTL7A and METTL7B thiol methyltransferase activity was initially tested by conducting gene expression modulation experiments in human cell culture. The primary method used for gene knockdown was transient siRNA transfection, optimized for transfection duration. Gene expression knockdown experiments were conducted in HepG2 cells due to their high basal levels of thiol methyltransferase that facilitated observation of a knockdown effect.

Using the optimized siRNA knockdown protocol, both *METTL7A* and *METTL7B* gene expression were significantly suppressed compared to control cells (Figure 2.9). Interestingly, downregulation of *METTL7A* results in an upregulation of *METTL7B* but the reverse is not true. The mechanism of *METTL7B* upregulation is unclear but it is possible that METTL7A or a metabolite helps to actively suppress *METTL7B* expression at basal levels. Upon the absence of the active suppression, *METTL7B* mRNA levels increase. Further experiments are required to understand the exact relationship between *METTL7A* and *METTL7B* expression and the potential physiological significance of their interaction at the mRNA level.

Thiol methylation activity in cells was measured using captopril as a marker substrate. HepG2 cells with decreased *METTL7A* and/or *METTL7B* expression exhibited significantly decreased captopril methylation compared to control cells even with the increase in *METTL7B* expression in cells treated with *METTL7A* siRNA (Figure 2.10). Cells treated with both siRNA exhibited an even greater decrease in captopril methylation, which implies that both METTL7A and METTL7B are involved in thiol methylation. Reduction in METTL7B protein expression was analyzed by western blot (Figure 2.11). The METTL7B band intensity was slightly decreased in cell lysates treated with METTL7B siRNA, indicating a reduction in intracellular protein concentrations. The remaining band signal intensity may be due to primary antibody cross-reactivity with METTL7A or remaining METTL7B. The decrease in METTL7B protein was directly correlated to a decrease in thiol methylation activity.

Gene overexpression experiments were conducted to further confirm that METTL7A and METTL7B act as thiol methyltransferase enzymes. HeLa cells were chosen due to their low basal expression of both *METTL7A* and *METTL7B*. HeLa cells were transfected with a mammalian expression plasmid which places expression of the gene of interest under the control of the constitutive cytomegalovirus promoter (Figure 2.12). Additionally, the expression plasmid adds a *C*-terminal affinity tag comprised of a c-Myc and FLAG sequence for western blot analysis and potential purification purposes.

Treatment with expression plasmids encoding *METTL7A* or *METTL7B* resulted in extremely large increases in each gene's mRNA levels (Figure 2.13). Gene expression levels increased 10,000-fold compared to control cells transfected with an empty expression plasmid. Interestingly, *METTL7A* mRNA concentrations were unaffected by the massive upregulation of

METTL7B and vice versa. It appears that the regulatory pathway controlled by *METTL7A* expression is only sensitive to decreased gene expression.

HeLa cells with increased expression of *METTL7A* and/or *METTL7B* displayed greater captopril methylation compared to control cells (Figure 2.14). Co-transfection with both expression plasmids did not yield higher captopril methylation than in cells transfected with an individual expression plasmid. It is possible that, due to the substantial increase in mRNA concentrations, that the amount of expressed METTL7A and METTL7B protein differed upon individual or co-transfection. Overexpression of a FLAG-tagged protein was confirmed by western blot (Figure 2.15), however the blot was not quantitative. Therefore, METTL7A and METTL7B protein concentrations may not have increased to the same extent and must be quantified using a different approach. The overexpression experiments confirmed that alteration of *METTL7A* and *METTL7B* expression in cells had a direct effect on thiol methylation.

Conclusions:

Over the years, multiple investigators attempted to identify the enzyme that accounts for thiol methyltransferase activity in humans, yet none have succeeded to date. Partial purification followed by proteomic analysis yielded two potential human genes encoding thiol methyltransferase proteins, namely *METTL7A* and *METTL7B*. Homology modeling and bioinformatic analysis of their amino acid sequences suggest that they are SAM-dependent small molecule methyltransferases. Modulation of their expression levels in two cell lines directly correlated with changes in the methylation of captopril; a marker reaction of thiol methyltransferase activity. Gene products of both *METLL7A* and *METTL7B* appear to be involved in thiol methylation. To unequivocally demonstrate that METTL7A and METTL7B

are thiol methyltransferases, expression and biochemical characterization of each enzyme is required.

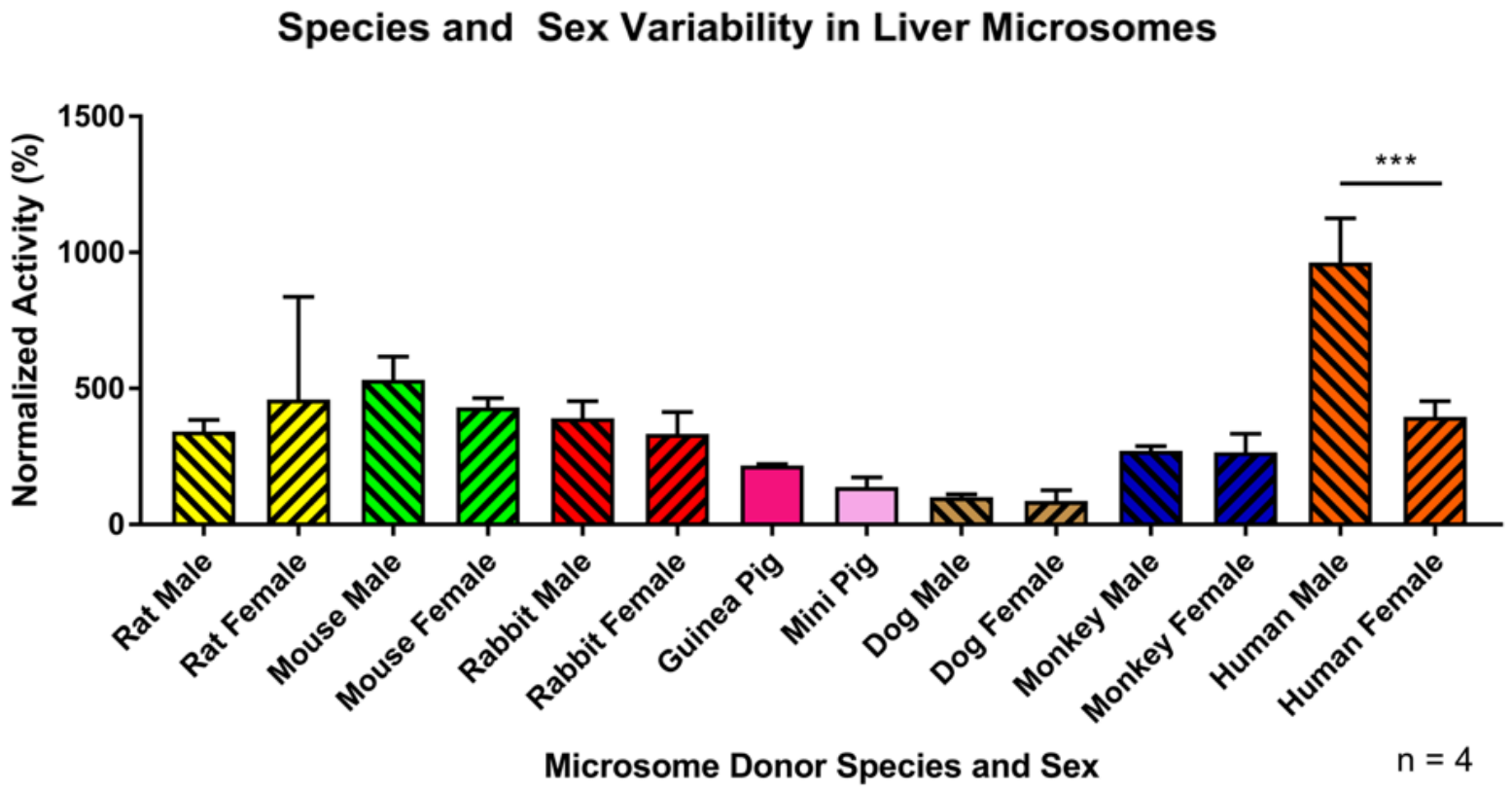

Figure 2.1. Inter-species and Inter-sex TMT Activity Variation: Species- and sex-specific liver microsomes were tested for TMT activity using the prasugrel active metabolite as a probe substrate. All species tested exhibited TMT activity at similar levels, except for dog which was relatively low. There were no significant differences between sexes for non-human species. All data are presented as the mean ± standard deviation. Significance was determined using unpaired two-tailed *t* test. ***$P<0.001$.

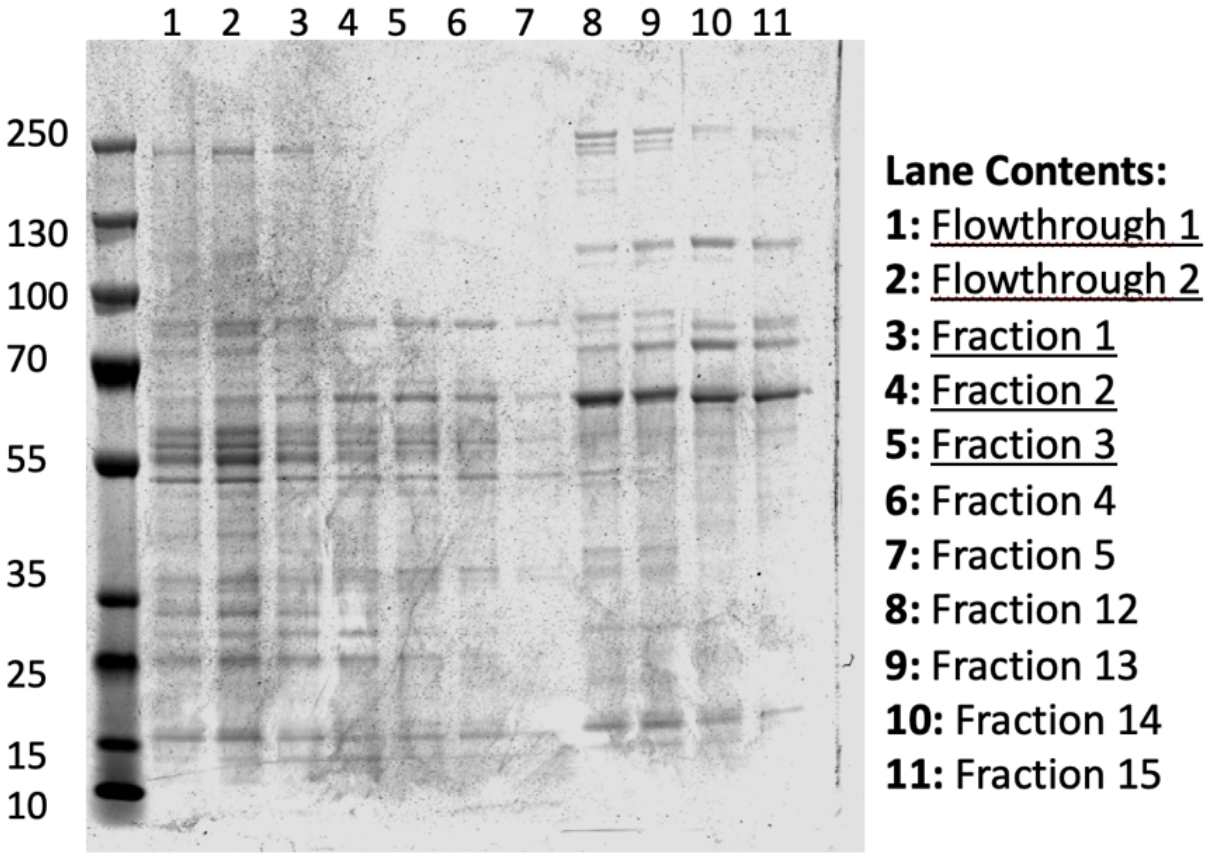

Figure 2.2. SDS-PAGE Silver Stain of DEAE Sepharose Separation: Lane contents are listed to the right of the gel image. Fractions containing thiol methyltransferase activity are underlined. All lanes were loaded with 0.25 mg/mL solutions as determined by BCA assay.

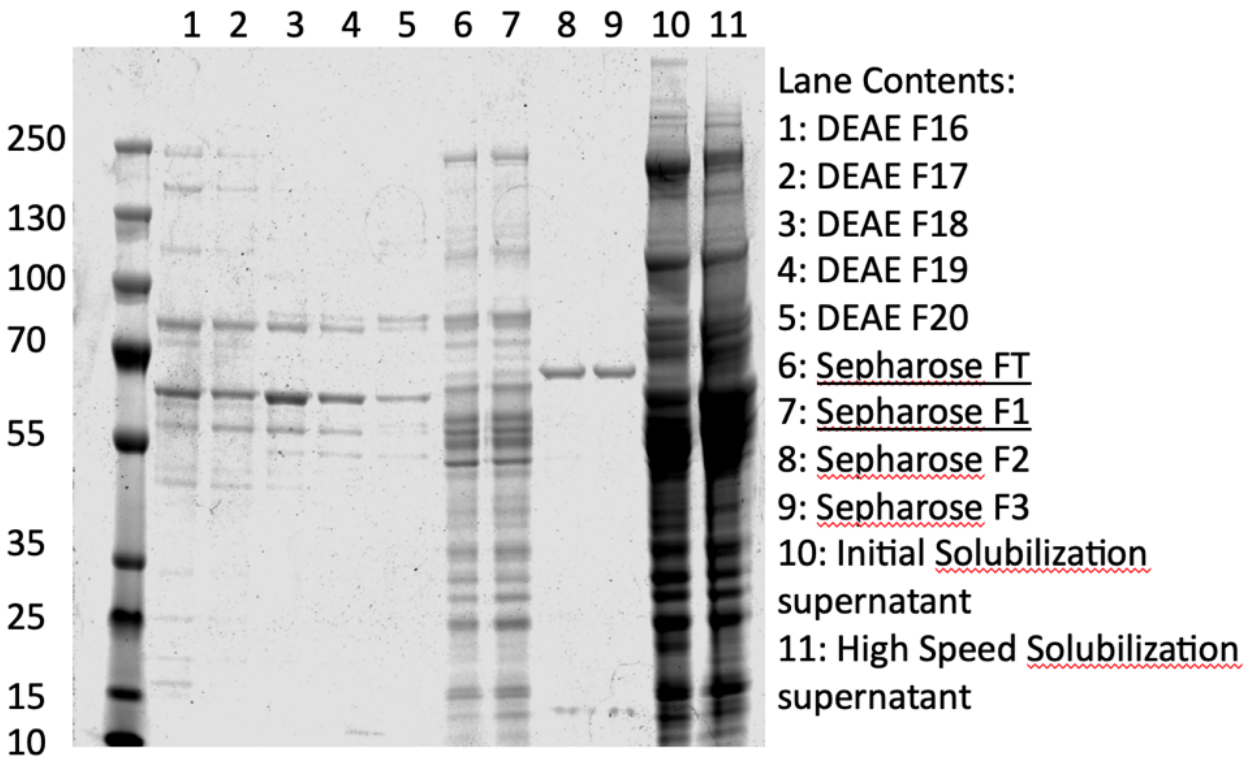

Figure 2.3. SDS-PAGE Silver Stain of SP Sepharose Separation: Lane contents are listed to the right of the gel image. Fractions containing thiol methyltransferase activity are underlined. All lanes were loaded with 0.25 mg/mL solutions as determined by BCA assay.

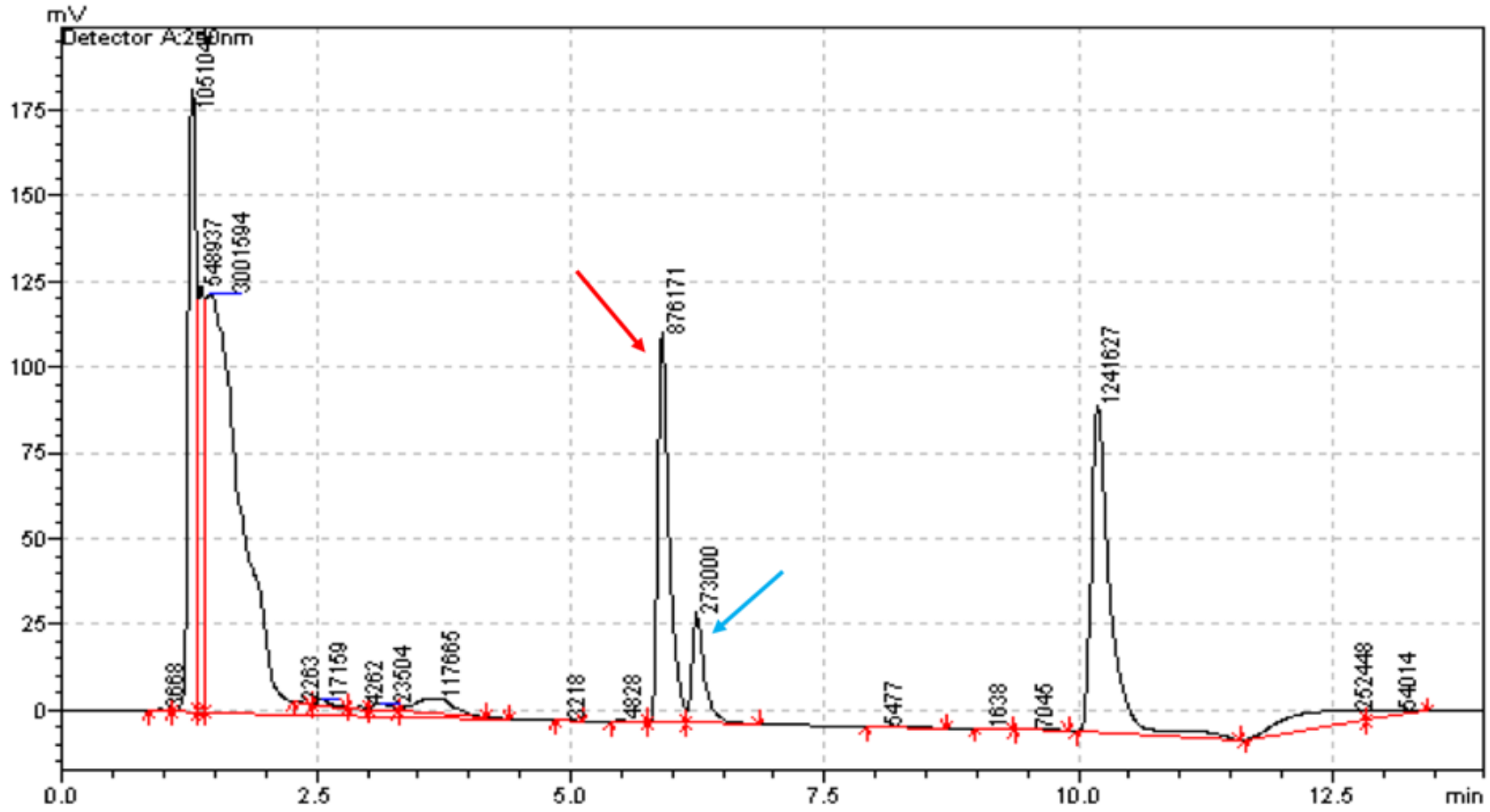

Figure 2.4. Representative HPLC UV Chromatogram for 7α-Thiospironolactone Methylation: Peaks were detected at 254 nm throughout the HPLC run. 7α-Thiospironolactone is noted with the red arrow with a retention time of 6 minutes. Methyl-7α-Thiospironolactone is noted with the blue arrow with a retention time of 6.5 minutes.

23 **Acc. #:** Q562C4 **Uniprot ID:** MET7B_RAT **Species:** RAT **Name:** Methyltransferase-like protein 7B
Organism: Rattus norvegicus **Gene:** Mettl7b **Existence:** Evidence at protein level **Version:** 1
Protein MW: 27904.1 **Protein pI:** 8.6 **Protein Length:** 244 **Index:** 234490

Num Unique	% Cov	Best Disc Score	Best Expect Val
6	36.5	3.73	2.1e-6

m/z	z	ppm	DB Peptide	Variable Mods	RT	Score	Expect	# in DB
1459.1781	2	-0.20	GTSNEVTLLELGCGTGANFQFYPPGCK		19.8035	25.5	2.1e-6	1
965.9870	2	-1.6	AQFSEVQLEWQPPPFK		19.3198	39.5	2.5e-6	1
774.3987	2	-1.6	TYFPYLMATLTAR		21.8432	17.9	1.1e-5	1
710.3300	2	-3.2	VTCVDPNPNFEK		12.7405	28.8	2.6e-5	1
583.2799	2	-0.50	HIGDGCHLTR		9.3841	23.9	7.8e-5	1
617.8422	2	0.50	WLPVGPHIMGK		16.7470	17.2	5.3e-4	1

Figure 2.5. METTL7B Peptides Identified from DEAE Sepharose-Separated Fractions: Multiple peptides unique to rat METTL7B were identified in a TMT-active fraction after separation by DEAE Sepharose. Peptides were identified using ProteinProspector and have very low error and expect values, which are measures of confidence of correct identification.

44 **Acc. #:** Q562C4 **Uniprot ID:** MET7B_RAT **Species:** RAT **Name:** Methyltransferase-like protein 7B
Organism: Rattus norvegicus **Gene:** Mettl7b **Existence:** Evidence at protein level **Version:** 1
Protein MW: 27904.1 **Protein pI:** 8.6 **Protein Length:** 244 **Index:** 234490

Num Unique	% Cov	Best Disc Score	Best Expect Val
3	16.0	1.98	3.4e-6

m/z	z	ppm	DB Peptide	Variable Mods	RT	Score	Expect	# in DB
638.8535	2	1.1	WLPVGPHIMGK		17.1607	23.1	3.4e-6	1
986.9995	2	0.076	AQFSEVQLEWQPPPFK		19.6178	22.3	1.7e-4	1
731.3400	2	-4.4	VTCVDPNPNFEK		13.3522	16.9	0.012	1

Figure 2.6. METTL7B Peptides Identified from SP-Sepharose-Separated Fractions:

Multiple peptides unique to rat METTL7B were identified in a TMT-active fraction after separation by SP-Sepharose. Peptides were identified using ProteinProspector.

Rank	Acc #	11_12_2015_005/DEAE Post-Void FT			Protein MW	Species	Protein Name
		Num Unique	% Cov	Best Expect Val			
1	P10634	20	46.2	2.0e-10	56684.4	RAT	Cytochrome P450 2D26
2	P06761	19	34.1	2.4e-10	72347.6	RAT	78 kDa glucose-regulated protein
3	P18163	18	37.5	2.7e-8	78179.4	RAT	Long-chain-fatty-acid--CoA ligase 1
4	P14141	14	85.8	1.8e-8	29431.6	RAT	Carbonic anhydrase 3
5	P07687	18	49.0	2.4e-7	52582.0	RAT	Epoxide hydrolase 1
6	P08683	14	39.0	3.9e-9	57181.6	RAT	Cytochrome P450 2C11
7	Q64573	11	31.6	1.5e-10	62309.0	RAT	Liver carboxylesterase 4
8	P46462	14	30.5	1.0e-7	89349.6	RAT	Transitional endoplasmic reticulum ATPase
9	P11442	10	9.4	1.7e-8	191600.4	RAT	Clathrin heavy chain 1
10	Q63081	9	34.3	8.4e-9	48173.8	RAT	Protein disulfide-isomerase A6
11	P02692	8	74.0	2.7e-9	14272.7	RAT	Fatty acid-binding protein, liver
12	P08541	10	24.5	3.6e-7	60986.1	RAT	UDP-glucuronosyltransferase 2B2
13	P08010	10	54.1	3.2e-7	25702.9	RAT	Glutathione S-transferase Mu 2
14	P04905	9	51.8	2.1e-6	25914.2	RAT	Glutathione S-transferase Mu 1
15	P30839	12	30.0	2.9e-7	54082.1	RAT	Fatty aldehyde dehydrogenase
16	P00173	8	56.7	2.8e-8	15355.3	RAT	Cytochrome b5
17	P10719	6	19.8	3.4e-8	56354.0	RAT	ATP synthase subunit beta, mitochondrial
18	Q9EQ76	6	14.3	1.1e-8	59960.9	RAT	Dimethylaniline monooxygenase [N-oxide-forming] 3
19	Q66HD0	7	13.4	4.7e-8	92771.7	RAT	Endoplasmin
20	P52759	5	60.6	7.0e-10	14303.6	RAT	2-iminobutanoate/2-iminopropanoate deaminase
21	P29147	6	23.3	4.2e-8	38202.2	RAT	D-beta-hydroxybutyrate dehydrogenase, mitochondrial
22	P55006	6	23.7	6.1e-11	35737.0	RAT	Retinol dehydrogenase 7
23	Q562C4	6	36.5	2.1e-6	27904.1	RAT	Methyltransferase-like protein 7B
24	P04797	6	27.9	2.3e-10	35828.3	RAT	Glyceraldehyde-3-phosphate dehydrogenase
25	P15999	7	20.1	2.5e-8	59754.1	RAT	ATP synthase subunit alpha, mitochondrial
26	P08011	4	23.9	6.6e-9	17471.7	RAT	Microsomal glutathione S-transferase 1
27	P60711	4	17.1	8.9e-8	41737.1	RAT	Actin, cytoplasmic 1
28	Q9Z0V5	6	34.8	3.7e-6	31007.7	RAT	Peroxiredoxin-4
29	P70580	3	19.5	7.0e-9	21598.2	RAT	Membrane-associated progesterone receptor component 1
30	P27364	5	16.6	4.3e-6	42206.6	RAT	3 beta-hydroxysteroid dehydrogenase type 5
31	P00502	4	22.5	2.0e-8	25607.3	RAT	Glutathione S-transferase alpha-1
32	Q6UPE0	4	12.5	3.6e-7	66389.1	RAT	Choline dehydrogenase, mitochondrial
33	P00388	4	10.0	5.3e-7	76963.5	RAT	NADPH--cytochrome P450 reductase
34	P02091	4	25.2	9.1e-7	15979.5	RAT	Hemoglobin subunit beta-1
35	P16232	5	15.6	7.8e-7	31883.6	RAT	Corticosteroid 11-beta-dehydrogenase isozyme 1
36	P05182	4	11.0	3.9e-6	56627.4	RAT	Cytochrome P450 2E1
37	P10867	3	9.3	2.8e-6	50615.8	RAT	L-gulonolactone oxidase

38	Q6UPE1	3	7.0	5.6e-8	68198.7	RAT	Electron transfer flavoprotein-ubiquinone oxidoreductase, mitochondrial
39	Q09073	3	16.8	4.5e-7	32901.6	RAT	ADP/ATP translocase 2
40	P27867	2	10.1	1.4e-7	38234.9	RAT	Sorbitol dehydrogenase
41	P11030	3	41.4	4.2e-7	10027.5	RAT	Acyl-CoA-binding protein
42	P55159	3	13.8	5.7e-6	39358.3	RAT	Serum paraoxonase/arylesterase 1
43	Q9ES38	4	9.3	1.6e-6	76266.3	RAT	Bile acyl-CoA synthetase
44	Q68FP2	2	7.9	2.1e-6	39458.5	RAT	Serum paraoxonase/lactonase 3
45	P01946	3	37.3	1.0e-6	15328.7	RAT	Hemoglobin subunit alpha-1/2
46	Q5PPL3	1	5.2	3.5e-8	40412.0	RAT	Sterol-4-alpha-carboxylate 3-dehydrogenase, decarboxylating
47	P20070	2	12.0	4.9e-7	34174.9	RAT	NADH-cytochrome b5 reductase 3
48	Q62730	1	4.5	5.5e-8	41967.5	RAT	Estradiol 17-beta-dehydrogenase 2
49	P13107	2	5.1	7.4e-7	56384.9	RAT	Cytochrome P450 2B3
50	P04642	2	8.7	3.8e-6	36450.8	RAT	L-lactate dehydrogenase A chain
51	P20816	2	5.0	4.6e-5	57969.5	RAT	Cytochrome P450 4A2
52	Q6AYS8	1	5.4	7.7e-8	32938.0	RAT	Estradiol 17-beta-dehydrogenase 11
53	P36365	3	8.1	3.8e-5	59825.9	RAT	Dimethylaniline monooxygenase [N-oxide-forming] 1
54	P24470	1	3.6	9.9e-7	56433.5	RAT	Cytochrome P450 2C23
55	P11240	2	21.9	6.2e-6	16129.7	RAT	Cytochrome c oxidase subunit 5A, mitochondrial
56	Q63276	1	4.0	1.9e-7	46465.1	RAT	Bile acid-CoA:amino acid N-acyltransferase
57	Q5XI60	1	6.2	1.5e-5	23313.3	RAT	Receptor expression-enhancing protein 6
58	P07632	1	8.4	4.1e-6	15911.8	RAT	Superoxide dismutase [Cu-Zn]
59	Q0ZHH6	1	3.3	1.9e-6	60586.5	RAT	Atlastin-3
60	Q02253	1	3.2	5.9e-6	57808.1	RAT	Methylmalonate-semialdehyde dehydrogenase [acylating], mitochondrial
61	P81828	1	13.9	3.2e-6	11068.0	RAT	Urinary protein 2
62	P05179	2	6.7	6.6e-5	56187.6	RAT	Cytochrome P450 2C7
63	P05183	1	2.6	8.5e-6	57732.2	RAT	Cytochrome P450 3A2
64	P51635	1	4.0	2.4e-6	36506.2	RAT	Alcohol dehydrogenase [NADP(+)]
65	P00884	1	4.1	2.3e-6	39618.5	RAT	Fructose-bisphosphate aldolase B
66	P02706	2	7.4	7.3e-5	32849.2	RAT	Asialoglycoprotein receptor 1
67	Q8K4C0	2	5.3	2.8e-5	60056.1	RAT	Dimethylaniline monooxygenase [N-oxide-forming] 5
68	Q5M9I5	1	20.2	7.5e-6	10423.7	RAT	Cytochrome b-c1 complex subunit 6, mitochondrial
69	P19225	2	4.1	2.6e-5	56157.2	RAT	Cytochrome P450 2C70
70	P97524	1	1.8	4.5e-5	70694.5	RAT	Very long-chain acyl-CoA synthetase
71	P50137	1	2.7	2.8e-5	67644.2	RAT	Transketolase
72	Q5I0E7	1	7.2	7.5e-5	27028.3	RAT	Transmembrane emp24 domain-containing protein 9
73	P81827	1	10.9	8.2e-5	10960.0	RAT	Urinary protein 1
74	Q9JJ46	1	6.1	1.7e-4	26737.8	RAT	3-beta-hydroxysteroid-Delta(8),Delta(7)-isomerase

Figure 2.7. Total Proteins Identified from TMT-Active DEAE Sepharose Fractions: Multiple proteins were identified from the semi-purified DEAE Sepharose fraction containing TMT-activity and are listed above. "Num Unique" notes how many unique peptides were identified in the tryptic digest that belong to that particular protein. "% Cov" shows how much of the total protein sequence was covered by the peptides used for identification. "Best Expect Val" gives a measure of the confidence of a false positive identification of that particular protein. Lower expect values indicate increased confidence. All of the expectation values listed are low and provide high confidence in the presence of those particular proteins in the tryptic digest sample.

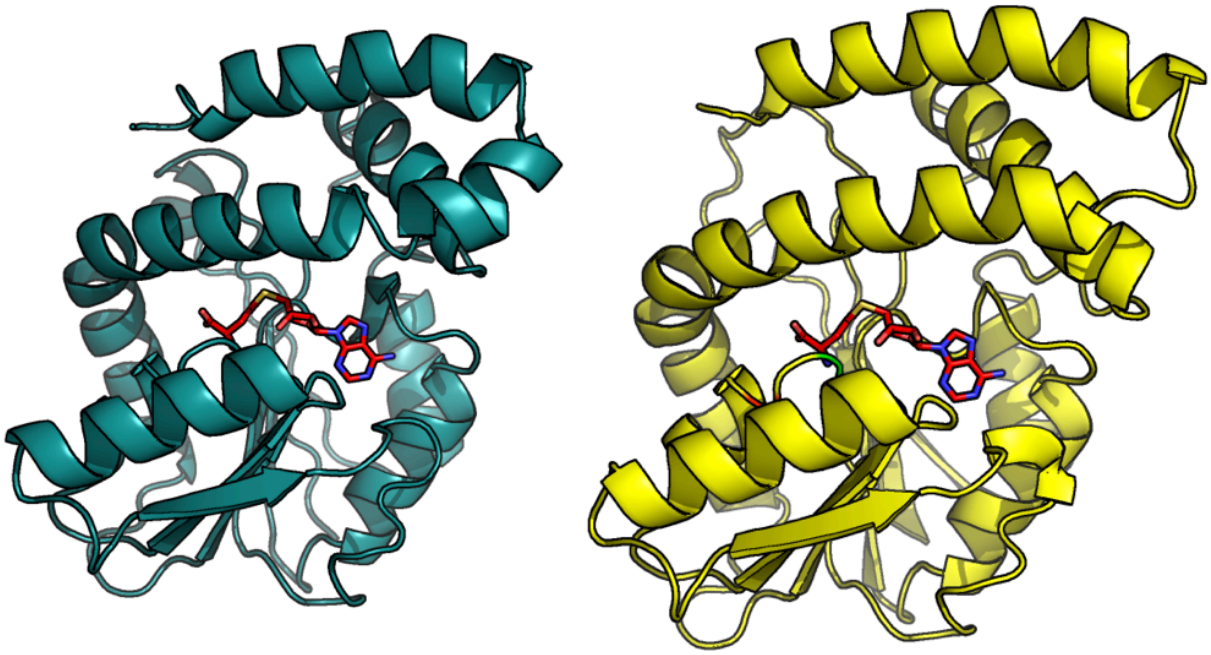

Figure 2.8. Homology models for human METTL7A and METTL7B with Docked SAH: Homology models were created by Dr. Abhi Nath. METTL7A is shown on the left in blue and METTL7B is shown on the right in yellow. Both models have docked SAH in the middle of the structure as a red ball and stick model.

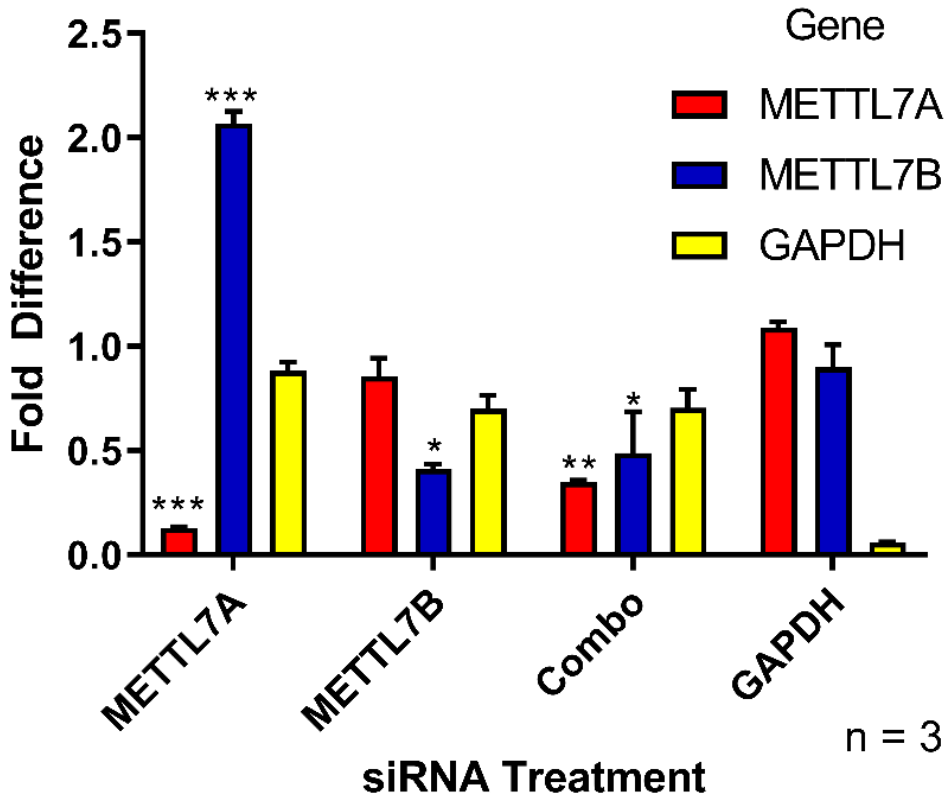

Figure 2.9. RT-PCR Analysis of *METTL7A* and *METTL7B* siRNA Gene Knockdown: *METTL7A* and *METTL7B* gene expression was significantly decreased compared to negative control cells when treated with their respective siRNA individually or in combination. Significant upregulation of *METTL7B* was observed upon treatment with *METTL7A* siRNA and the *GAPDH* positive control siRNA showed high levels of gene knockdown. Data are presented as the mean ± standard deviation. Significance was determined using unpaired two-tailed *t* test. ***$P<0.001$, **$P<0.01$, *$P<0.05$.

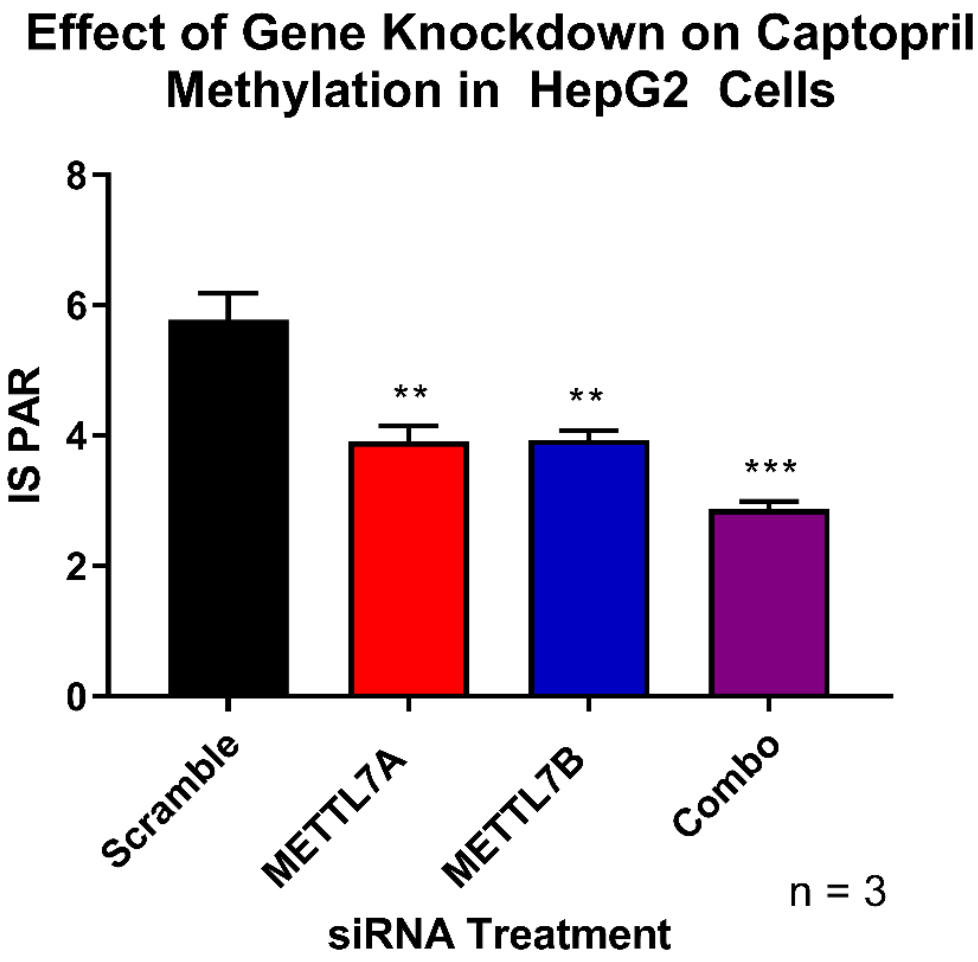

Figure 2.10. Captopril Methylation following *METTL7A* and *METTL7B* siRNA knockdown in HepG2 Cells: Cells with reduced *METTL7A* and/or *METTL7B* gene expression showed significantly decreased captopril methylation compared to negative control cells. Captopril methylation was reduced a greater extent upon co-treatment with both siRNA than either individually. All data are presented as the mean ± standard deviation. Significance was determined using unpaired two-tailed *t* test. ***$P<0.001$, **$P<0.01$.

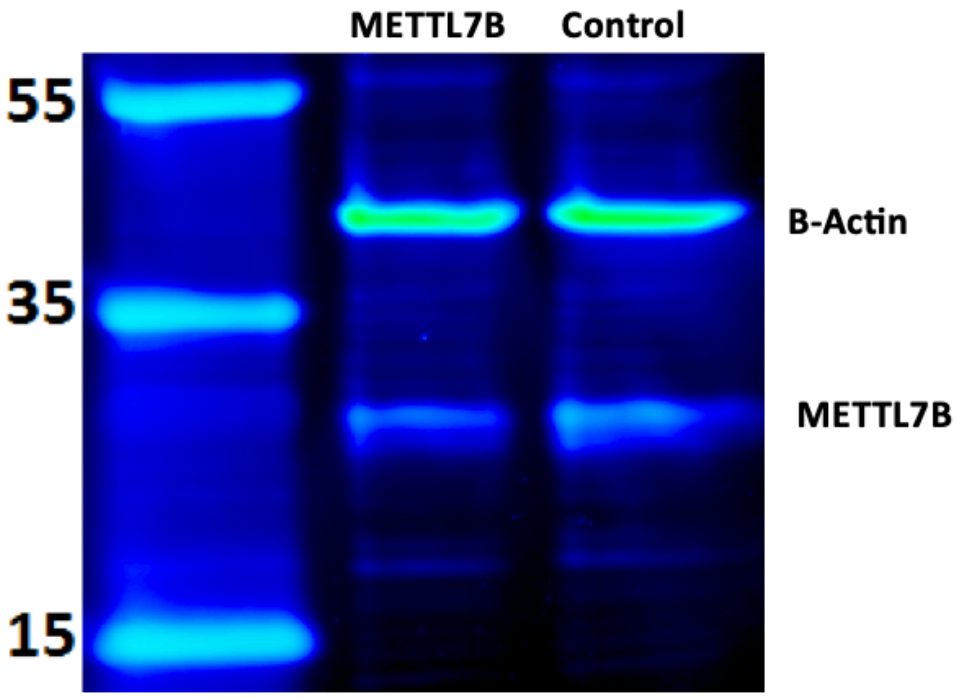

Figure 2.11. Western Blot Analysis of HepG2 Cell Knockdown Cell Lysate: Cell lysate from HepG2 cells treated with a *METTL7B* siRNA and a scrambled negative control siRNA. A METTL7B protein band is present in both lanes near the expected molecular weight of 28 kDa with slightly reduced intensity in the experimental sample lane. The ß-actin loading control band is visible in both samples.

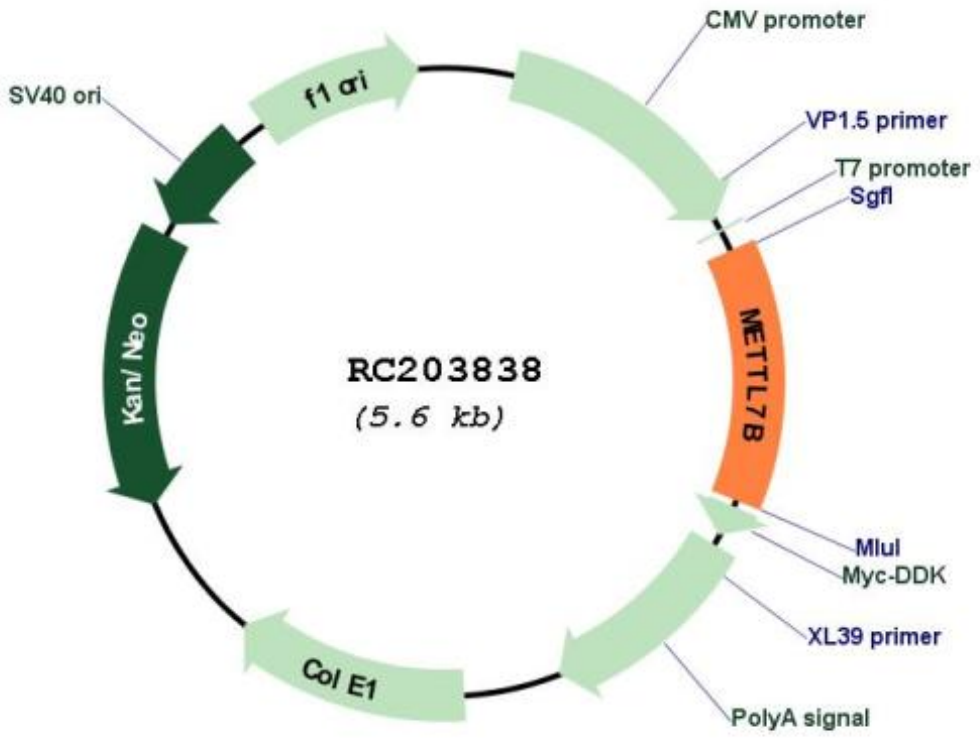

Figure 2.12. Map of the Constitutive Overexpression Plasmid: The overexpression plasmid encoding the *METTL7B* gene contains a constitutive cytomegalovirus (CMV) promoter. The expression plasmid also adds a *C*-terminal combination c-Myc/FLAG affinity tag.

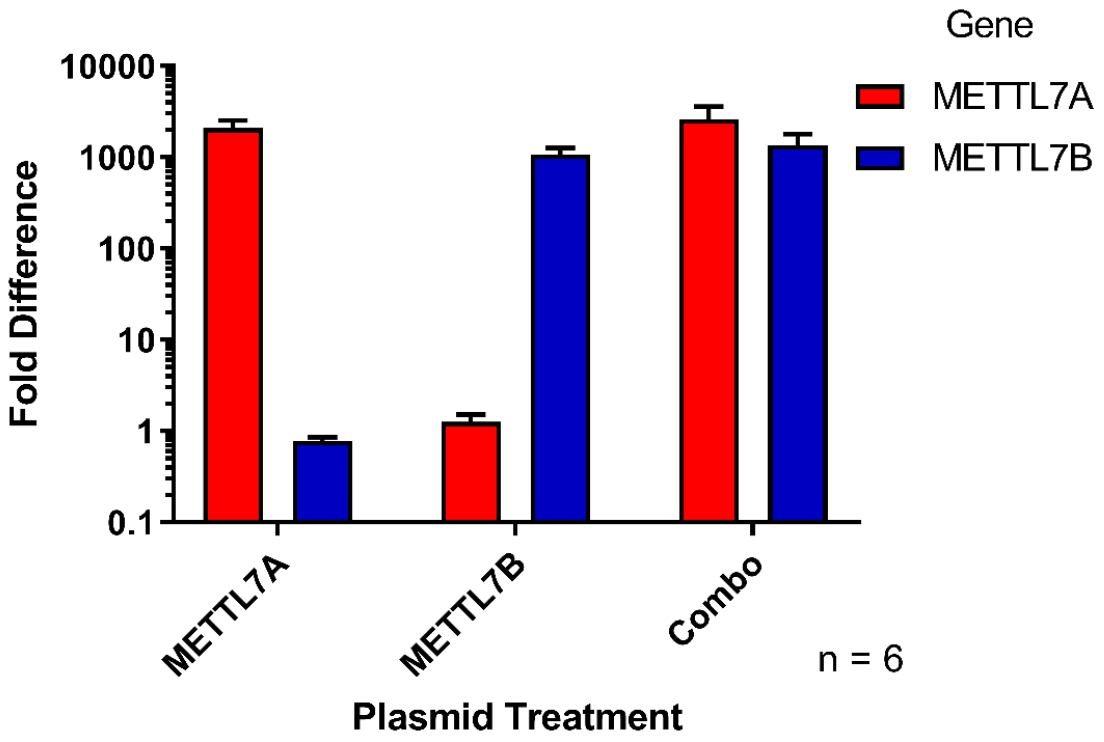

Figure 2.13. RT-PCR Analysis of *METTL7A* and *METTL7B* overexpression: Cells transfected with *METTL7A* or *METTL7B* overexpression plasmids for 48 hours showed a 10,000-fold increase in gene expression compared to negative control cells treated with an expression plasmid lacking a gene insert. Co-transfection with both plasmids resulted in the same level of gene expression increase as observed when dosed individually. All data are presented as the mean ± standard deviation.

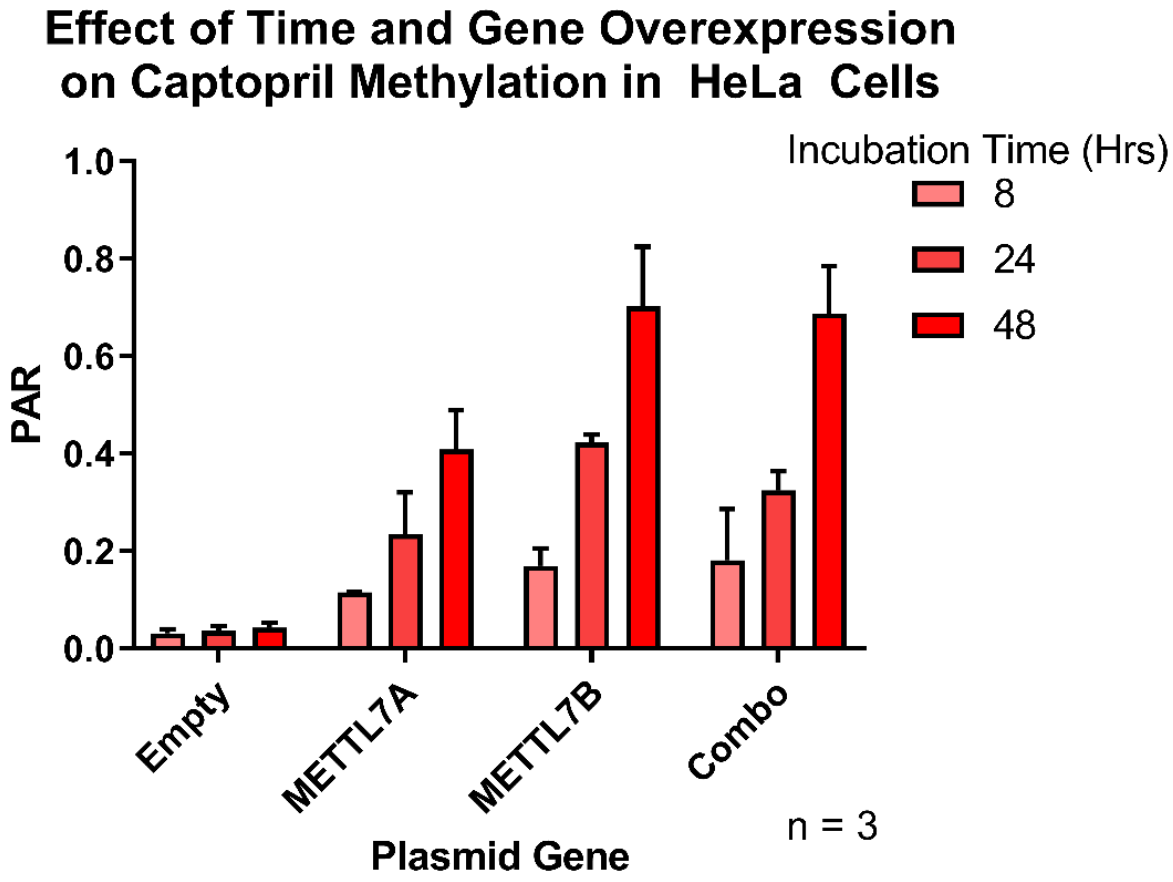

Figure 2.14. Captopril Methylation in Overexpressing HeLa Cells: Cells with increased *METTL7A* and/or *METTL7B* gene expression also exhibited increased captopril methylation over time compared to negative control cells. Captopril methylation was increased in cells co-treated with both overexpression plasmids. All data are presented as the mean ± standard deviation.

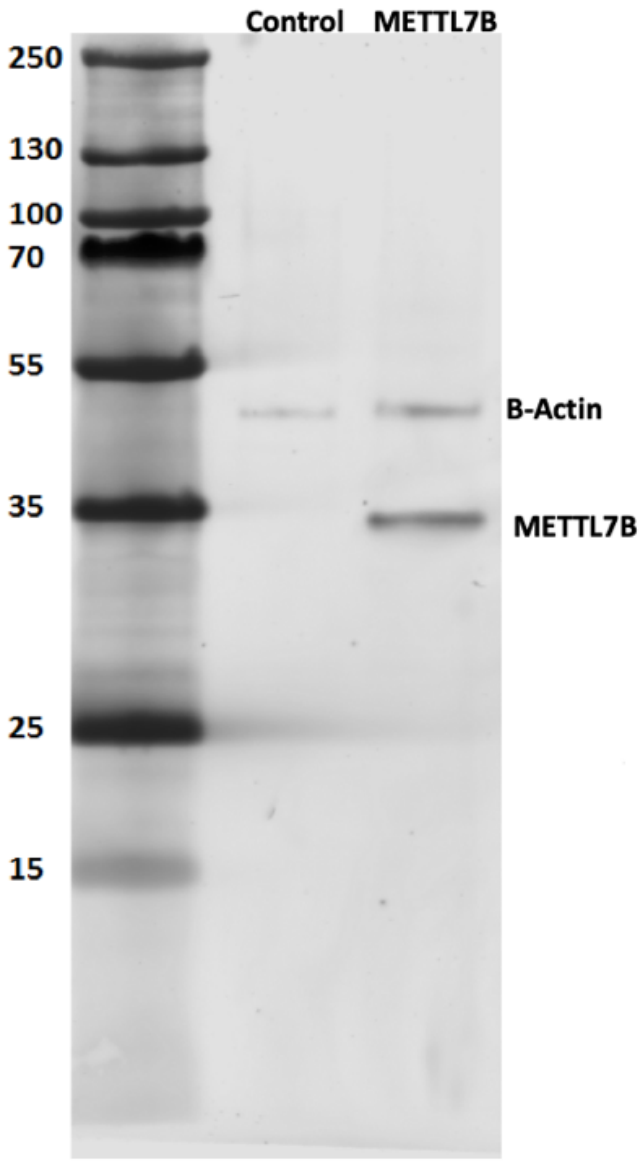

Figure 2.15. Western Blot Analysis of HeLa Cell Overexpression Cell Lysate: Cell lysate from HeLa cells treated with a *METTL7B* overexpression plasmid and a non-coding control plasmid. A FLAG-tagged METTL7B protein band is present near the expected molecular weight of 31 kDa in the overexpressed cell lysate and is absent in the control. The ß-actin loading control band is visible in both samples.

Bibliography:

1. Bremer, J. & Greenberg, D. M. Enzymic methylation of foreign sulfhydryl compounds. *Biochim. Biophys. Acta* **46**, 217–224 (1961).

2. Borchardt, R. & Cheng, C. Purification and Characterization of Rat Liver Microsomal Thiol Methyltransferase. *Biochim. Biophys. Acta* **522**, 340–353 (1978).

3. Weisiger, R. A. & Jakoby, W. B. Thiol S-methyltransferase from rat liver. *Arch. Biochem. Biophys.* **196**, 631–7 (1979).

4. Weinshilboum, R. Pharmacogenetics of methylation: relationship to drug metabolism. *Clin. Biochem.* **21**, 201–10 (1988).

5. Keith, R. A., Van Loon, J., Wussow, L. F. & Weinshilboum, R. M. Thiol methylation pharmacogenetics: heritability of human erythrocyte thiol methyltransferase activity. *Clin. Pharmacol. Ther.* **34**, 521–8 (1983).

6. Weinshilboum, R. M. & Sladek, S. L. Mercaptopurine pharmacogenetics: Monogenic inheritance of erythrocyte thiopurine methyltransferase activity. *Am. J. Hum. Genet.* **32**, 651–662 (1980).

7. Krynetski, E. Y. & Evans, W. E. Genetic Polymorphism of Thiopurine S-Methyltransferase: Molecular Mechanisms and Clinical Importance. *Pharmacology* **61**, 136–146 (2000).

8. Lennard, L., Van Loon, J. A. & Weinshilboum, R. M. Pharmacogenetics of acute azathioprine toxicity: Relationship to thiopurine methyltransferase genetic polymorphism.

Clin. Pharmacol. Ther. **46**, 149–154 (1989).

9. Chocair, P. R., Duley, J. A., Simmonds, H. A. & Cameron, J. S. The importance of thiopurine methyltransferase activity for the use of azathioprine in transplant recipients. *Transplantation* **53**, 1051–1055 (1992).

10. Black, A. J. *et al.* Thiopurine methyltransferase genotype predicts therapy-limiting severe toxicity from azathioprine. *Ann. Intern. Med.* **129**, 716–718 (1998).

11. Rosenbaum, J., Katz, W. A. & Schumacher, H. R. Hepatotoxicity associated with use of D-penicillamine in rheumatoid arthritis. *Ann. Rheum. Dis.* **39**, 152–154 (1980).

12. Keshmiri, H., Behal, A., Shroff, S. & Berkelhammer, C. Clopidogrel-Induced Severe Hepatitis: A Case Report and Literature Review. *Case Reports Hepatol.* 8068276 (2016). doi:10.1155/2016/8068276

13. Howell, P. *et al.* Clopidogrel-induced liver failure. *J. R. Soc. Med. Short Reports* **2**, (2011).

14. Shevchenko, A., Tomas, H., Havliš, J., Olsen, J. V. & Mann, M. In-gel digestion for mass spectrometric characterization of proteins and proteomes. *Nat. Protoc.* **1**, 2856–60 (2006).

15. Livak, K. J. & Schmittgen, T. D. Analysis of Relative Gene Expression Data Using Real-Time Quantitative PCR and the 2−ΔΔCT Method. *Methods* **25**, 402–408 (2001).

16. Petrossian, T. & Clarke, S. Bioinformatic Identification of Novel Methyltransferases. *Epigenomics* **1**, 163–175 (2009).

17. Price, R. A. *et al.* Major gene polymorphism for human erythrocyte (RBC) thiol

methyltransferase (TMT). *Genet. Epidemiol.* **6**, 651–662 (1989).

18. Lundby, A. *et al.* Quantitative maps of protein phosphorylation sites across 14 different rat organs and tissues. *Nat. Commun.* **3**, 876 (2012).

Chapter 3: Expression, Purification, and Characterization of Recombinant METTL7B

Introduction:

In this chapter we took on the task to recombinantly express and purify METTL7B, to optimize reaction conditions, and define the substrate specificity and steady state kinetic properties of the enzyme. Proteins can be recombinantly expressed in many different host species, each possessing their own strengths and weaknesses. In general, recombinant protein expression in mammalian cells helps maximize proper folding and allows for accurate post-translational modifications such as glycosylation patterns[1–3]. Unfortunately, the total amount of expressed protein can be very low, especially for membrane-bound proteins. To overcome this obstacle, many researchers instead express recombinant protein in *E. coli* which replicate exponentially and can generate much higher overall yields of recombinant protein[4,5]. It is important to note that bacteria lack the same folding and post-translational modification machinery as mammalian cells[6,7]. Therefore, expression of recombinant protein is often a balance between quality and quantity.

Once an appropriate expression system has been identified, recombinant protein can be expressed with a number of different modifications to aid downstream purification processes. Most commonly, an affinity tag is added to the expressed protein that can be used to isolate the protein of interest from heterogenous cell lysates by binding a specific ligand immobilized to agarose resin[8]. Additionally, many affinity tags are available for recombinant protein expression that can alter the major biophysical characteristics of the tagged protein of interest[9]. For example, glutathione *S*-transferase (GST) affinity tags can prevent membrane insertion, thus increasing the amount of soluble protein expressed in the cytosol[10,11]. This tagging approach is very useful for the expression and purification of membrane proteins, especially if removal of the

hydrophobic sequences impacts protein function. The specific choice of affinity tag is usually determined empirically and is impacted by both the expression system and downstream applications of the recombinant protein.

The ability to remove an affinity tag after purification is a desirable quality for all expressed recombinant protein. This is achieved by placing a protease recognition sequence between the tag and the protein of interest, which allows for site-specific cleavage[12]. This is most useful when the presence of the affinity tag significantly impacts the function of the protein of interest[13]. However, tag removal can lead to other problems such as aggregation and precipitation of the protein of interest, particularly with hydrophobic membrane proteins[14]. Overall, when expressing and purifying recombinant proteins, specifically those that are membrane bound, it is important to consider the expression host and affinity tag design. Ultimately the goal is to use an appropriate affinity tag and expression system that will produce active, soluble fusion protein that can be purified with ease.

Expression and purification of recombinant METTL7A and METTL7B proteins proved to be difficult and required significant optimization, multiple rounds of various fusion protein design, and sampling of different expression systems. Appendix II expands on the various systems we evaluated prior to designing the current successful protein construct. In this chapter, we report our final, and most successful, purification of active recombinant METTL7B fusion protein. We purified the recombinant protein to near homogeneity using a dual-stage affinity chromatography approach and validated the purification of the target using western blot and proteomic analysis. We successfully cleaved the fusion protein affinity tag but were unable to separate it from the remaining free METTL7B protein in solution. Subsequently, we used the recombinant fusion protein to define METTL7B's biochemical characteristics including

optimum pH and lipid environment for enzymatic activity, methylation kinetics, and substrate specificity.

Materials and Methods:

Materials:

HisPur Ni-NTA resin, *E. coli* growth reagents, and Pierce HRV3C protease were purchased from ThermoFisher (Waltham, MA). GSTrapFF column were purchased from Cytiva, formerly GE Healthcare Life Sciences (Marlborough, MA). Buffer salts and ion exchange resins were acquired from Sigma-Aldrich (St. Louis, MO) as well as methyltransferase probe substrates unless otherwise stated. *S*-adenosyl-*L*-methionine was obtained from New England Biolabs (Ipswich, MA). 7α-Thiospironolactone was purchased from Santa Cruz Biotechnology (Dallas, TX). LOBSTR-BL21(DE3) competent *E. coli* cells were bought from Kerafast (Boston, MA). Competent Stellar *E. coli* cells were purchased from Takara (Mountain View, CA). CHAPS detergent, glutathione, and UPLC-grade solvents were obtained from Fisher Scientific (Hampton, NH). Sequencing grade porcine trypsin and MTase-Glo Methyltransferase Assays were purchased from Promega (Madison, WI). 1,2-Dimyristoyl-*sn*-glycero-3-PG (DMPG) and mertansine were obtained from Cayman Chemical (Ann Arbor, MI). The prasugrel active metabolite was a gift from Dr. Allan Rettie.

Design and Development of the Expression Plasmid:

The general molecular biology techniques used to create the various pET21 expression plasmids are detailed in Appendix I.

pET21 METTL7B Expression and Purification:

Recombinant METTL7B was produced in *E. coli* using a unique expression plasmid created in our lab. The expression plasmid backbone was obtained from pET21-10XHis-GST-HRV-dL5 which was a gift from Marcel Bruchez (Addgene plasmid # 73214; http://n2t.net/addgene:73214; RRID:Addgene_73214). The human *METTL7B* gene sequence was inserted into the plasmid using BamHI and EcoRI restriction sites and general molecular biology techniques. All plasmid inserts were sequenced by Eurofins Genomics and sequencing histograms were analyzed using FinchTV software.

Expression plasmids were propagated using heat-shocked Stellar cells. Individual colonies were used to create glycerol stocks and purify expression plasmids that were then sequenced for mutations. Plasmids with the correct sequence were used to transform competent LOBSTR-BL21(DE3) *E. coli* via heat shock. Unless otherwise noted, all *E. coli* growth occurred on an orbital shaker at 250 rpm, 37 ºC, and under the selection pressure of 100 µg/mL ampicillin.

To express recombinant protein, LOBSTR-BL21(DE3) overnight cultures were added to ampicillin-containing TB expression media at a ratio of 1:100. Briefly, cells were grown for 3 hours at 37 ºC. Then, METTL7B production was induced via addition of isopropyl ß-D-1-thiogalactopyranoside (IPTG) to a final concentration of 1 mM. The temperature was reduced to 15 ºC and the cells were grown for an additional 24 hours. Cells were harvested via gentle centrifugation and the pellets stored at -80 ºC until future processing.

Frozen cell pellets were thawed on ice in a 4 ºC cold cabinet overnight prior to lysis. Lysis was performed by resuspending the cell pellet in cell lysis buffer (50 mM KPi pH 7.0, 20% glycerol, 150 mM NaCl, 10 mM CHAPS, EDTA-free Halt Protease Inhibitor Cocktail)

supplemented with 100 µg/mL lysozyme (Sigma Aldrich). The cell solution was rotated end-over-end at 4 °C until the solution had become extremely viscous. The cell lysate was then treated with 100 µg/mL DNA Nuclease I (Sigma Aldrich) and rotated at 4 °C or until no longer viscous. The lysate was then centrifuged at 48,000 g for 30 minutes at 4 °C and the resulting supernatant was retained for subsequent purification steps.

Purification was conducted using the ÄKTA start chromatography system (GE Healthcare). Cell lysate supernatant was applied to a pre-packed and conditioned HisPur Ni-NTA column (ThermoFisher) overnight at a low flow rate (0.5 mL/min). The column was subsequently washed with Ni-NTA purification buffer (50 mM KPi pH 7.0, 20% glycerol, 10 mM CHAPS, 300 mM NaCl) containing 50 mM imidazole until A_{280} readings stabilized. Protein was eluted from the column with Ni-NTA purification buffer containing 300 mM imidazole until A_{280} readings stabilized.

The HisPur Ni-NTA column eluent was directly applied to a pre-conditioned GSTrapFF column at a flow rate of 1 mL/min for 4 hours. The column was then washed with GSTrapFF purification buffer (50 mM KPi pH 7.0, 20% glycerol, 10 mM CHAPS, 150 mM NaCl) until A_{280} had decreased to baseline. Recombinant protein was eluted from the column using GSTrapFF purification buffer containing 10 mM reduced glutathione and adjusted to pH 8.0. Pooled eluent was concentrated to appropriate working concentrations using Amicon Centriprep 10K molecular weight cutoff centrifugal filter units. Final protein concentration was determined by A_{280} measurement and stocks were aliquoted and stored at -80 °C until future use.

Protein Purity Analysis:

All SDS-PAGE analyses were conducted using NuPAGE 4-12% Bis-Tris gels in the XCell SureLock Mini-Cell Electrophoresis system using PageRuler Plus Prestained Protein Ladder as a molecular weight marker. Samples were prepared using NuPAGE LDS Sample Buffer and 1.4 M ß-mercaptoethanol before boiling for 5 minutes. Gels were run at room temperature, at a constant 200 volts, and developed using previously published silver staining protocols[15].

All western blot analyses were conducted using the XCell SureLock Mini-Cell electrophoresis system, PageRuler Plus Prestained Protein Ladder, and NuPAGE 10-20% Tricine gels. Samples were prepared using 4X Protein Loading Buffer (LiCor) and 0.7 M ß-mercaptoethanol prior to boiling for 5 minutes. After initial SDS-PAGE separation, the gel was removed from the cassette and placed with PVDF blotting membrane into the XCell II Blot Module according to the manufacturer protocol. Blot transfer was conducted over 1 hour at a constant 30 volts on ice. The blot was blocked using Odyssey Blocking Buffer (LiCor) for 1 hour at room temperature. A primary antibody incubation was conducted overnight using the suggested dilution factor for the rabbit anti-METTL7B (Sigma Aldrich) or anti-GST (Cell Signaling) antibodies. The secondary antibody incubation was conducted for 1 hour at room temperature using IRDye 680RD goat anti-rabbit antibody (LiCor). Western blots were imaged using an Odyssey gel scanner. Blot images were visualized using Image Studio Version 4.0 software.

Tryptic Digest:

In-gel tryptic digests of silver stained SDS-PAGE gels were conducted following the method published by Shevchenko[15,16]. Briefly, the protein band was excised from the gel and

dehydrated with neat acetonitrile. Protein bands were then treated with 10 mM dithiothreitol (DTT) solution and incubated at 56 ºC to reduce all proteins. The reduced bands were treated with 55 mM iodoacetamide at room temperature in the dark to alkylate all exposed cysteines. Finally, the bands were incubated overnight at 37 ºC with 13 ng/µL trypsin-containing solution. Digested peptides were extracted from gel bands the following day and concentrated in a centrifugal evaporator. The protocol for in-solution tryptic digest is similar to one used for in-gel digestion. The main difference is that samples do not require acetonitrile dehydration, therefore dithiothreitol and iodoacetamide are sequentially added to the same sample tube containing up to 10.5 µg total protein.

The LC-MS system used for proteomic analysis was a Finnigan LTQ Orbitrap coupled to a Waters Acquity LC. Peptides were separated using a 1x150 mm Acquity UPLC CSH C18 column and 0.1% formic acid in water and 0.1% formic acid in acetonitrile as solvents A and B. Peptide separation was achieved using the following gradient: solvent B was held at 5% for the first two minutes, increased to 40% over the next 90 min, then increased to 90% over the next five minutes and held for an additional 8 minutes, then re-equilibrated over five minutes. The flow rate was held at 0.06 mL/min and flow as diverted to the mass spectrometer from 2 to 95 minutes.

Peptides were analyzed using a data dependent scan method in positive mode. The initial high-resolution scan from 300-2,000 m/z was conducted in the FTMS with 60,000 resolution. Four data dependent scans were completed in the ion trap to obtain fragmentation. Dynamic exclusion was enabled which excluded the top 25 most intense ions after they had been selected twice over a four second window. The following mass spectrometer settings were used:

sheath gas flow rate was 12 arb, spray voltage was 3.5 kV, capillary temperature was 350 ^{o}C, capillary voltage was 22 V, and tube lens voltage was 100 V.

Proteolytic Cleavage of pET21 METTL7B:

Purified pET21 METTL7B was diluted with Nanopure water and HRV3C buffer (ThermoFisher, Waltham, MA) prior to adding HRV3C protease. The concentration of pET21 METTL7B present in the final purified protein fraction was determined using A_{280} values obtained by Nanodrop and a predicted extinction coefficient of 89,560 M^{-1} cm^{-1} obtained from ExPASy ProtParam. The final ratio achieved was 2 units of HRV3C to 15 µg pET21 METTL7B.

To optimize digestion times, aliquots were taken at 0, 1, 2, 3, 4, 6, 8, and 12 hours and immediately boiled in SDS-PAGE sample buffer. Samples were kept at room temperature overnight followed by western blot analysis using an anti-METTL7B primary antibody.

Future HRV3C cleavage experiments were incubated for 4 hours prior to affinity purification clean-up by overnight loading onto cleaned GSTrapFF or HisPur Ni-NTA columns. After loading, the columns were washed at a low flow rate with each column's respective purification buffer until A_{280} values had stabilized. The flow-through and wash fractions were retained for potential cleaved METTL7B protein. Cleaved affinity tag protein was eluted using either 10 mM glutathione or 300 mM imidazole depending on the column chemistry. All samples were analyzed by western blot, using either an anti-GST or anti-METTL7B primary antibody.

Substrate Screening Using the MTase-Glo Kit and High-Resolution Mass Spectrometry:

Substrate screening was primarily conducted using the MTase-Glo Assay (Promega, Madison, WI). Briefly, recombinant METTL7B was prepared similar to captopril methylation assays. SAM was added to the METTL7B protein stock for a final concentration of 50 µM and aliquoted into a 384-well plate. Substrate was added to each well and the plate was covered with Parafilm before incubation at 37 ^{o}C for 1 hour. The incubation was quenched by a 1:5 addition of 0.5% trifluoro acetic acid. The samples were processed according to the manufacturer's protocol and luminescence was recorded for each well using a Synergy HTX Multi-Mode Reader (BioTek).

Additional substrate screening was conducted using high-resolution mass spectrometry. Briefly, pET21 METTL7B was incubated for an hour at 37 ^{o}C with 750 µM SAM and the test compounds at a concentration at least three times higher than reported K_m values. Boiled and buffer-only controls were conducted to account for non-enzymatic turnover of more reactive compounds. The reaction was quenched via a 2:1 addition of ice cold 50:50 acetonitrile:methanol. The samples were incubated on ice to further enable precipitation and then centrifuged for 15 minutes at 4,000 x g. The supernatant was analyzed by LC-MS.

The LC-MS system used for substrate screening was an AB Sciex 5600 mass spectrometer paired with a Waters Acquity LC. Compound separation was achieved using a 2.1x150 mm Acquity UPLC BEH Shield RP column and 0.1% formic acid in water and 0.1% formic acid in 50:50 acetonitrile:methanol as solvents A and B respectively. Column temperature was maintained at 50 ^{o}C at all times. Chromatographic separation was achieved using the following gradient: solvent B was held at 0% from 0 to 1.5 minutes, ramped to 100% from 1.5 to 6 minutes, held at 100% from 6 to 7 minutes followed by re-equilibration to the

starting conditions for another 3 minutes. Flow rate was held constant at 0.3 mL/min and flow was only diverted to the mass spectrometer between 1.5 to 9.5 minutes.

Compounds were analyzed in positive mode using a unique information dependent acquisition (IDA) experiment. An initial survey scan from 50-2000 m/z was conducted with an accumulation time of 100 msec. Ions of interest were selected using a mass defect filter of ±30 mDa and mass filter of ±37.5 Da in relation to the parent compound. Fragmentation was induced using rolling collision energy and daughter ions were collected. Repeat analysis was excluded for 1 second to increase sensitivity to low abundance ions. Metabolites were identified using MetabolitePilot (AB Sciex). Incubations without enzyme were used as control samples and neat standards of parent compounds were used to collect reference spectra. Potential metabolites were identified using the programmed Phase II set of biotransformations. Ions were only flagged as metabolites if they were present at twice the intensity in experimental samples compared to controls. All potential methylated metabolites were then confirmed using PeakView software from raw data.

In vitro Captopril Methylation Using Recombinant pET21 METTL7B:

Captopril methylation was conducted using purified pET21 METTL7B fusion protein. The optimized activity assay buffer (50 mM KPi pH 7.0, 10 mM CHAPS, 20% glycerol, 150 mM NaCl, and 9 mg/mL DMPG) was placed in a sonication water bath until the solution was clear to help form DMPG liposomes. Recombinant enzyme was added at a ratio of 85:1 DMPG:pET21 METTL7B and allowed to incubate on ice for 30 minutes. Following the addition of captopril, the enzyme was pre-equilibrated at 37 ^{o}C for 2 minutes prior to initiation by addition of SAM to a reaction volume of 150 µL. The final concentration of captopril was

increased to collect the kinetic information and the final concentration of SAM was held at 750 μM. The reaction was incubated for 25 minutes then quenched via addition of 15% (w/v) zinc sulfate in a 1:5 dilution to total reaction volume. The quenched solution was incubated on ice for 10 minutes followed by a 1:6 addition of a saturated barium hydroxide solution containing the d_3-S-methyl captopril internal standard. Following a second 10-minute incubation on ice, the solution was centrifuged at 5,000 x g for 15 minutes to pellet all precipitated proteins and salts.

After centrifugation, 75 μL of supernatant was transferred to an opaque polypropylene strip-well tube containing 5 μL of 2 M sodium hydroxide. Unreacted captopril was derivatized at room temperature for 1 hour in the dark via addition of 20 μL of 2.5 M maleimide to reduce ion suppression from non-methylated captopril. Derivatized samples were centrifuged and the supernatant was analyzed by LC-MS/MS.

Analytical Measurement of Captopril Methylation:

A Waters Xevo TQS mass spectrometer paired with a Waters Acquity LC was used to measure the methylated metabolite of captopril. Chromatographic separation was achieved using a 2.1x100 mm Ascentis Express RP Amide column and 0.1% formic acid in water and 0.1% formic acid in methanol as solvents A and B respectively. Column temperature was maintained at 50 ^{o}C at all times. The following gradient was employed: solvent B was held at 30% from 0 to 3 min, then held at 90% from 3 to 7 min, followed by re-equilibration to the starting conditions for another 3 min for a total run time of 10 min. Flow rate was held constant at 0.2 mL/min and flow was only diverted to the mass spectrometer between 2 to 7.5 min.

S-methyl captopril and the internal standard, d_3-*S*-methyl captopril, were monitored in positive ionization mode. The monitored mass transitions m/z+ were 232.1 > 89 and 232.1 >

116 (S-methyl captopril) as well as 235.1 > 91.9 and 235.1 > 115.9 (internal standard). The MS conditions were as follows: collision energy 15 V, cone voltage 30 V, capillary voltage 3.2 kV, desolvation temperature 450 ^{o}C, desolvation gas flow 1,000 L/hr and cone gas 150 L/hr.

Hydrogen Sulfide Methylation:

Protein concentration and incubation with DMPG liposomes was similar to the protocol described above. All steps were conducted in a glove box under atmospheric nitrogen unless otherwise indicated. Recombinant enzyme was aliquoted into a polypropylene deep-well plate on ice along with SAM and NaSH for a final volume of 150 µL and 0.09 mg/mL and 83.3 µM for protein and SAM concentrations respectively. The plate was capped with a silicon mat and placed in a 37 ^{o}C water bath for 45 min under normal atmosphere. After incubation, the plate was placed on ice under nitrogen and quenched via a 1:15 addition of 0.3 M sodium hydroxide. Quenched reaction solution (110 µL) was added to 50 µL of 20 mM monobromobimane (MBB), following published H_2S derivatization methods[17–19]. Once capped under nitrogen, the reaction plate was incubated at room temperature on an orbital shaker at 450 rpm for 30 min.

The MBB derivatization was quenched by addition of 50 µL of 200 mM 5-sulfosalicylic acid and 10 µL of the ethyl 2-aminothiazole carboxylate (EATC) internal standard. Protein was precipitated by addition of 15% (w/v) zinc sulfate and barium hydroxide as detailed above. Samples were centrifuged at 4,000 x g for 15 min and the supernatant was analyzed by LC-MS/MS.

Analytical Measurement of Methanethiol:

The LC-MS/MS system used for hydrogen sulfide methylation analysis was a Waters Xevo TQS mass spectrometer paired with a Waters Acquity LC. Compound separation was achieved using a 2.1x150 mm Acquity UPLC BEH Shield RP column and 0.2% acetic acid in water and 0.2% acetic acid in acetonitrile as solvents A and B respectively. Column temperature was maintained at 25 ^{o}C at all times. Chromatographic separation was obtained using the following gradient: solvent B was held at 40% from 0 to 1 minutes, ramped to 90% from 1 to 3.5 minutes, held at 90% from 4.5 to 5 minutes followed by re-equilibration to the starting conditions for another minute. Flow rate was held constant at 0.3 mL/min and flow was only diverted to the mass spectrometer from 1 to 4.5 minutes.

Derivatized methanethiol and the internal standard, EATC, were monitored in positive ionization mode. The monitored mass transitions m/z+ were 239.22 > 175.24 and 239.22 > 192.2 (derivatized methanethiol) as well as 173.17 > 72.11 and 173.17 > 127.06 (internal standard). The MS conditions were as follows: collision energy 24, 10, 24, 16 V for each transition respectively, cone voltage 56 V, capillary voltage 2.9 kV, desolvation temperature 450 ^{o}C, desolvation gas flow 1,000 L/hr and cone gas 150 L/hr.

Data Analysis:

All experiments were conducted with biological triplicates, and repeated at least two times on two separate days. All data are reported as the mean ± standard deviation, however individual data points from multiple experiments are presented when possible. Statistical significance was determined by a two-tailed unpaired *t* test with a threshold *P* value of 0.05. Kinetic parameter K_m values were obtained through non-linear regression analysis using GraphPad Prism, version 8.3.1 for Windows (GraphPad Software, La Jolla, CA).

Results:

Expression of pET21 METTL7B:

The *METTL7B* gene sequence (NCBI CCDS8887.2) was inserted into a pET21 *E. coli* expression vector, downstream of a 10xHis-GST combination affinity tag (Figure 3.1). The plasmid sequence incorporated a HRV3C protease site for affinity tag cleavage. Additionally, a rigid peptide linker was inserted between the protease recognition site and the *N*-terminus of the *METTL7B* gene sequence. The linker encoded five sequential alanine-proline repeats and was designed to maintain separation between the hydrophobic METTL7B *N*-terminus and the HRV3C cleavage site.

Three additional *N*-terminal truncations were created, removing either the first three, six, or nine amino acids of the METTL7B protein sequence. In frame plasmid insert sequences were confirmed by DNA sequencing and verified plasmids were expressed in *E. coli*. The most conservative three-residue truncation construct was not fully verified due to incomplete DNA sequencing reads, therefore the protein was not expressed and tested for activity. Induced *E. coli* lysates containing full-length METTL7B exhibited high specific activity however little to no activity was observed in lysates containing the six- or nine-residue truncated forms of METTL7B (Figure 3.2). Future purification efforts focused entirely on the full-length METTL7B construct, henceforth referred to as pET21 METTL7B.

Purification of pET21 METTL7B:

Recombinant pET21 METTL7B was solubilized from BL21(DE3) *E. coli* lysates via incubation with lysis buffer (50 mM KPi pH 7.0, 20% glycerol, 150 mM NaCl, 10 mM CHAPS,

EDTA-free Halt Protease Inhibitor Cocktail) followed by centrifugation. The supernatant was applied to HisPur Ni-NTA nickel affinity resin overnight. The loaded affinity resin was washed with Ni-NTA purification buffer (50 mM KPi pH 7.0, 20% (v/v) glycerol, 10 mM CHAPS, 300 mM NaCl) containing increasing imidazole concentrations. Finally, the resin was cleaned with 6 M guanidine hydrochloride. Aliquots of all purification steps were analyzed for purity and the presence of METTL7B was confirmed via SDS-PAGE silver stain and western blot respectively (Figures 3.3 and 3.4). The majority of pET21 METTL7B eluted from the HisPur Ni-NTA resin at 300 mM imidazole and very little eluted at 50 mM imidazole. The pET21 METTL7B band was visible by SDS-PAGE silver stain in the 300 mM imidazole eluent however numerous proteins co-eluted from the column despite extensive intermediate washing.

HisPur Ni-NTA purification of pET21 METTL7B was repeated using protein expressed in LOw Background STRain (LOBSTR) *E. coli* cells and compared to prior purifications conducted using protein expressed in BL21(DE3) *E. coli*. Less protein contamination was observed in purification eluents when LOBSTR cells were used. Specifically, the expression of two major protein contaminants, at 25 and 75 kDa, was reduced in LOBSTR cell purifications compared to BL21(DE3) cell purifications. The specific proteins are marked by red stars in the SDS-PAGE silver stain (Figure 3.5). LOBSTR *E. coli* were used for all subsequent expression and purification of pET21 METTL7B.

HisPur Ni-NTA column eluent was directly applied to an immobilized glutathione GSTrapFF affinity column, washed with GSTrapFF buffer (50 mM KPi pH 7.0, 20% (v/v) glycerol, 10 mM CHAPS, 150 mM NaCl), and eluted using GSTrapFF buffer adjusted to pH 8.0 and containing 10 mM reduced glutathione. The secondary GSTrapFF cleanup step removed many contaminating proteins present in the HisPur Ni-NTA eluent, leaving only the pET21

METTL7B protein and minor protein contaminants in the GSTrapFF eluent (Figure 3.6). A small amount of pET21 METTL7B was observed in the 6 M guanidine hydrochloride resin wash but the majority of the recombinant protein was eluted successfully.

The presence of pET21 METTL7B at ~55 kDa was confirmed by western blot using an anti-GST and anti-METTL7B primary antibody (Figure 3.7). The lower molecular weight contaminating bands around 35 kDa were identified as GST-tagged proteins because they were visible on the anti-GST western blot but not the anti-METTL7B western blot (Figure 3.7)

The presence of METTL7B was orthogonally confirmed using in-solution and in-gel tryptic digestion followed by proteomic analysis. Ten peptides unique to METTL7B were identified by in-solution digest of the GSTrapFF eluent fraction (Figure 3.8). Additionally, samples were analyzed against the *E. coli* proteome to identify potential contaminants (Figure 3.9). The most abundant bacterial protein identified was the chaperone protein DnaK which is roughly 70 kDa in size. The chaperone protein DnaJ and low molecular weight ribosomal subunits were also observed albeit at lower abundance.

In-gel tryptic digest was conducted on the ~55 kDa band observed in SDS-PAGE silver stain analysis of the final eluent fraction (Figure 3.7). Six peptides unique to METTL7B were identified (Figure 3.10). In general, parent mass m/z ratios were measured with less than 2 ppm error.

Cleavage of the pET21 METTL7B Affinity Tag:

Purified pET21 METTL7B eluent was treated with commercial HRV3C protease in a 1:15 protease:protein ratio. Aliquots were removed at several time points to assess cleavage

efficiency by SDS-PAGE silver stain (Figure 3.11) and anti-METTL7B western blot (Figure 3.12). Only the ~55 kDa pET21 METTL7B fusion protein band intensity decreased over time when analyzed by SDS-PAGE. Western blot analysis confirmed a decrease in the ~55 kDa pET21 METTL7B fusion protein band intensity over time. In parallel, a 30 kDa band appeared in HRV3C-treated samples and increased in intensity over time. A four-hour protease cleavage incubation time was chosen for future experiments.

Captopril methylation was used to measure and compare the activity of cleaved pET21 METTL7B, non-cleaved protein incubated at 4 ^{o}C for four hours, or non-cleaved protein stored at -80 ^{o}C (Figure 3.13). Methylation activity was slightly reduced in protein samples stored at 4 ^{o}C for four hours compared to protein stored at -80 ^{o}C. Enzyme activity was further reduced upon cleavage of the GST tag compared to non-cleaved fusion protein under identical storage conditions. The combined fusion tag removal and four-hour incubation at 4 ^{o}C resulted in a 65% reduction in captopril methylation compared to non-cleaved fusion protein stored frozen.

Separation of the cleaved GST tag from the free METTL7B was initially attempted using HisPur Ni-NTA affinity chromatography. Cleaved pET21 METTL7B was incubated overnight with a clean HisPur Ni-NTA column to bind all non-cleaved fusion protein and free GST affinity tag. The column was washed with three column volumes of Ni-NTA purification buffers containing either 10 mM reduced glutathione, 10 mM captopril, 250 μM SAM, 0.5% (w/v) Triton X-100, 50 mM imidazole, or 300 mM imidazole. Each wash fraction was collected and aliquots were analyzed for free GST tag and free METTL7B by anti-GST and anti-METTL7B western blots respectively (Figures 3.14 and 3.15). Both western blots displayed efficient cleavage by HRV3C protease and little protein present in the flow-through and initial wash

fractions. Full-length fusion protein and the free GST and METTL7B proteins both only eluted from the HisPur column after washing with 300 mM imidazole.

An alternative separation approach was also tested using GSTrapFF resin affinity chromatography. Cleaved pET21 METTL7B was incubated overnight with GSTrapFF resin, washed with GSTrapFF buffer until A_{280} absorbance readings had stabilized, and eluted with GSTrapFF buffer containing 10 mM reduced glutathione and adjusted to pH 8.0. Anti-METTL7B western blot analysis showed that moderate amounts of cleaved METTL7B bound to the GSTrapFF column and that full length pET21 METTL7B was mostly present in the column flow-through and eluent (Figure 3.16). Very little cleaved METTL7B was present in the column flow-through when analyzed by SDS-PAGE silver stain (Figure 3.17).

Anti-GST western blot analysis of a GSTrapFF binding timecourse revealed that the non-cleaved pET21 METTL7B and the free GST tags were present in column flow-through fractions even after six hours of incubation. The amount of free GST tag was relatively consistent across all time points tested and did not appear to decrease with increasing incubation time (Figure 3.18). Subsequent biochemical characterization experiments were conducted using non-cleaved pET21 METTL7B because of the large reduction in enzymatic activity upon HRV3C cleavage and the inability to isolate free METTL7B from cleaved GST tag protein.

Biochemical Characterization of pET21 METTL7B:

Aside from pH optimization, all biochemical characterization was conducted with the pET21 METTL7B fusion protein without cleaving the affinity tag. pH optimization was conducted using the full length METTL7B construct encoded in the pGEX-3X vector (detailed in Appendix II). This construct also contained an *N*-terminal GST fusion protein tag, was active

for captopril methylation *in vitro*, and assumed to behave similarly to the pET21 METTL7B fusion protein. The optimum pH for captopril methylation was 7.0 using recombinant METTL7B (Figure 3.19). Each data point was corrected for the rate of non-enzymatic methylation.

The effects of different buffer components on captopril methylation were also tested using purified pET21 METTL7B. The addition of magnesium chloride, nickel sulfate, and reduced glutathione significantly decreased enzyme activity (Figure 3.20). Addition of 2,3-dichloro-α-methylbenzylamine (DCMB) did not significantly decrease captopril methylation by pET21 METTL7B.

Incubating pET21 METTL7B with 1,2-dimyristoyl-sn-glycero-3-phosphorylglycerol (DMPG) liposomes in activity assay buffer (50 mM KPi pH 7.0, 20% (v/v) glycerol, 10 mM CHAPS, 150 mM NaCl) for 30 minutes on ice greatly increased the specific activity as reflected by the increase in captopril methylation. The ratio of liposome:protein was directly related to the increase in specific activity, with a 75:1 (w/w) liposome:protein ratio resulting in the highest activity (Figure 3.21). The non-enzymatic rate of methylation was not changed by the presence of DMPG liposomes in the activity assay buffer (Figure 3.22). All further substrate screening and kinetic experiments were conducted using pET21 METTL7B reconstituted with DMPG liposomes in activity assay buffer. A final ratio of 85:1 liposome:protein was used as this was the highest ratio achievable without altering the activity assay parameters.

Characterization of pET21 METTL7B Substrate Specificity:

Several small molecule methyltransferase probe substrates were screened for methylation activity with recombinant pET21 METTL7B in DPMG liposomes. The substrate concentrations

used were at least three times above the published K_m values to ensure detection of potential methylation. For all substrates, non-enzymatic methylation with both boiled enzyme and buffer-only controls were also measured.

Only compounds containing aliphatic thiol functional groups, namely 7α-Thiospironolactone, coenzyme A, thioglucose, and captopril, exhibited significant methylation activity compared to the dopamine non-substrate control (Figure 3.23). Canonical substrates for catechol *O*-methyltransferase, histamine *N*-methyltransferase, and thiopurine methyltransferase were not methylated by pET21 METTL7B. Endogenous thiols, glutathione and cysteine also did not appear to be methylated by pET21 METTL7B.

Substrate specificity was further characterized using several additional aliphatic thiol-containing compounds, including *D*- and *L*-penicillamine, the active metabolite of prasugrel, and mertansine (Figure 3.24). All substrates, except for diethyldithiocarbamate, were methylated above background levels. The qualitative results of multiple rounds of substrate screening are presented in Table 3.1.

High-resolution mass spectrometry confirmed site-specific methylation of the aliphatic thiol functional group for captopril, prasugrel active metabolite, and 7α-Thiospironolactone. Multiple shared daughter ions were identified in the fragmentation spectra of captopril and *S*-methyl captopril (Figure 3.25). Specific daughter ion transitions were used to assign certain fragments for both captopril and *S*-methyl captopril (Figures 3.26 and 3.27).

Similarly, fragmentation of the prasugrel active metabolite and the methylated compound share multiple daughter ion transitions (Figure 3.28). Fragments containing the methylated aliphatic thiol group were not identified however the parent masses for both compounds match

theoretical masses with less than 2 ppm error. Both the prasugrel active metabolite and methylated prasugrel active metabolite share similar fragmentation patterns (Figures 3.29 and 3.30). Fragments directly reporting on thiol methylation were not observed.

Finally, fragmentation spectra for 7α-Thiospironolactone and *S*-methyl-7α-Thiospironolactone were also obtained (Figure 3.31). Both compounds also share multiple daughter ions and parent compound masses match theoretical masses with less than 2 ppm error. Both 7α-Thiospironolactone and *S*-methyl-7α-Thiospironolactone fragmentation spectra contained daughter ions representing the loss of the aliphatic thiol or the methyl-thioether (Figures 3.32 and 3.33). Additionally, multiple dehydration events were observed but were not assigned.

Kinetic Characterization of pET21 METTL7B Methylation:

As previously mentioned, select aliphatic thiol substrates exhibited non-enzymatic turnover in the absence of METTL7B. This was most evident in captopril methylation assays. Non-enzymatic methylation was linear with respect to both captopril and SAM concentrations (Figures 3.34 and 3.35). Therefore, all further kinetic analyses of METTL7B were adjusted for non-enzymatic methylation at each substrate and co-factor concentrations.

Captopril methylation with pET21 METTL7B was linear with respect to incubation time and protein concentration (Figures 3.36 and 3.37). Future kinetic experiments were conducted within the linear range, specifically a 25-minute incubation time and 15 µL of pET21 METTL7B in DMPG liposomes.

Captopril methylation kinetics were measured with pET21 METTL7B (Figure 3.38). The highest concentration tested was 10 mM due to solubility limitations. Therefore, all tested concentrations were below the predicted K_m and saturation was not achieved.

Kinetic parameters were also determined for multiple known thiol methyltransferase substrates, namely 7α-Thiospironolactone, dithiothreitol and hydrogen sulfide (Figure 3.39). 7α-Thiospironolactone and dithiothreitol methylation was measured using a bioluminescent kit that reports formation of *S*-adenosyl-*L*-homocysteine formation. Hydrogen sulfide methylation was measured directly by LC-MS/MS. Similarly, SAM kinetic parameters were measured using LC-MS/MS and with captopril as a substrate. Each substrate exhibited saturable enzyme kinetics and measurements were taken above and below apparent K_m values. Eadie-Hofstee transformations of the kinetic curves produced linear plots (Figure 3.40). Linear regression line *R* squared values were consistently above 0.75 for all substrates measured.

Discussion:

We have investigated several different avenues to express and purify METTL7B, which are discussed in detail in Appendix II. We found that addition of an *N*-terminal GST tag to METTL7B sequence enabled purification from *E. coli* lysate however proteolytic cleavage of the fusion protein could not be achieved likely due to strong interaction with the hydrophobic *N*-terminus of METTL7B. Therefore, the *METTL7B* gene sequence was inserted into a new expression vector downstream of an engineered linker and fused to a combination GST-His tag. The linker consisted of five repeats of alanine-proline and was predicted to adopt a rigid and extended backbone geometry due to the inflexibility of the alternating proline residues[8,12]. The

new expression vector also contained an HRV3C protease site that is enzymatically cleavable at 4 ^{o}C, thus preventing thermal degradation during cleavage incubations.

Several *N*-terminally truncated forms of METTL7B were also created and expressed. Removal of the first six or nine amino acids of the METTL7B protein sequence reduced activity more than an order of magnitude compared to the full-length protein. These results are similar to those observed with other truncated METTL7B fusion proteins (Appendix II). Therefore, it appears that the METTL7B *N*-terminus is required for either protein stability, enzymatic activity, or both. All subsequent purification experiments were conducted entirely using full-length METTL7B protein, referred to as pET21 METTL7B, in order to obtain maximally active enzyme.

The new fusion protein, pET21 METTL7B, was retained on HisPur Ni-NTA resin however overall purity was relatively low. As discussed in Appendix II, there are multiple endogenous *E. coli* proteins that will bind to nickel ions and may copurify with His-tagged proteins, specifically ArnA and SlyD[20–22]. To reduce contamination, pET21 METTL7B was expressed in the LOBSTR strain of *E. coli* which contains mutated ArnA and SlyD proteins with impaired binding to nickel resin.[23]. Expression and purification using LOBSTR cells reduced contamination, however overall enzyme purity was still sub-optimal.

Overall purity was substantially increased by a second round of purification utilizing the GST portion of the pET21 METTL7B fusion tag and GSTrapFF immobilized glutathione affinity resin. The most prominent bands in the final eluent belonged to the full length pET21 METTL7B fusion protein and aborted synthesis products containing the affinity tag. Faint SDS-PAGE silver stain bands indicated slight contamination of higher molecular weight chaperone

proteins. These proteins were confirmed by multiple western blots as well as in-solution and in-gel tryptic digest and proteomic analysis. All methyltransferase activity observed in later characterization experiments was attributed to METTL7B because no other identified proteins are known to bind SAM or catalyze methylation reactions.

The purified pET21 METTL7B was efficiently cleaved by HRV3C protease within four hours, resulting in a free GST tag and free METTL7B protein. Captopril methylation activity decreased during incubation at 4 ºC and was further decreased upon HRV3C cleavage. The decrease in activity was perhaps a result of a conformational change in METTL7B structure after removal of the GST tag. As previously noted, truncation of the METTL7B *N*-terminus significantly decreased captopril methylation activity. Additionally, homology modeling presented in Chapter 2 indicated that the SAM binding site may partially include the *N*-terminal alpha helix. Therefore, HRV3C cleavage may potentially affect the *N*-terminus position, impacting enzyme activity by altering SAM or substrate binding. Alternatively, free METTL7B could remain associated with the free GST tag to help provide a hydrophobic environment for the *N*-terminal alpha helix, which may cause similar conformational changes or even block access to the active site. Further biophysical experiments are required to understand the underlying mechanism leading to loss of enzymatic activity that seems to be dependent on the *N*-terminus.

Separation of free METTL7B and free GST proteins was attempted using affinity chromatography in order to evaluate METTL7B substrate specificity and steady state kinetics in the absence of the fusion tag. Unfortunately, the free METTL7B was retained on the HisPur resin along with the free GST affinity tag protein and could not be selectively eluted. Similarly, free GST affinity tag would not bind to GSTrapFF affinity resin, instead remaining in solution

with the free METTL7B. A possible explanation is that the free GST and free METTL7B proteins continue to interact even after proteolytic cleavage. It may be that the free GST binds to free METTL7B in order to decrease solvent accessibility to the hydrophobic METTL7B *N*-terminal alpha helix. Future cleavage experiments should be conducted in the presence of DMPG liposomes. Purification of free METTL7B may be possible if the *N*-terminal alpha helix is better stabilized by insertion into liposomes than by interaction with free GST, which might allow removal of the free GST tags.

Biochemical characterization was conducted with non-cleaved METTL7B fusion protein constructs. The observed optimum pH for captopril methylation was 7.0 which is lower than previously reported values[24–26]. Additionally, captopril methylation with recombinant pET21 METTL7B was unaffected by the addition of magnesium ions to the activity assay buffer, contrary to the results observed with pooled human liver microsomes (HLMs) and further discussed in Chapter 4.

Recombinant pET21 METTL7B was not inhibited by DCMB, a known inhibitor of microsomal thiol methyltransferase activity. The concentration tested was ten times higher than the reported K_i in microsomes, therefore inhibition should have been observed[27]. Interestingly, captopril and hydrogen sulfide methylation were inhibited with the same concentration of DCMB in pooled HLMs as a positive control. Therefore, the specificity of DCMB needs to be further investigated, especially with other potential thiol methyltransferase enzymes such as METTL7A. Additionally, METTL7B inhibition by DCMB was only tested using tagged recombinant protein and must be revisited once active cleaved protein is purified.

Addition of DMPG liposomes significantly increased pET21 METTL7B captopril methylation activity, but did not change the non-enzymatic rate of methylation. The increase in activity was heavily dependent upon the liposome:protein ratio. DPMG liposomes may help stabilize the hydrophobic *N*-terminus of METTL7B or help prevent potential aggregation of multiple METTL7B fusion proteins. Future investigation of the effect of DMPG liposomes on the activity of truncated METTL7B fusion protein constructs is warranted.

pET21 METTL7B was screened with a panel of thiol-containing compounds as well as other canonical methyltransferase probe substrates. As predicted, methylation activity was only observed in the presence of compounds containing aliphatic thiol functional groups. No methylation activity was observed with substrates for catechol *O*-methyltransferase, histamine *N*-methyltransferase, or thiopurine methyltransferase[28–31]. While most confirmed substrates had been previously reported in literature, mertansine and coenzyme A were novel substrates for the methyltransferase.

Mertansine is a cytotoxic agent that binds to microtubules and is the "warhead" in the antibody-drug conjugate, trastuzumab emtansine[32]. Upon release from the antibody, mertansine contains an aliphatic thiol that has been shown to undergo methylation *in vivo* to a cytotoxic metabolite[33–35]. This methylation appears to be catalyzed by METTL7B. Methylation of coenzyme A was an intriguing finding and has not been reported *in vivo*. Like mertansine, coenzyme A methylation requires mass spectrometric confirmation. Metabolomics experiments are underway to potentially identify methylated coenzyme A in biological samples.

Methylation of 7α-Thiospironolactone, captopril, and the active metabolite of prasugrel was validated by high-resolution mass spectrometry. Methylation was demonstrated specifically

on the aliphatic thiol functional group for 7α-Thiospironolactone. Fragmentation patterns for captopril and the methylated metabolite also suggest specific methylation on the aliphatic thiol. The prasugrel active metabolite fragmentation pattern was not as informative but suggest that the methylation event occurred on the ring-opened thiophene moiety. Thiol methylation is consistent with the observed activity for METTL7B and has been observed *in vivo*[36,37].

Kinetic characterization of METTL7B was complex and required a large number of control experiments due to non-enzymatic methylation of specific probe substrates, namely captopril. The rate of non-enzymatic methylation exhibited first order kinetics with respect to both SAM and captopril. Therefore, every concentration on a kinetic curve must be accompanied by a specific control sample to account for non-enzymatic methylation at that substrate concentration. Kinetic experiments were also conducted within the linear range for both incubation time and protein concentration to permit steady state assumptions.

Apparent kinetic constants were measured for 7α-Thiospironolactone, dithiothreitol, hydrogen sulfide, and SAM. These compounds all displayed typical Michalis-Menten kinetics as evidenced by the linear Eadie-Hofstee transformed data. Captopril methylation was also catalyzed by pET21 METTL7B, however the methylation kinetics were only partly characterized given that saturation was not achieved. The apparent K_m values measured for *S*-adenosyl-*L*-methionine and 7α-Thiospironolactone were relatively similar to published values measured in human tissue fractions[24,38,39]. This suggests that METTL7B may account for a significant amount of thiol methyltransferase activity measured in humans.

All characterized substrates displayed classic Michaelis-Menten kinetics supported by the linear Eadie-Hofstee transformations of the velocity-concentration curves. This is relatively

surprising considering that several thiol methyltransferase probe substrates, including 7α-Thiospironolactone, have exhibited biphasic kinetics in human tissues[26,38]. This phenomenon could possibly be explained by the contribution of METTL7A to substrate methylation in human tissue. METTL7A and METTL7B may have distinct binding affinities and maximal rates of methylation for the same substrate. Therefore, steady state kinetics obtained from complex subcellular fractions will reflect a combination of the individual kinetics of both enzymes. Ideally, the same kinetic experiments listed here should be performed using recombinant METTL7A protein once purified, to allow direct kinetic comparisons.

Finally, the fact that METTL7B catalyzes the methylation of hydrogen sulfide is highly significant and should not be understated. Hydrogen sulfide is a signaling gasotransmitter that is important in human health[40,41]. Dysregulation of hydrogen sulfide homeostasis has been observed in many disease states, including rheumatoid arthritis and multiple cancers[42–47]. Alterations in METTL7B expression and activity can potentially play a role in the etiology of these diseases. Alternatively, chemical inhibition of METTL7B could be used as a potential treatment in diseases with increased hydrogen sulfide catabolism. Overall, a better understanding of the effect of METTL7B on hydrogen sulfide homeostasis is required and is currently under investigation in our lab.

Conclusions:

Recombinant pET21 METTL7B has been purified to near homogeneity using a dual affinity chromatography approach. As designed, the purified protein could be cleaved by HRV3C protease. Unfortunately, the free METTL7B could not be separated from the free GST affinity tag and captopril methylation activity was significantly decreased compared to full-

length fusion protein. Therefore, kinetic analysis and substrate specificity testing was conducted using full-length pET21 METTL7B incubated with DMPG liposomes, which increase enzymatic activity. Substrate screening further confirmed specificity towards aliphatic thiol groups and no methylation of catechols, amines, or thiopurines. The most clinically relevant substrates are hydrogen sulfide and mertansine, both of which are potential targets for cancer treatment. Michaelis-Menten kinetics were observed for a number of probe substrates and the apparent binding affinities closely matched literature values. Overall, these results unequivocally demonstrate that METTL7B is an aliphatic thiol methyltransferase that accounts for a significant portion of the thiol methylation activity observed in humans. Future research should focus on better defining its role in human health and disease, particularly in relation to hydrogen sulfide homeostasis.

Table 3.1: Relative Turnover of Probe Substrates with METTL7B

Substrate	Activity	Non-Substrate	Activity
7α-Thiospironolactone	+++	6-mercaptopurine	-
Dithiothreitol	+++	Arsenic Trioxide	-
Thioglucose	++	Cantharidin	-
L-penicillamine	++	Coenzyme M	-
D-penicillamine	++	Cysteine	-
Hydrogen Sulfide	++	Dopamine	-
Captopril	+	Glutathione	-
Prasugrel Active Metabolite	+	Histamine	-
		N-acetylcysteine	-
		Phenylethanolamine	-

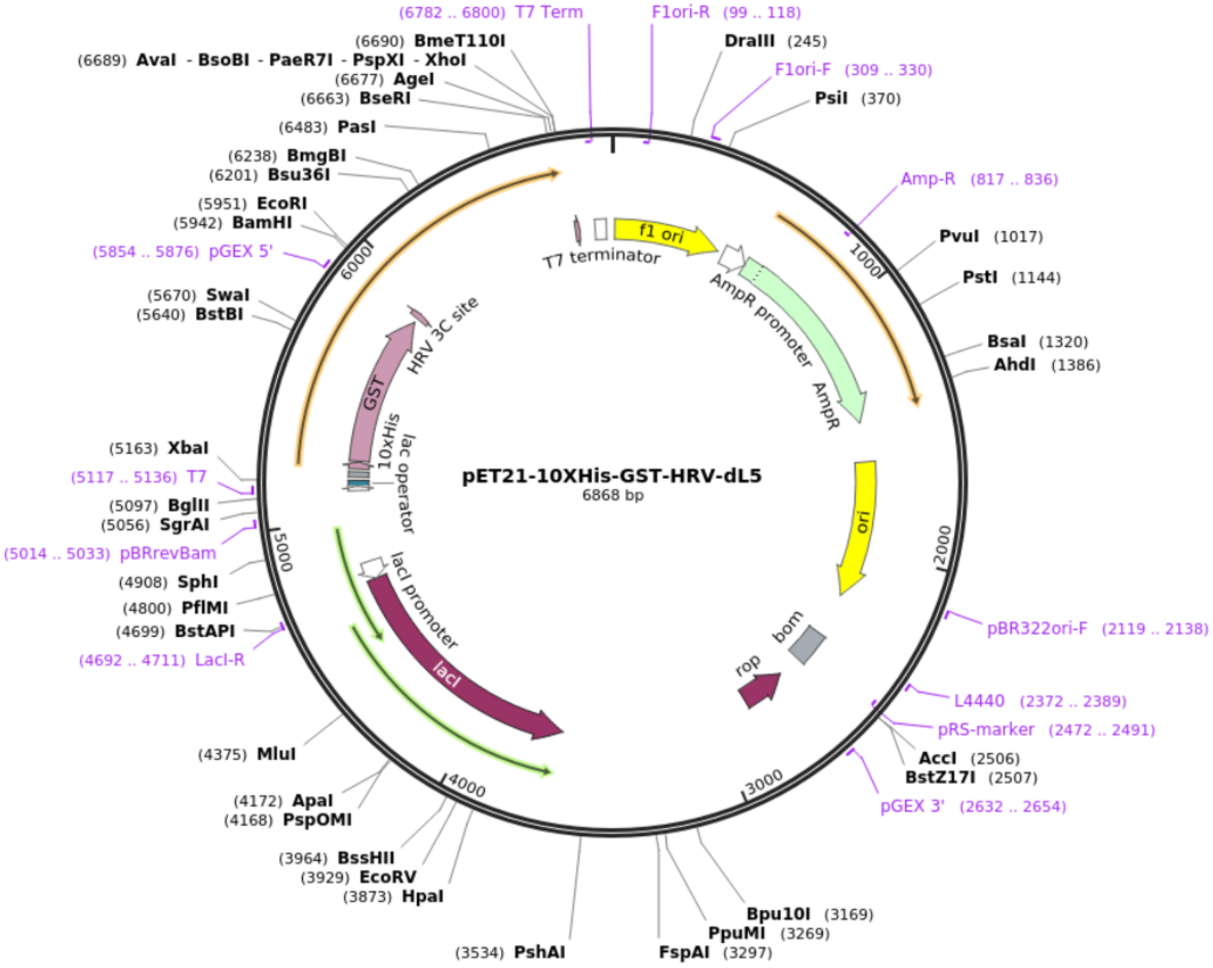

Figure 3.1. Plasmid Map for Expression of pET21 METTL7B: The *METTL7B* gene sequence was inserted directly downstream of a HRV3C protease site and a poly alanine-proline steric linker was added to the METTL7B *N*-terminus. The plasmid map was provided courtesy of SnapGene.

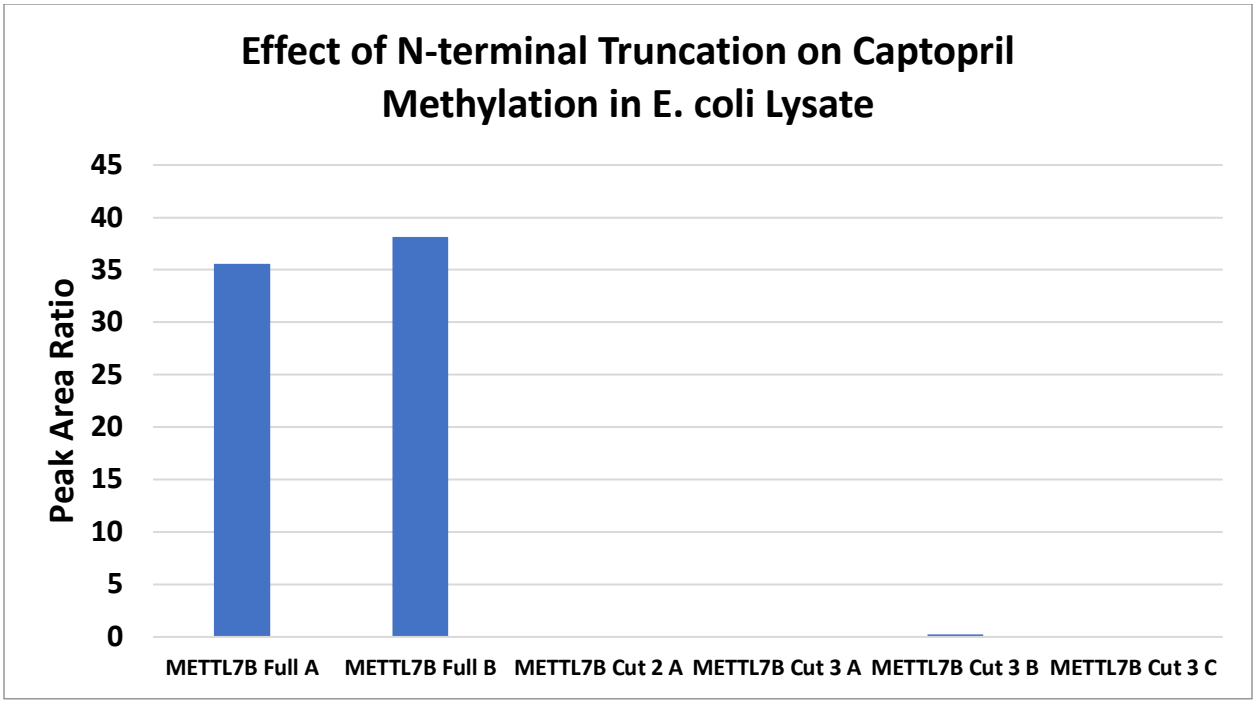

Figure 3.2. Effect of *N*-terminal Truncation on Captopril Methylation in Overexpressed *E. coli* Lysate: *Y*-axis is the *S*-methyl captopril ratio to internal standard in protein-normalized *E. coli* lysates. Individual activities are shown for colonies containing verified expression plasmids. Colonies containing non-verified expression plasmids were excluded.

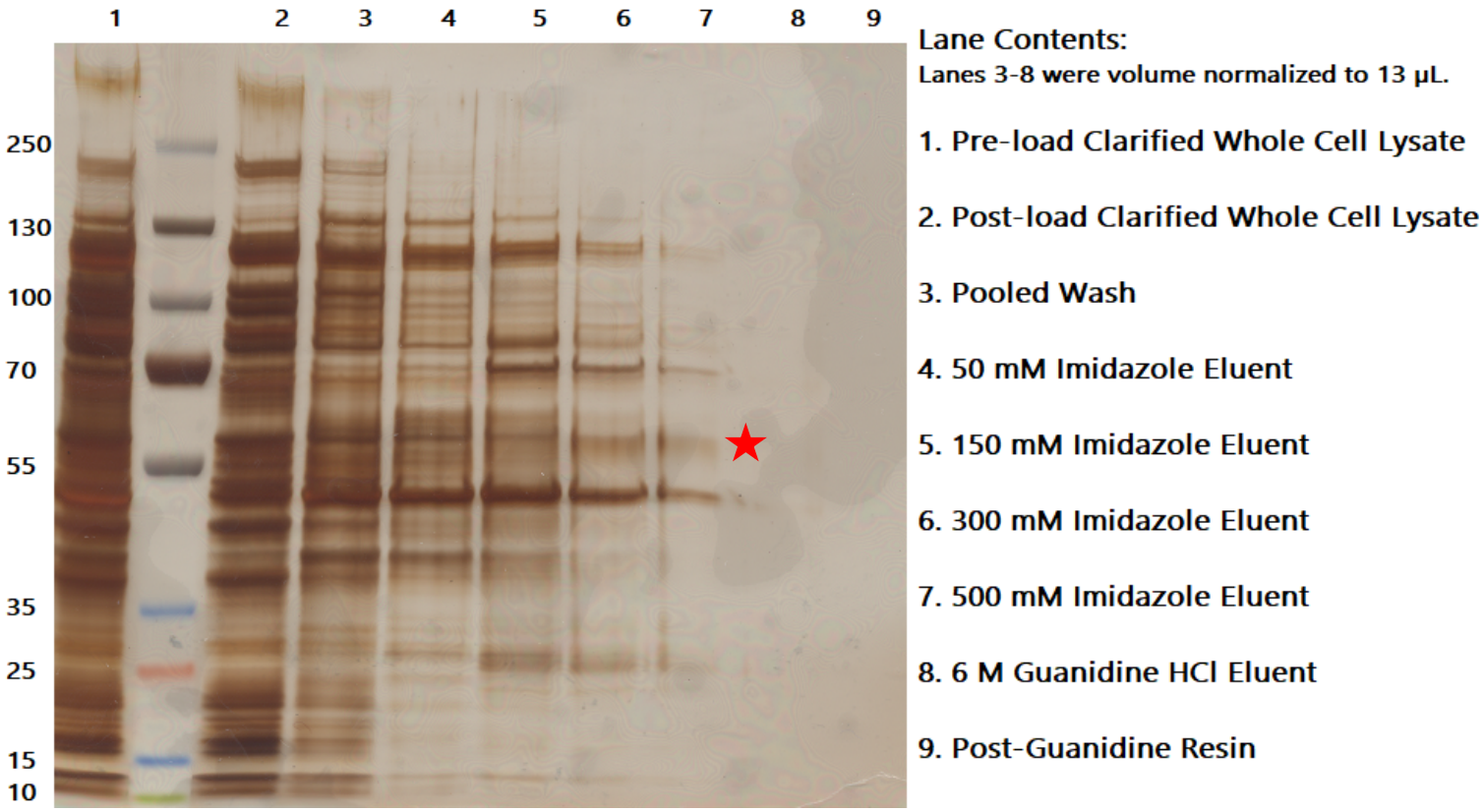

Figure 3.3. SDS-PAGE Silver Stain of Varying Imidazole Concentrations during HisPur Ni-NTA Purification of pET21 METTL7B: *E. coli* cell lysate containing pET21 METTL7B was loaded onto HisPur Ni-NTA resin and eluted with various concentrations of imidazole. Aliquots were taken from each elution fraction and equal volumes were analyzed by SDS-PAGE silver stain. A visible near 55 kDa band was present in lanes 6 and 7, as marked by the red star.

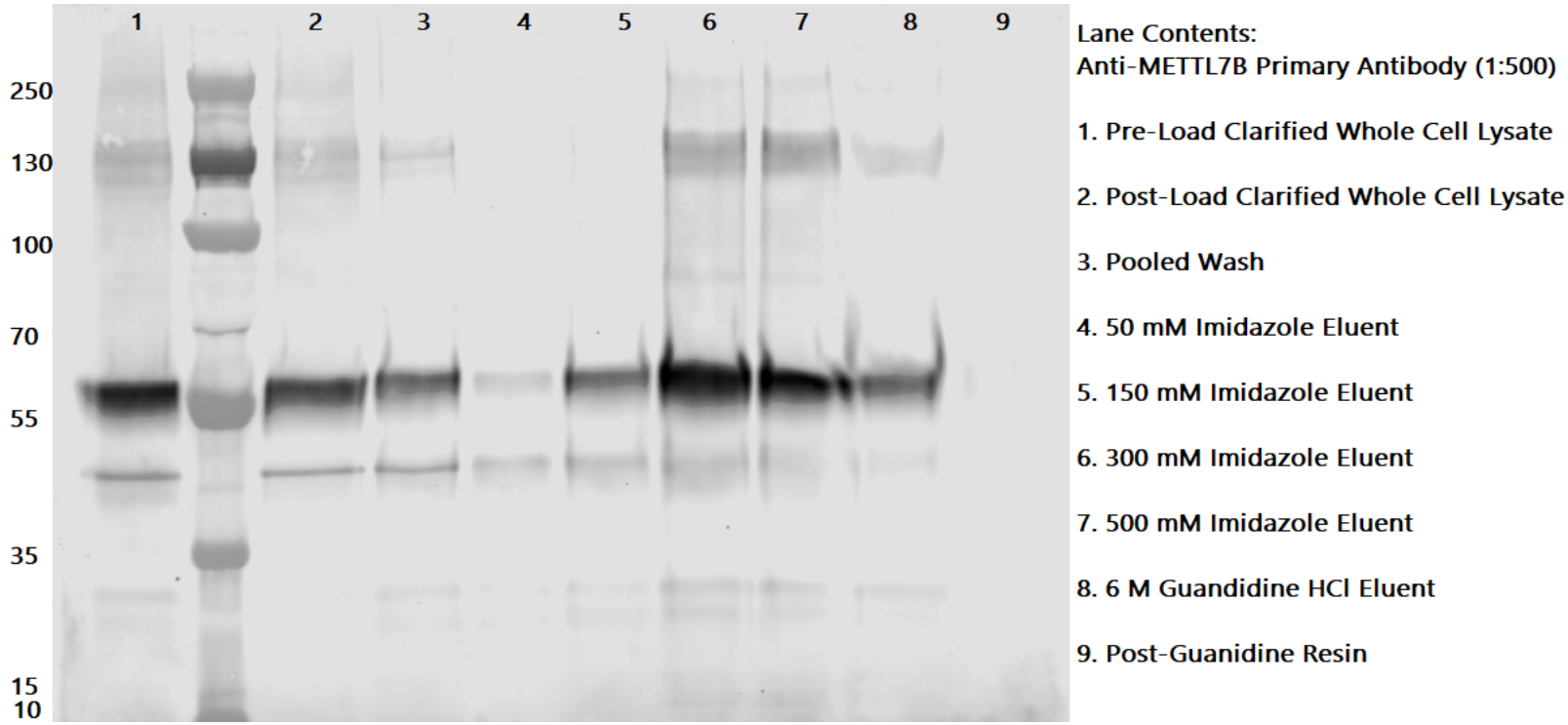

Figure 3.4. Anti-METTL7B Western Blot of Varying Imidazole Concentrations During HisPur Ni-NTA Purification of pET21 METTL7B: *E. coli* lysate containing pET21 METTL7B was purified using HisPur Ni-NTA and eluted with varying imidazole concentrations. Aliquots of each fraction were analyzed by western blot using a primary anti-METTL7B antibody. A distinct ~55 kDa band was present in cell lysates and the highest concentration imidazole elution fractions. Band intensity was decreased in the 50 mM and 150 mM imidazole elution fractions.

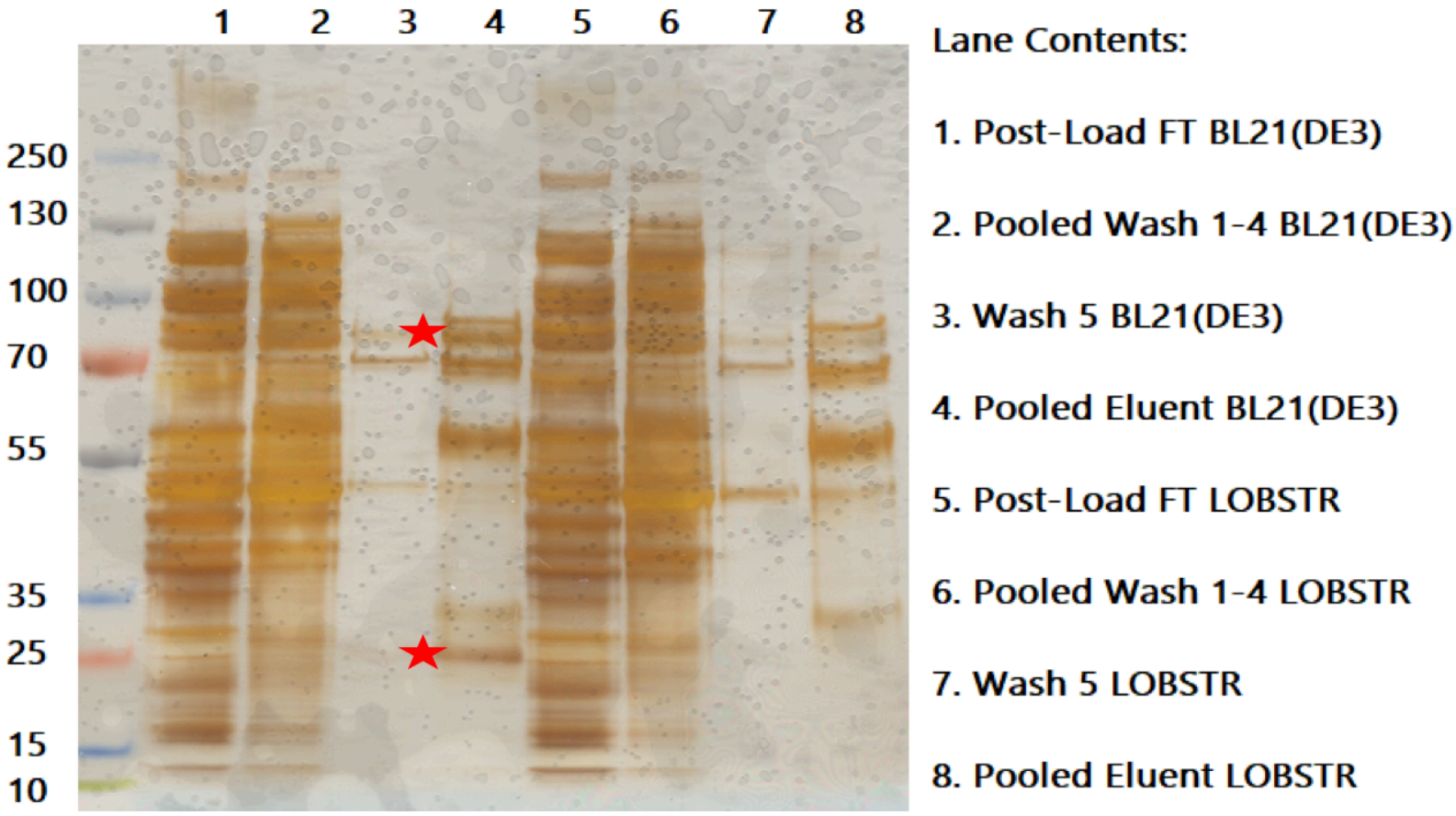

Figure 3.5. SDS-PAGE Silver Stain Comparison of BL21(DE3) *E. coli* and LOBSTR *E. coli* Endogenous Protein Contamination: Recombinant pET21 METTL7B was expressed in either BL21(DE3) *E. coli* or LOBSTR *E. coli*. Fusion protein was purified from each lysate using HisPur Ni-NTA resin and eluent fractions are shown in lanes 4 and 8. The two bands marked with red stars at 25 kDa and 70 kDa displayed the greatest difference between the two bacterial strains.

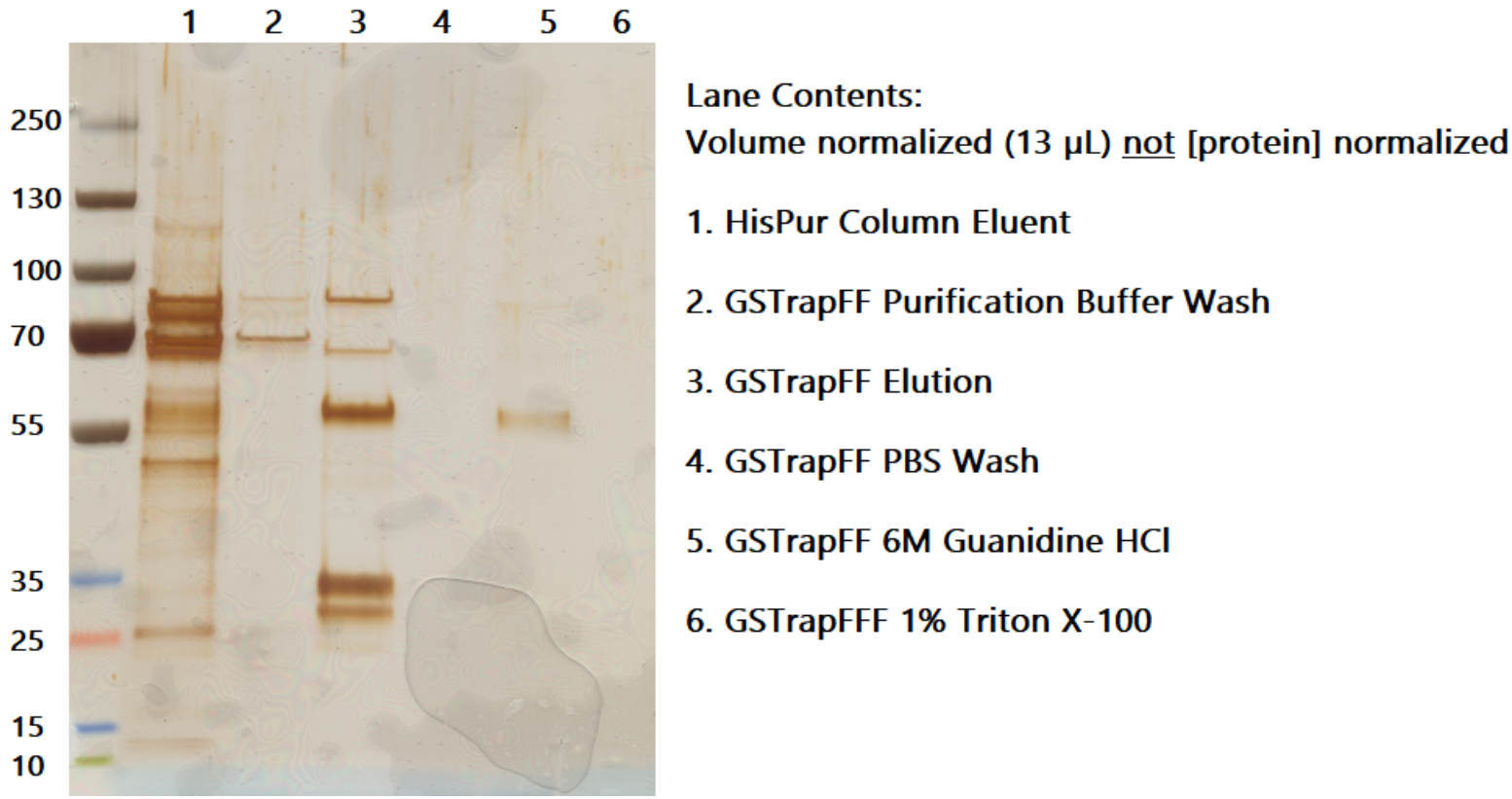

Figure 3.6. SDS-PAGE Silver Stain of GSTrapFF Secondary Purification of HisPur Ni-NTA Eluent: Elution fractions from GSTrapFF purification of HisPur Ni-NTA resin eluent. Equal volumes of flow-through, wash, elution, and subsequent column cleaning fractions were analyzed by SDS-PAGE silver stain. The GSTrapFF eluent contained intense bands at 55 kDa and 35 kDa as well as some higher molecular weight contaminants. Very few protein bands were observed in either the guanidine hydrochloride or Triton X-100 column wash fractions.

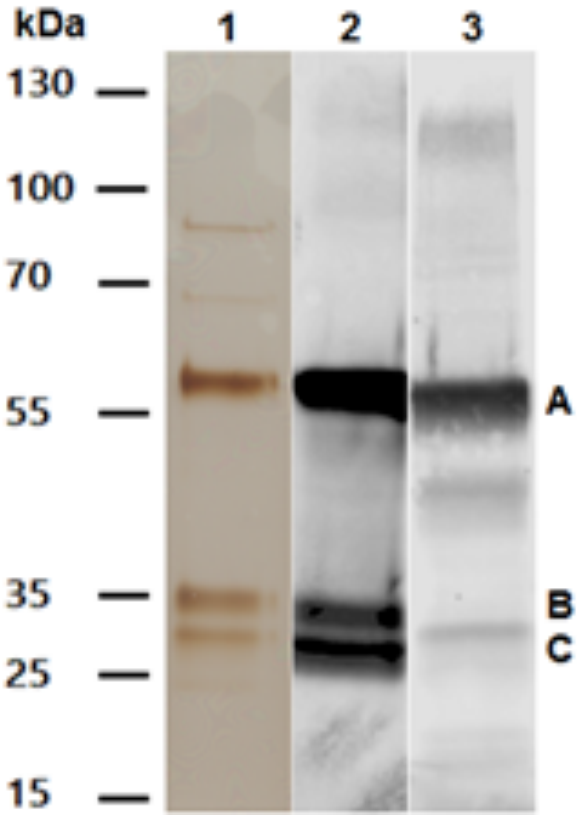

Figure 3.7. Purity Analysis of Purified pET21 METTL7B: Lane 1) SDS-PAGE silver stain of a representative gel showing purified 1µg pET21 METTL7B. **Lane 2)** Immunodetection of purified pET21 METTL7B (0.1 µg total protein) using anti-GST. **Lane 3)** Immunodetection of purified pET21 METTL7B (with 0.1 µg total protein) using anti-METTL7B. The pET21 METTL7B band is marked by the letter A and GST-containing aborted synthesis products are marked by the letters B and C.

1 **Acc. #:** Q6UX53 **Uniprot ID:** MET7B_HUMAN **Species:** HUMAN **Name:** Methyltransferase-like protein 7B
Organism: Homo sapiens **Gene:** METTL7B **Existence:** Evidence at protein level **Version:** 2
Protein MW: 27775.1 **Protein pI:** 8.7 **Protein Length:** 244 **Index:** 234488

Num Unique	% Cov	Best Disc Score	Best Expect Val
10	63.1	5.16	5.9e-9

m/z	z	ppm	DB Peptide	Score	Expect	# in DB
1214.0861	2	2.7	VALLELGCGTGANFQFYPPGCR	49.8	5.9e-9	1
855.3956	2	2.3	DLENAQFSEIQMER	45.0	1.3e-8	1
1127.5265	2	0.55	ETWKDLENAQFSEIQMER	52.1	1.1e-7	1
728.8484	2	0.41	VTCLDPNPHFEK	47.6	1.4e-7	1
765.4084	2	1.5	SYFPYLMAVLTPK	39.8	5.6e-7	1
594.7665	2	0.75	HIGDGCCLTR	31.6	2.3e-6	1
1071.0376	4	-0.80	RVLRPGGVLFFWEHVAEPYGSWAFMWQQVFEPTWK	30.3	5.5e-6	1
845.4191	3	0.63	QLADGSMDVVVCTLVLCSVQSPR	31.7	5.8e-6	1
560.7768	2	0.68	FVVAPGEDMR	31.6	1.7e-5	1
617.8421	2	0.33	WLPVGPHIMGK	26.5	2.0e-5	1

Figure 3.8. Human Peptides Identified from In-Solution Digest of Purified pET21 METTL7B: Several peptides unique to METTL7B were identified in the final GSTrapFF eluent fraction after in-solution tryptic digest. Peptides were identified using ProteinProspector and have low expect values and mass error.

Rank	Acc #	1_11_2019_001a/1_11_19 pET21 METTL7B GSTrapFF Eluent E coli 1				Protein MW	Species	Protein Name
		Num Unique	% Cov	Best Disc Score	Best Expect Val			
1	P0A6Y8	5	11.6	4.67	4.8e-8	69115.5	ECOLI	Chaperone protein DnaK
2	P0A6N2	4	12.7	2.78	1.6e-5	43314.0	ECOL6	Elongation factor Tu
3	P0A7L0	3	17.9	3.61	2.7e-6	24729.8	ECOLI	50S ribosomal protein L1
4	P02413	2	18.1	4.82	2.5e-8	14980.5	ECOLI	50S ribosomal protein L15
5	P0A7J3	3	23.6	2.76	1.2e-5	17711.7	ECOLI	50S ribosomal protein L10
6	P0A7J7	2	16.2	4.32	2.1e-7	14875.5	ECOLI	50S ribosomal protein L11
7	P0A7K2	2	19.0	3.83	1.8e-6	12295.3	ECOLI	50S ribosomal protein L7/L12
8	P60723	3	15.9	3.76	6.3e-8	22086.7	ECOLI	50S ribosomal protein L4
9	Q1RGI7	2	8.8	3.58	3.6e-7	41044.7	ECOUT	Chaperone protein DnaJ
10	P0A7R5	2	24.3	3.93	5.9e-7	11735.7	ECOLI	30S ribosomal protein S10
11	P0C054	2	15.3	2.85	1.7e-5	15773.8	ECOLI	Small heat shock protein IbpA
12	P60422	3	16.8	3.13	9.5e-7	29860.7	ECOLI	50S ribosomal protein L2
13	P0A7W1	1	11.4	5.30	3.3e-9	17603.5	ECOLI	30S ribosomal protein S5
14	P62399	3	22.3	2.56	1.7e-6	20301.8	ECOLI	50S ribosomal protein L5
15	P0ADB7	1	39.6	4.80	2.8e-8	4809.6	ECOLI	Entericidin B
16	P0A7S9	2	26.3	2.74	8.6e-6	13099.5	ECOLI	30S ribosomal protein S13
17	P0A7L3	2	16.1	2.62	4.0e-6	13497.1	ECOLI	50S ribosomal protein L20
18	P0A7W7	1	10.8	4.05	8.0e-8	14126.7	ECOLI	30S ribosomal protein S8
19	P0A7L8	1	16.5	3.41	3.4e-6	9124.5	ECOLI	50S ribosomal protein L27
20	P0A7V3	1	5.2	3.35	7.5e-6	25983.4	ECOLI	30S ribosomal protein S3
21	P0C058	2	12.7	2.04	3.5e-5	16093.3	ECOLI	Small heat shock protein IbpB
22	P62593	2	8.0	1.43	2.0e-4	31515.5	ECOLX	Beta-lactamase TEM
23	P02359	3	14.0	1.69	4.0e-5	20019.3	ECOLI	30S ribosomal protein S7
24	P0AA10	1	7.0	2.18	1.8e-6	16018.7	ECOLI	50S ribosomal protein L13
25	P60438	1	4.8	2.04	6.6e-5	22243.7	ECOLI	50S ribosomal protein L3
26	P0A7V8	1	4.4	1.90	1.2e-4	23469.3	ECOLI	30S ribosomal protein S4
27	P60624	1	9.6	1.43	4.4e-5	11316.3	ECOLI	50S ribosomal protein L24
28	P0A9X9	1	21.4	1.01	2.0e-4	7403.3	ECOLI	Cold shock protein CspA
29	P0A6A8	1	11.5	0.30	0.0038	8639.6	ECOLI	Acyl carrier protein

Figure 3.9. *E. coli* Proteins Identified Alongside Purified pET21 METTL7B: Multiple *E. coli* proteins were identified by in-solution tryptic digest of GSTrapFF eluent containing pET21 METTL7B. The most abundant protein contaminants were chaperone proteins such as DnaK and DnaJ. Numerous ribosomal subunits were also present.

1 **Acc. #:** Q6UX53 **Uniprot ID:** MET7B_HUMAN **Species:** HUMAN **Name:** Methyltransferase-like protein 7B
Organism: Homo sapiens **Gene:** METTL7B **Existence:** Evidence at protein level **Version:** 2
Protein MW: 27775.1 **Protein pI:** 8.7 **Protein Length:** 244 **Index:** 234488

1 MDILVPLLQL LVLLLTLPLH LMALLGCWQP LCKSYFPYLM AVLTPKSNRK MESKKRELFS QIKGLTGASG KVALLELGCG
81 TGANFQFYPP GCRVTCLDPN PHFEKFLTKS MAENRHLQYE RFVVAPGEDM RQLADGSMDV VVCTLVLCSV QSPRKVLQEV
161 RRVLRPGGVL FFWEHVAEPY GSWAFMWQQV FEPTWKHIGD GCCLTRETWK DLENAQFSEI QMERQPPPLK WLPVGPHIMG
241 KAVK

Num Unique	% Cov	Best Disc Score	Best Expect Val
6	27.9	3.47	3.4e-6

m/z	z	ppm	Score	Expect	# in DB
828.7350	3	4.3	30.9	3.4e-6	1
891.9000	2	-2.0	28.9	7.7e-6	1
757.3594	2	0.75	38.0	1.9e-5	1
883.9045	2	0.19	34.8	3.1e-5	1
589.2875	2	0.60	28.9	1.4e-4	1
623.2773	2	0.82	16.4	1.9e-4	1

Figure 3.10. METTL7B Peptides Identified from SDS-PAGE In-Gel Digest: The ~55 kDa band shown in Lane 1 of Figure 3.7 was excised. Multiple METTL7B peptides were identified by in-gel tryptic digest and proteomic analysis using ProteinProspector.

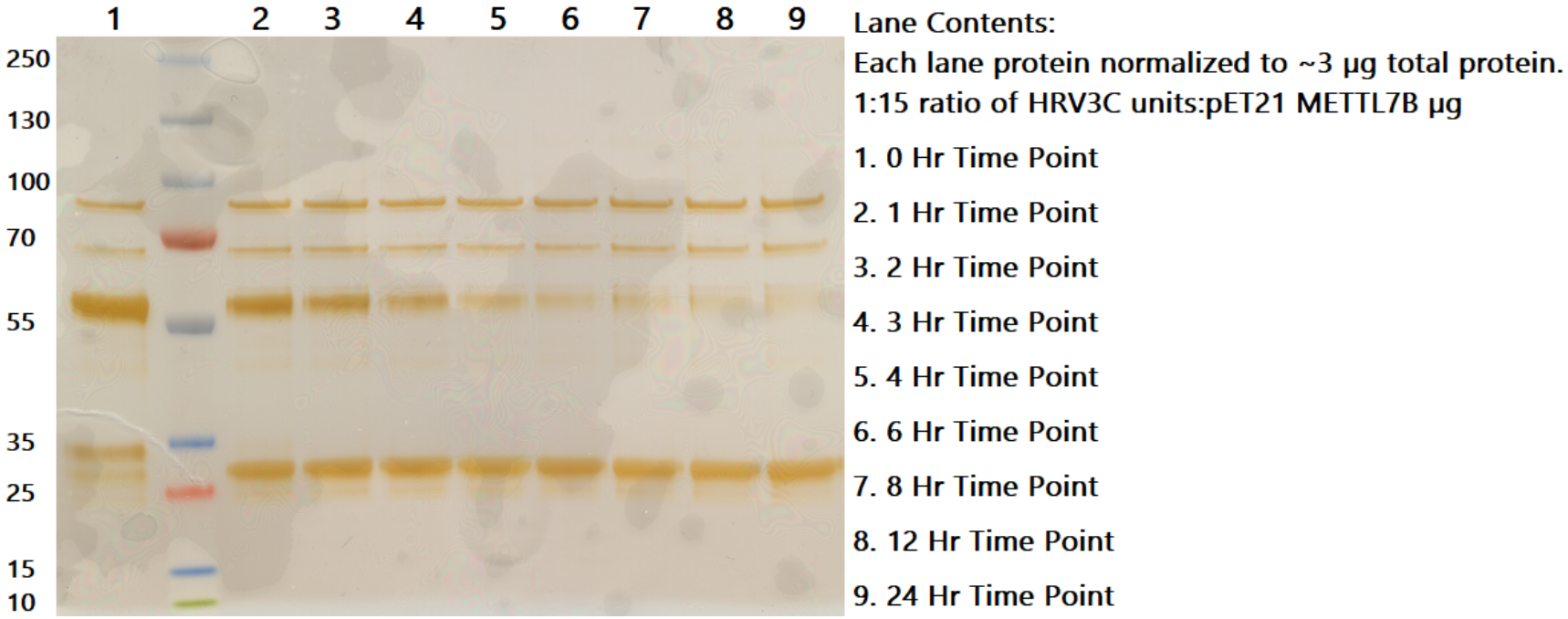

Figure 3.11. SDS-PAGE Analysis of pET21 METTL7B HRV3C Cleavage Time Course: Aliquots of an HRV3C digestion at various time points and analyzed by SDS-PAGE silver stain. Lane contents are noted on the right side of the gel.

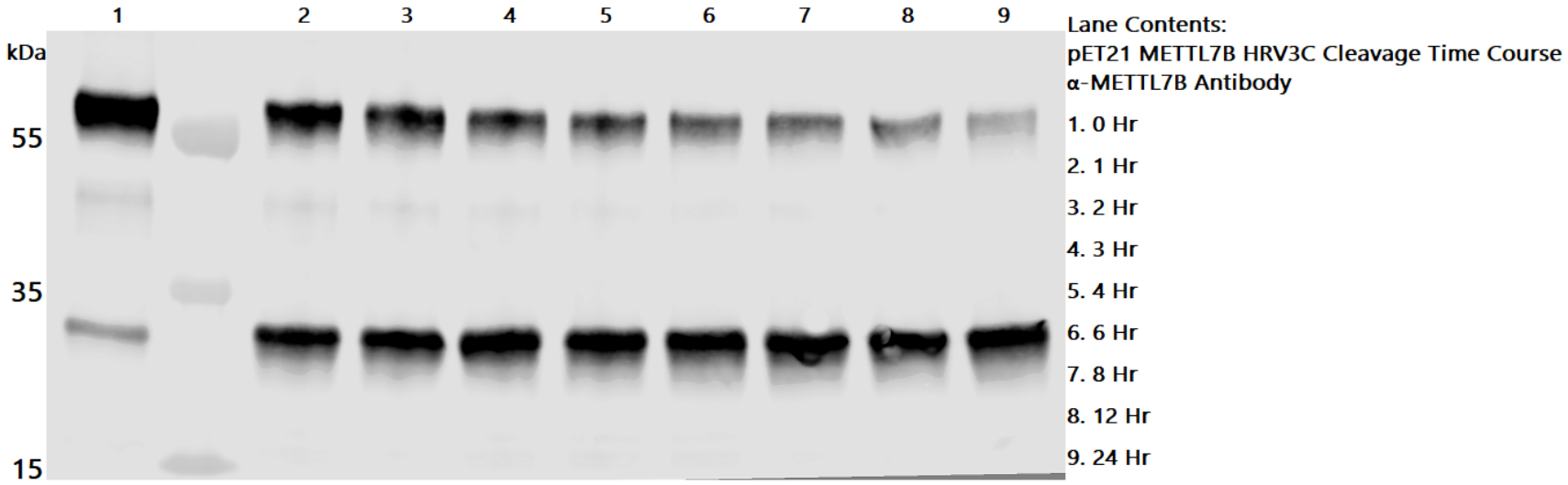

Figure 3.12. Western Blot Analysis of pET21 METTL7B HRV3C Cleavage Time Course: Aliquots of an HRV3C digestion at various time points analyzed via western blot using an anti-METTL7B primary antibody. Lane contents are noted on the right side of the gel as time points after digestion.

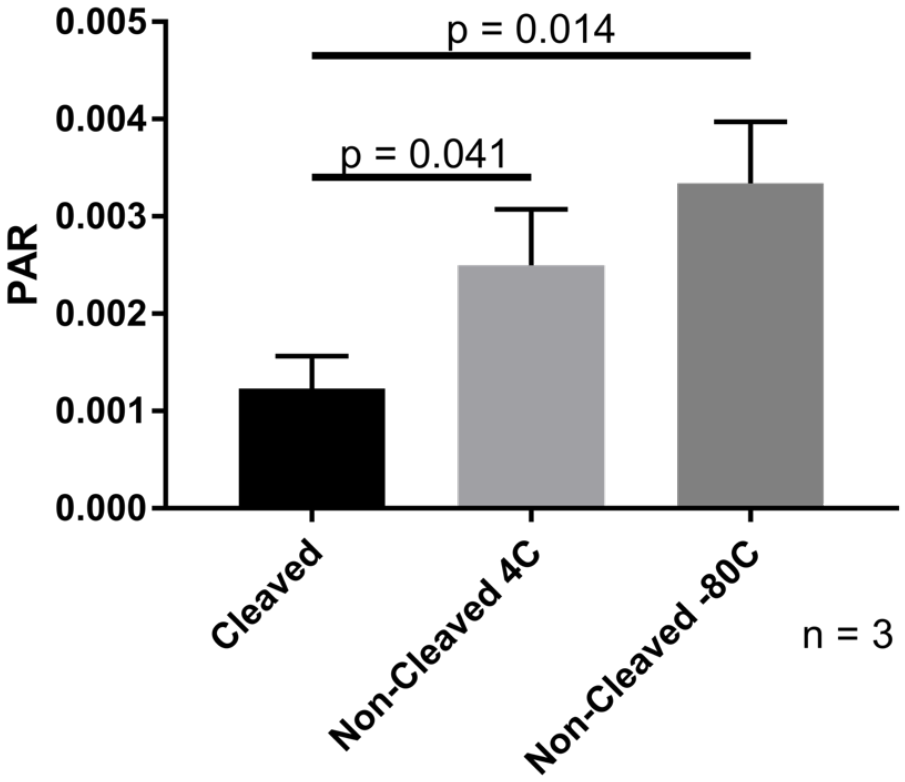

Figure 3.13. Effect of HRV3C Cleavage and Storage Temperature on Captopril Methylation Activity: Recombinant pET21 METTL7B was incubated at 4 ºC for four hours with or without HRV3C protease and captopril methylation activity was compared to full length protein stored at -80 ºC. Significance was determined using unpaired two-tailed *t* test. Data are presented as mean ± standard deviation.

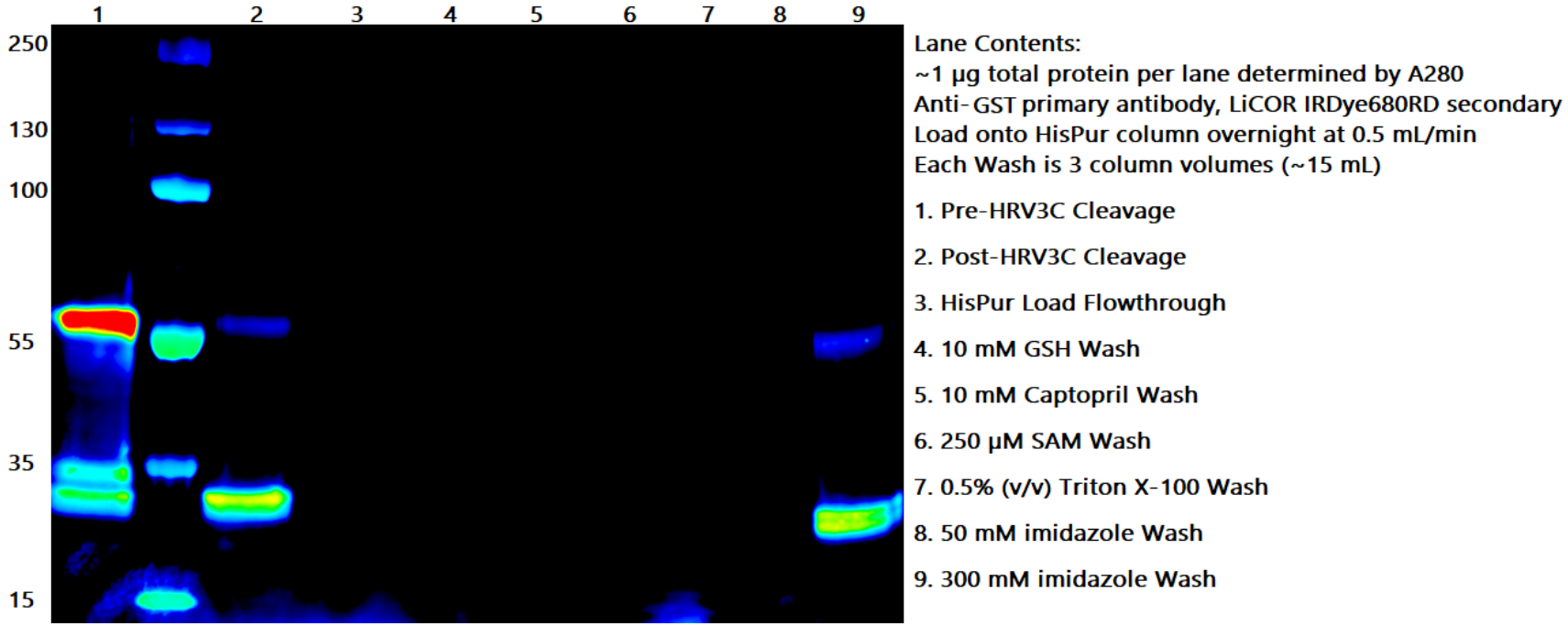

Figure 3.14. Anti-GST Western Blot of Cleaved pET21 METTL7B HisPur Cleanup: Cleaved pET21 METTL7B incubated overnight with HisPur Ni-NTA resin. The cleaved GST fusion protein eluted only in the presence of 300 mM imidazole.

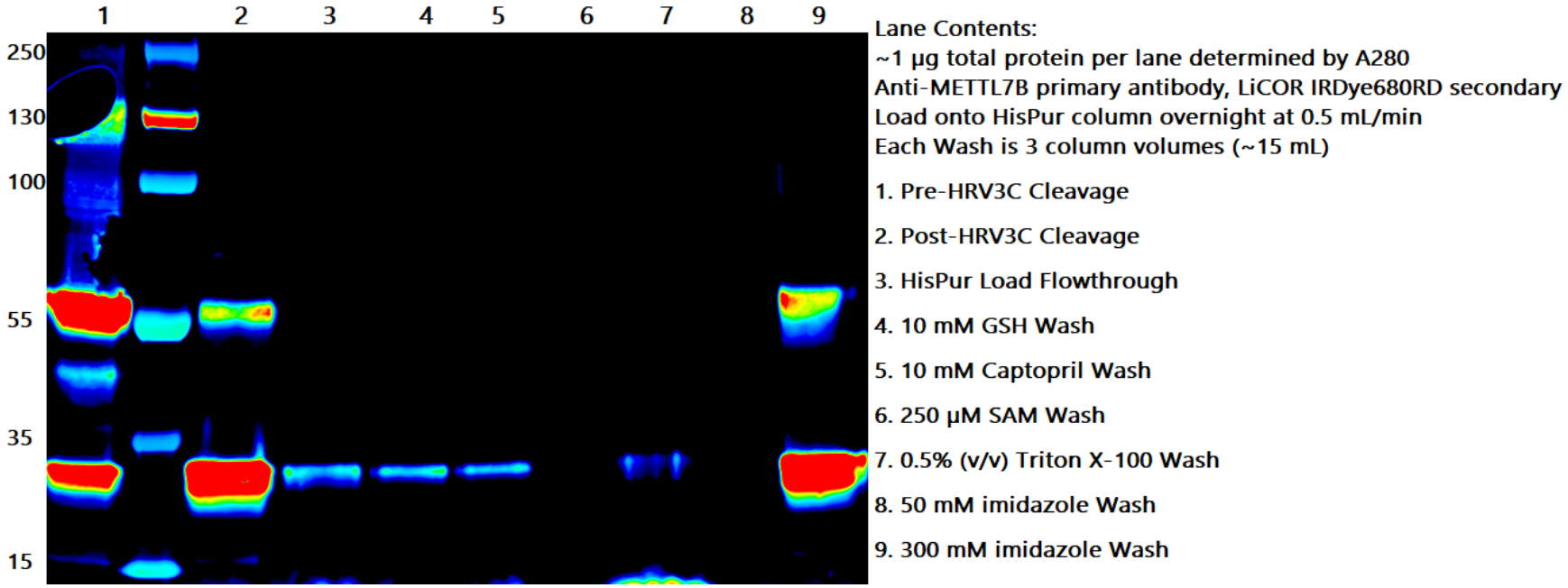

Figure 3.15. Anti-METTL7B Western Blot of Cleaved pET21 METTL7B HisPur Cleanup: pET21 METTL7B was cleaved with HRV3C protease and incubated overnight with HisPur Ni-NTA resin. Small amounts of cleaved METTL7B protein were present in the glutathione, captopril, and Triton X-100 wash steps.

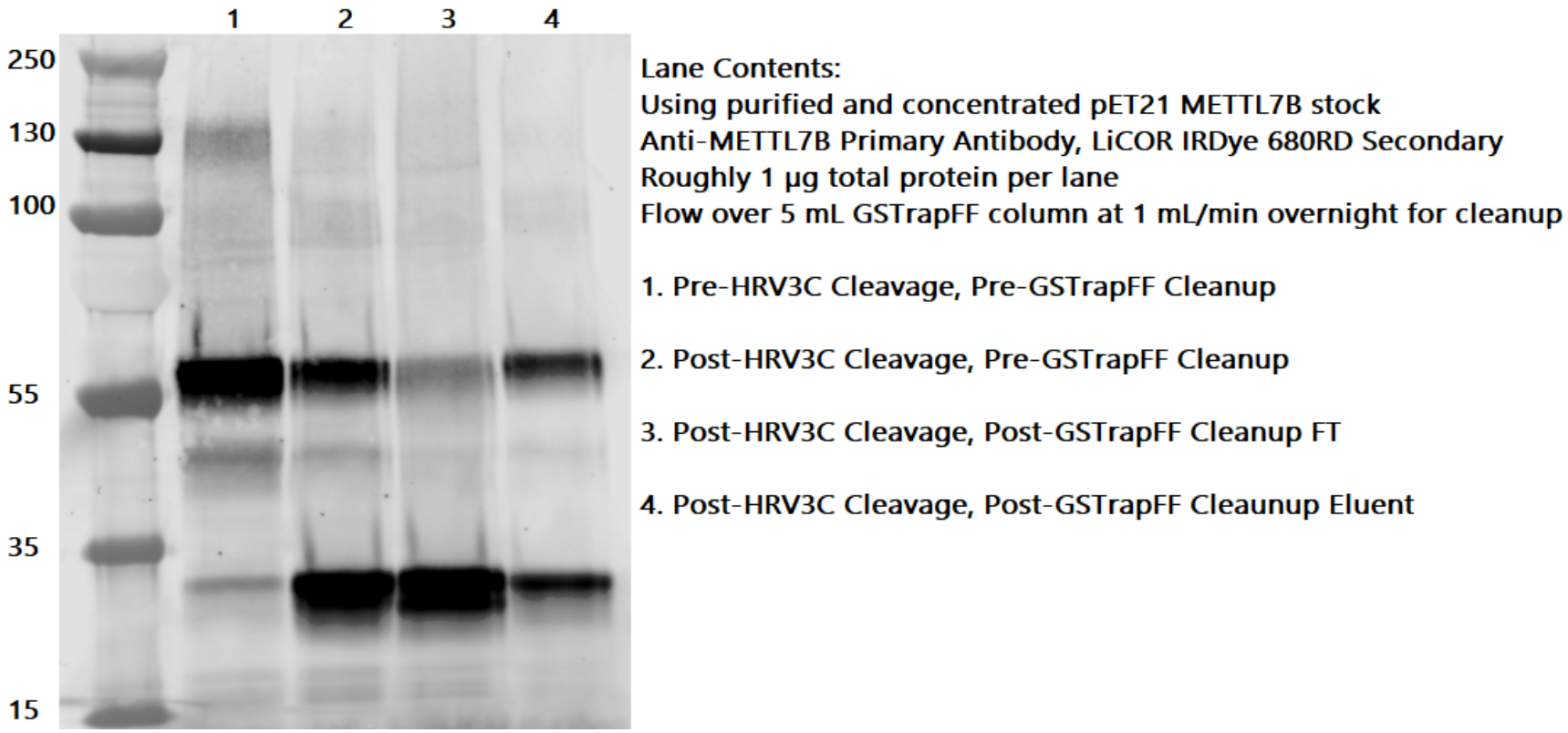

Figure 3.16. Anti-METTL7B Western Blot of Cleaved pET21 METTL7B GSTrapFF Cleanup: Cleaved pET21 METTL7B was passed over GSTrapFF resin overnight. The majority of the cleaved METTL7B did not bind to the GSTrapFF resin.

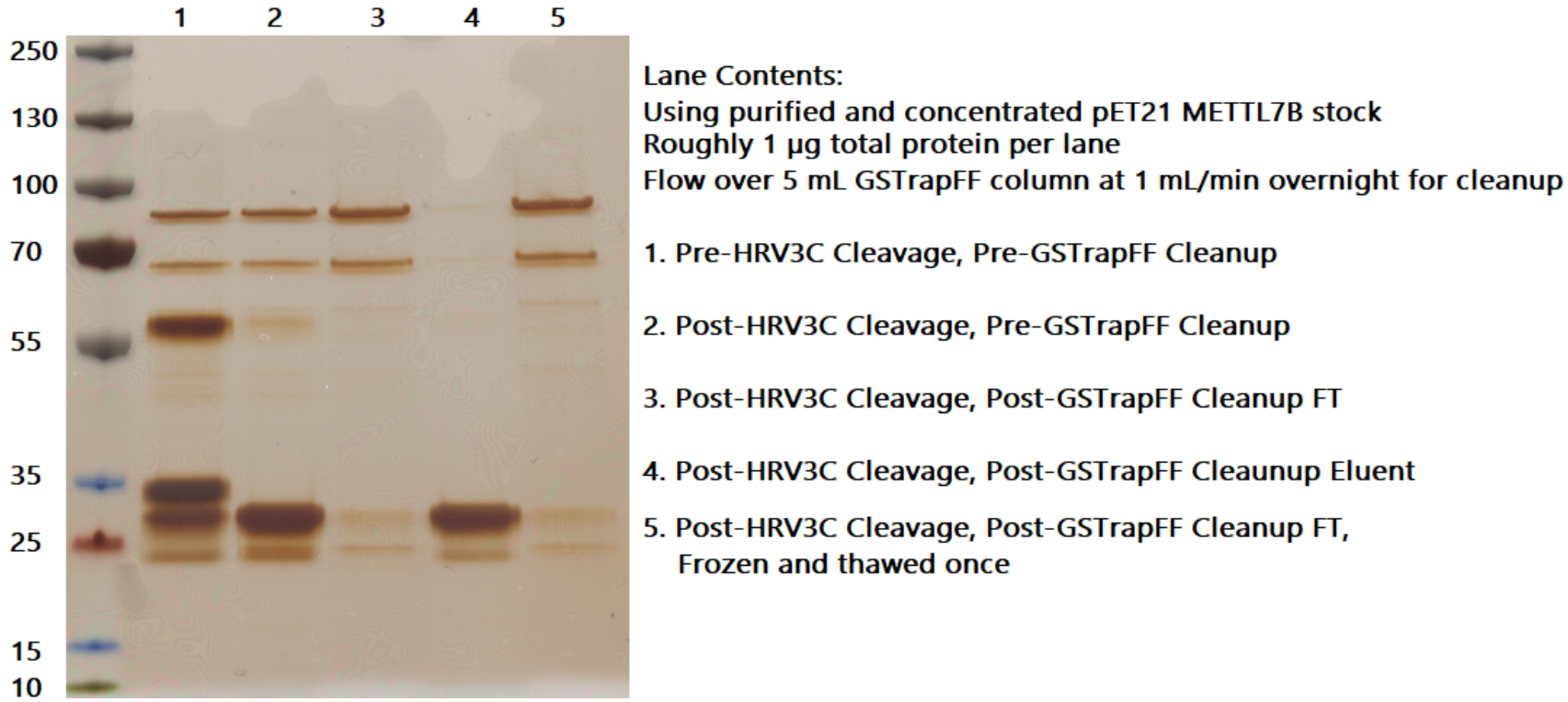

Figure 3.17. SDS-PAGE Silver Stain of Cleaved pET21 METTL7B GSTrapFF Cleanup: Cleaved pET21 METTL7B was separated from uncleaved fusion protein and the free GST tag by affinity chromatography. Very little free METTL7B was observed in the resin flow-through fraction.

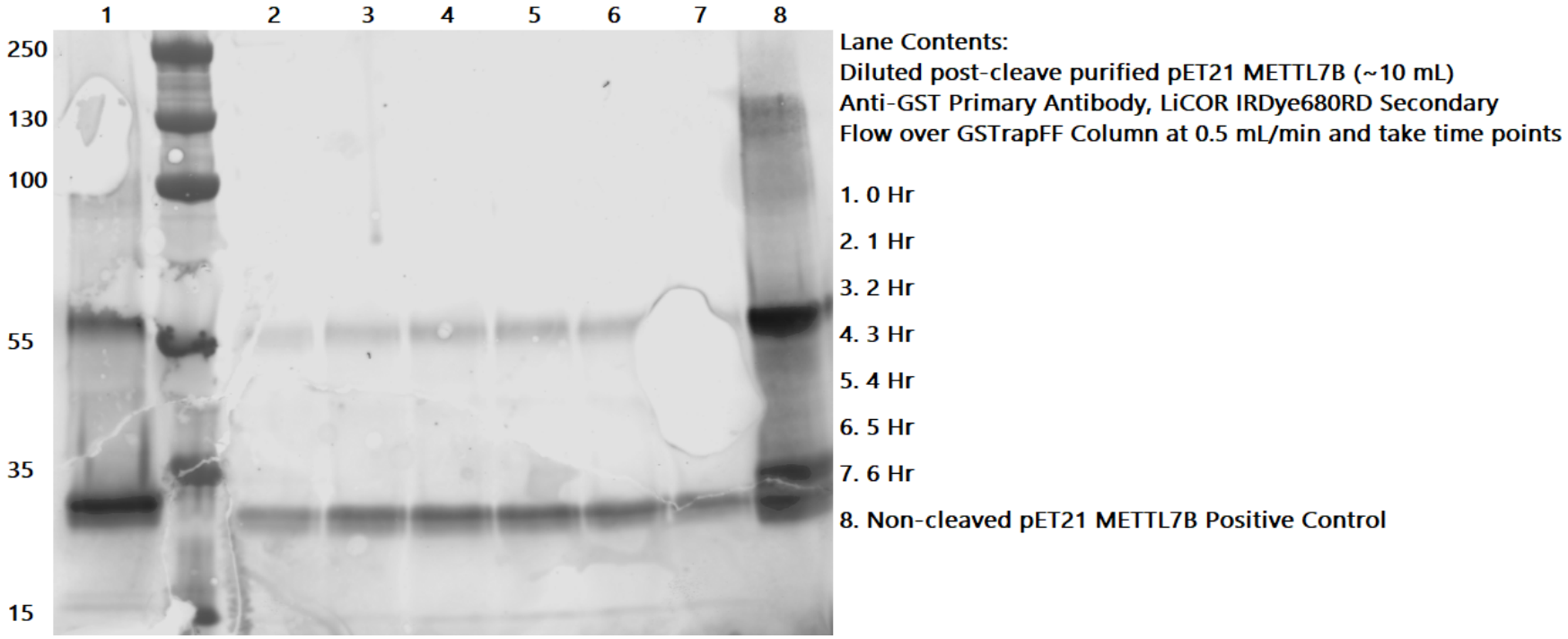

Figure 3.18. Anti-GST Western Blot Analysis of GST Tag Removal by Affinity Chromatography: Cleaved pET21 METTL7B was incubated with GSTrapFF resin overnight and aliquots were removed at certain time points. Free GST affinity tag protein was present at all time points and band intensity did not appear to decrease over time.

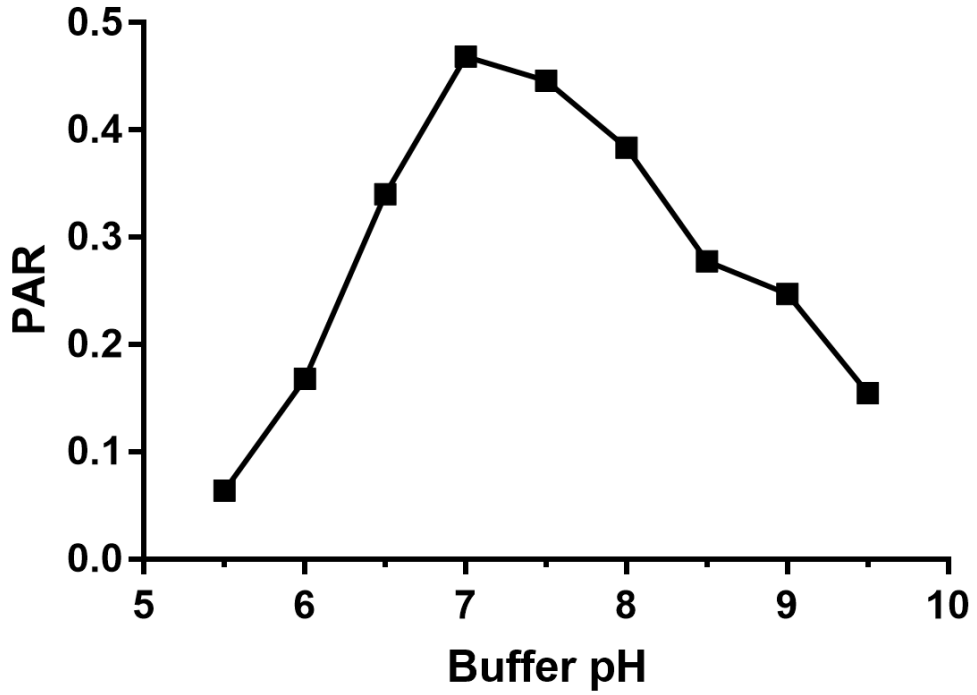

Figure 3.19. pGEX-3X METTL7B pH Dependence for Captopril Methylation: Purified full-length pGEX-3X METTL7B exhibited optimal captopril methylation activity at pH 7.0. Each data point was corrected for non-enzymatic methylation.

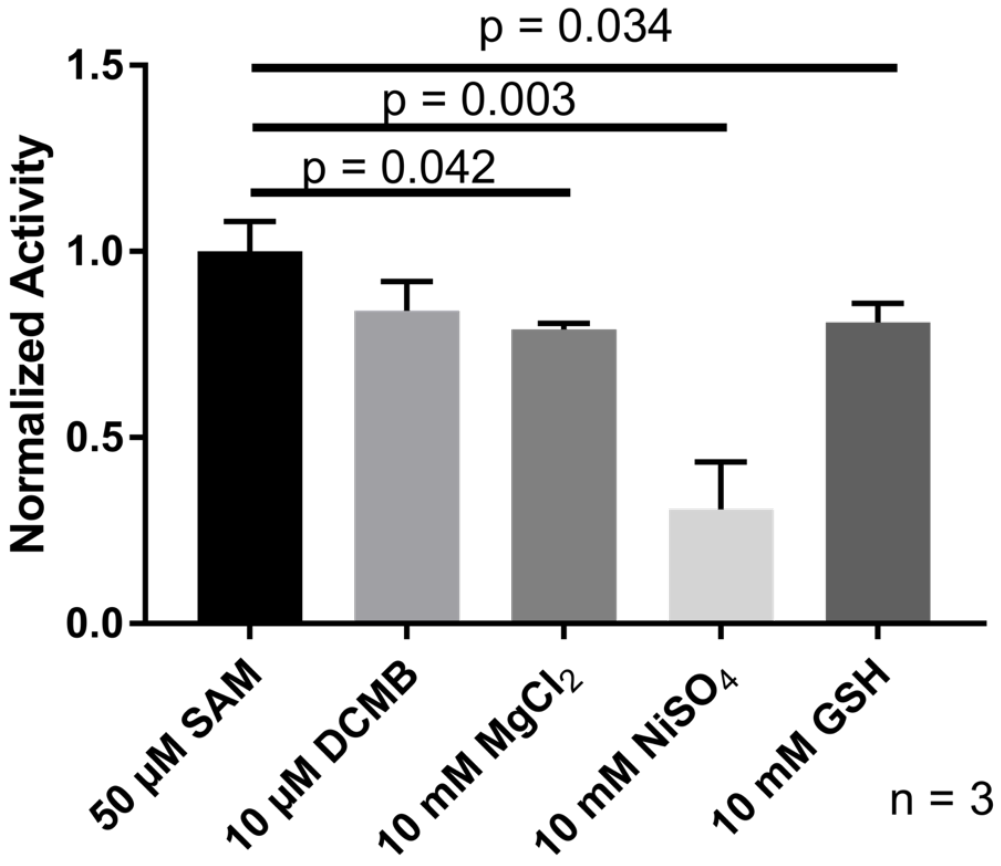

Figure 3.20. pET21 METTL7B Captopril Methylation in Different Buffers: Activity assay buffer was 50 mM KPi pH 7.0, 20% (v/v) glycerol, 10 mM CHAPS, and 150 mM NaCl. The 50 µM SAM sample is considered maximally active. Data are presented as the mean ± standard deviation of triplicate measurements. Significance was determined using the unpaired two-tailed *t* test.

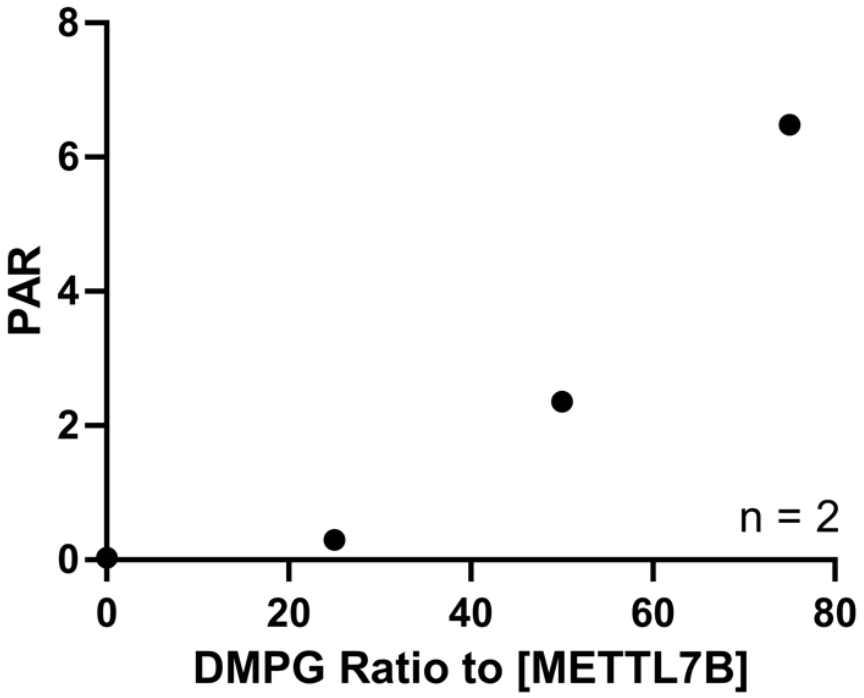

Figure 3.21. Effect of DMPG:Protein Ratio on pET21 METTL7B Captopril Methylation: Methylation activity was higher in samples with increased DMPG:METTL7B ratios. Data are presented as the mean ± standard deviation.

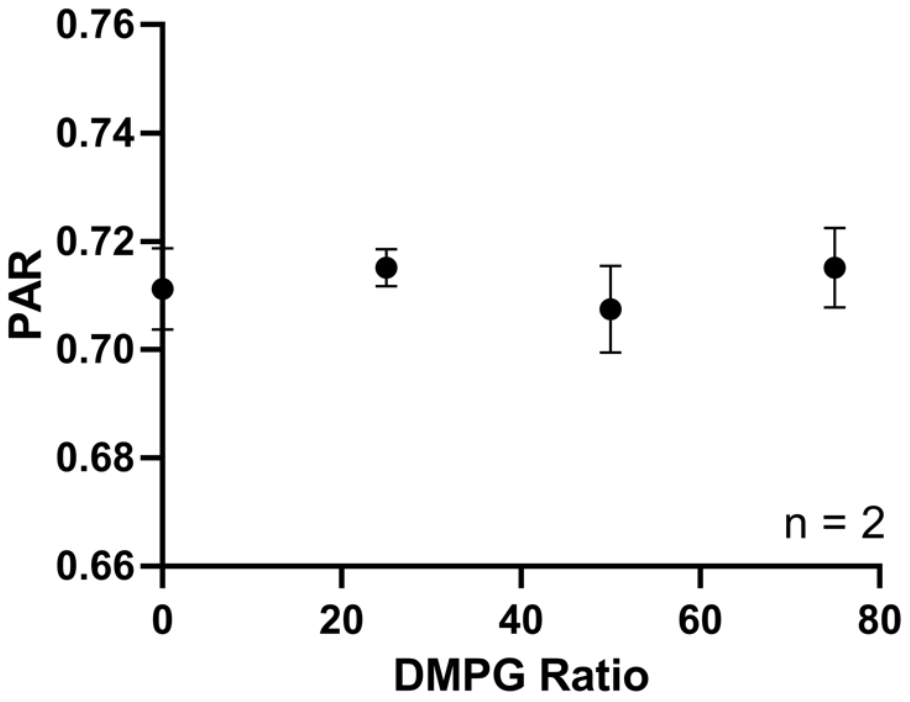

Figure 3.22. Effect of DMPG Ratio on Non-enzymatic Captopril Methylation: The background rate of non-enzymatic captopril methylation measured in incubations without METTL7B is unaffected by increasing DMPG liposomes. Data are presented as the mean ± standard deviation of replicates

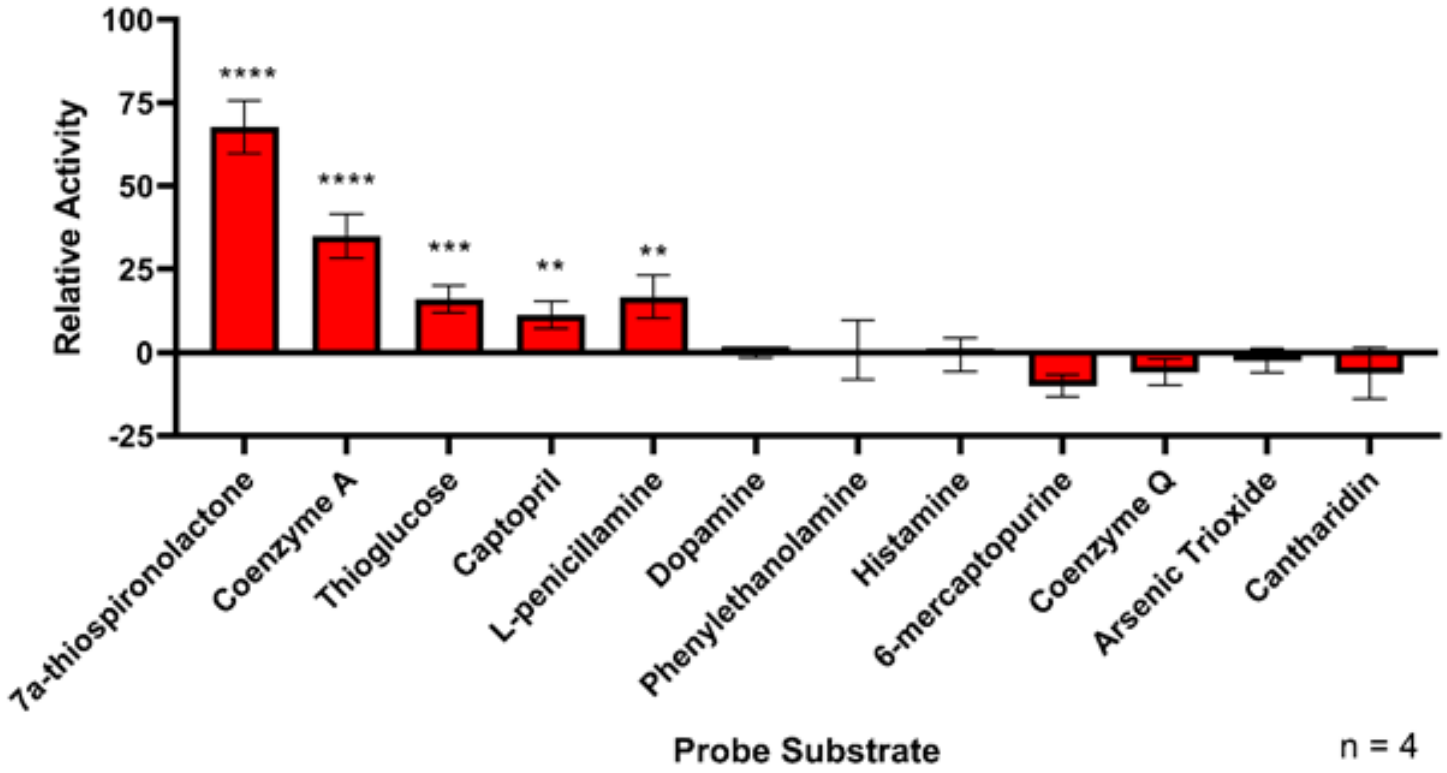

Figure 3.23. Screening of Select Methyltransferase Probe Substrates. Small molecule methyl transferase probe substrates were incubated for 1 hour with pET21 METTL7B at concentrations above K_m. Formation of *S*-adenosyl-*L*-homocysteine was measured using the Promega MTase-Glo kit. Activity was normalized to dopamine, a catechol *O*-methyltransferase probe. Negative values indicate reduced background signal compared to dopamine. All data are presented as the mean ± standard deviation. Significance was determined using unpaired two-tailed *t* test. ****P<0.0001. ***P<0.001. **P<0.01

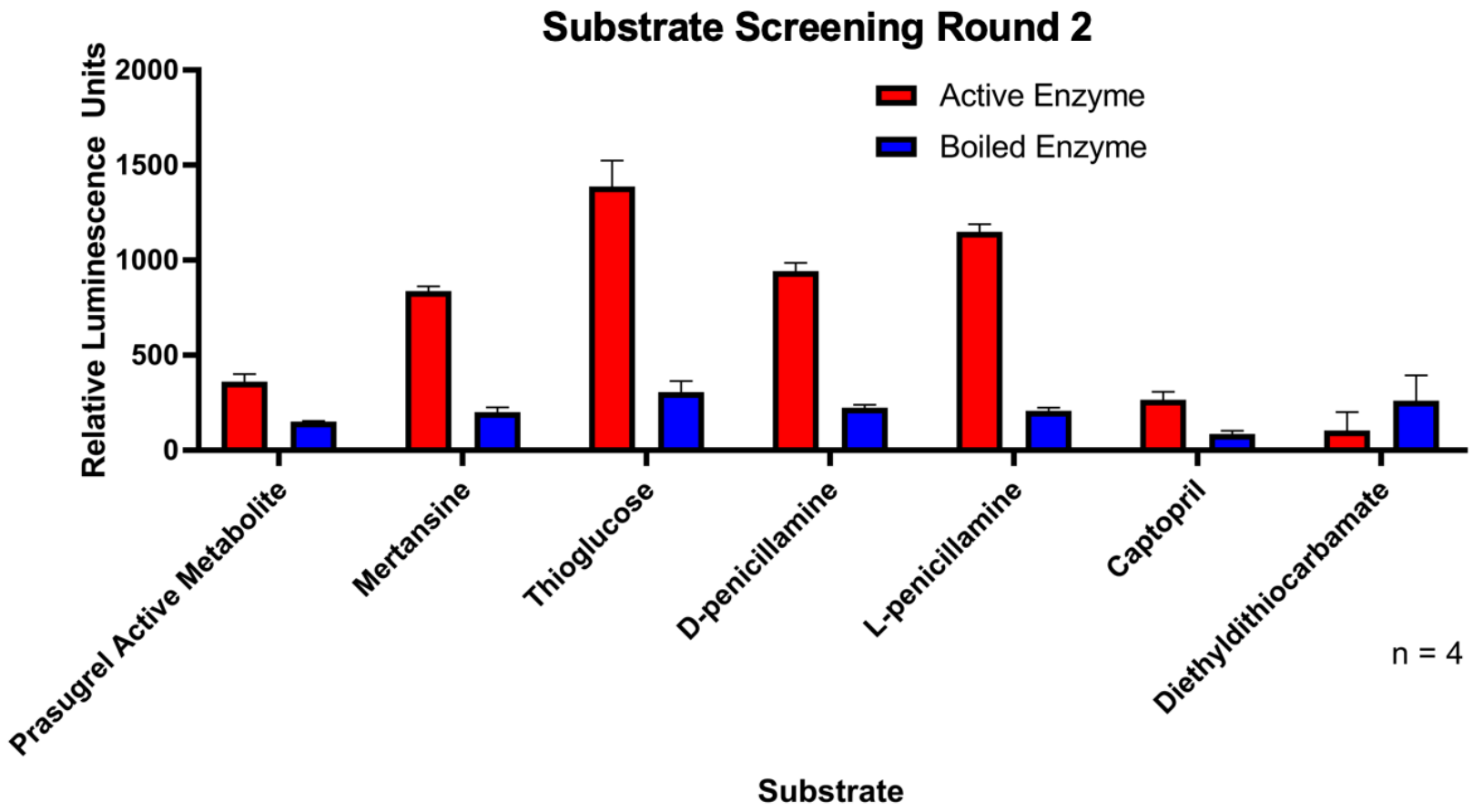

Figure 3.24. Semi-Quantitative Screening of Thiol-Containing Compounds: Thiol-containing probe substrates were incubated with pET21 METTL7B for 1 hour. Formation of *S*-adenosyl-*L*-homocysteine was measured using a Promega MTase-Glo kit. Substrate turnover was compared between active and boiled enzyme. Data are presented as the mean ± standard deviation.

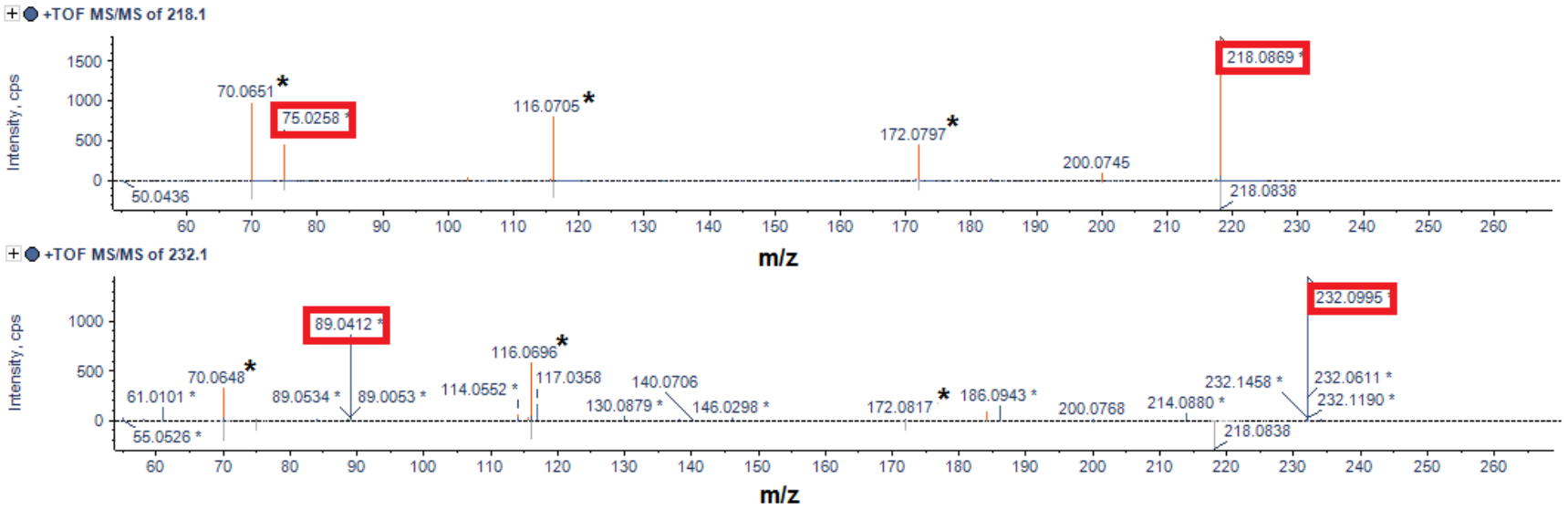

Figure 3.25. High-resolution Fragmentation Spectra of Captopril and *S*-methyl Captopril: Fragmentation pattern of captopril (top panel) and methylated metabolite (lower panel). Fragments unique to each compound are boxed in red and shared masses are marked by asterisks.

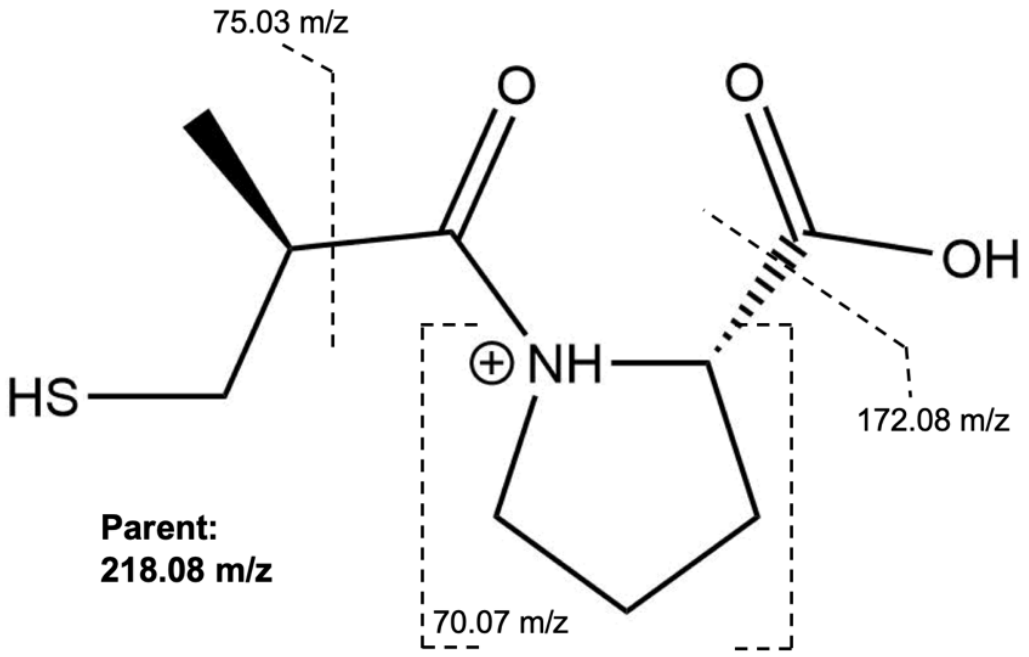

Figure 3.26. Predicted Fragmentation of Captopril: Potential fragments of captopril are shown by the dashed lines.

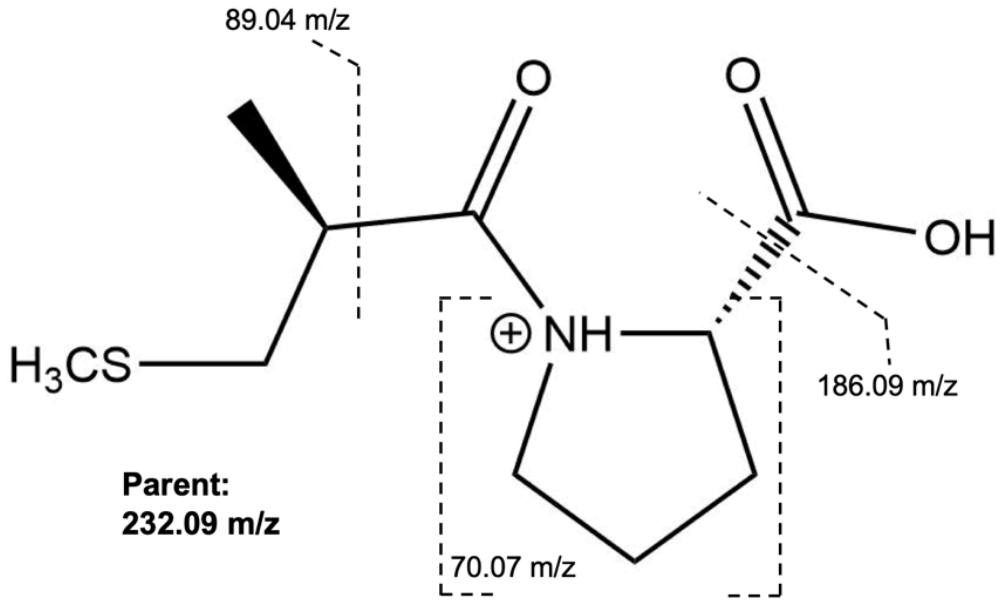

Figure 3.27. Predicted Fragmentation of *S*-methyl Captopril: Potential fragments of methylated captopril are denoted by the dashed lines.

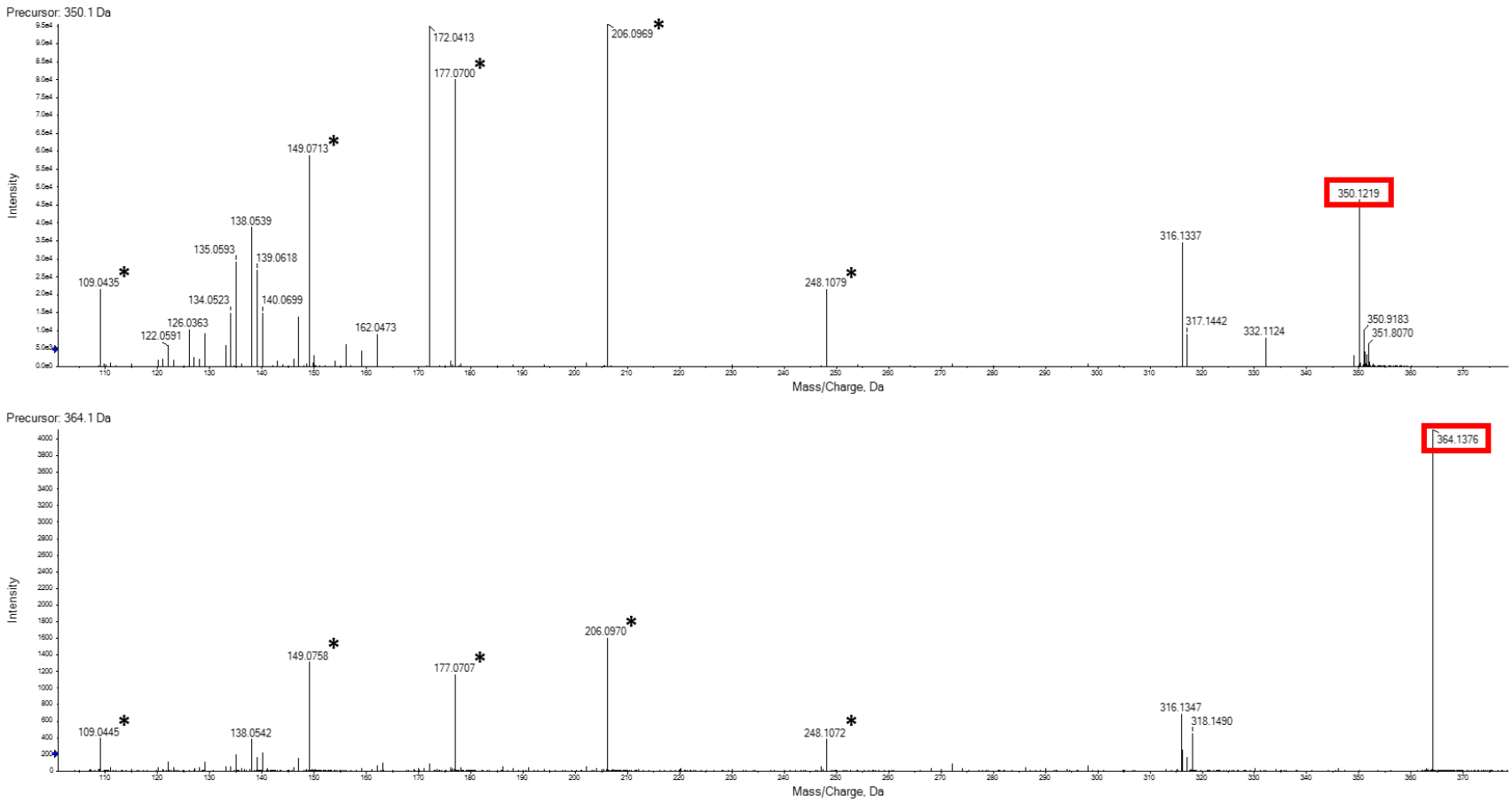

Figure 3.28. High-resolution Fragmentation Spectra of Prasugrel Active Metabolite and *S*-methyl Prasugrel Active Metabolite: The fragmentation pattern of the prasugrel active metabolite (upper panel) and the methylated active metabolite (lower panel). Masses unique to each compound are boxed in red and shared masses are marked by asterisks.

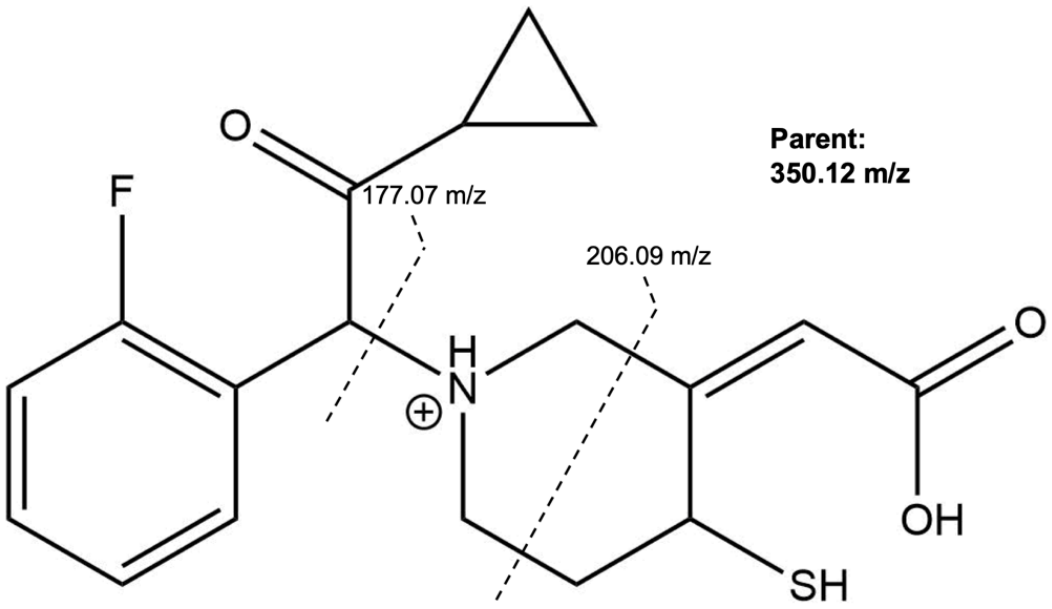

Figure 3.29. Predicted Fragmentation of the Prasugrel Active Metabolite: Potential fragments of the prasugrel active metabolite are denoted by the dashed lines.

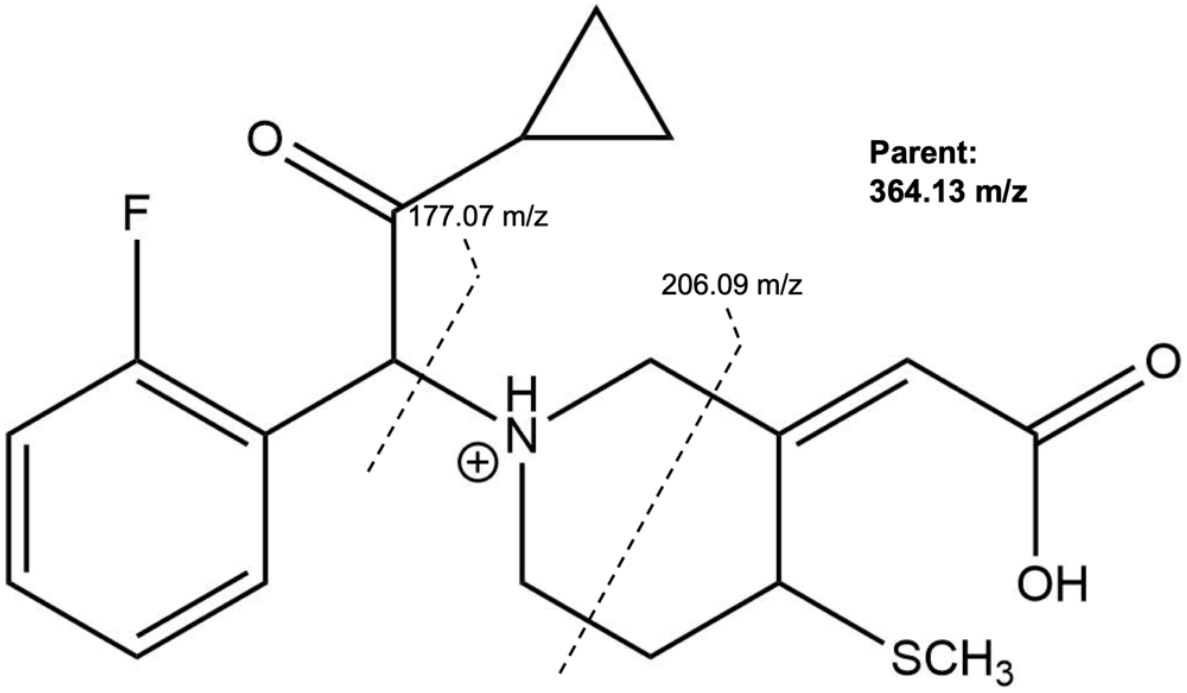

Figure 3.30. Predicted Fragmentation of the *S*-Methyl Prasugrel Active Metabolite: Potential fragments of the methylated prasugrel active metabolite are denoted by the dashed lines.

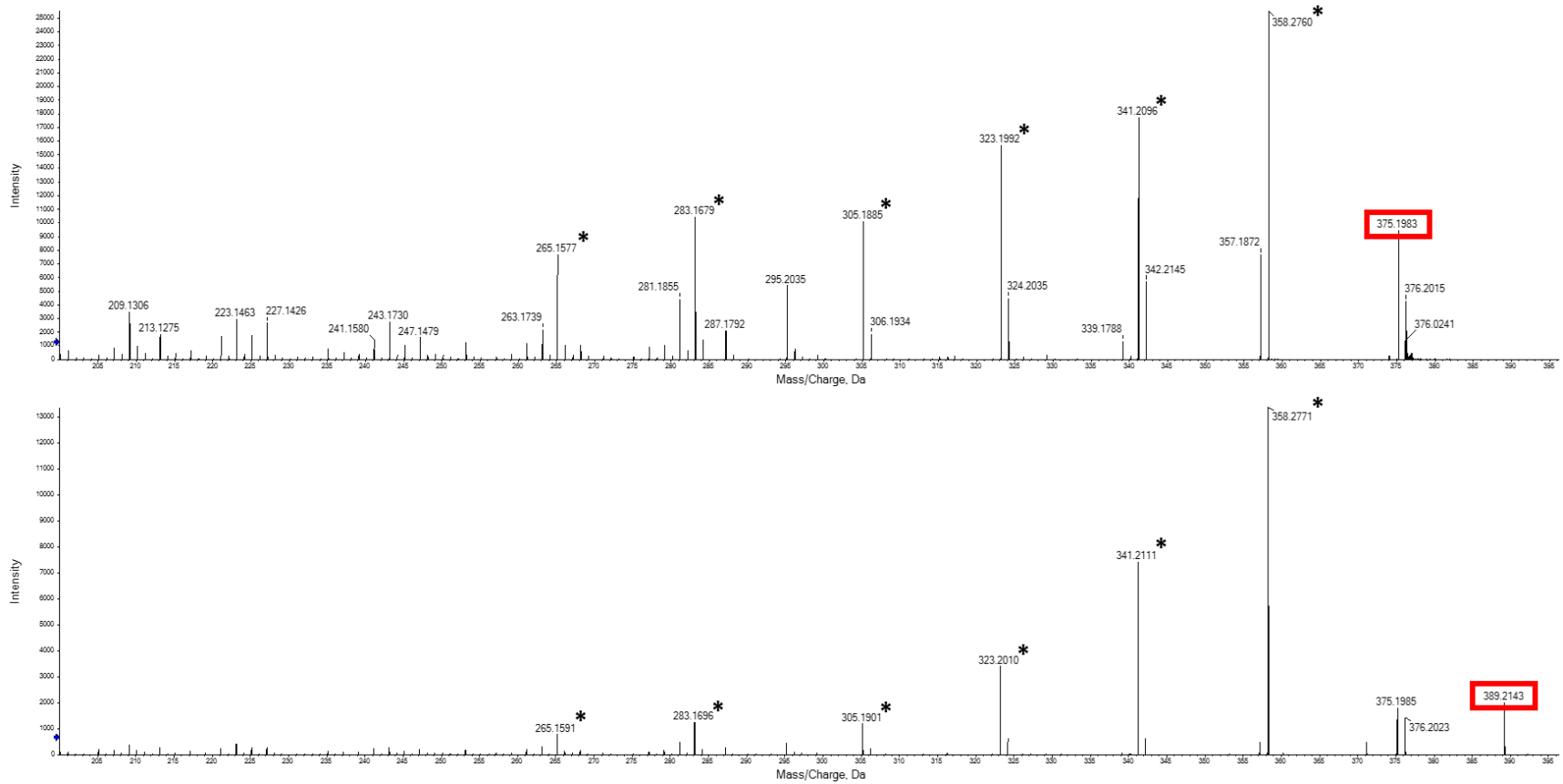

Figure 3.31. High-resolution Fragmentation Spectra of 7α-Thiospironolactone and *S*-methyl 7α-Thiospironolactone: he fragmentation spectra of 7α-Thiospironolactone is shown in the upper panel and the fragmentation spectra of the methylated 7α-Thiospironolactone is shown in the lower panel. Masses unique to each compound are boxed in red and shared masses are marked by asterisks.

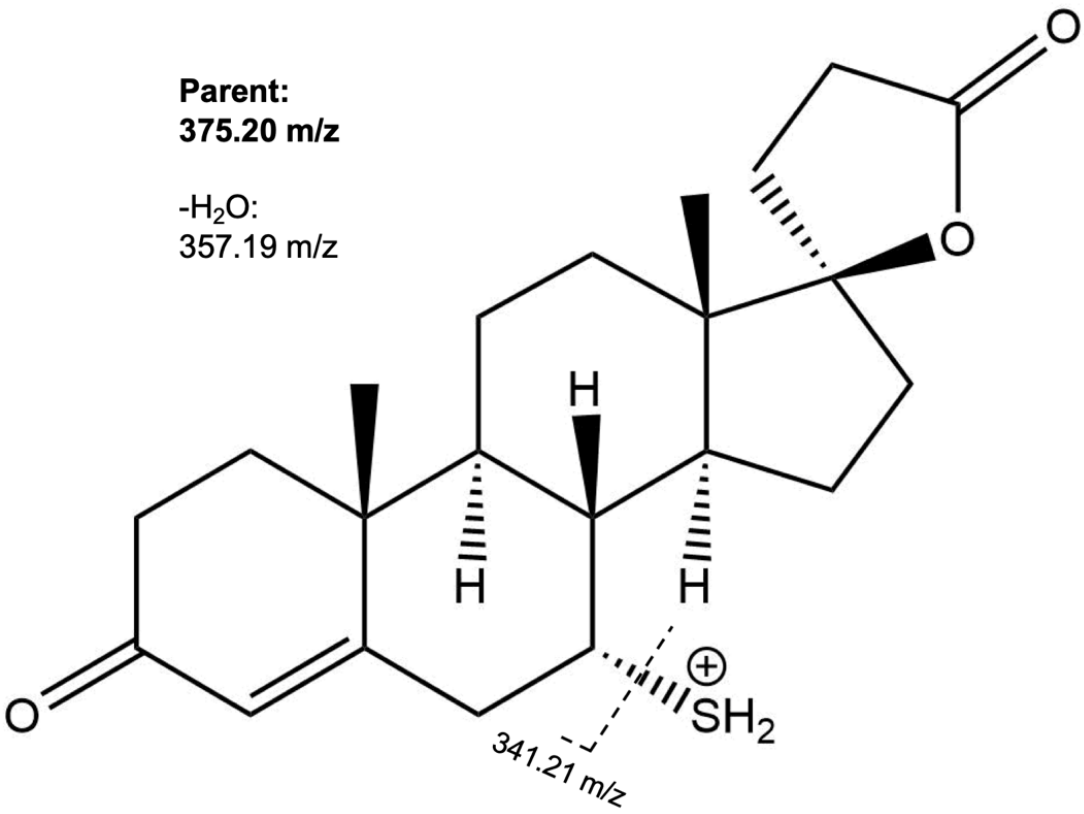

Figure 3.32. Predicted Fragmentation of 7α-Thiospironolactone: Potential fragments of 7α-Thiospironolactone are denoted by the dashed lines.

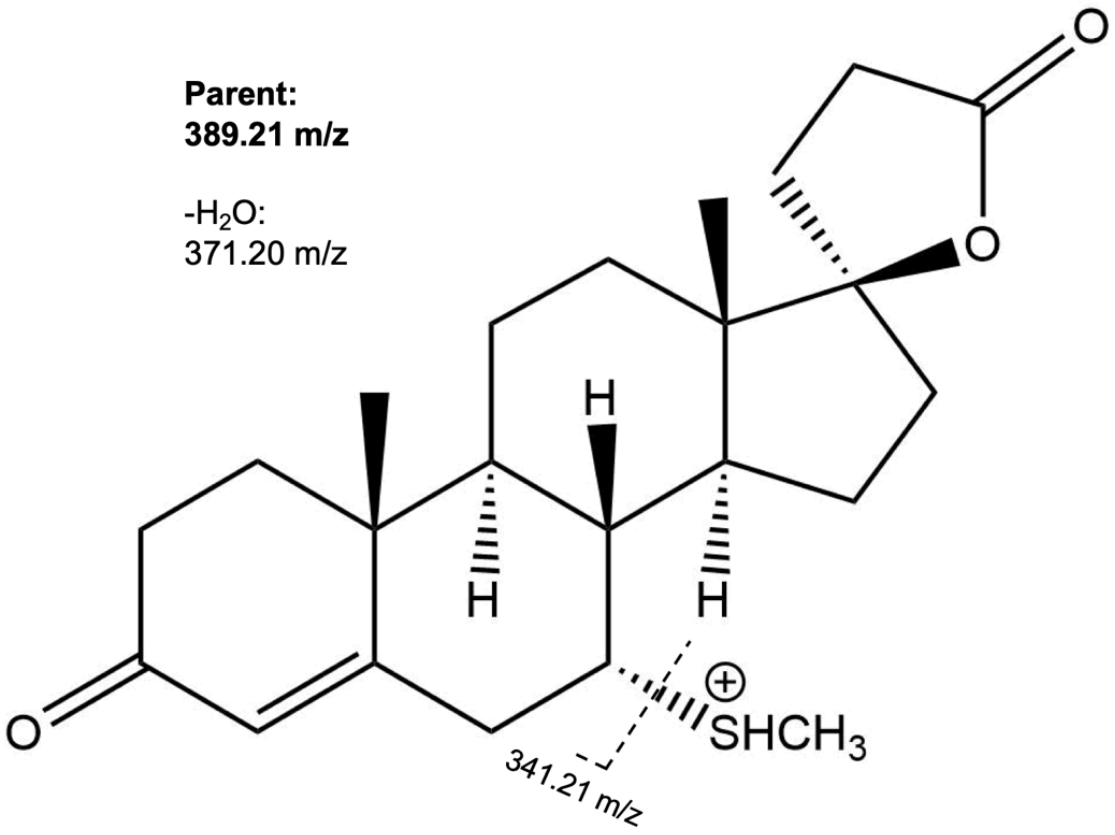

Figure 3.33. Predicted Fragmentation of *S*-Methyl 7α-Thiospironolactone: Potential fragments of methylated 7α-Thiospironolactone are denoted by the dashed lines.

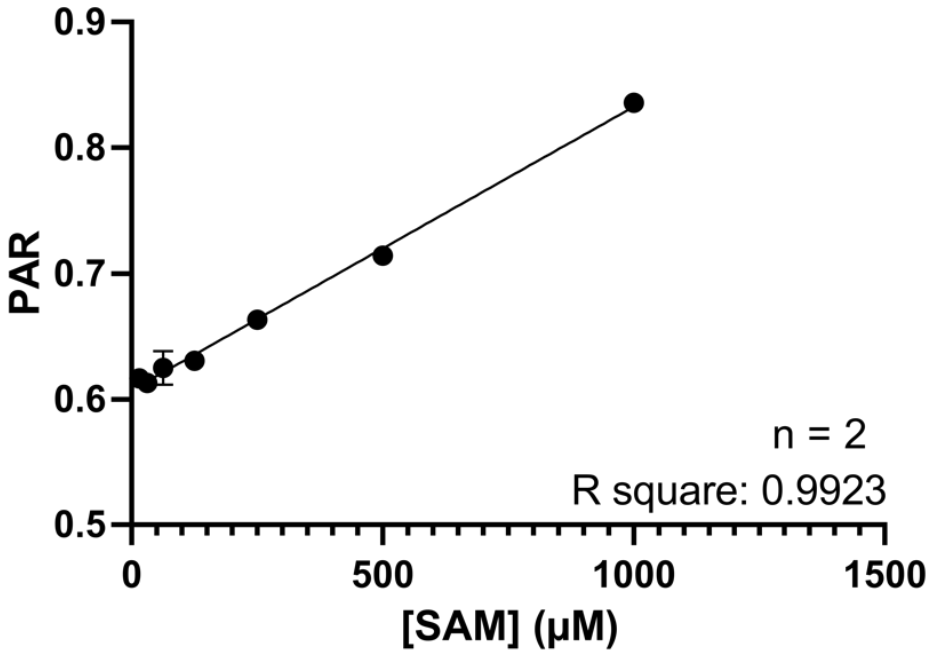

Figure 3.34. Effect of SAM Concentration on Non-enzymatic Captopril Methylation: Data are presented as the mean ± standard deviation.

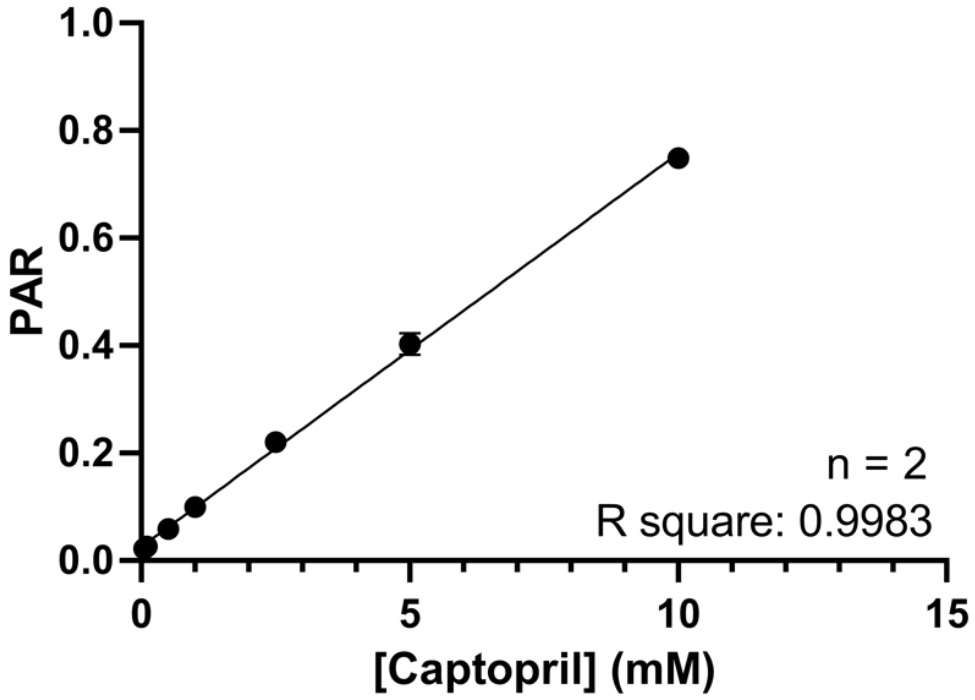

Figure 3.35. Effect of Captopril Concentration on Non-enzymatic Captopril Methylation:

Data are presented as the mean ± standard deviation.

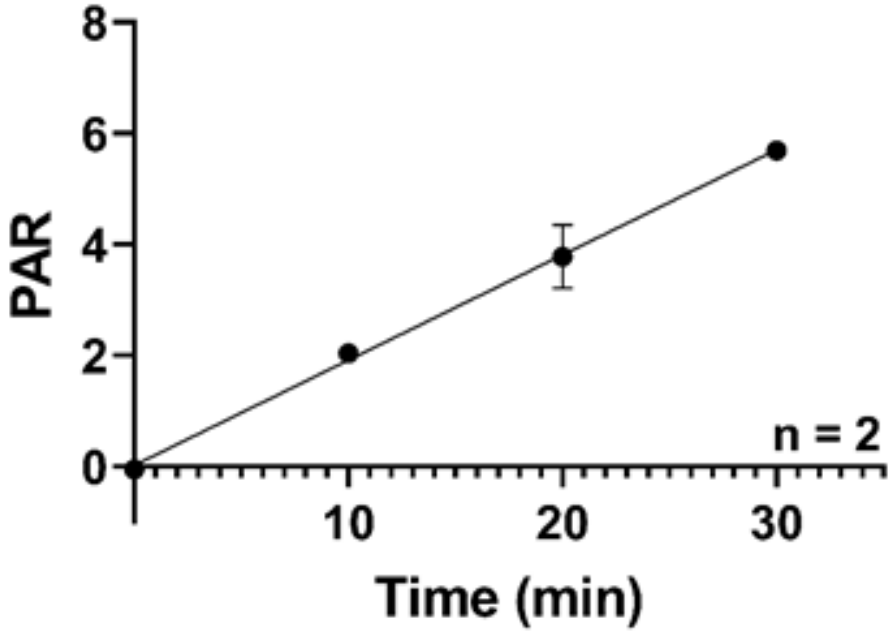

Figure 3.36: Time Linearity of pET21 METTL7B Captopril Methylation. All data are presented as the mean ± standard deviation.

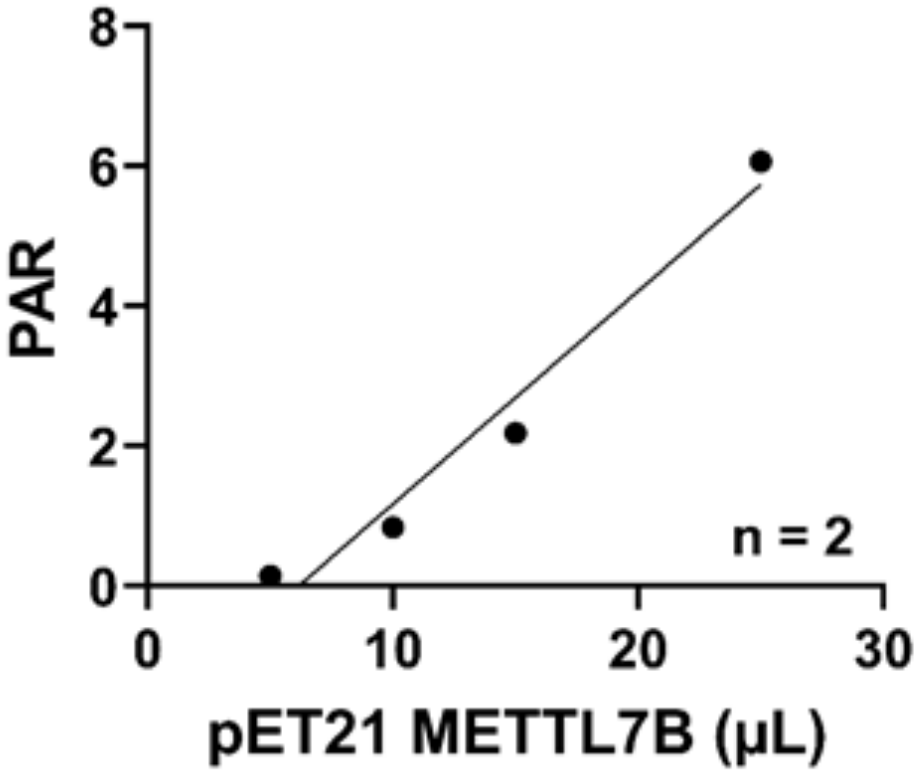

Figure 3.37: Protein Linearity of pET21 METTL7B Captopril Methylation. All data are presented as the mean ± standard deviation.

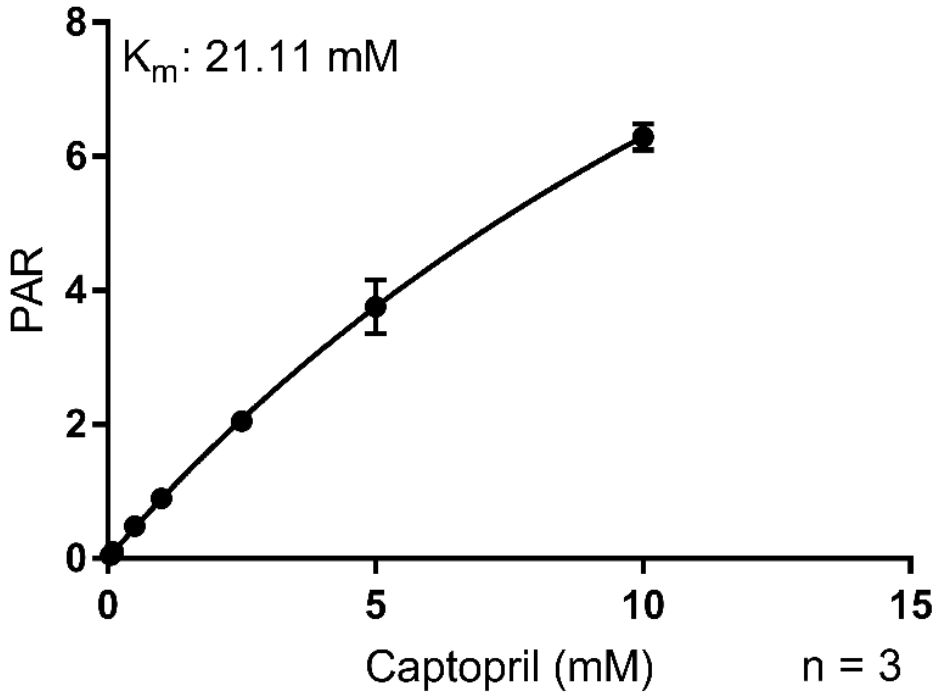

Figure 3.38. Rate of Captopril Methylation for pET21 METTL7B: Peak area ratio of captopril to internal standard vs concentration curve for captopril methylation as measured by formation of *S*-methyl captopril. Data presented as the mean ± standard deviation.

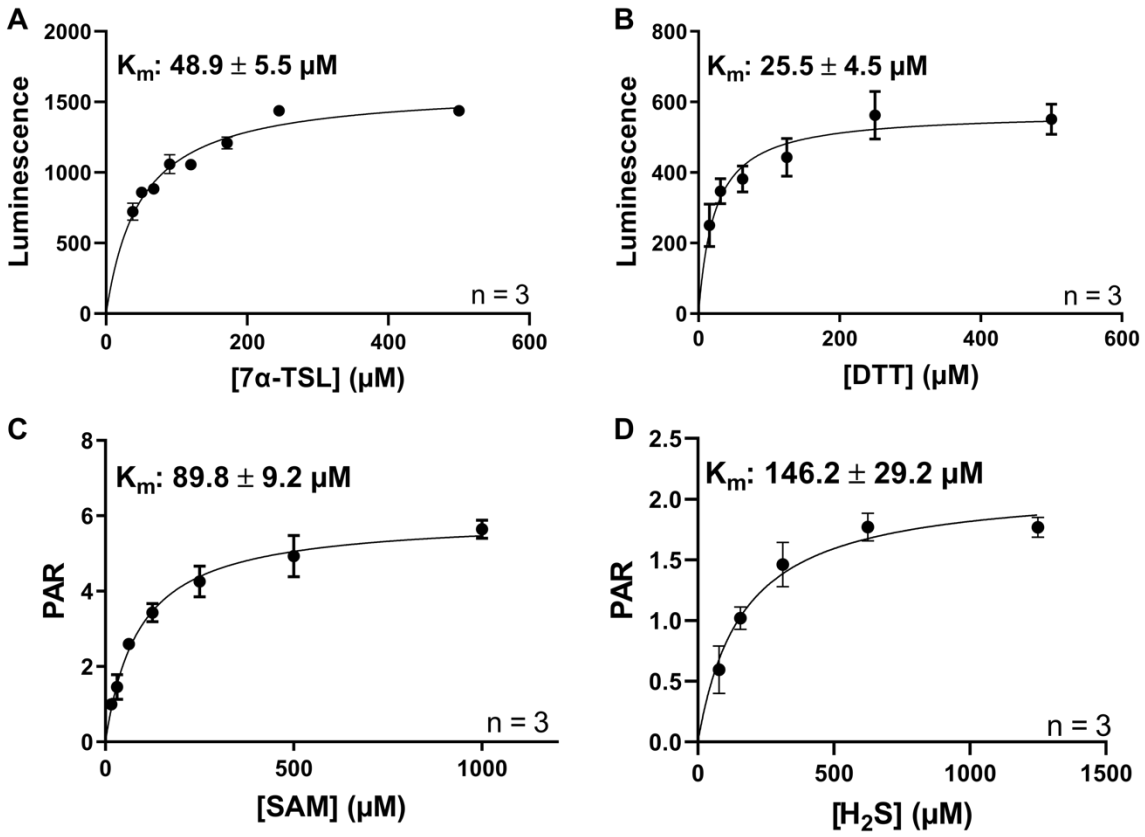

Figure 3.39. Rate of Thiol Methyl Formation for pET21 METTL7B with Multiple Probe Substrates: A) Luminescence vs. concentration curves for 7α-Thiospironolactone methylation as measured by SAH formation. **B)** Luminescence vs. concentration curve for dithiothreitol methylation as measured by SAH formation. **C)** Peak area ratio (PAR) vs concentration curve for *S*-adenosyl-*L*-methionine use as measured by captopril methylation. **D)** PAR vs concentration curve for hydrogen sulfide methylation as measured by formation of methanethiol. All data are presented as the mean ± standard deviation.

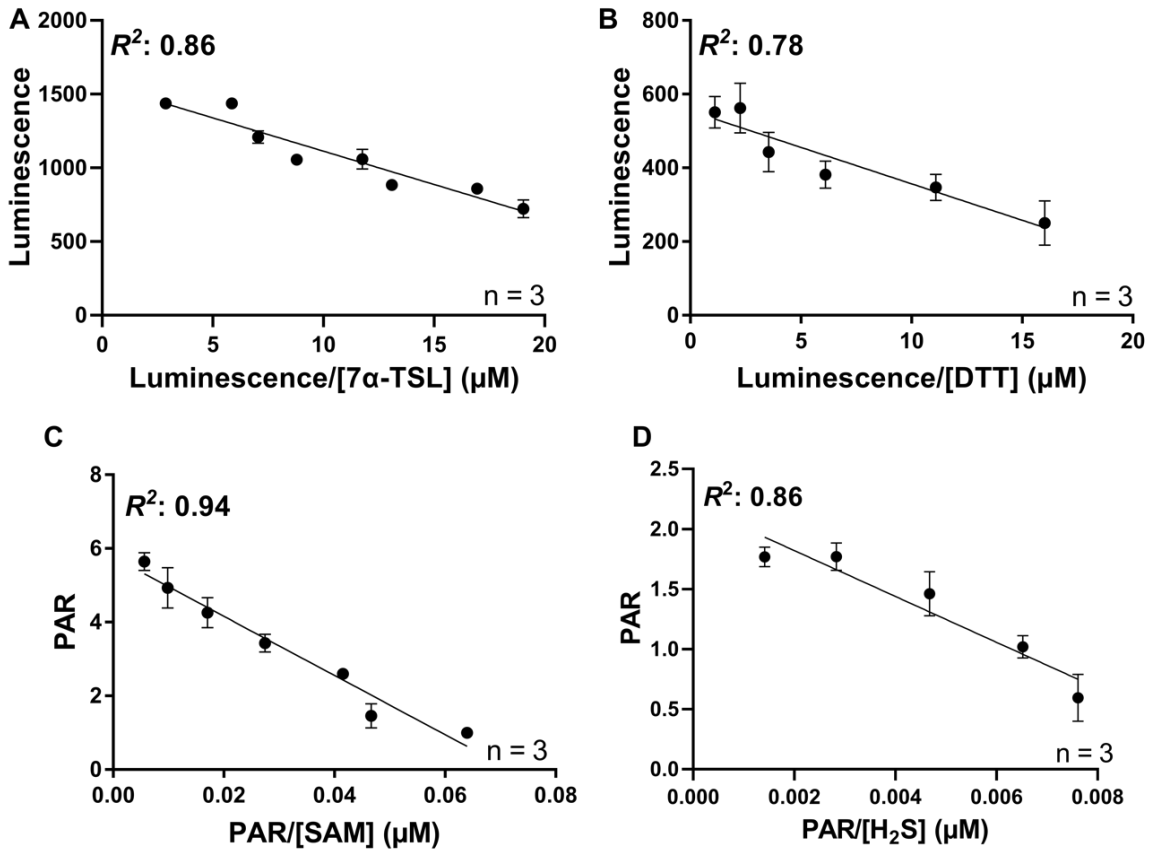

Figure 3.40. Eadie-Hofstee Transformations of Thiol Methylation by pET21 METTL7B. A) 7α-Thiospironolactone methylation measured by SAH formation. **B)** Dithiothreitol methylation measured by SAH formation. **C)** *S*-adenosyl-*L*-methionine use measured by captopril methylation. **D)** Hydrogen sulfide methylation measured by formation of methanethiol. Data presented as the mean ± standard deviation.

Bibliography:

1. AU - Subedi, G. P., AU - Johnson, R. W., AU - Moniz, H. A., AU - Moremen, K. W. & AU - Barb, A. High Yield Expression of Recombinant Human Proteins with the Transient Transfection of HEK293 Cells in Suspension. *JoVE* e53568 (2015). doi:doi:10.3791/53568
2. Thomas, P. & Smart, T. G. HEK293 cell line: A vehicle for the expression of recombinant proteins. *J. Pharmacol. Toxicol. Methods* **51**, 187–200 (2005).
3. Urbanowicz, R. A. *et al.* Antigenicity and Immunogenicity of Differentially Glycosylated Hepatitis C Virus E2 Envelope Proteins Expressed in Mammalian and Insect Cells. *J. Virol.* **93**, e01403-18 (2019).
4. Studier, F. W. & Moffattf, B. A. *Use of Bacteriophage T7 RNA Polymerase to Direct Selective High-level Expression of Cloned Genes*. *J. MoZ. Biol* **189**, (1986).
5. Baneyx, F. Recombinant protein expression in Escherichia coli. *Curr. Opin. Biotechnol.* **10**, 411–421 (1999).
6. Xiong, S. *et al.* Solubility of disulfide-bonded proteins in the cytoplasm of Escherichia coli and its “oxidizing” mutant. *World J. Gastroenterol.* **11**, 1077–1082 (2005).
7. Baneyx, F. & Mujacic, M. Recombinant protein folding and misfolding in Escherichia coli. *Nat. Biotechnol.* **22**, 1399–1408 (2004).
8. Cook, J. M. & Charlesworth, A. Insertion of inter-domain linkers improves expression and bioactivity of Zygote arrest (Zar) fusion proteins. *Protein Eng. Des. Sel.* **30**, 313–319 (2017).
9. Zuo, X. *et al.* Enhanced expression and purification of membrane proteins by SUMO fusion in Escherichia coli. doi:10.1007/s10969-005-2664-4

10. Harper, S. & Speicher, D. W. Purification of proteins fused to glutathione S-transferase. *Methods Mol. Biol.* **681**, 259–280 (2011).

11. Frangioni, J. V & Neel, B. G. Solubilization and Purification of Enzymatically Active Glutathione S-Transferase (pGEX) Fusion Proteins. *Anal. Biochem.* **210**, 179–187 (1993).

12. Chen, X., Zaro, J. L. & Shen, W.-C. Fusion protein linkers: property, design and functionality. *Adv. Drug Deliv. Rev.* **65**, 1357–1369 (2013).

13. Chant, A., Kraemer-Pecore, C. M., Watkin, R. & Kneale, G. G. Attachment of a histidine tag to the minimal zinc finger protein of the Aspergillus nidulans gene regulatory protein AreA causes a conformational change at the DNA-binding site. *Protein Expr. Purif.* **39**, 152–159 (2005).

14. Lebendiker, M. & Danieli, T. Production of prone-to-aggregate proteins. *FEBS Lett.* **588**, 236–246 (2014).

15. Shevchenko, A., Wilm, M., Vorm, O. & Mann, M. Mass Spectrometric Sequencing of Proteins from Silver-Stained Polyacrylamide Gels. *Anal. Chem.* **68**, 850–858 (1996).

16. Shevchenko, A., Tomas, H., Havliš, J., Olsen, J. V. & Mann, M. In-gel digestion for mass spectrometric characterization of proteins and proteomes. *Nat. Protoc.* **1**, 2856–60 (2006).

17. Shen, X. *et al.* Measurement of plasma hydrogen sulfide in vivo and in vitro. *Free Radic. Biol. Med.* **50**, 1021–31 (2011).

18. Shen, X., Peter, E. A., Bir, S., Wang, R. & Kevil, C. G. Analytical measurement of discrete hydrogen sulfide pools in biological specimens. *Free Radic. Biol. Med.* **52**, 2276–2283 (2012).

19. Shen, X., Kolluru, G. K., Yuan, S. & Kevil, C. G. Measurement of H2S in vivo and in vitro by the monobromobimane method. *Methods Enzymol.* **554**, 31–45 (2015).

20. Mokhonov, V. V *et al.* SlyD-deficient Escherichia coli strains: A highway to contaminant-free protein extraction. *Biochem. Biophys. Res. Commun.* **499**, 967–972 (2018).

21. Parsy, C. B., Chapman, C. J., Barnes, A. C., Robertson, J. F. & Murray, A. Two-step method to isolate target recombinant protein from co-purified bacterial contaminant SlyD after immobilised metal affinity chromatography. *J. Chromatogr. B* **853**, 314–319 (2007).

22. Kaluarachchi, H. *et al.* Metal selectivity of the Escherichia coli nickel metallochaperone, SlyD. *Biochemistry* **50**, 10666–10677 (2011).

23. Andersen, K. R., Leksa, N. C. & Schwartz, T. U. Optimized E. coli expression strain LOBSTR eliminates common contaminants from His-tag purification. *Proteins* **81**, 1857–1861 (2013).

24. Otterness, D. M., Keith, R. A., Kerremans, A. L. & Weinshilboum, R. M. Mouse liver thiol methyltransferase. Assay conditions, biochemical properties, and strain variation. *Drug Metab. Dispos.* **14**, 680–8 (1986).

25. Weinshilboum, R. M., Sladek, S. & Klumpp, S. Human erythrocyte thiol methyltransferase: Radiochemical microassay and biochemical properties. *Clin. Chim. Acta* **97**, 59–71 (1979).

26. Glauser, T. A., Kerremans, A. L. & Weinshilboum, R. M. Human hepatic microsomal thiol methyltransferase. Assay conditions, biochemical properties, and correlation studies. *Drug Metab. Dispos.* **20**, 247–55 (1992).

27. Glauser, T. A., Saks, E., Vasova, V. M. & Weinshilboum, R. M. Human liver microsomal thiol methyltransferase: inhibition by arylalkylamines. *Xenobiotica* **23**, 657–69 (1993).

28. Käenmäki, M. *et al.* Quantitative role of COMT in dopamine clearance in the prefrontal cortex of freely moving mice. *J. Neurochem.* **114**, 1745–1755 (2010).

29. Brown, D. D., Axelrod, J. & Tomchick, R. Enzymatic N-Methylation of Histamine. *Nature* **183**, 680 (1959).

30. Krynetski, E. Y. & Evans, W. E. Genetic Polymorphism of Thiopurine S-Methyltransferase: Molecular Mechanisms and Clinical Importance. *Pharmacology* **61**, 136–146 (2000).

31. Weinshilboum, R. M. & Sladek, S. L. Mercaptopurine pharmacogenetics: Monogenic inheritance of erythrocyte thiopurine methyltransferase activity. *Am. J. Hum. Genet.* **32**, 651–662 (1980).

32. Barok, M., Joensuu, H. & Isola, J. Trastuzumab emtansine: mechanisms of action and drug resistance. *Breast Cancer Res.* **16**, 209 (2014).

33. Lopus, M. Antibody-DM1 conjugates as cancer therapeutics. *Cancer Lett.* **307**, 113–118 (2011).

34. Lopus, M. *et al.* Maytansine and cellular metabolites of antibody-maytansinoid conjugates strongly suppress microtubule dynamics by binding to microtubules. *Mol. Cancer Ther.* **9**, 2689–2699 (2010).

35. Shen, B.-Q. *et al.* Non-Clinical Disposition and Metabolism of DM1, a Component of Trastuzumab Emtansine (T-DM1), in Sprague Dawley Rats. *Drug Metabolism Letters* **9**, 119–131 (2015).

36. Farid, N. A. *et al.* The Disposition of Prasugrel, a Novel Thienopyridine, in Humans. *Drug Metab. Dispos.* **35**, 1096 LP – 1104 (2007).

37. Smith, R. L., Gillespie, T. A., Rash, T. J., Kurihara, A. & Farid, N. A. Disposition and metabolic fate of prasugrel in mice, rats, and dogs. *Xenobiotica* **37**, 884–901 (2007).

38. Keith, R. A., Jardine, I., Kerremans, A. & Weinshilboum, R. M. Human erythrocyte

membrane thiol methyltransferase. S-methylation of captopril, N-acetylcysteine, and 7 alpha-thio-spirolactone. *Drug Metab. Dispos.* **12**, 717–24 (1984).

39. Babidge, W. J., Millard, S. H. & Roediger, W. E. Thiol methyltransferase activity in colonocytes and erythrocyte membranes. *J. Clin. Pathol.* **48**, 641–4 (1995).

40. Whiteman, M. & Winyard, P. G. Hydrogen sulfide and inflammation: the good, the bad, the ugly and the promising. *Expert Rev. Clin. Pharmacol.* **4**, 13–32 (2011).

41. Mustafa, A. K. *et al.* H2S Signals Through Protein S-Sulfhydration. *Sci. Signal.* **2**, (2010).

42. Li, L. *et al.* Hydrogen sulfide is a novel mediator of lipopolysaccharide-induced inflammation in the mouse. *FASEB J.* **19**, 1196–1198 (2005).

43. Pitcher, M. C. L., Beatty, E. R., Harris, R. M., Waring, R. H. & Cummings, J. H. Sulfur metabolism in ulcerative colitis: Investigation of detoxification enzymes in peripheral blood. *Dig. Dis. Sci.* **43**, 2080–5 (1998).

44. Whiteman, M. *et al.* Detection of hydrogen sulfide in plasma and knee-joint synovial fluid from rheumatoid arthritis patients: relation to clinical and laboratory measures of inflammation. *Ann. N. Y. Acad. Sci.* **1203**, 146–150 (2010).

45. Wu, D. *et al.* Hydrogen sulfide acts as a double-edged sword in human hepatocellular carcinoma cells through EGFR/ERK/MMP-2 and PTEN/AKT signaling pathways. *Sci. Rep.* **7**, 5134 (2017).

46. Wu, D. *et al.* Hydrogen sulfide in cancer: Friend or foe? *Nitric Oxide* **50**, 38–45 (2015).

47. Sen, N. & Snyder, S. H. Protein modifications involved in neurotransmitter and gasotransmitter signaling. *Trends Neurosci.* **33**, 493–502 (2011).

Chapter 4: Gene, Protein Expression, and Interindividual Variability of METTL7A and METTL7B in Human Liver Microsomes

Introduction:

Interindividual variability in drug metabolism pathways or drug targets can cause unintended toxicity or lack of efficacy for pharmaceutical compounds[1]. The presence of single nucleotide polymorphisms (SNPs) in the coding region of certain genes can alter enzyme function, is primarily responsible for interindividual variability, and is therefore the focus of the field of pharmacogenetics[2,3]. Many drugs exhibit some level of variable exposure within a population, however variability is most notable with narrow therapeutic index drugs where therapeutic and toxic serum concentrations are not very different, such as warfarin[4]. Warfarin is an oral anti-coagulant that is notoriously difficult to dose due to the presence of several SNPs in both the metabolic clearance pathways and the pharmacological target[5,6]. High levels of exposure can cause fatal bleeding while sub-therapeutic concentrations can lead to dangerous blood clots. Multiple clinical trials have been conducted to investigate the benefit of genotyping patients prior to dosing[7–9].

Thiol methylation is a pathway with well-known pharmacogenetic consequences. Thiopurine methyltransferase (TPMT) catalyzes the *S*-methylation of thiopurine cancer agents such as 6-mercaptopurine and azathioprine, which is a major route of metabolism and deactivation for these drugs[10,11]. Multiple SNPs present in the *TPMT* gene significantly impact enzyme activity, and subsequently, clearance of thiopurine compounds[12,13]. Impaired metabolism of thiopurine compounds increases their serum concentrations and can result in severe myelosuppression and bone marrow failure, which can be fatal[14]. Studies have successfully demonstrated that genotyping of patients prior to initiating azathioprine treatment can prevent toxic side effects in the presence of certain *TMPT* SNPs with reduced activity[15]. The

presence of these SNPs can be observed at the population level, where TPMT activity can vary up to five-fold between individuals[16].

Similar to TPMT, thiol methyltransferase (TMT) activity is also highly variable. TMT activity measured using 7α-Thiospironolactone methylation in single donor erythrocyte membranes exhibits a five-fold variation[17]. This variability appears to have a genetic component as there is a strong correlation between sibling-sibling and parent-offspring activities compared to parent-parent variability[18]. Therefore, TMT drug substrates may exhibit potential toxicity or lack of efficacy in certain populations with naturally low enzyme activity. So, in this chapter, we report the interindividual TMT activity variability in single donor human liver microsomes (HLMs) using multiple probe substrates.

METTL7B has a close ortholog in METTL7A and so we also investigated the gene, and relative protein expression, of METTL7A and METTL7B from proteomic and RNA-seq analyses respectively. There was no correlation between *METTL7A* and *METTL7B* gene expression in our samples. Methylation activity using hydrogen sulfide or captopril as substrates did not correlate with either relative protein expression of METTL7A, METTL7B, or both. Analysis of RNA-seq data suggested that *METTL7A* gene expression is correlated with other small molecule methyltransferases as well as oxidative stress proteins, whereas *METTL7B* gene expression was not correlated with any of the genes present in our subset. Finally, experiments in human cardiomyocytes subjected to doxorubicin vs. control indicated that *METTL7A* and *METTL7B* expression are sensitive to changes in cellular oxidative stress.

Materials and Methods:

Materials:

Buffer salts and captopril were acquired from Sigma-Aldrich (St. Louis, MO). *S*-adenosyl-*L*-methionine was obtained from New England Biolabs (Ipswich, MA). UPLC-grade solvents were obtained from Fisher Scientific (Hampton, NH). The prasugrel active metabolite was a gift from Dr. Allan Rettie. Single donor human livers were obtained from the University of Washington School of Pharmacy human liver bank.

Human Liver Microsome Preparation:

Frozen tissue was taken from individual donor livers and placed in labeled Falcon tubes on dry ice until further processing. The tissues samples were thawed on ice in homogenization buffer (50 mM KPi pH 7.4, 250 mM sucrose, 1 mM EDTA, and 1X Halt Protease inhibitor cocktail). The thawed tissue was transferred to a sterile petri dish on ice and a razor blade was used to remove fibrotic tissue. Next, the samples were placed in a 55 mL Dounce homogenizer and homogenized using 4-6 passes of a powered Teflon pestle. The homogenate was transferred to a centrifuge tube and spun at 8,000 x g for 30 minutes at 4 ^{o}C to pellet all unbroken cells, nuclei, and mitochondria. The supernatant was transferred to a clean ultracentrifuge tube and spun at 100,000 x g for 60 minutes at 4 ^{o}C. The supernatant, containing the cytosolic fraction, was collected and kept in Falcon tubes at -80 ^{o}C. The pellet, containing the microsomal fraction, was resuspended in 2 mL of homogenization buffer via Dounce homogenization, aliquoted, and stored at -80 ^{o}C until future use.

In vitro Captopril Methylation Optimization in Human Liver Microsomes:

Captopril methylation was optimized in human liver microsomes (HLMs) using a pooled 1 mg/mL HLM stock created by adding equal amounts of total protein from the following donor

livers: HL-145, HL-150, HL-154, HL-159, and HL-170. The pooled HLM stock was distributed across 1.5 mL Eppendorf tubes so that each tube contained 250 mg total protein. The tubes were centrifuged for 15 minutes at 25,000 x g to pellet the microsomes. The supernatant was aspirated and microsomes were resuspended in a variety of activity buffers using polypropylene pestles to 1 mg/mL final protein concentration. The first round of optimization began with 10 mM KPi pH 8.0, 20% glycerol buffer and buffer components were altered as shown on the X-axis of Figure 3.1. The second round of optimization began with 50 mM KPi pH 7.0, 20% glycerol, 10 mM $MgCl_2$, and 10 mM CHAPS. Buffer components were altered as listed on the X-axis of Figure 3.2.

Resuspended HLMs were added to clean 1.5 mL Eppendorf tubes. An aqueous captopril stock solution was added to a final concentration of 500 µM. The samples were pre-incubated at 37 ^oC for 2 minutes and the reaction was initiated by addition of SAM to a final concentration of 50 µM and a final volume of 250 µL. The samples were incubated for 30 minutes and enzyme activity was quenched via 1:6 addition of 15% (w/v) $ZnSO_4$. The internal standard was d_3-*S*-methyl-6-mercaptopurine and added as 15 µL of a 1 µg/mL solution. Samples were incubated on ice for 10 minutes, centrifuged, and the supernatant was analyzed via LC-MS/MS as detailed below.

The LC-MS/MS system used for initial captopril methylation analysis is an AB Sciex API 4000 mass spectrometer paired with a Waters Acquity LC. Compound separation was achieved using a 2.1x150 mm Acquity UPLC C18 RP Shield column and 0.1% formic acid in water and 0.1% formic acid in acetonitrile as solvents A and B respectively. Chromatographic separation was obtained using the following gradient: solvent B was initially set at 10% and increased to 30% from 0 to 1 minutes, held at 30% from 1 to 3 minutes, increased to 70% from 3

to 7 minutes, reduced to 10% from 6 to 7 minutes, and held at 10% from 7 to 10 minutes to allow for re-equilibration. Flow rate was held constant at 0.3 mL/min and flow was only diverted to the mass spectrometer from 2 to 8 minutes.

Methylated captopril, captopril, and the internal standard, d_3-*S*-methyl-6-mercaptopurine, were monitored in positive ionization mode. The monitored mass transitions m/z+ were 232.1 > 89.0, 232.1 > 184.0, 232.1 > 116.2 and 232.1 > 70.2 (methylated captopril), 217.9 > 116.4 (captopril), and 1701. > 126.2 (internal standard). The MS conditions were as follows: collision energy 25, 25, 19, 25, 25, 31 V for each transition respectively, declustering potential 80, 80, 76, 76, 80, 106 V for each transition respectively, entrance potential 10 V, curtain gas 10, medium collision gas, IonSpray 5000 V, desolvation temperature 350 ^{o}C, ion source gas #1 40 and ion source gas #2 50.

In vitro Prasugrel Active Metabolite Methylation Assay in Human Liver Microsomes:

Single donor human liver microsomes (240 µL of 0.15 mg/mL) were aliquoted into a 1.5 mL Eppendorf tube on ice along with 5 µL of 100 µM prasugrel active metabolite for a final concentration of 2 µM. Reaction tubes were pre-incubated at 37 ^{o}C for 2-3 minutes. Enzymatic activity was initiated via addition of 5 µL of 2.5 mM SAM for a final concentration of 50 µM and a final reaction volume of 250 µL. The samples were incubated at 37 ^{o}C for 25 min and quenched via a 1:10 addition of an aqueous 15% (w/v) $ZnSO_4$ solution and chilled on ice for 10 min. The d_3-6-mercaptopurine internal standard was added for a final concentration of 150 ng/mL. The tubes were vortexed and centrifuged at 13,000 x g for 5 min to pellet precipitated proteins. Supernatants were analyzed by liquid chromatography-tandem mass spectrometry (LC-MS/MS).

Analytical Measurement of Prasugrel Active Metabolite Methylation:

The LC-MS/MS system used for prasugrel active metabolite methylation analysis was an AB Sciex 4000 QTrap paired with a Waters Acquity LC. Compound separation was achieved using a 2.1x150 mm Acquity BEH C18 column and 0.1% formic acid in water and 0.1% formic acid in acetonitrile as solvents A and B respectively. The analytical column was not heated however the samples were kept at 5 ^{o}C. Chromatographic separation was obtained using the following gradient: solvent B was set at 10% initially, then increased to 50% during the first minute, followed by a decrease to 35% over the next three minutes, and re-equilibrated to the starting conditions for another 3.5 min for a total run time of 7.5 min. Flow rate was held constant at 0.3 mL/min and flow was only diverted to the mass spectrometer between 1.8 to 5.5 min.

S-methyl prasugrel active metabolite, prasugrel active metabolite, and the internal standard, d_3-6-mercaptopurine, were monitored in negative mode. The monitored mass transitions m/z^- were 349.0 > 99.0 and 349.0 > 215.0 (prasugrel active metabolite), 362.0 > 177.0 (*S*-methyl prasugrel active metabolite) and 170.1 > 128.2 (internal standard). The MS conditions were as follows: collision energy -30.0, declustering potential -50.0, entrance potential -10.0, collision cell exit potential -15.0, IonSpray voltage -4500.0, desolvation temperature 350 ^{o}C, curtain gas 10.0, ion source gas #1 40.0, and ion source gas #2 50.0.

In vitro Captopril Methylation Using Single Donor PRINCE HLMs:

In vitro captopril methylation was conducted using single donor HLMs diluted to 0.5 mg/mL in reaction buffer (50 mM KPi pH 7.0, 10 mM CHAPS, 20% glycerol, 150 mM NaCl). Dilute HLMs were added to the reaction vessel with captopril for a final concentration of 20 mM. The samples were pre-equilibrated at 37 ^{o}C for 2 minutes before initiation by addition of

SAM to a final concentration of 100 µM and final reaction volume of 150 µL. The reaction was incubated for 20 minutes and then quenched via addition of 15% (w/v) zinc sulfate in a 1:3 dilution to total reaction volume. The quenched solution was incubated on ice for 10 minutes followed by a 1:4 addition of a saturated barium hydroxide solution containing the d_3-S-methyl captopril internal standard. Following a second 10-minute incubation on ice, the solution was centrifuged at 5,000 x g for 15 minutes to pellet all precipitated proteins and salts.

After centrifugation, 75 µL of supernatant was transferred to an opaque polypropylene strip-well tube containing 5 µL of 2 M sodium hydroxide. Unreacted captopril was derivatized at room temperature for 1 hour in the dark via addition of 20 µL of 2.5 M maleimide to reduce ion suppression from non-methylated captopril. Derivatized samples were centrifuged and the supernatant was analyzed by LC-MS/MS as previously described.

Protein linearity optimization was conducted using an identical protocol as detailed above except for adjusting the final protein concentration to either 0.1, 0.5 or 1 mg/mL and the final captopril concentration to either 0.1, 1, or 10 mM.

Analytical Measurement of Captopril Methylation:

A Waters Xevo TQS mass spectrometer paired with a Waters Acquity LC is used to measure the methylated metabolite of captopril. Chromatographic separation was achieved using a 2.1x100 mm Ascentis Express RP Amide column and 0.1% formic acid in water and 0.1% formic acid in methanol as solvents A and B respectively. Column temperature was maintained at 50 ^{o}C at all times. The following gradient was employed: solvent B was held at 30% from 0 to 3 min, then held at 90% from 3 to 7 min, followed by re-equilibration to the starting conditions for another 3 min for a total run time of 10 min. Flow rate was held constant at 0.2 mL/min and flow was only diverted to the mass spectrometer between 2 to 7.5 min.

S-methyl captopril and the internal standard, d_3-*S*-methyl captopril, were monitored in positive ionization mode. The monitored mass transitions m/z+ were 232.1 > 89 and 232.1 > 116 (S-methyl captopril) as well as 235.1 > 91.9 and 235.1 > 115.9 (internal standard). The MS conditions were as follows: collision energy 15 V, cone voltage 30 V, capillary voltage 3.2 kV, desolvation temperature 450 °C, desolvation gas flow 1,000 L/hr and cone gas 150 L/hr.

In vitro Hydrogen Sulfide Methylation Using Single Donor PRINCE HLMs:

In vitro hydrogen sulfide methylation was conducted using single donor HLMs diluted to 0.5 mg/mL in reaction buffer (50 mM KPi pH 7.0, 10 mM CHAPS, 20% glycerol, 150 mM NaCl). All steps were conducted in a glove box under nitrogen unless otherwise indicated. Dilute HLMs were aliquoted into a polypropylene deep-well plate on ice along with SAM and NaSH for a final volume of 150 µL and 1.5 mM and 100 µM for NaSH and SAM concentrations respectively. The plate was capped with a silicon mat and placed in a 37 °C water bath for 45 min under normal atmosphere. After incubation, the plate was placed back on ice under nitrogen and quenched via a 1:15 addition of 0.3 M sodium hydroxide. 110 µL of the quenched reaction solution was added to 50 µL of 20 mM monobromobimane (MBB), based off of published H_2S derivatization method[19–21]. Once capped under nitrogen, the reaction plate was incubated at room temperature on an orbital shaker at 450 rpm for 30 min.

The MBB derivatization was quenched by addition of 50 µL of 200 mM 5-sulfosalicylic acid and 10 µL of the ethyl 2-aminothiazole carboxylate (EATC) internal standard. Protein was precipitated by addition of 15% (w/v) zinc sulfate and barium hydroxide as previously detailed. Samples were centrifuged at 4,000 x g for 15 min and the supernatant was analyzed by LC-MS/MS.

Analytical Measurement of Methanethiol:

The LC-MS/MS system used for hydrogen sulfide methylation analysis was a Waters Xevo TQS mass spectrometer paired with a Waters Acquity LC. Compound separation was achieved using a 2.1x150 mm Acquity UPLC BEH Shield RP column and 0.2% acetic acid in water and 0.2% acetic acid in acetonitrile as solvents A and B respectively. Column temperature was maintained at 25 ^{o}C at all times. Chromatographic separation was obtained using the following gradient: solvent B was held at 40% from 0 to 1 minutes, ramped to 90% from 1 to 3.5 minutes, held at 90% from 4.5 to 5 minutes followed by re-equilibration to the starting conditions for another minute. Flow rate was held constant at 0.3 mL/min and flow was only diverted to the mass spectrometer from 1 to 4.5 minutes.

Derivatized methanethiol and the internal standard, EATC, were monitored in positive ionization mode. The monitored mass transitions m/z+ were 239.22 > 175.24 and 239.22 > 192.2 (derivatized methanethiol) as well as 173.17 > 72.11 and 173.17 > 127.06 (internal standard). The MS conditions were as follows: collision energy 24, 10, 24, 16 V for each transition respectively, cone voltage 56 V, capillary voltage 2.9 kV, desolvation temperature 450 ^{o}C, desolvation gas flow 1,000 L/hr and cone gas 150 L/hr.

RNA Sequencing:

RNA sequencing was conducted by Dr. Katrina Claw (HLM samples) and Dr. Eric Evangelista (human cardiomyocytes). Detailed protocols can be found in published works[22,23].

Relative Proteomic Analysis:

Relative proteomic analysis was conducted by various members of the Prasad lab using published methodology[24,25].

Data Analysis:

All experiments were conducted with biological triplicates and repeated at least two times on two separate days when possible. All data are reported as the mean ± standard deviation or mean ± range for duplicate measurements. Correlation analysis was conducted using Spearman correlation and significance was assigned by a two-tailed *P* value below 0.05. All statistical analysis was conducted using GraphPad Prism, version 8.3.1 for Windows (GraphPad Software, La Jolla, CA).

Results:

Optimization of Thiol Methyltransferase Activity in Human Liver Microsomes:

TMT activity was optimized in human liver microsomes (HLMs) by altering incubation conditions. A 1 mg/mL stock of pooled HLMs was created using equivalent amounts of protein from HL-145, HL-150, HL-154, HL-159, and HL-170 microsomes which were prepared fresh following published protocols[26]. Captopril methylation did not change with the addition, or increased concentrations, of sodium chloride, or cryopreservants such as glycerol or sucrose. Addition of EDTA did not alter enzyme activity but lowering the buffer pH or adding specific divalent cations at high concentrations enhanced methylation activity (Figure 4.1). Both potassium phosphate and Tris buffered solutions displayed similar levels of activity above 50 mM. Non-ionic detergents such as Triton X-100, Tween-20, and *n*-dodecyl ß-D-maltoside (DDM) severely reduced captopril methylation, while enzyme activity increased with the addition of the zwitterionic detergent CHAPS (Figure 4.1).

Based on the different conditions tested, 50 mM KPi pH 7.0, 20% glycerol, 10 mM $MgCl_2$, and 10 mM CHAPS was chosen as the optimal buffer to measure captopril methylation and for experiments investigating the impact of several divalent cations on activity.

The effect of adding divalent cation salts to the incubation buffer was further tested using the same set of pooled HLMs above. TMT activity decreased upon removal of CHAPS, magnesium chloride, or both, from the reaction buffer. Chelating the magnesium ions via addition of EDTA reduced turnover. Other divalent cations consistently reduced captopril methylation in HLMs compared to the optimized reaction buffer (Figure 4.2). A white cloudy precipitate was observed over time in many tested activity assay buffers, including those containing magnesium chloride.

Optimization of HLM Incubation Parameters:

To be consistent with the proteomics results, a second preparation of pooled HLM stock was created using equal protein amounts of freshly prepared microsomes from the same 20 individual donor livers used in the Prasad lab Proteomics-based Research Initiative for Non-CYP Enzymes (PRINCE) study. The specific donor livers are noted in later figures. Captopril methylation was linear with respect to total protein at all substrate concentrations tested (Figure 4.3). A similar experiment was repeated for hydrogen sulfide methylation however only a subset of the data points were analyzed due to instrumentation issues. Preliminary data analysis indicated that hydrogen sulfide methylation was also linear within the same protein concentration range tested for captopril. A final protein concentration of 0.5 mg/mL was chosen for all subsequent HLM screening experiments for both captopril and hydrogen sulfide.

A range of captopril concentrations was tested at each HLM concentration in order to roughly estimate kinetic parameters (Figure 4.4). The apparent K_m values were below 7 mM at all concentrations tested. Therefore, a final concentration of 20 mM was chosen to test for variability of methylation activity in individual HLMs.

Investigation of Interindividual Variability for Various Substrates:

TMT activity was initially tested using all single donor human liver microsomes available in the Totah lab HLM bank from many different HLM preparations. Captopril methylation activity varied up to 60-fold (Figure 4.5) across all samples however activity was potentially impacted by differences in preparation date or length of storage at -80 ºC (Figure 4.6). Therefore, fresh HLMs were prepared from PRINCE liver samples to investigate preparation- and storage-independent variation.

PRINCE liver HLMs exhibited a 9-fold variation in captopril methylation (Figure 4.7) and an 8-fold variation in hydrogen sulfide methylation (Figure 4.8). Activity was normalized to the least active liver, HL-136.

Correlation Analysis of Single Donor HLM Methyltransferase Variability:

A subset of the HLMs presented in Figure 4.5 were also tested for methylation of the prasugrel thiol active metabolite in addition to captopril. Methyltransferase activity for both substrates was highly correlated between single donors (Figure 4.9). All associations were conducted using non-parametric Spearman rank correlation, which does not assume a normal distribution of data points or homoscedasticity. Similar correlation analysis was conducted using the PRINCE liver HLMs. A strong positive correlation was observed between the formation of *S*-methyl captopril and methanethiol (Figure 4.10).

Correlation Analysis of METTL7A and METTL7B Gene and Protein Expression:

METTL7A and METTL7B expression was measured in the PRINCE livers by the Prasad lab. Individual METTL7B or METTL7A expression levels were corrected relative to the amount of protein measured in HLMs pooled from all the individual samples tested. It is unclear which

protein is expressed at higher levels in individual samples however both METTL7A and METTL7B were measurable in every liver.

RNA sequencing analysis of the University of Washington School of Pharmacy human liver bank was conducted by Dr. Katrina Claw in the Thummel lab. METTL7A and METTL7B relative protein did not correlate with gene expression in PRINCE livers (Figure 4.11, Panels A and B). Similarly, gene expression of *METTL7A* did not correlate with *METTL7B* (Figure 4.11, Panel C). Relative protein expression between both enzymes was significantly positively correlated (Figure 4.11, Panel D).

Correlation Analysis of Methyltransferase Activity and Relative Protein Expression:

Correlation of methyltransferase activity with several substrates was investigated with respect to relative METTL7A and METTL7B expression levels in PRINCE livers. No correlation was observed between methyltransferase activity and protein expression for captopril (Figure 4.12) or hydrogen sulfide (Figure 4.13).

Analysis of RNA-seq Gene Expression Correlation to METTL7A and METTL7B:

Over four hundred single donor samples were subjected to RNA-seq analysis in the Thummel lab. A subset of genes involved in small molecule methylation and redox response pathways was mined from the original dataset and examined in detail. *METTL7A* gene expression was highly correlated with multiple genes involved in cellular redox and arachidonic acid signaling pathways, including cytochrome P450 2J2 (*CYP2J2),* epoxide hydrolase 2 (*EPHX2),* catalase (*CAT),* and both superoxide dismutase 1 and 2 (*SOD1* and *SOD2*) (Figure 4.14, Panels A-E). *METTL7A* gene expression was also highly correlated with numerous small molecule methyltransferases, such as histamine *N*-methyltransferase (*HNMT),* catechol *O*-

methyltransferase (*COMT),* glycine *N*-methyltransferase (*GNMT),* phosphatidylethanolamine *N*-methyltransferase (*PEMT),* and thiopurine methyltransferase (*TPMT)* (Figure 4.14, Panels F-J).

METTL7B gene expression only weakly correlated with *TPMT* and heme oxygenase 1 (*HMOX1)* gene expression (Figure 4.15).

Effect of Doxorubicin Treatment on Gene Expression in Human Cardiomyocytes:

RNA sequencing analysis was performed on human ventricular cardiomyocytes that were treated with 20 μM doxorubicin (a clinically relevant concentration) for 24 hours compared to un-treated control cells. Treatment with doxorubicin significantly decreased gene expression of *METTL7A, METTL7B*, and *PEMT* (Figure 4.16). The expression levels of other small molecule methyltransferases such as *TPMT* and *COMT* were not affected (Figure 4.16).

The effect of doxorubicin treatment on genes involved in hydrogen sulfide anabolism and catabolism was also investigated (Figure 4.17). Expression of hydrogen sulfide-producing enzymes, namely cystathionine beta-synthase (*CBS),* cystathionine gamma-lyase (*CTH),* and 3-mercaptopyruvate sulfurtransferase (*3MST)*, was not significantly altered upon doxorubicin treatment. Hydrogen sulfide-depleting enzymes, such as *METTL7B, METTL7A,* and sulfide-quinone reductase (*SQR)*, were significantly downregulated with doxorubicin treatment. Rhodanese was the only significantly upregulated gene in the presence of doxorubicin.

Discussion:

Captopril methylation activity was optimized in pooled human liver microsomes prior to variability screening. Multiple conditions were altered such as buffer pH, detergent, ionic strength, and cryoprotectant. Methylation activity measured using captopril as a probe substrate was increased by lowering the buffer pH from 8.0 to 7.0, adding magnesium chloride, or adding

the zwitterionic detergent CHAPS. The increase in enzymatic activity at lower pH was surprising because the aliphatic thiols should be more reactive towards S_N2 reactions when deprotonated. Therefore, the lower pH may instead stabilize the protein structure, resulting in increased rates of enzymatic methylation. Captopril methylation activity decreased only following addition of non-ionic detergents such as Triton X-100, Tween-20, and *n*-dodecyl ß-D-maltoside. These detergents may disrupt the microsomal vesicle integrity or induce protein conformational changes, which has been reported previously for non-ionic detergents with other proteins[27].

The increased activity with the addition of magnesium ions was very interesting because other methyltransferases are known to require divalent cation cofactors, such as catechol *O*-methyltransferase, which is magnesium-dependent[28]. TMT activity was not changed upon addition of EDTA alone which suggests that either the enzyme does not bind magnesium directly, or that it loses any bound cations during microsome preparation. However, the increase in enzyme activity is magnesium-dependent because the increase was not observed upon chelation of free magnesium by EDTA. Interaction between METTL7B and chaperone proteins in HLMs could also explain the altered activity upon the addition of magnesium. Chaperone proteins require the presence of magnesium and ATP to dissociate from their binding targets[29]. If residual ATP is present in the microsomal preparations, addition of magnesium could help dissociate chaperone proteins from thiol methyltransferase proteins, resulting in an increase in specific activity. In contrast, addition of magnesium did not increase the activity of purified recombinant METTL7B (Chapter 3). This observation supports the idea that the effect observed in microsomes is mediated by altering protein-protein interactions.

Further buffer optimization demonstrated that removal of magnesium or CHAPS from the activity assay buffer decreased captopril methylation in HLMs. Additional divalent cations were tested (Figure 4.2) however none produced the same level of activity as that observed with magnesium. Unfortunately, a white precipitate formed over time in magnesium-containing buffers, likely due to formation of insoluble magnesium phosphate. Therefore, magnesium was omitted from future incubation conditions to keep reaction conditions as consistent as possible between samples.

Multiple batches of single donor human liver microsomes were prepared at different times from donor livers of the University of Washington School of Pharmacy liver bank. Initially, captopril methylation activity was tested across all batched and varied up to 60-fold, however older stocks exhibited lower activity that may have artifactually increased the observed variability. Nonetheless, high correlation of captopril methylation to prasugrel active metabolite methylation in the same HLM sample set suggested that thiol methyltransferase activity is catalyzed by one enzyme or perhaps multiple co-regulated enzymes, as previously proposed[17].

The new batch of HLMs was processed and stored using a single common protocol for activity and proteomic analysis in order to reduce artifacts in future variability studies. Both captopril and hydrogen sulfide methylation were highly correlated and displayed 8- to 9-fold variation in activity. The high correlation indicates that each compound is methylated by a single enzyme or co-regulated enzymes. Additionally, prior studies have likely underestimated the interindividual variability in thiol methyltransferase activity, possibly due to using erythrocyte membranes rather than liver microsomal fractions[17,30,31]. Our results are more appropriate for studying the impact of variability on drug exposure and clearance. The observed thiol methylation variability may have clinical implications, especially since up to 20% of orally

dosed captopril undergoes *S*-methylation[32]. The clinical impact of the variable methylation activity will be most relevant for thiol-containing drugs with narrow therapeutic indices.

The co-regulation of METTL7A and METTL7B was investigated using RNA sequencing gene expression data as well as relative proteomic protein expression data. Neither *METTL7A* nor *METTL7B* gene expression correlated with their respective relative protein expression. Additionally, no correlation existed between *METTL7A* and *METTL7B* gene expression levels which indicates that co-regulation is not occurring at the transcriptional level. Interestingly, relative protein expression was highly correlated despite the disconnect to gene expression. This suggests that METTL7A and METTL7B may be co-regulated at the translational or post-translational level given the lack of mRNA expression correlation. Preliminary work using intact protein mass spectrometry did not identify major post-translational modifications however further investigation is required. The apparent co-regulation of METTL7 protein concentration also supports the unimodal distribution of activity observed in prior studies as well as the reported biphasic kinetics[33,34]. Kinetic characterization of METTL7B did not indicate biphasic turnover, therefore the reported biphasic activity may be due to the presence of METTL7A. Purification and kinetic characterization of recombinant METTL7A is a high priority. Additionally, the correlation between METTL7A and METTL7B proteins will be further investigated with quantitative measurement to determine if they are truly correlated.

Unfortunately, the relative expression of either METTL7A, METTL7B, or both did not correlate with the observed variable methylation activity in single donor HLMs. There are many reasons for the lack of correlation including the presence of activity-modifying post-translational modifications, co-enzymes, or other potential thiol methyltransferases that have not been identified. Quantitative proteomic analysis on the same PRINCE liver HLM samples used for

interindividual variability will be performed to confirm if methylation of captopril and hydrogen sulfide are correlated to either protein. Additionally, kinetic parameters will be measured for purified recombinant METTL7A which can be compared to METTL7B and HLM kinetics.

Finally, both *METTL7A* and *METTL7B* mRNA expression levels are correlated to other genes involved in methylation and oxidative stress pathways. *METTL7A* expression appears to be tightly regulated with several genes that are known to respond to reactive oxygen species (ROS), either directly or through arachidonic acid signaling. This is likely due to the fact that METTL7A can efficiently methylate hydrogen sulfide which is highly tuned to the redox state of the cell[35–37]. Therefore, METTL7A may be part of major redox-sensitive signaling pathways governing cellular response to stress. Further experimentation is required to elucidate the exact relationships and their implications in cell health. Additionally, *METTL7A* expression was correlated with multiple other small molecule methyltransferases. The implications of this are currently unknown however the intracellular ratio of SAM to SAH is tightly controlled[38,39]. Since SAM is also used as a cofactor for epigenetic DNA methylation, it is possible that other enzymatic sources of SAM degradation are under some type of epigenetic control.

METTL7B expression was slightly correlated with a different methyltransferase, *TPMT,* and a redox response enzyme, *HMOX1*. Therefore, *METTL7B* is likely not as tightly regulated by redox signaling pathways as *METTL7A* but could still be impacted by other regulatory pathways not investigated at this time. While METTL7B can also methylate hydrogen sulfide, the lack of correlation to redox signaling genes suggests that hydrogen sulfide methylation may not be its primary role in the cell. The siRNA results presented in Chapter 2 indicate that METTL7B may act as a backup enzyme in case *METTL7A* expression is decreased. Therefore, our working hypothesis is that METTL7A primarily methylates hydrogen sulfide while

METTL7B preferentially methylates xenobiotics or other, yet to be identified, endogenous substrates. Measuring the rate of METTL7A-mediated hydrogen sulfide methylation is warranted. Also, more extensive RNA-seq pathway analysis is required to fully characterize *METTL7A* and *METTL7B* signaling pathways.

Finally, the role of METTL7A and METTL7B as redox enzymes was further confirmed by RNA-seq data in human cardiomyocytes. Cardiomyocytes were treated with doxorubicin that increases ROS signaling pathways, mimicking severe oxidative stress. While the expression of most small molecule methyltransferases did not change, both *METTL7A* and *METTL7B* were downregulated, which indicates that they are regulated separately from other methyltransferase enzymes in cardiomyocytes. Sulfide-quinone reductase, the first step in oxidative hydrogen sulfide metabolism, was also highly downregulated yet hydrogen sulfide-producing enzyme expression levels did not change significantly. It appears that, in times of oxidative stress, the cell limits hydrogen sulfide catabolism by downregulating *METTL7A, METTL7B,* and *SQR* but not *CBS, CTH,* or *3-MST*. This may lead to an increase in intracellular hydrogen sulfide concentrations, which could act to help mitigate the effects of reactive oxygen species, however further testing is required.

Conclusions:

Overall, TMT activity was highly variable (almost 10-fold) between individuals in single donor HLM experiments. Variability was somewhat larger than previously reported, increasing potential for toxicity or lack of efficacy for TMT-metabolized drugs. Methylation of multiple probe substrates was highly correlated, which suggests that one enzyme is responsible or there is a less likely set of co-regulated enzymes not yet identified. *METTL7A* and *METTL7B* gene

expression was not correlated however protein expression levels were highly correlated. Relative protein expression levels of either METTL7A or METTL7B did not explain the observed methyltransferase activity variation, which suggests that perhaps there are other thiol methyltransferase enzymes to be discovered. *METTL7A* expression was highly correlated with other small molecule methyltransferases and redox enzymes, however *METTL7B* expression was not. Oxidative stress experiments in human cardiomyocytes suggest that both METTL7A and METTL7B are important in the cellular response to oxidation, likely due to their metabolism of hydrogen sulfide. Further experiments are needed to determine their exact role in health and disease, as well as whether interindividual variation in their expression predisposes certain populations to drug toxicity or diseases.

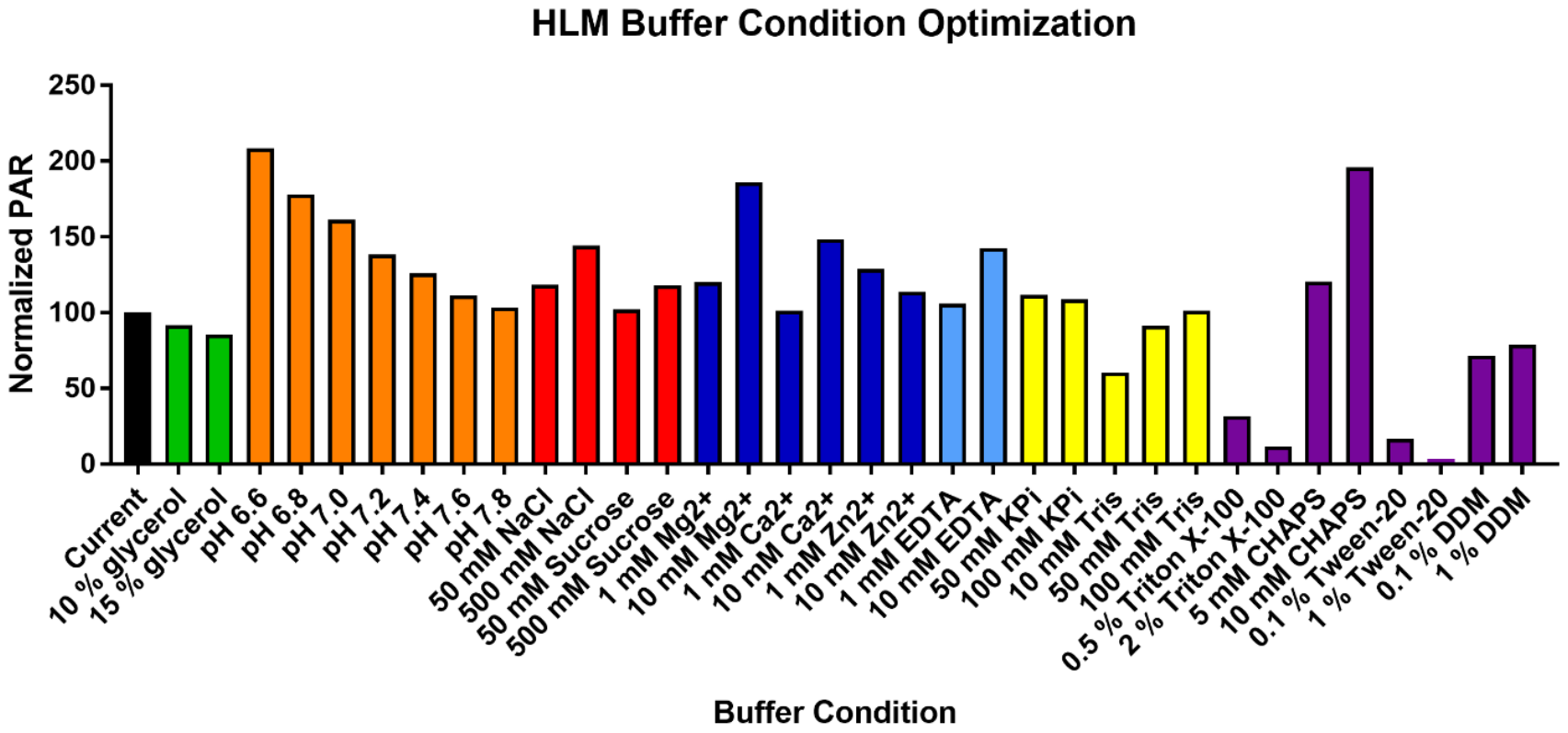

Figure 4.1. Buffer Optimization for Captopril Methylation in Human Liver Microsomes: Different activity assay buffer conditions tested with pooled HLMs. "Current" buffer conditions are 10 mM KPi pH 8.0 with 20% (v/v) glycerol. Buffer conditions were tested with a single replicate due to limited microsomal stocks.

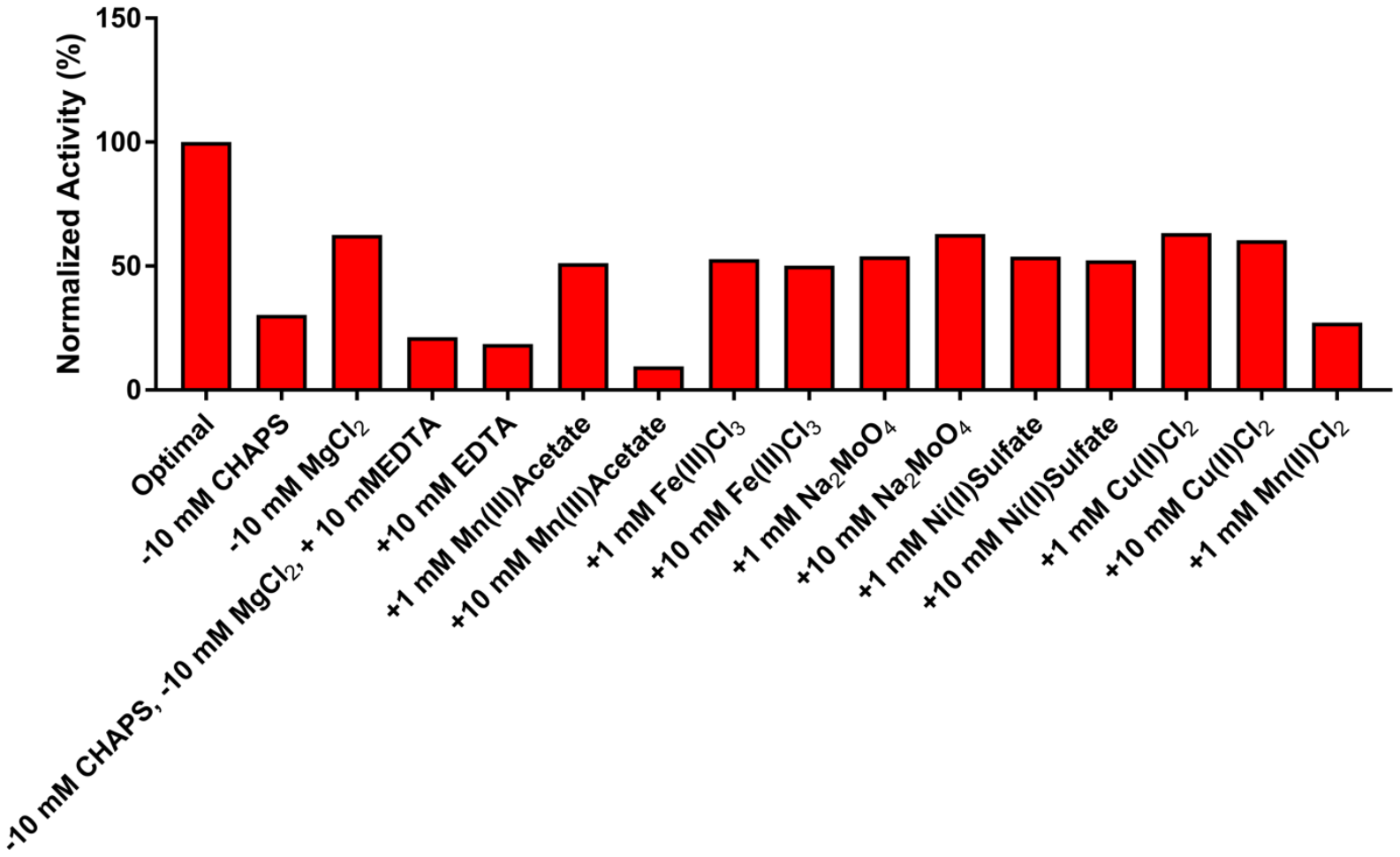

Figure 4.2. Secondary Buffer Optimization for Captopril Methylation in Human Liver Microsomes: Pooled HLMs were exposed to numerous divalent cations at multiple concentrations. "Optimal" buffer consisted of 50 mM KPi pH 7.0, 20% glycerol, 10 mM $MgCl_2$, and 10 mM CHAPS. Buffer conditions were tested in single replicates due to limited amounts of pooled microsomes.

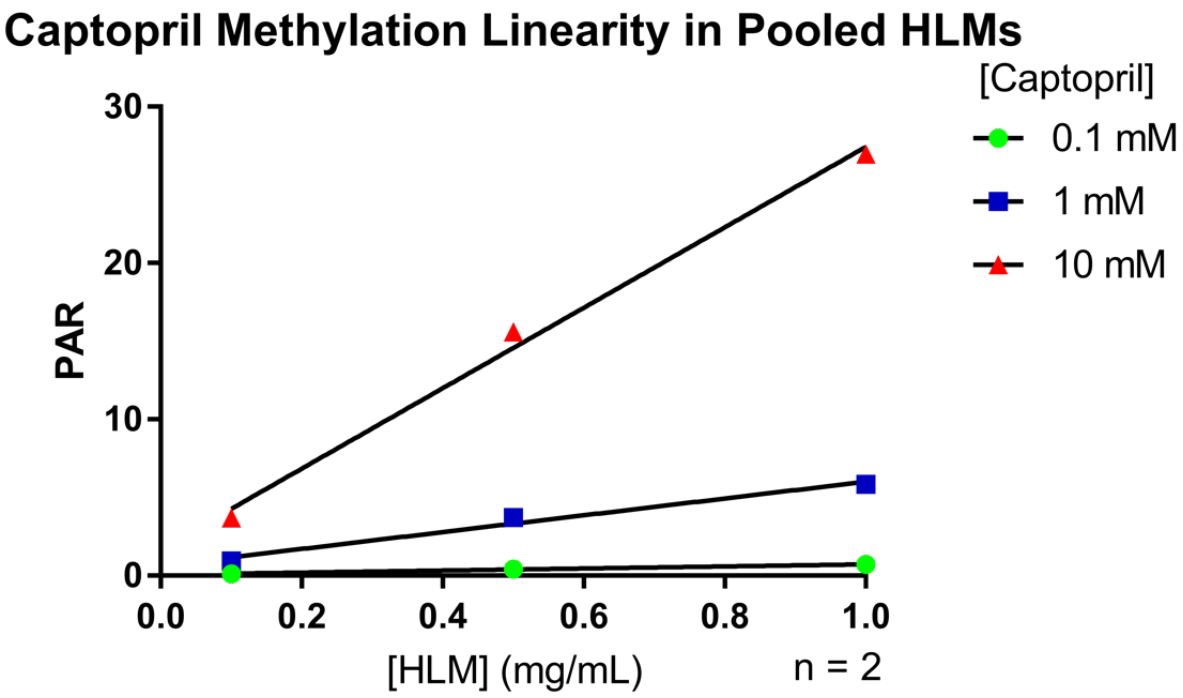

Figure 4.3. Protein Linearity Testing for Captopril Methylation in Pooled HLMs: The ratio of *S*-methyl captopril to the internal standard as a function of protein concentration at three different concentrations of captopril. Data are presented as mean ± range of duplicate measurements.

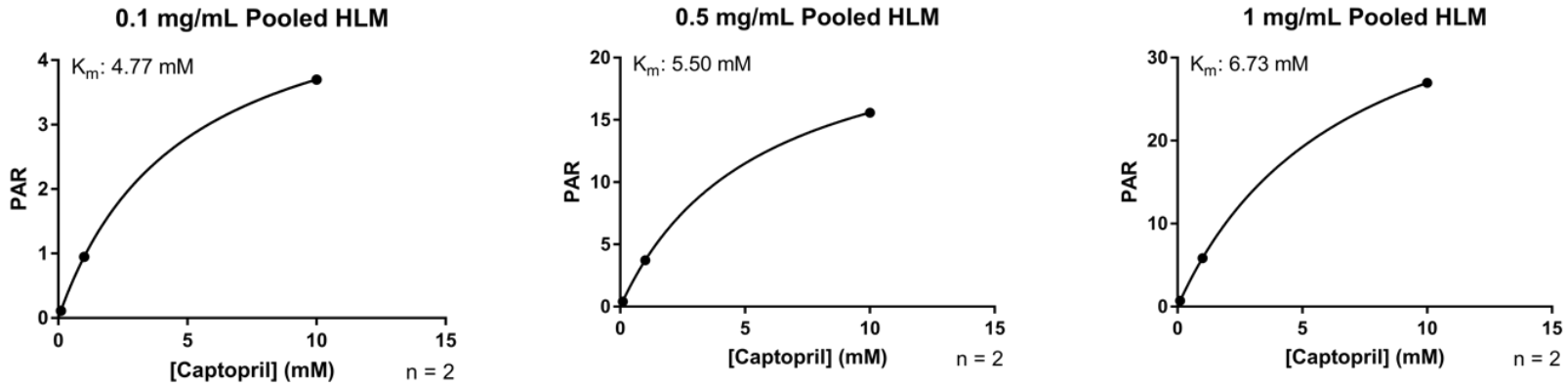

Figure 4.4. Kinetic Parameter Estimation for Captopril Methylation in Pooled HLMs: The ratio of *S*-methyl captopril to internal standard as a function of substrate concentration at three different concentrations of captopril. Data are presented as mean ± range of duplicate measurements.

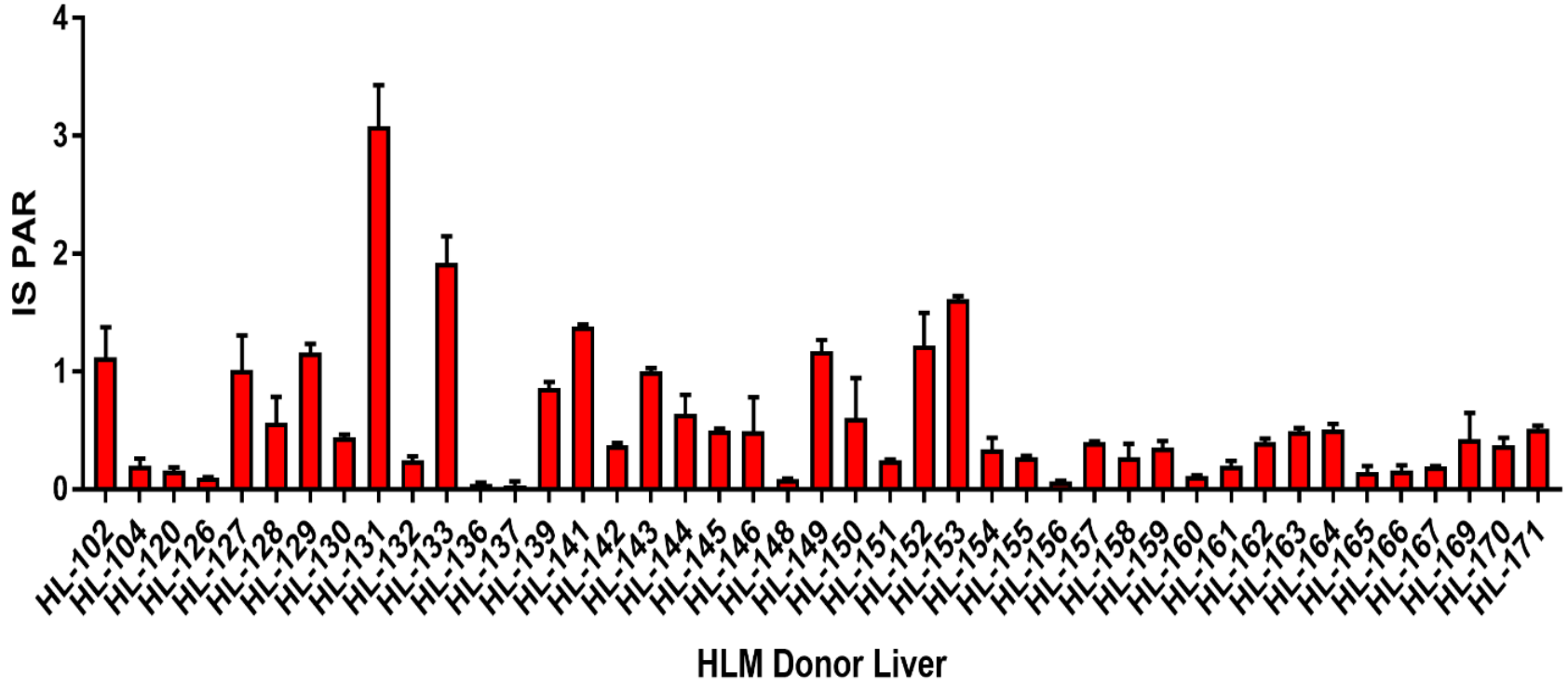

Figure 4.5. Single Donor HLM Captopril Methylation Variability in Older Livers: Ratio of *S*-methyl captopril to internal standard across 43 single donor HLM stocks. Data are presented as mean ± S.D. (n = 3)

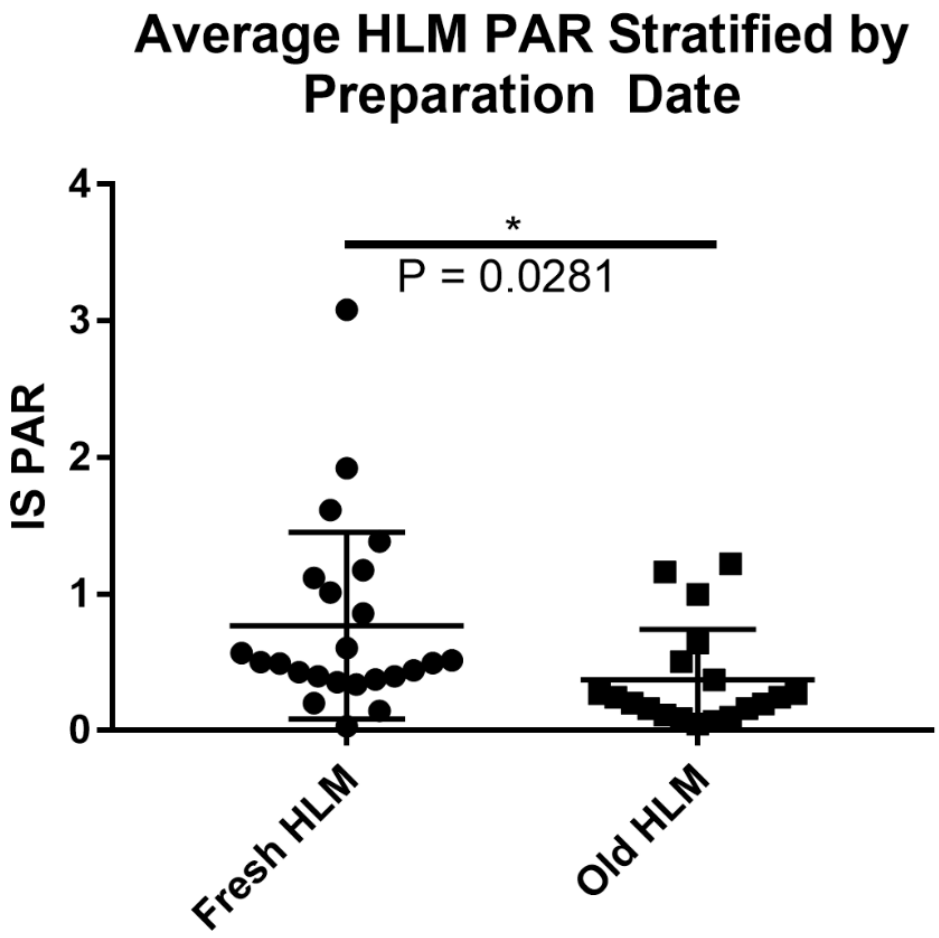

Figure 4.6. Captopril Methylation Activity Stratified by Preparation Date: Ratio of *S*-methyl captopril to internal standard in HLMs stratified by preparation date. Individual liver methylation rates are plotted and significance was determined by two-tailed *t*-test.

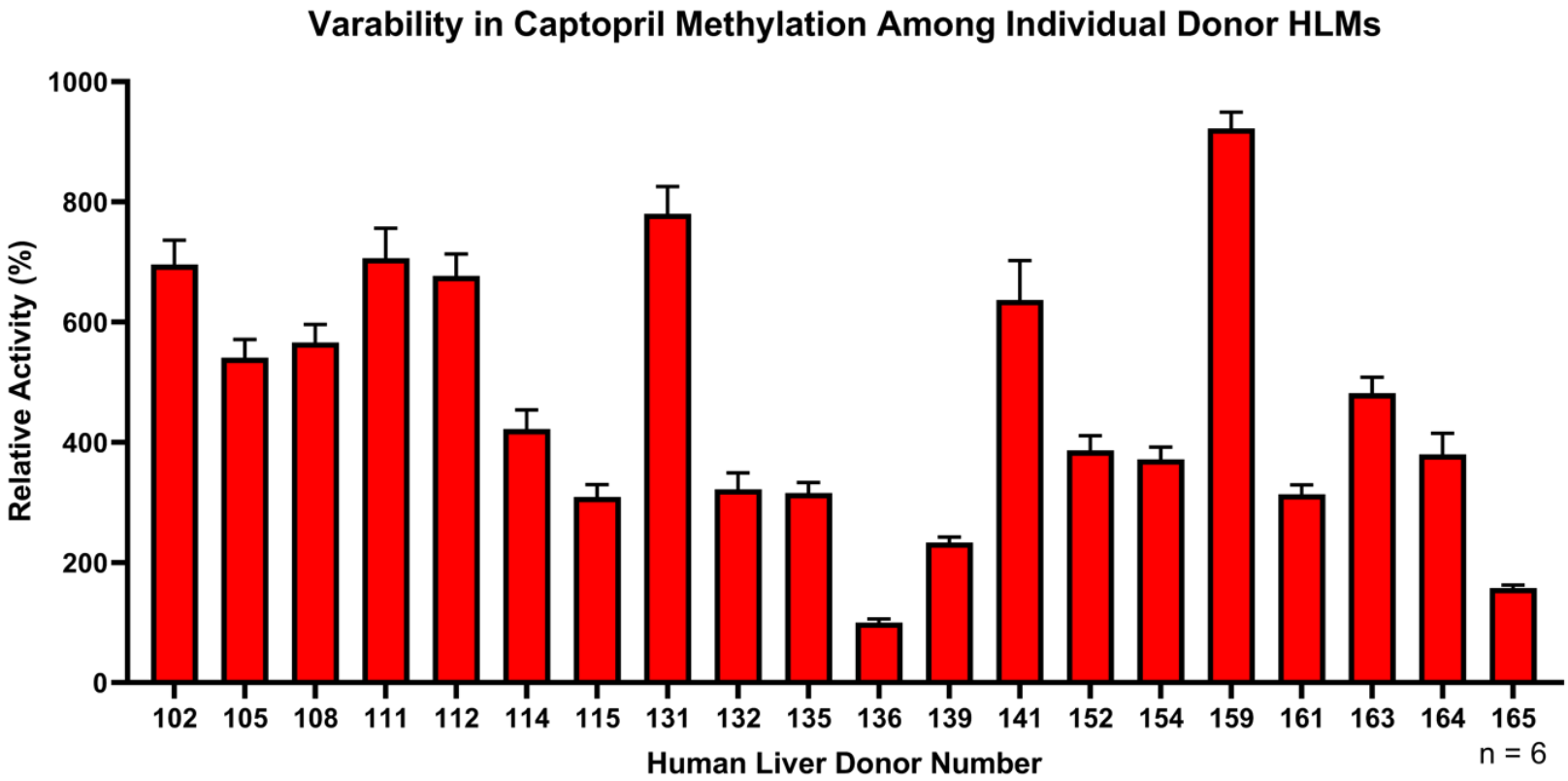

Figure 4.7. Single Donor HLM Captopril Methylation Variability in PRINCE Livers: Captopril methylation activity across twenty single donor HLM stocks, normalized to HL-136 activity. Data are presented as mean ± S.D.

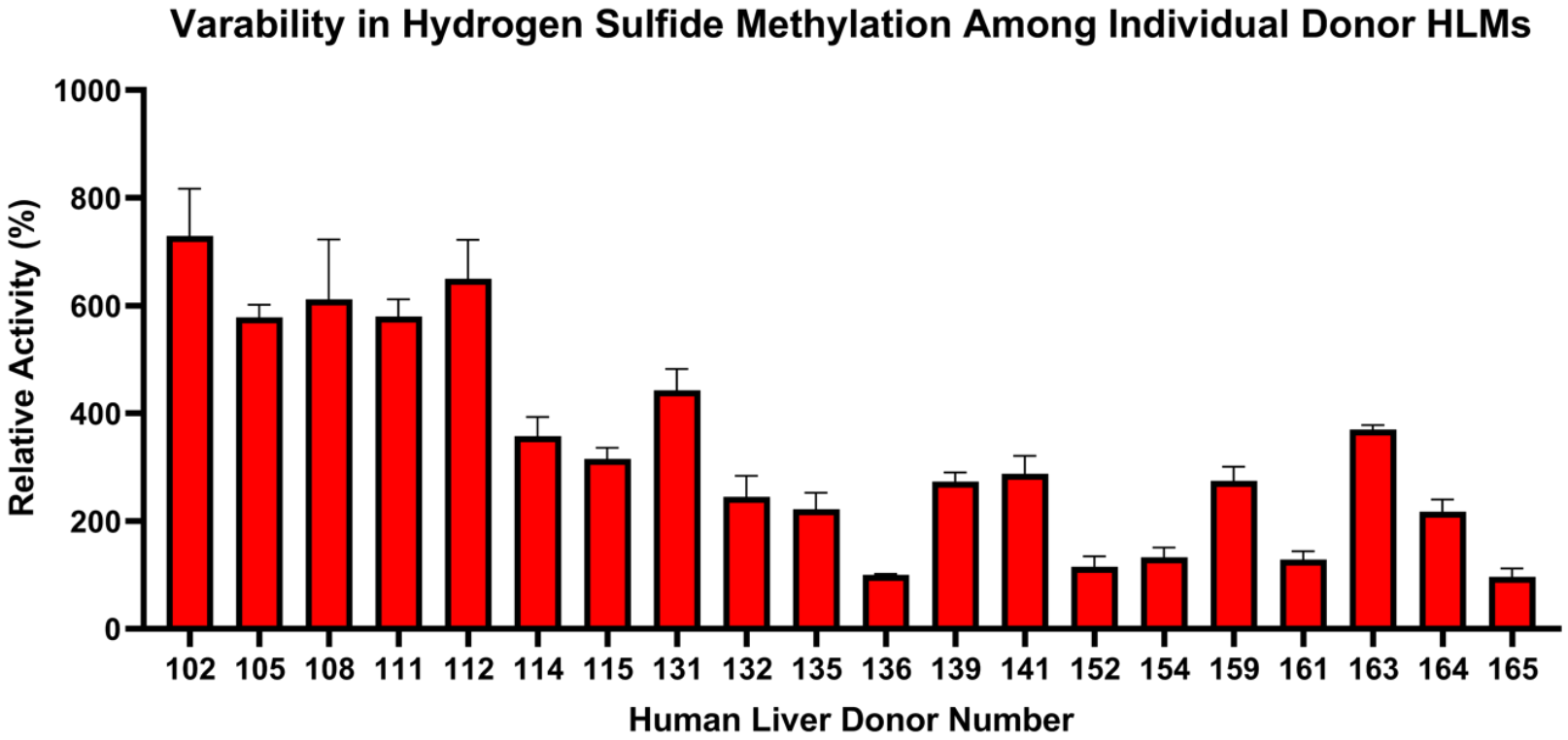

Figure 4.8. Single Donor HLM Hydrogen Sulfide Methylation Variability in PRINCE Livers: Hydrogen sulfide methylation activity across twenty single donor HLM stocks, normalized to HL-136 activity. Data are presented as mean ± S.D.

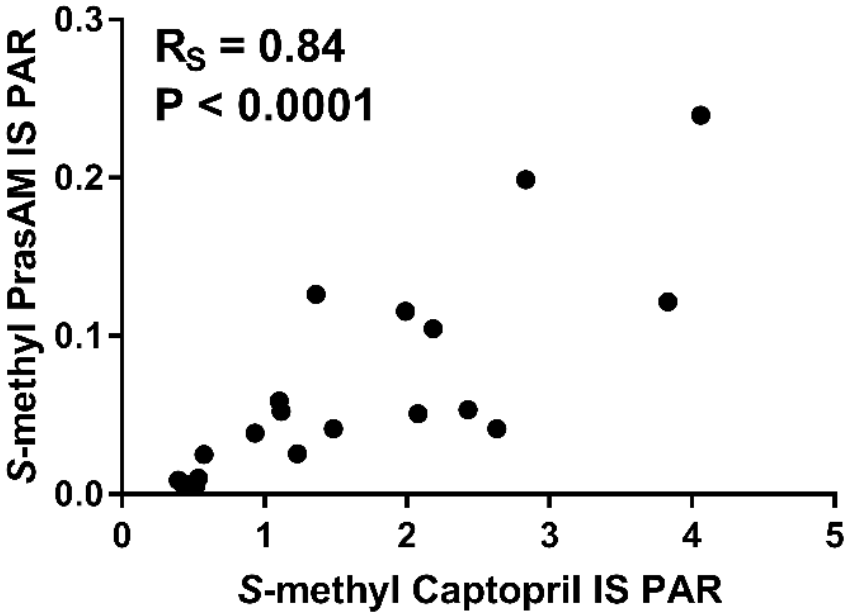

Figure 4.9. Correlation of Captopril and Prasugrel Active Metabolite Methylation in non-PRINCE Livers: Formation of *S*-methyl captopril vs. *S*-methyl prasugrel active metabolite in 20 single donor human liver microsomes. Both compounds are normalized to internal standard. Correlation was calculated using Spearman correlation.

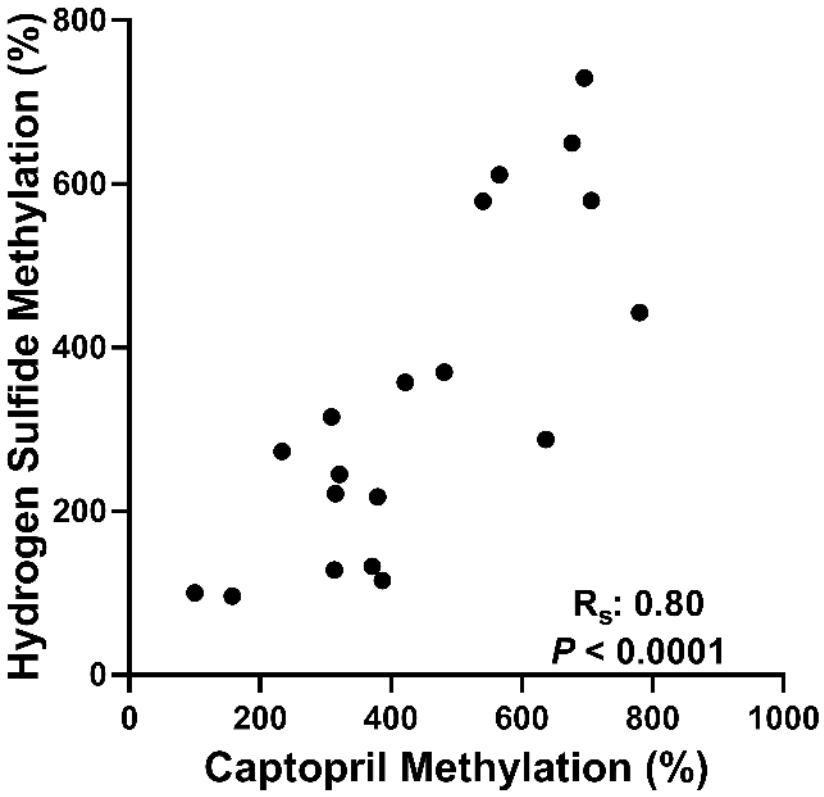

Figure 4.10. Correlation of *S*-methyl Captopril and Methanethiol Formation in PRINCE Liver HLMs: Activity measured in PRINCE liver HLMs using specific LC-MS/MS assays. Correlations were calculated using Spearman correlation.

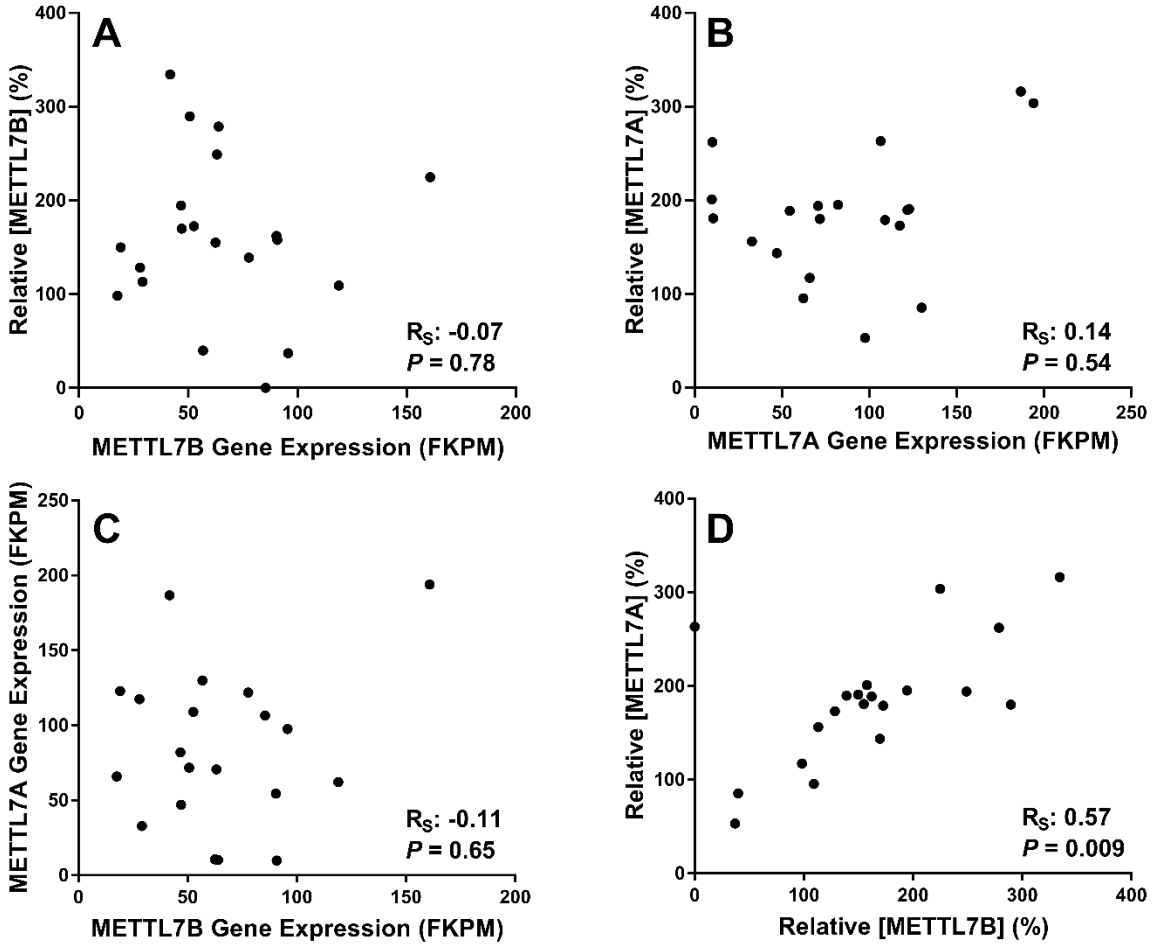

Figure 4.11. Correlation of METTL7A and METTL7B Relative Protein Expression and RNA-seq Gene Expression in PRINCE Liver HLMs: A) Correlation of METTL7A gene and protein expression. B) Correlation of METTL7B gene and protein expression. C) Correlation of *METTL7A* and *METTL7B* gene expression. D) Correlation of METTL7A and METTL7B relative protein expression. Correlations were calculated using Spearman correlation.

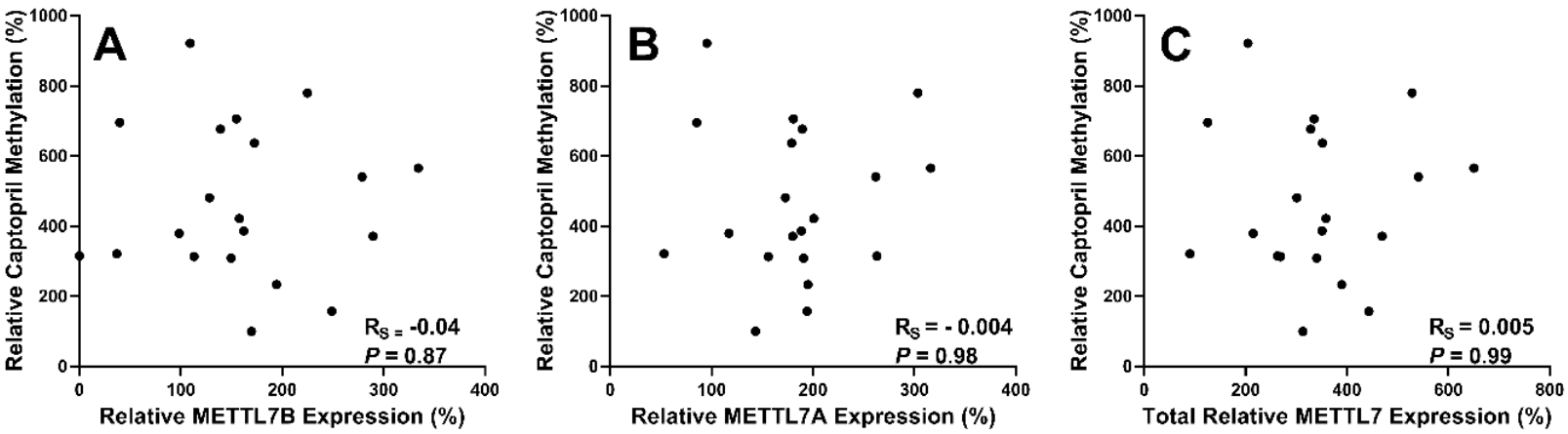

Figure 4.12. Correlation of METTL7A and METTL7B Relative Protein Expression with Captopril Methylation Activity in PRINCE Liver HLMs: A) Correlation of relative METTL7B protein expression and captopril methylation. B) Correlation of relative METTL7A protein expression and captopril methylation. C) Correlation of total relative METTL7 protein expression and captopril methylation. Correlations were calculated using Spearman correlation.

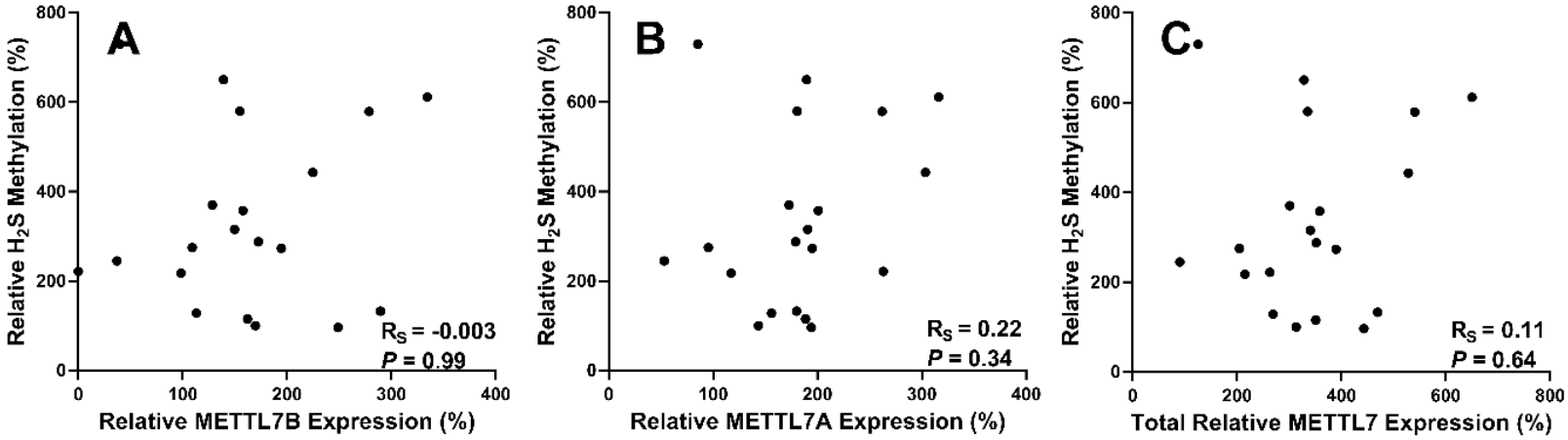

Figure 4.13. Correlation of METTL7A and METTL7B Relative Protein Expression with Hydrogen Sulfide Methylation Activity in PRINCE Liver HLMs: A) Correlation of relative METTL7B protein expression and hydrogen sulfide methylation. B) Correlation of relative METTL7A protein expression and hydrogen sulfide methylation. C) Correlation of total relative METTL7 protein expression and hydrogen sulfide methylation. Correlations were calculated using Spearman correlation.

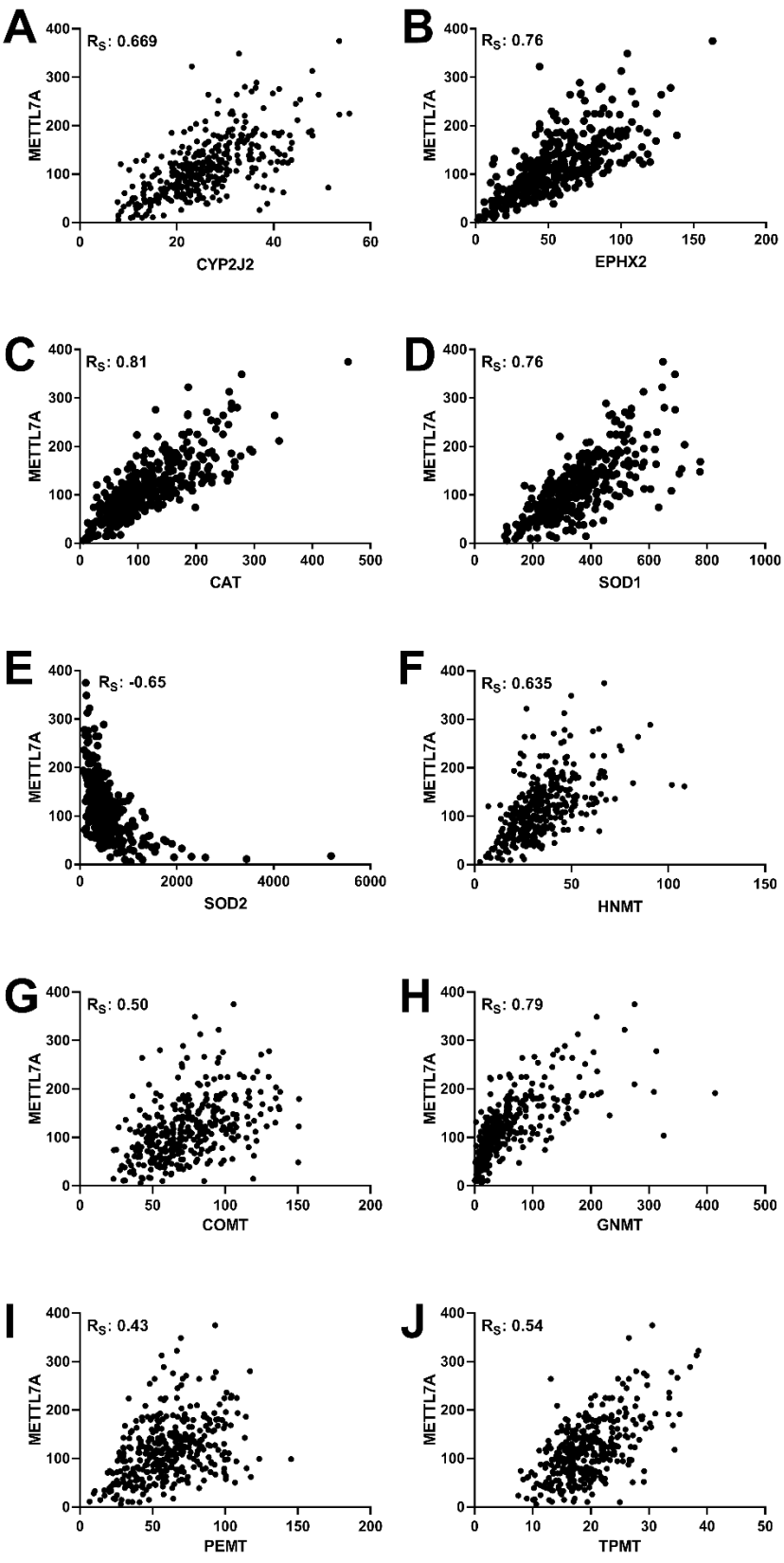

Figure 4.14. Correlation of *METTL7A* Gene Expression with Other Methyltransferases and Redox Genes in Human Liver Tissue: Correlation of *METTL7A* gene expression to A) *CYP2J2* B) *EPHX2* C) *CAT* D) *SOD1* E) *SOD2* F) *HNMT* G) *COMT* H) *GNMT* I) *PEMT* J) *TPMT*. Correlations were calculated using Spearman correlation.

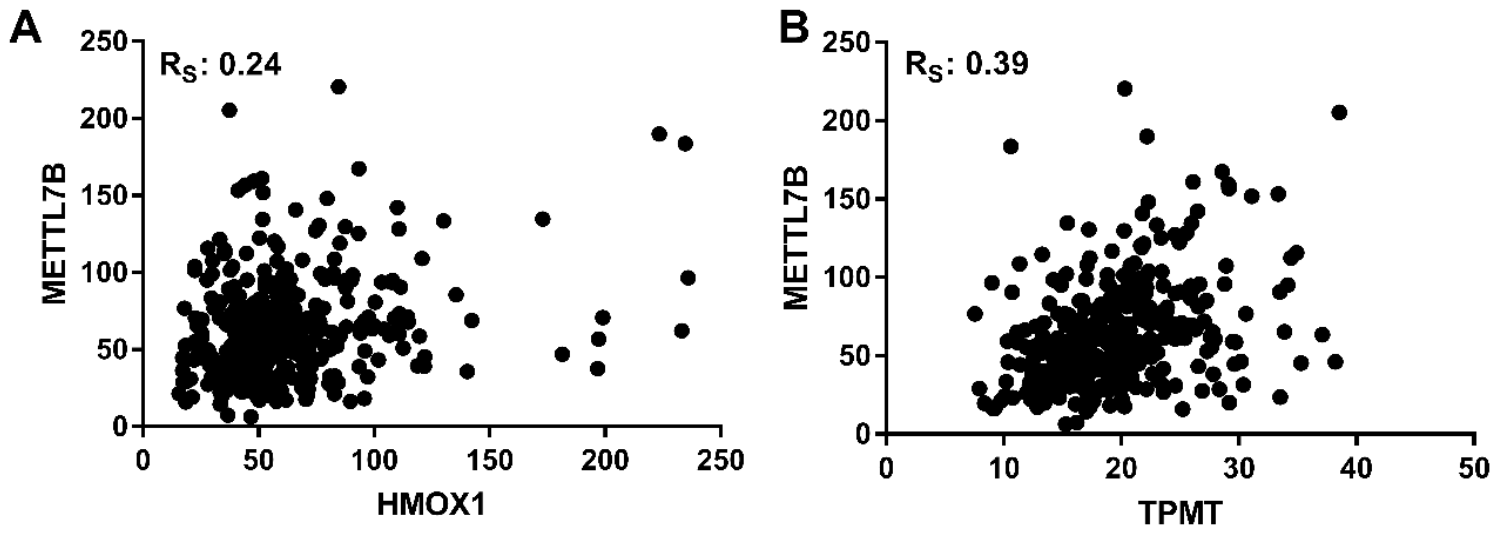

Figure 4.15. Correlation of *METTL7B* Gene Expression with A) *HMOX1* B) *TPMT* in Human Liver Tissue. Correlations were calculated using Spearman correlation.

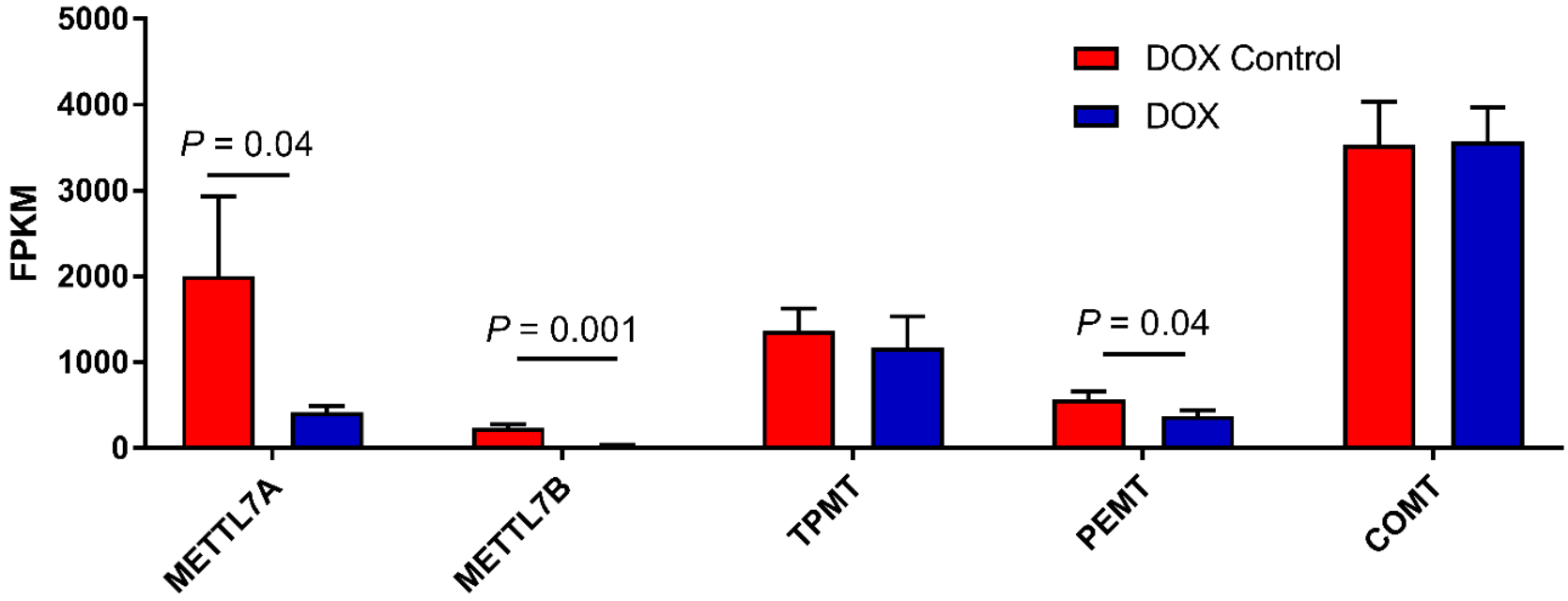

Figure 4.16. Effect of Doxorubicin Treatment on Methyltransferase Gene Expression in Human Ventricular Cardiomyocytes: RNA expression levels measured by RNA-seq in human cardiomyocytes upon treatment with doxorubicin for 24 hours. Data are presented as mean ± S.D (n=3). Significance was determined using a two-tailed *t*-test.

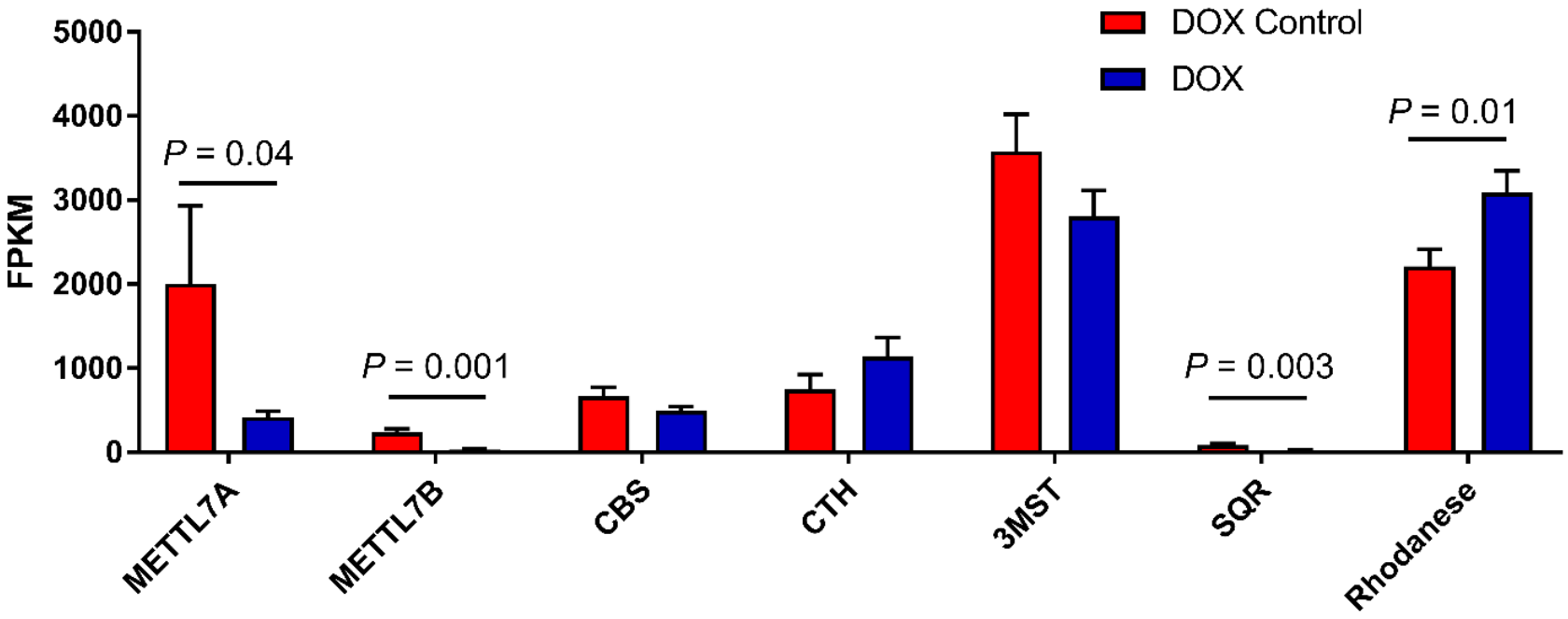

Figure 4.17. Effect of Doxorubicin Treatment on Hydrogen Sulfide-Related Gene Expression in Human Ventricular Cardiomyocytes: RNA expression levels measured by RNA-seq in human cardiomyocytes following treatment with doxorubicin (20uM) for 24 hours. Data are presented as mean ± S.D. (n=3). Significance was determined using a two-tailed *t*-test

Bibliography:

1. Lee, Y.-S., Kim, H., Wu, T.-X., Wang, X.-M. & Dionne, R. A. Genetically mediated interindividual variation in analgesic responses to cyclooxygenase inhibitory drugs. *Clin. Pharmacol. Ther.* **79**, 407–418 (2006).
2. Alwi, Z. Bin. The Use of SNPs in Pharmacogenomics Studies. *Malays. J. Med. Sci.* **12**, 4–12 (2005).
3. Shastry, B. S. SNPs in disease gene mapping, medicinal drug development and evolution. *J. Hum. Genet.* **52**, 871–880 (2007).
4. Witt, D. M., Clark, N. P., Kaatz, S., Schnurr, T. & Ansell, J. E. Guidance for the practical management of warfarin therapy in the treatment of venous thromboembolism. *J. Thromb. Thrombolysis* **41**, 187–205 (2016).
5. Zhang, X., Li, L., Ding, X. & Kaminsky, L. S. Identification of cytochrome P450 oxidoreductase gene variants that are significantly associated with the interindividual variations in warfarin maintenance dose. *Drug Metab. Dispos.* **39**, 1433–1439 (2011).
6. Johnson, J. A. *et al.* Clinical Pharmacogenetics Implementation Consortium (CPIC) Guideline for Pharmacogenetics-Guided Warfarin Dosing: 2017 Update. *Clin. Pharmacol. Ther.* **102**, 397–404 (2017).
7. Gage, B. F. *et al.* Effect of Genotype-Guided Warfarin Dosing on Clinical Events and Anticoagulation Control Among Patients Undergoing Hip or Knee Arthroplasty: The GIFT Randomized Clinical Trial. *JAMA* **318**, 1115–1124 (2017).
8. Pirmohamed, M. *et al.* A Randomized Trial of Genotype-Guided Dosing of Warfarin. *N. Engl. J. Med.* **369**, 2294–2303 (2013).
9. L., A. J. *et al.* Randomized Trial of Genotype-Guided Versus Standard Warfarin Dosing in

Patients Initiating Oral Anticoagulation. *Circulation* **116**, 2563–2570 (2007).

10. Chocair, P. R., Duley, J. A., Simmonds, H. A. & Cameron, J. S. The importance of thiopurine methyltransferase activity for the use of azathioprine in transplant recipients. *Transplantation* **53**, 1051–1055 (1992).
11. Weinshilboum, R. M. & Sladek, S. L. Mercaptopurine pharmacogenetics: Monogenic inheritance of erythrocyte thiopurine methyltransferase activity. *Am. J. Hum. Genet.* **32**, 651–662 (1980).
12. Black, A. J. *et al.* Thiopurine methyltransferase genotype predicts therapy-limiting severe toxicity from azathioprine. *Ann. Intern. Med.* **129**, 716–718 (1998).
13. Lennard, L., Van Loon, J. A. & Weinshilboum, R. M. Pharmacogenetics of acute azathioprine toxicity: Relationship to thiopurine methyltransferase genetic polymorphism. *Clin. Pharmacol. Ther.* **46**, 149–154 (1989).
14. Lennard, L., Gibson, B. E., Nicole, T. & Lilleyman, J. S. Congenital thiopurine methyltransferase deficiency and 6-mercaptopurine toxicity during treatment for acute lymphoblastic leukaemia. *Arch. Dis. Child.* **69**, 577 LP – 579 (1993).
15. Black, A. J. *et al.* Thiopurine Methyltransferase Genotype Predicts Therapy-Limiting Severe Toxicity from Azathioprine. *Ann. Intern. Med.* **129**, 716–718 (1998).
16. Kasirer, Y. *et al.* Thiopurine S-methyltransferase (TPMT) Activity Is Better Determined by Biochemical Assay Versus Genotyping in the Jewish Population. *Dig. Dis. Sci.* **59**, 1207–1212 (2014).
17. Keith, R. A., Jardine, I., Kerremans, A. & Weinshilboum, R. M. Human erythrocyte membrane thiol methyltransferase. S-methylation of captopril, N-acetylcysteine, and 7 alpha-thio-spirolactone. *Drug Metab. Dispos.* **12**, 717–24 (1984).

18. Keith, R. A., Van Loon, J., Wussow, L. F. & Weinshilboum, R. M. Thiol methylation pharmacogenetics: heritability of human erythrocyte thiol methyltransferase activity. *Clin. Pharmacol. Ther.* **34**, 521–8 (1983).

19. Shen, X., Peter, E. A., Bir, S., Wang, R. & Kevil, C. G. Analytical measurement of discrete hydrogen sulfide pools in biological specimens. *Free Radic. Biol. Med.* **52**, 2276–2283 (2012).

20. Shen, X. *et al.* Measurement of plasma hydrogen sulfide in vivo and in vitro. *Free Radic. Biol. Med.* **50**, 1021–31 (2011).

21. Shen, X., Kolluru, G. K., Yuan, S. & Kevil, C. G. Measurement of H2S in vivo and in vitro by the monobromobimane method. *Methods Enzymol.* **554**, 31–45 (2015).

22. Evangelista, E. A. *et al.* CYP2J2 Modulates Diverse Transcriptional Programs in Adult Human Cardiomyocytes. *Sci. Rep.* **10**, 5329 (2020).

23. Dalton, R. *et al.* Interrogation of CYP2D6 Structural Variant Alleles Improves the Correlation Between CYP2D6 Genotype and CYP2D6-Mediated Metabolic Activity. *Clin. Transl. Sci.* **13**, 147–156 (2020).

24. Basit, A., Radi, Z., Vaidya, V. S., Karasu, M. & Prasad, B. Kidney Cortical Transporter Expression across Species Using Quantitative Proteomics. *Drug Metab. Dispos.* **47**, 802 LP – 808 (2019).

25. Zhang, H. *et al.* Regional proteomic quantification of clinically relevant non-cytochrome P450 enzymes along the human small intestine. *Drug Metab. Dispos.* dmd.120.090738 (2020). doi:10.1124/dmd.120.090738

26. Friedberg, T. *et al.* The identification, solubilization, and characterization of microsome-associated glutathione S-transferases. *J. Biol. Chem.* **254**, 12028–12033 (1979).

27. Zhao, K.-H. *et al.* Nonenzymatic chromophore attachment in biliproteins: conformational control by the detergent Triton X-100. *Biochim. Biophys. Acta - Bioenerg.* **1657**, 131–145 (2004).

28. Sparta, M. & Alexandrova, A. N. How Metal Substitution Affects the Enzymatic Activity of Catechol-O-Methyltransferase. *PLoS One* **7**, 47172 (2012).

29. Clare, D. K. & Saibil, H. R. ATP-driven molecular chaperone machines. *Biopolymers* **99**, 846–859 (2013).

30. Bremer, J. & Greenberg, D. M. Enzymic methylation of foreign sulfhydryl compounds. *Biochim. Biophys. Acta* **46**, 217–224 (1961).

31. Drummer, O. H., Miach, P. & Jarrott, B. S-methylation of captopril. Demonstration of captopril thiol methyltransferase activity in human erythrocytes and enzyme distribution in rat tissues. *Biochem. Pharmacol.* **32**, 1557–62 (1983).

32. Migdalof, B. H. *et al.* Captopril: Pharmacology, Metabolism, and Disposition. *Drug Metab. Rev.* **15**, 841–869 (1984).

33. Weisiger, R. A. & Jakoby, W. B. Thiol S-methyltransferase from rat liver. *Arch. Biochem. Biophys.* **196**, 631–7 (1979).

34. Glauser, T. A., Kerremans, A. L. & Weinshilboum, R. M. Human hepatic microsomal thiol methyltransferase. Assay conditions, biochemical properties, and correlation studies. *Drug Metab. Dispos.* **20**, 247–55 (1992).

35. Bhatia, M. Role of Hydrogen Sulfide in the Pathology of Inflammation. *Sci.* **2012**, 12 (2012).

36. Wallace, J. L., Vong, L., McKnight, W., Dicay, M. & Martin, G. R. Endogenous and Exogenous Hydrogen Sulfide Promotes Resolution of Colitis in Rats. *Gastroenterology*

137, 569-578.e1 (2009).

37. Whiteman, M. & Winyard, P. G. Hydrogen sulfide and inflammation: the good, the bad, the ugly and the promising. *Expert Rev. Clin. Pharmacol.* **4**, 13–32 (2011).

38. Finkelstein, J. D., Kyle, W. E. & Harris, B. J. Methionine metabolism in mammals: Regulatory effects of S-adenosylhomocysteine. *Arch. Biochem. Biophys.* **165**, 774–779 (1974).

39. Caudill, M. A. *et al.* Intracellular S-Adenosylhomocysteine Concentrations Predict Global DNA Hypomethylation in Tissues of Methyl-Deficient Cystathionine β-Synthase Heterozygous Mice. *J. Nutr.* **131**, 2811–2818 (2001).

Chapter 5: Conclusions and Future Directions

Conclusions:

The main goal of this dissertation project was to identify, purify and characterize the enzyme or enzymes responsible for aliphatic thiol methylation in humans. This was achieved by fractionating solubilized microsomal proteins and tracking thiol methyltransferase activity using specific enzyme activity assays. Two candidate proteins, METTL7A and METTL7B, were identified using a shotgun proteomics and bioinformatics approach and subsequently validated via altered gene expression experiments in two cell lines. METTL7B was successfully expressed in *E. coli* and purified to near homogeneity. The purified protein selectively catalyzed aliphatic thiol methylation, particularly hydrogen sulfide, in a time and SAM-dependent fashion. Furthermore, thiol methyltransferase activity in human liver microsomal preparations was highly variable between individuals but did not correlate with *METTL7* gene or relative protein expression. Interestingly, RNA sequencing results suggested that both proteins are responsive to intracellular oxidative stress.

Initial purification attempts using rat liver microsomes failed to isolate a thiol methyltransferase candidate protein. Therefore, fractions containing thiol methyltransferase enzymatic activity were subjected to tryptic digest and shotgun proteomics to overcome the sample heterogeneity. Rat METTL7B protein was only present in TMT-active fractions and therefore became our candidate thiol methyltransferase protein. Rat METTL7A was also considered a candidate thiol methyltransferase despite not being directly observed in tryptic digest experiments, likely due to low abundance or instability. The human orthologs of each

protein had high sequence similarity to the rat proteins and were further tested in cell culture models.

METTL7A and *METTL7B* gene expression was modulated and correlated to changes in thiol methyltransferase activity in two different cell lines. siRNA-mediated gene knockdown in HepG2 cells reduced protein expression and significantly decreased captopril methylation. Alternatively, captopril methylation was significantly increased in HeLa cells overexpressing *METTL7A* and *METTL7B* mRNA and protein. These results indicated that both proteins are involved in thiol methylation in some capacity. We then proceeded to express and purify recombinant protein to test for direct thiol methylation activity.

Active METTL7A and METTL7B were overexpressed in *E. coli* as His-GST fusion proteins. The fusion tag enabled multiple affinity purification approaches and decreased overall protein hydrophobicity, a major hurdle in previous purification attempts. METTL7A fusion protein was still difficult to solubilize from bacterial membranes compared to the METTL7B fusion protein, likely due to a more hydrophobic *N*-terminal alpha helix. Unfortunately, both METTL7A and METTL7B enzyme activity was severely decreased upon modest truncation of the *N*-terminus, which may result from active site destabilization. As such, all efforts were focused on purifying the full-length METTL7B fusion protein. The dual-stage affinity chromatography approach yielded pure recombinant METTL7B with minimal contamination as verified by western blot and proteomic analysis.

Recombinant METTL7B catalyzed the methylation of several compounds, including captopril, 7α-Thiospironolactone, and hydrogen sulfide, which is an important inflammatory signaling molecule. Classic Michaelis-Menten kinetics were observed for all measured substrates and the SAM methyl donor cofactor. Substrate specificity testing showed that

METTL7B had a clear preference for aliphatic thiol-containing molecules, including several known thiol methyltransferase substrates[1–4]. No methylation was observed with thiopurines, canonical *O*- and *N*-methyltransferase substrates, cysteine, or glutathione. Enzymatic activity was greatly increased upon incubation with DMPG liposomes which may be due to protein stabilization effects. Overall, our results unequivocally demonstrate that METTL7B is an aliphatic thiol methyltransferase that metabolizes both exogenous and endogenous thiol substrates.

Variability in thiol methyltransferase activity was also investigated using single donor human liver microsomes to better characterize potential interindividual variability and possible clinical relevance. We found that the rate of thiol methylation for multiple probe substrates varied up to 9-fold within a population of 20 individuals. This indicates that thiol-containing drugs or metabolites may exhibit widely variable levels of systemic exposure between individuals, which could precipitate toxic effects for narrow therapeutic window drugs. The catalytic variability did not correlate with either gene or protein expression of METTL7A and METTL7B however more appropriate analysis will be conducted using quantitative protein expression data. Preliminary RNA-seq results indicated that *METTL7A* expression was correlated with genes involved in redox and arachidonic acid signaling pathways in liver. *METTL7A* and *METTL7B* also appear to be responsive to doxorubicin-induced oxidative stress in human cardiomyocytes, likely due to their role in hydrogen sulfide catabolism.

Future Directions:

The fundamental discovery nature of this dissertation project paves the way for many future research directions to elucidate the broader impact that METTL7A and METTL7B have on health and disease. However, the immediate focus of future work, however, should be on the

purification of recombinant METTL7A followed by biochemical characterization and comparison to METTL7B. Preliminary data indicates that METTL7A methylates hydrogen sulfide efficiently and could be the primary enzyme responsible for methanethiol formation *in vivo*. This hypothesis is supported by RNA-seq data and the fact that *METTL7A* gene knockdown triggers compensatory upregulation of *METTL7B,* but not vice versa. We believe that recombinant METTL7A is required to fully characterize both exogenous and endogenous thiol methylation in humans.

Further optimization and biochemical characterization of recombinant METTL7B activity is also required. Truncation experiments and DMPG-mediated enzyme activation suggest that the *N*-terminal alpha helix plays a large role in thiol methyltransferase function. Additionally, both METTL7A and METTL7B are predicted to localize to lipid droplets because their *N*-terminal sequences may gravitate towards extremely hydrophobic triglyceride-rich portions of the endoplasmic reticulum membrane. Therefore, METTL7B's function should be studied in different reconstituted lipid environments that will stabilize the *N*-terminus to different degrees. Similarly, subcellular lipid droplet isolates should be tested for thiol methyltransferase activity. Together, these results may shed light on the role of the METTL7 *N*-terminus, their subcellular localization, and possibly increase the accuracy of our *in vitro* characterization for *in vivo* extrapolation.

Finally, the RNA sequencing and cardiomyocyte oxidative stress experiments indicate that both *METTL7A* and *METTL7B* are sensitive to cellular redox states, likely due to their role in hydrogen sulfide catabolism. As discussed in Chapter 1, many cancers exhibit dysregulated hydrogen sulfide homeostasis and differential gene expression of *METTL7A* and *METTL7B*. Therefore, further investigation is required to determine if there is a mechanistic link between the

two. The gene expression and intracellular hydrogen sulfide concentrations should be measured in tissues from several disease states such as diabetes, rheumatoid arthritis, and solid tumor cancers and compared to controls. Additionally, RNA-seq pathway analysis should be conducted in appropriate human cell culture models treated with either *METTL7A* or *METTL7B* siRNA. Together, these data may help explain the physiological role of METTL7A and METTL7B in healthy tissue and the potential cellular benefit for dysregulation during cancer progression.

Bibliography:

1. Kröplin, T. & Iven, H. Methylation of 6-mercaptopurine and 6-thioguanine by thiopurine S-methyltransferaseA comparison of activity in red blood cell samples of 199 blood donors. *Eur. J. Clin. Pharmacol.* **56**, 343–345 (2000).
2. Brown, D. D., Axelrod, J. & Tomchick, R. Enzymatic N-Methylation of Histamine. *Nature* **183**, 680 (1959).
3. Axelrod, J. Purification and Properties of Phenylethanolamine-N-methyl Transferase. *J. Biol. Chem.* **237**, 1657–1660 (1962).
4. Sparta, M. & Alexandrova, A. N. How Metal Substitution Affects the Enzymatic Activity of Catechol-O-Methyltransferase. *PLoS One* **7**, 47172 (2012).

Appendix I: Creating the pGEX-3X METTL7B full-length vector for expression and purification: A Guide to Shuttling Genes of Interest Between Expression Plasmids

A generalized protocol for shuttling gene sequences into new expression vector backbones is detailed below. I will use the creation of the pGEX-3X METTL7B full-length vector as a specific example, but this protocol can be applied to any other expression vector with appropriate restriction enzyme digestion sites. The main differences that occur when using new vectors is the design of the PCR primer overhangs and the re-optimization of PCR annealing temperatures. Additionally, this method allows for easy *N*- and *C*-terminal truncations of the protein sequence expressed from the gene of interest.

Before discussing specific primer design, it is important to understand that DNA is a double helix which is read in a certain direction. The upstream portion, or 5' end, is where a gene sequence will start, and the downstream portion, or 3' end, is where a gene sequence ends on the "sense" strand of DNA. The other DNA strand is called the reverse complement, or "anti-sense" strand, and it is an inverted complementary sequence to the gene of interest. This is only important when conducting PCR and sequencing because reverse primers must be reverse complementary to the downstream portion of the sequence of interest on the sense strand of DNA.

Step 1: Primer Design

BamHI and EcoRI restriction sites were added upstream and downstream of the *METTL7B* gene sequence respectively. This was conducted using overhang polymerase chain reaction (PCR). Briefly, a linear oligonucleotide forward primer is designed that is only complementary to the gene of interest in the downstream half of the primer. The upstream half

of the primer, which will not anneal during the initial round of PCR, contains a 5' "CTAGCTAG" handle, followed by the BamHI restriction site, and any spacers or linkers required to maintain reading frame or add specific peptide sequences. Restriction enzyme binding is not as efficient at the ends of PCR products. Therefore, the "CTAGCTAG" handle, suggested by Dr. Mike Guttman, helps increase restriction enzyme binding by adding random nucleotides to the end of the PCR products, thus moving the restriction enzyme consensus sequences further into the middle.

In this case, an "AG" sequence is added prior to the *METTL7B* gene sequence to keep the correct reading frame after ligation. The downstream portion of the primer should be complementary to the gene of interest, either the start of the gene sequence or further downstream if N-terminal truncations of the protein product are required.

The reverse primer is designed such that the downstream portion contains the EcoRI restriction site, a 3' "CTAGCTAG" handle, and two stop codons to ensure termination of protein synthesis. The upstream portion of the primer is complementary to the 3' end of the gene of interest, usually the end of the gene of interest or further upstream if C-terminal truncations are desired. After appropriate design, the sequence is converted to the reverse complement for use in PCR. **If you do not use the reverse complement primer, PCR amplification will not occur.**

The forward primer sequence is shown below. The red portion is the "GTAGCTAG" handle, the purple section is the BamHI recognition site, the green section is the added "AG" sequence to correct the reading frame shift, and the bolded and underlined section is the start of the METTL7B gene sequence.

Forward primer sequence (5’ to 3’):

5’ CTAGCTAGGGATCCAG<u>ATGGATATTTTAGTGCCA</u> 3’

The reverse primer sequence is shown below as the reverse complement. The red portion is the handle, the purple section is the EcoRI recognition site, the green section is two stop codons, and the bolded and underlined section binds to the end of the METTL7B gene sequence.

Reverse primer sequence (5’ to 3’) followed by the reverse complement (3’ to 5’):

5’ CTAGCTAGGAATTCTTATTA<u>TTTGACAGCCTTTCCCAT</u> 3’

3’ <u>ATGGGAAAGGCTGTCAAA</u>TAATAAGAATTCCTAGCTAG 5’

<u>Additional Primer Design Example:</u>

Below is a separate forward primer that was designed to incorporate a poly-alanine/proline peptide linker prior to the start of the METTL7B sequence. This added sequence is shown in green and significantly increases the length of the forward primer that will not bind to the template sequence in the first round of PCR, making it very difficult to predict appropriate annealing temperatures. Therefore, it is even more important to empirically optimize the PCR conditions in this case. The rest of the primer is designed the same way as usual.

Forward Primer with Linker (5’ to 3’):

5’ CTAGCTAGGGATCCGCTCCGGCACCGGCTCCGGCACCGGCACCG<u>ATGGATA</u>

<u>TTTTAGTGCCATTGTTACAGCTT</u> 3’

Experimental Note:

Use the highest fidelity DNA polymerase available, preferably Q5 High-Fidelity DNA Polymerase available from New England Biolabs. For comparison, *Taq* DNA polymerase error rate is roughly 1 per 3,300 bases while Q5 polymerase error rate is roughly 1 per 1,000,000 bases. Therefore, if your PCR amplicon length is around 3.3 kilobase pairs, you are almost guaranteed to incorporate at one single nucleotide polymorphism (SNP) by using *Taq* DNA polymerase. Using Q5 DNA polymerase instead will provide more correct PCR products and yield better results in the future after DNA ligation and plasmid sequencing. The only valid reason to use *Taq* instead of Q5 is if SNPs are desired to test the effect of amino acid substitutions. Even then, the SNP incorporation is random which may lead to a silent mutation. Additionally, there are better options for site-directed mutagenesis available.

Step 2: PCR and Gel Purification

The following components were added to a single PCR tube, with all final concentrations noted. 1X ThermoPol Reaction buffer, 200 μM dNTP mixture, 200 nM forward primer, 200 nM reverse primer, 1 ng total synthesized pEX-C-His METTL7B plasmid template DNA, 1.25 units of *Taq* DNA Polymerase, and nuclease-free water to a final volume of 50 μL.

Samples were initially denatured at 95 ºC for 30 seconds, followed by 30 PCR cycles. Each cycle consisted of heating to 95 ºC for 15 seconds, dropping the temperature to 42-57 ºC for 45 seconds, and then holding at 68 ºC for one minute. The exact annealing temperature is

dependent upon the primer design and must be determined empirically. Finally, samples were held at 68 ^{o}C for five minutes before being stored at 4 ^{o}C until further use.

Subsequently, PCR reactions were run on a 0.8% Agarose E-gel (Invitrogen) to determine the total DNA yield and the primer specificity. After imaging, gel cassettes were forced open and the DNA band of interest was excised while visualized using long-wave UV light. The PCR products were isolated from the DNA gel using the Monarch DNA Gel Extraction kit from New England Biolabs (NEB) using the manufacturer protocol. DNA yield was quantified via NanoDrop. If the PCR reaction has been previously validated and does not need to be run on a DNA gel, the PCR products can also be purified using a Qiagen QiaQuick PCR Purification kit which will remove contaminating unused nucleotides and DNA polymerase before future use.

Sample Results #1:

These results were compiled when shuttling the full and truncated METTL7A and METTL7B gene sequences into a pGEX-3X plasmid backbone. The same concepts apply to all other PCR annealing temperature optimizations. All lanes shown below were volume normalized.

Gel #1:

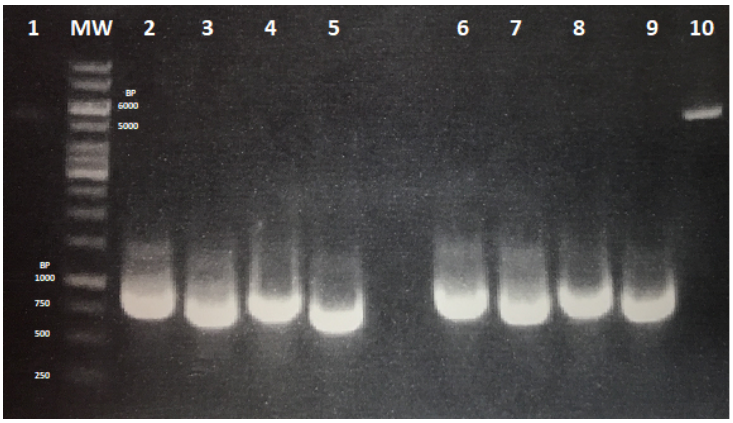

Lane Contents:

1: 20 ng Dabrowski METTL7B pEX-C-His Plasmid
2: METTL7B Full Anneal 42 °C
3: METTL7B Truncated Anneal 42 °C
4: METTL7A Full Anneal 42 °C
5: METTL7A Truncated Anneal 42 °C
6: METTL7B Full Anneal 47 °C
7: METTL7B Truncated Anneal 47 °C
8: METTL7A Full Anneal 47 °C
9: METTL7A Truncated Anneal 47 °C
10: 20 ng Dabrowski METTL7A pEX-C-His Plasmid

As shown in the gel, lower annealing temperatures result in significantly more DNA produced during the PCR run, resulting in brighter and larger bands. Unfortunately, as annealing temperature drops, primer binding becomes less specific for the correct complementary sequence. This is evident by the higher molecular weight bands evident in lanes 2, 3, 5, 6, and 7. In general, off-target PCR products should be avoided as they could result in incorrect sequences being ligated into the final expression plasmid.

Gel #2:

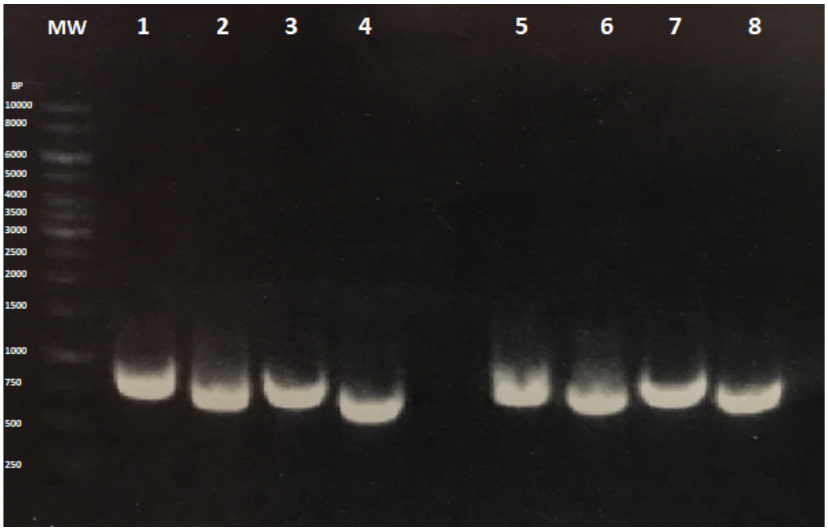

Lane Contents:

1: METTL7B Full Anneal 54 °C
2: METTL7B Truncated Anneal 54 °C
3: METTL7A Full Anneal 54 °C
4: METTL7A Truncated Anneal 54 °C
5: METTL7B Full Anneal 57 °C
6: METTL7B Truncated Anneal 57 °C
7: METTL7A Full Anneal 57 °C
8: METTL7A Truncated Anneal 57 °C

The higher molecular weight bands are no longer present in the second gel. This is because specificity for the correct complementary sequence increases when annealing temperatures are raised. It is also evident that total yield decreases, but is not a concern as multiple PCR reactions can be run in parallel and combined prior to further use.

It is important to note that DNA gel analysis of PCR reactions not only provides an idea of off-target DNA synthesis but also acts as a convenient way of confirming correct primer design. The total PCR amplicon length for the full length METTL7B PCR product is predicted to be 774 base pairs long, which coincides nicely with the gel band. Similarly, the truncated METTL7B PCR product is predicted to be 711 base pairs long which is also in line with the gel results. Therefore, while the PCR products have not been sequenced at this point, there is high confidence that the correct sequence is being amplified and experiments can proceed.

Step 3: Restriction Enzyme Digest

Both BamHI and EcoRI are active in the same buffer conditions so both enzymes can be used at the same time in one incubation. The following components are added to a single PCR tube: 1 µg of DNA, 10 units of BamHI-HF, 10 units of EcoRI-HF, 10X CutSmart Buffer from NEB, and nuclease-free water to 50 µL. The reaction was incubated at 37 ^{o}C for 15 minutes followed by a DNA gel. If the restriction enzymes are not fully functional in a single buffer, then the buffer must be adjusted between two sequential restriction digests. New England Biolabs has an online protocol calculator to determine if this is the case, which is the tool I suggest using.

The linearized plasmid backbone and digested PCR products were isolated using the NEB Monarch DNA Gel Extraction kit.

Experimental Note:

Gel extraction requires a significant amount of DNA loaded per gel lane. Ignore the DNA load amounts suggested in the E-gel user manual and load as much as possible. The band size may increase and possibly smear but it will give better yield after gel isolation. As long as the linearized backbone is significantly different in size from the excised section and non-restricted plasmid, there will not be any issues with contamination even if the gel bands spread.

Sample Results #2:

Similar to above, these results come from shuttling the full and truncated METTL7A and METTL7B gene sequences into a pGEX-3X plasmid backbone. The same protocols can be adapted to any other backbone digest and DNA ligation.

Gel #1:

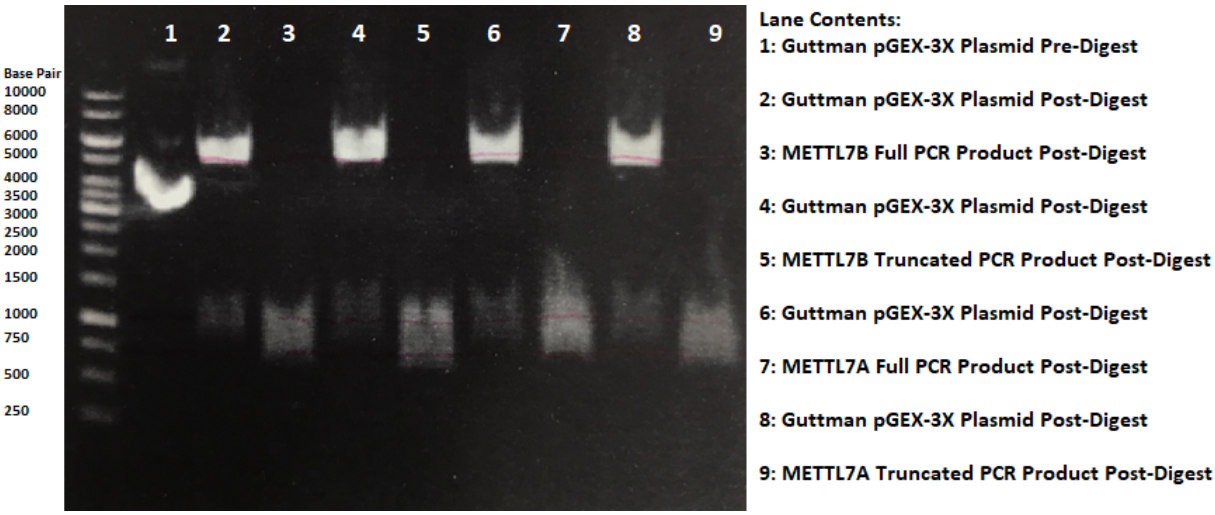

The even numbered lanes contain the pGEX-3X plasmid after it has been digested by two separate restriction enzymes. The predicted linearized backbone length is 4,942 base pairs which aligns well with the bright upper band. The non-restricted plasmid was run in lane 1 and exhibits a different retention in the DNA gel. This is likely because plasmids exist as coiled pieces of circular DNA so they will not run accurately on a DNA gel compared to linear fragments. The doubly restricted PCR products are shown in the odd lanes 3, 5, 7, and 9. There is no discernable difference in length compared to prior gels because the double restriction digest should only remove ~20 base pairs which is too small of a shift to see on this particular DNA gel. The presence of the PCR products does confirm that there were no internal restriction sites, otherwise there would be multiple smaller bands below the molecular weight of the starting material. These results suggest that the restriction digestion of the PCR products and expression plasmid proceeded as planned and that they should be purified and ligated.

Step 4: DNA Ligation

The DNA ligation was conducted using a 1:3 backbone:insert molar ratio. The following components were added to a single PCR tube: 0.02 pmol linearized backbone, 0.06 pmol digested PCR products, 10X T4 DNA Ligase buffer, 1 µL T4 DNA Ligase, and nuclease-free water to 20 µL. The reaction mixture was incubated at room temperature for 20 minutes and then heat inactivated via incubation at 65 ^{o}C for 10 minutes.

Step 5: E. coli Transformation and Plasmid Propagation

Chemically competent Stellar cells were transformed using the manufacturer-provided heat shock protocol and 2 µL of the DNA Ligase reaction solution. Transformed cells were plated onto LB-agar plates containing 100 µg/mL ampicillin and incubated overnight at 37 ^{o}C. Adjust the concentration and type of antibiotic used depending on the selection marker present in the plasmid backbone. Several online resources exist for suggested concentrations for multiple different commonly used antibiotics.

The following day, five individual colonies were picked using a flame-sterilized pipette tip and used to create 5 mL overnight cultures in ampicillin-containing LB media. The overnight cultures were split to create glycerol stocks and to purify plasmids using the QIAprep Spin Miniprep kit (Qiagen). Plasmid stocks were sequenced by Eurofins and nucleotide sequences were confirmed by hand using FinchTV histogram-viewing software.

Experimental Note:

When designing sequencing primers, make sure that they are located 40-60 nucleotides upstream or downstream of the sequence of interest for forward and reverse primers

respectively. The nucleotides closest to the primer binding site will not be easily identifiable and the histogram will only be easily readable after ~30 nucleotides have been amplified. Additionally, a sequencing run will identify 400-800 base pairs depending on the specific plasmid preparation and primer binding efficiency. Therefore, if the desired sequence is greater than 1 kb, it is likely worthwhile to design additional primers that can sequence the middle section.

Appendix II: Optimization steps for the Expression and Purification of Recombinant METTL7A and METTL7B

This appendix will detail the various approaches attempted to purify recombinant METTL7A and METTL7B. Each purification approach will be broken down into three separate sections. I will first discuss why the specific approach was chosen and what set-up was required. I will then present and discuss experimental results focusing on analysis of protein expression and activity. Finally, I will discuss the downsides associated with that specific expression and purification approach as well as possible fixes. Overall, this appendix will demonstrate the iterative nature of optimizing recombinant protein expression and purification.

First Purification Attempt: C-terminal Myc-FLAG Tag

Set-Up and Choice of Method:

The first purification approach attempted was a pCMV6 mammalian entry vector which constitutively expresses either METTL7A or METTL7B protein as shown below in Figure 1. This method was chosen because it had been previously validated in HeLa cells and shown to produce FLAG-tagged recombinant protein. The supporting data are presented and further discussed in Chapter 2.

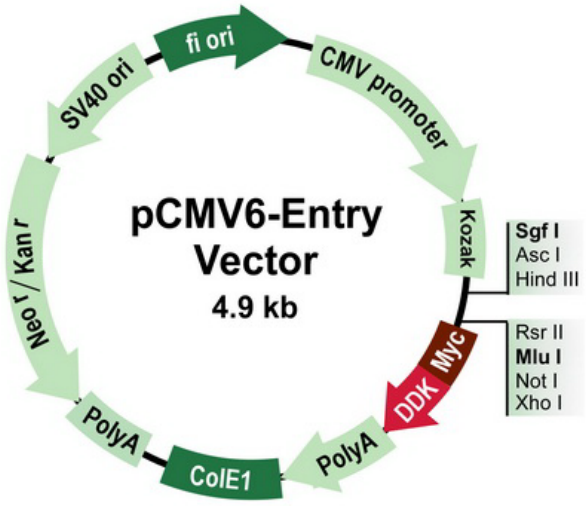

Figure 1. pCMV6 Entry Vector Plasmid Map: The gene sequence for the protein of interest is inserted downstream of the CMV promoter sequence and has a combination Myc-FLAG tag added to the C-terminus. The plasmid map is courtesy of Origene.

HEK293F cells were chosen as the most appropriate expression cell line due to their ability to be cultured in suspension. This allows a much higher cell density, and therefore higher total expression of recombinant protein, compared to adherent cell culture. The main set-up required for mammalian cell suspension culture is the presence of a shaker-incubator that can maintain a 5% CO_2 atmosphere. This equipment was readily available in the Lee lab and all HEK293F growth was conducted in their incubators.

Experimental Results:

HEK293F cells were transfected with a pCMV6-METTL7B expression vector using Lipofectamine3000 (ThermoFisher) according to the manufacturer protocol. Cell aliquots were taken at various time points and analyzed for METTL7B expression via western blot. The addition of the C-terminal affinity tag increased the fusion protein molecular weight to 31 kDa in total. As shown in Figure 2, METTL7B expression increased over time, peaked at 24 hours post-transfection, and gradually decreased until no protein expression was observed. Future experiments used a 24-hour transfection period prior to harvesting.

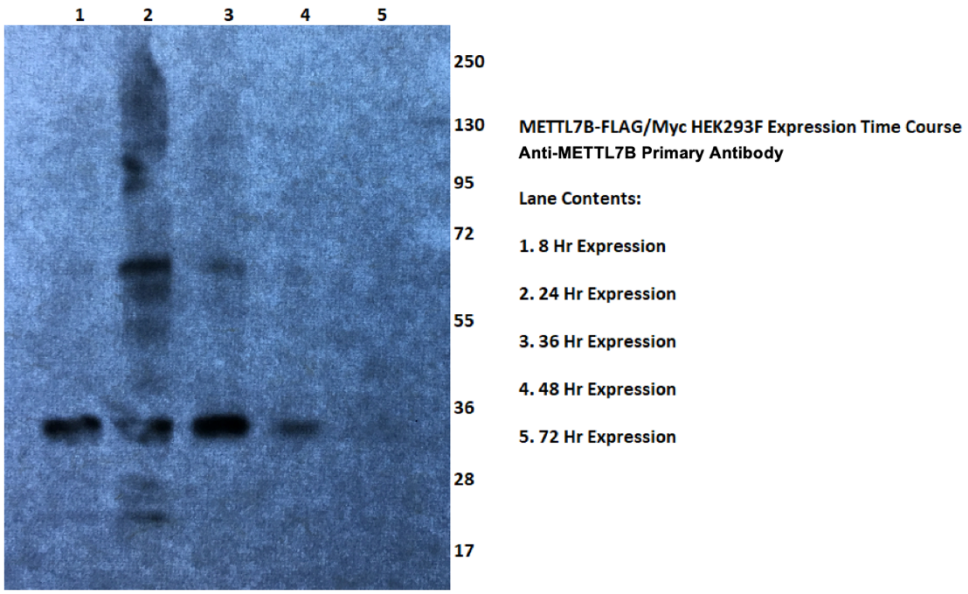

Figure 2. Recombinant METTL7B Expression Time Course in HEK293F Cells: METTL7B expression was measured by western blot at various time points in post-transfection cell lysate. Lane contents are as follows: 1) 8 hours post-transfection 2) 24 hours post-transfection 3) 36 hours post-transfection 4) 48 hours post-transfection 5) 72 hours post-transfection. The METTL7B band was visible between the 28 and 36 kDa markings.

Both METTL7A and METTL7B are membrane-bound proteins and thus require solubilization from lipid membranes prior to purification. While many purifications tend to use non-ionic detergents such as Triton X-100, we found that this detergent inhibited thiol methyltransferase activity in human liver microsomes (as discussed in Chapter 3). Therefore, we decided to use the zwitterionic detergent CHAPS, which did not inhibit captopril methylation in microsomal screens. Overexpressed HEK293F cell lysates were treated with varying concentrations of CHAPS and rotated end-over-end at 4 ^{o}C for an hour before high-speed centrifugation. Western blot analysis of the supernatant and pellet fractions showed that there was little difference in solubilization between the CHAPS concentrations tested and that some METTL7B was present as soluble protein in all tested conditions as shown in Figure 3.

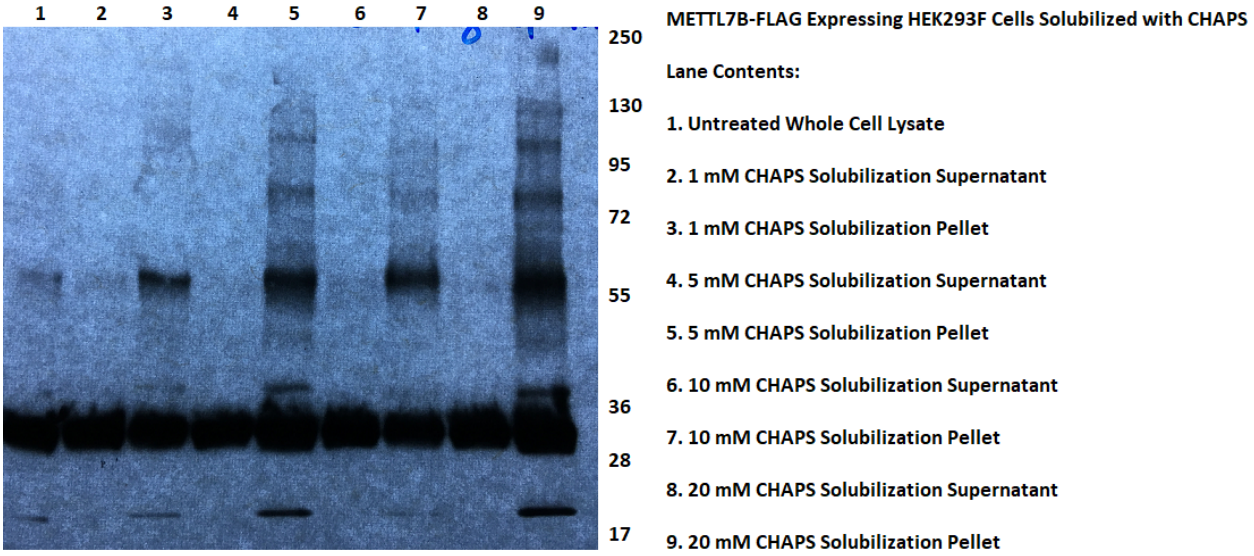

Figure 3. Effect of CHAPS Concentration on METTL7B Solubilization: HEK293F cell lysates were treated with a solubilization buffer containing 1-20 mM CHAPS. METTL7B western blot bands, visible at ~31 kDa, were present at similar intensities in both the supernatant and pellet fractions following high-speed centrifugation.

Lower concentrations of CHAPS tended to maintain captopril methylation activity better than higher concentrations as shown in Figure 4. Even though zwitterionic detergents are generally less denaturing than non-ionic detergents, it is possible that high CHAPS concentrations could disrupt the native structure of METTL7B. Since all concentrations seemed to solubilize the same amount of METTL7B, 1 mM CHAPS was chosen as the final concentration for all future purifications from HEK293F cells.

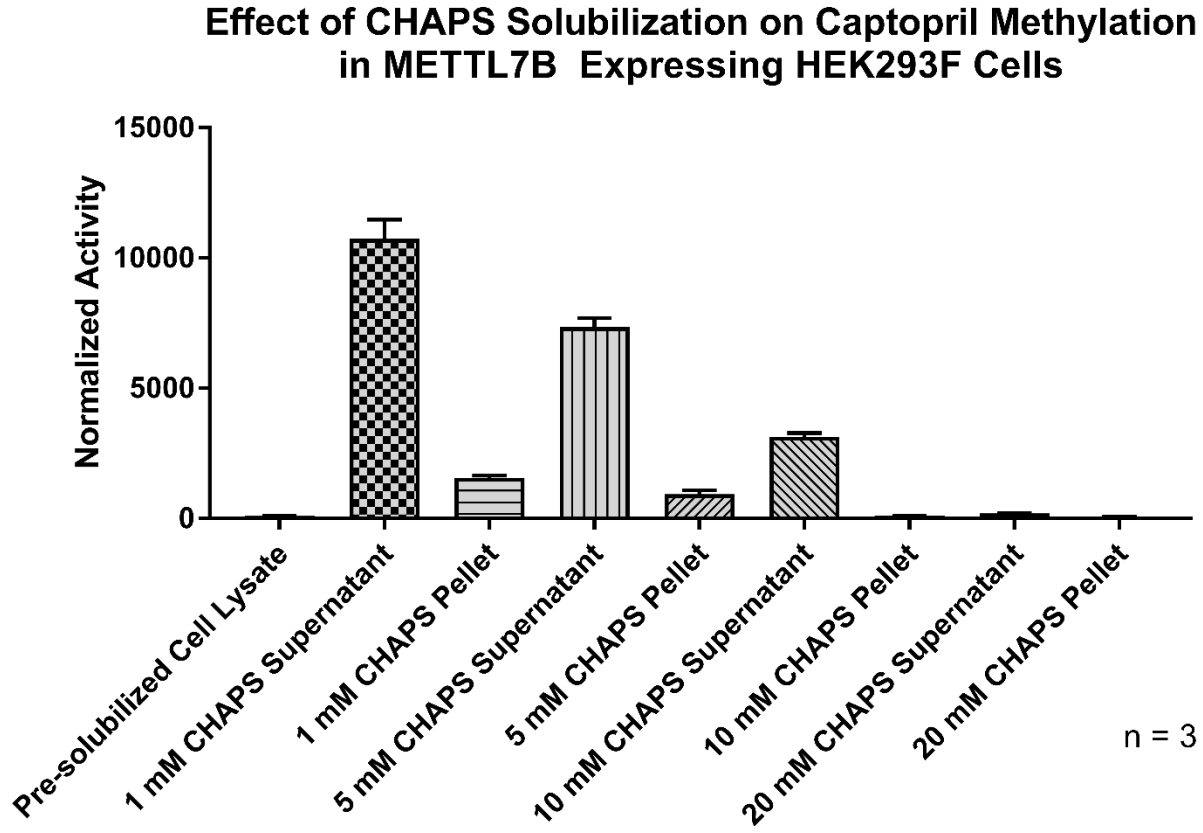

Figure 4. Effect of CHAPS Concentration on Captopril Methylation in HEK293F Subcellular Fractions: HEK293F cells overexpressing METTL7B were lysed and solubilized using various concentrations of CHAPS. The solubilized cells were centrifuged to separate soluble proteins and membrane fractions. Protein-normalized fractions were tested for captopril methylation in triplicate. Data are presented as the mean ± standard deviation.

Affinity purification of METTL7B was attempted using the optimized expression and solubilization conditions determined for HEK293F cells. Anti-FLAG affinity purification was initially chosen over anti-Myc affinity purification because the FLAG tag was further removed from the METTL7B protein sequence and more likely to be exposed in solution. The first purification attempt was conducted using anti-FLAG M2 affinity resin (Sigma) according to the manufacturer batch purification protocol. The results are shown below in Figure 5, where SDS-PAGE analysis discovered significant protein contamination even after multiple rounds of elution. The band pattern in elution fractions was distinct from wash fractions meaning that

contaminating proteins were being selectively retained. It is unclear whether the protein contaminants were interacting with the bound METTL7B or the affinity resin. Both tryptic digest and proteomic analysis confirmed the presence of METTL7B in elution fractions as well as identified a number of contaminating proteins, detailed in Figures 6 and 7 respectively.

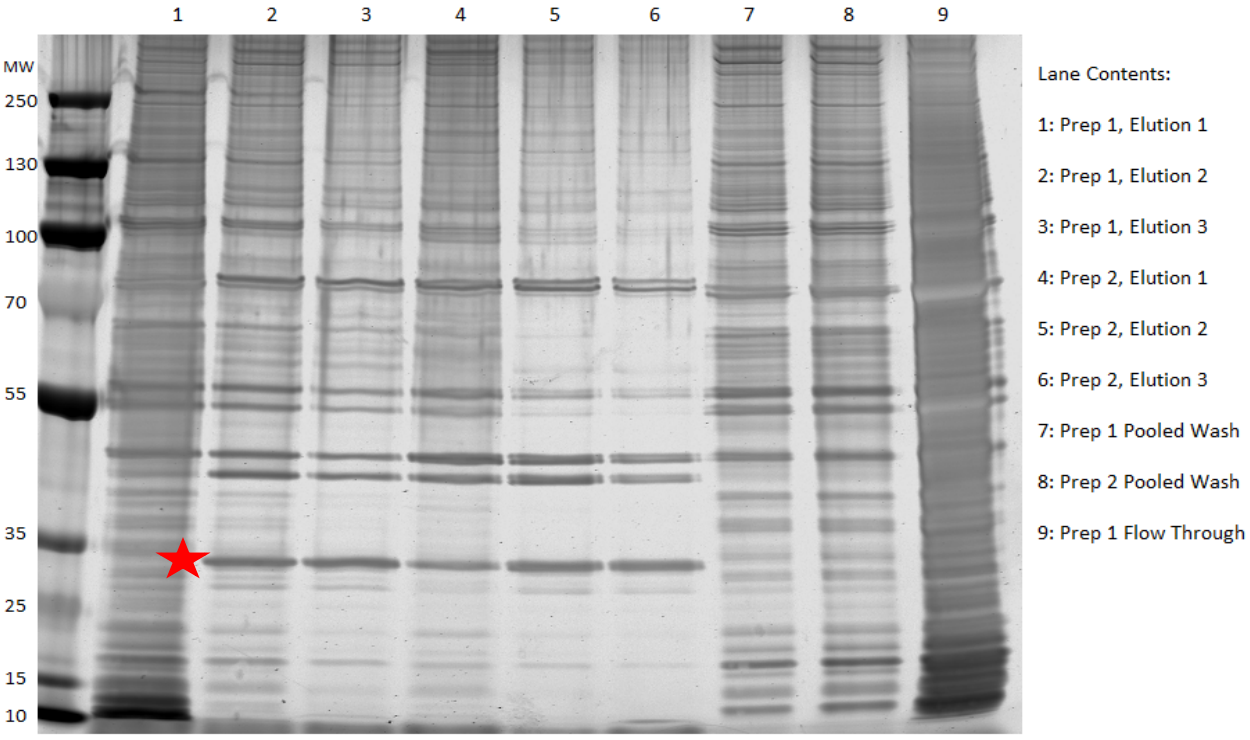

Figure 5. SDS-PAGE Silver Stain Analysis of M2 Purification of METTL7B: Elution and wash fractions from two separate batch purifications of FLAG-tagged METTL7B from solubilized HEK293F cell lysate were run on SDS-PAGE. Lanes 1-3 correspond to three sequential elutions from the same M2 affinity resin, similar to lanes 4-6. The pooled washes for each purification are shown in lanes 7 and 8 respectively. Lane 9 shows the loading flow-through which contains proteins that did not bind to the M2 affinity resin. The putative METTL7B band is marked by the red star.

3 **Acc. #:** Q6UX53 **Uniprot ID:** MET7B_HUMAN **Species:** HUMAN **Name:** Methyltransferase-like protein 7B
Organism: Homo sapiens **Gene:** METTL7B **Existence:** Evidence at protein level **Version:** 2
Protein MW: 27775.1 **Protein pI:** 8.7 **Protein Length:** 244 **Index:** 231643

Num Unique	% Cov	Best Disc Score	Best Expect Val
15	64.8	5.08	8.5e-9

m/z	z	ppm	DB Peptide	Variable Mods	RT	Score	Expect	# in DB
1214.0813	2	-1.3	VALLELGCGTGANFQFYPPGCR		17.1545	53.5	8.5e-9	1
855.3916	2	-2.3	DLENAQFSEIQMER		12.9342	54.8	1.6e-8	1
765.4059	2	-1.8	SYFPYLMAVLTPK		19.8592	44.2	8.3e-8	1
728.8463	2	-2.5	VTCLDPNPHFEK		9.9211	49.0	2.2e-7	1
1375.6809	3	-0.66	VLRPGGVLFFWEHVAEPYGSWAFMWQQVFEPTWK		23.7028	29.6	8.1e-7	1
594.7645	2	-2.6	HIGDGCCLTR		7.6631	32.0	9.0e-7	1
752.0198	3	0.17	ETWKDLENAQFSEIQMER		14.5450	35.0	2.5e-6	1
568.7727	2	-2.1	FVVAPGEDMR	Oxidation@9	9.4643	30.1	4.8e-6	1
560.7800	2	6.4	FVVAPGEDMR		11.0980	31.5	5.1e-6	1
617.8413	2	-0.96	WLPVGPHIMGK		13.3720	27.5	2.6e-5	1
345.6926	2	-0.23	GLTGASGK		3.5080	22.5	6.2e-4	1
423.2200	2	7.4	HLQYER		5.8127	23.5	0.0023	1
436.2707	2	-2.1	KVLQEVR		6.3538	31.3	0.0062	1
372.2241	2	-0.12	VLQEVR		7.0601	16.9	0.041	2
432.7441	2	-1.9	ELFSQIK		11.7764	16.9	0.048	1

Figure 6. METTL7B Peptides Identified in M2 Elution Fractions: Multiple peptides unique to METTL7B were identified by proteomic analysis in a M2 eluent fraction. Mass error was generally below 3 ppm error which indicates high confidence in defining parent m/z ratios. These results were generated using ProteinProspector.

9_13_2016_002/METTL7B M2 Eluent				Protein MW	Species	Protein Name
Num Unique	% Cov	Best Disc Score	Best Expect Val			
32	66.9	5.79	4.1e-10	70052.8	HUMAN	Heat shock 70 kDa protein 1A
6	12.5	3.71	2.9e-6	70898.7	HUMAN	Heat shock cognate 71 kDa protein
18	65.3	4.92	1.7e-8	49671.3	HUMAN	Tubulin beta chain
15	64.8	5.08	8.5e-9	27775.1	HUMAN	Methyltransferase-like protein 7B
13	38.2	5.83	3.4e-10	50228.5	HUMAN	RuvB-like 1
15	38.0	4.78	3.1e-8	72684.5	HUMAN	Protein arginine N-methyltransferase 5
12	30.7	4.28	2.6e-7	51157.0	HUMAN	RuvB-like 2
9	27.9	5.40	2.1e-9	50152.1	HUMAN	Tubulin alpha-1B chain
9	20.3	4.94	1.6e-8	83264.9	HUMAN	Heat shock protein HSP 90-beta
9	13.8	4.93	1.6e-8	84660.4	HUMAN	Heat shock protein HSP 90-alpha
3	9.6	3.24	2.1e-5	39365.1	HUMAN	Heat shock protein HSP 90-alpha A2
5	19.9	3.80	2.0e-6	36724.7	HUMAN	Methylosome protein 50
5	13.9	3.54	5.9e-6	50141.3	HUMAN	Elongation factor 1-alpha 1
5	20.1	3.33	1.5e-5	25761.8	HUMAN	Polyubiquitin-B
3	13.9	5.38	2.3e-9	32575.3	HUMAN	Nucleophosmin
2	8.6	4.13	2.6e-7	61055.2	HUMAN	60 kDa heat shock protein, mitochondrial
2	6.9	4.38	1.7e-7	45374.5	HUMAN	Nucleosome assembly protein 1-like 1
2	4.2	3.49	7.4e-6	62639.8	HUMAN	Stress-induced-phosphoprotein 1
2	5.1	3.62	1.5e-6	59751.1	HUMAN	ATP synthase subunit alpha, mitochondrial
1	16.8	5.05	9.6e-9	13281.7	HUMAN	Small nuclear ribonucleoprotein Sm D1
1	11.3	4.81	2.6e-8	12676.4	HUMAN	Ig kappa chain V-II region Cum
1	5.5	4.36	1.8e-7	59671.6	HUMAN	T-complex protein 1 subunit epsilon
1	5.3	4.24	6.0e-8	37564.2	HUMAN	Eukaryotic translation initiation factor 3 subunit F
1	2.5	3.91	1.2e-6	56560.4	HUMAN	ATP synthase subunit beta, mitochondrial
1	10.4	3.50	6.2e-6	11665.0	HUMAN	60S acidic ribosomal protein P2
1	8.6	3.05	2.2e-6	16272.9	HUMAN	40S ribosomal protein S14
1	3.0	3.01	4.9e-6	38738.3	HUMAN	Putative heat shock protein HSP 90-alpha A5

Figure 7. M2 Purification Protein Contaminants: Many contaminating proteins were identified by proteomic analysis of a M2 eluent fraction. Expect values were low which increases confidence in accurate protein identification. Most contaminants are chaperone proteins, such as heat shock proteins, or cytoskeletal proteins such as tubulin.

Captopril methylation was observed in M2 eluent fractions and not in the wash fractions, suggesting that METTL7B binds tightly to the affinity resin. Unfortunately, the activity measured in elution fractions was much lower compared to the relatively high activity measured in the HEK293F cell lysate. This could indicate inactivation of the protein over the course of the purification. Alternatively, the METTL7B protein could remain associated with the M2 affinity resin even after incubating the resin in elution conditions. This appeared to be the case, as evidenced by the large amount of METTL7B activity associated with M2 resin after elution with FLAG peptide, shown in Figure 8.

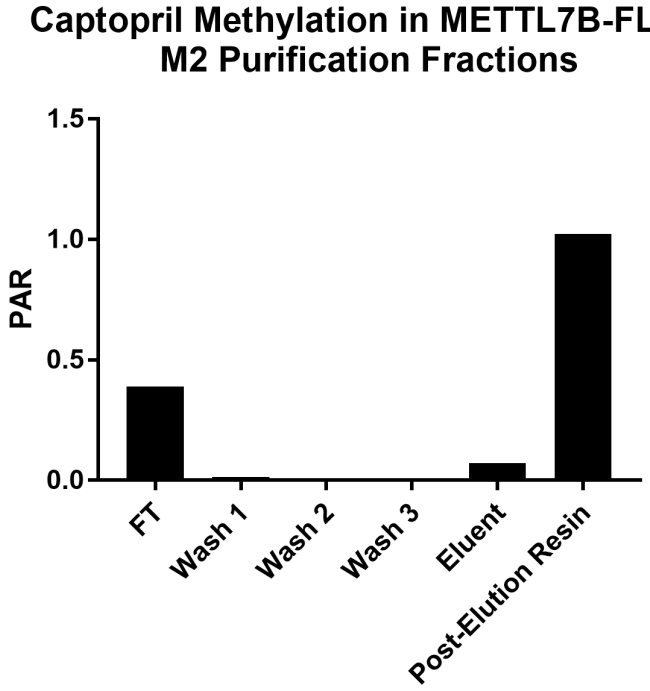

Figure 8. Captopril Methylation in M2 Purification Fractions: The majority of captopril methylation activity was associated with M2 resin eluted by incubation in a FLAG peptide-containing solution. Small amounts of activity were also observed in the eluent fraction and the initial wash. No activity was observed in the second and third wash fractions.

The initial elution conditions, 1-hour incubation with 200 ng/µL FLAG peptide, were insufficient to release the majority of the METTL7B from the M2 resin. Both the elution incubation time and the FLAG peptide concentration were varied in an attempt to increase the amount of METTL7B released from the affinity resin. Elution efficacy was monitored by SDS-PAGE (Figure 9) and by measuring eluent captopril methylation activity (Figure 10). The SDS-PAGE analysis did not indicate any major 31 kDa bands present in any eluent fraction, meaning that the METTL7B yield is extremely low. Additionally, captopril methylation was not significantly increased in any eluent fraction compared to the initial elution conditions. Therefore, the METTL7B fusion protein is retaining on the M2 resin in a FLAG-independent fashion.

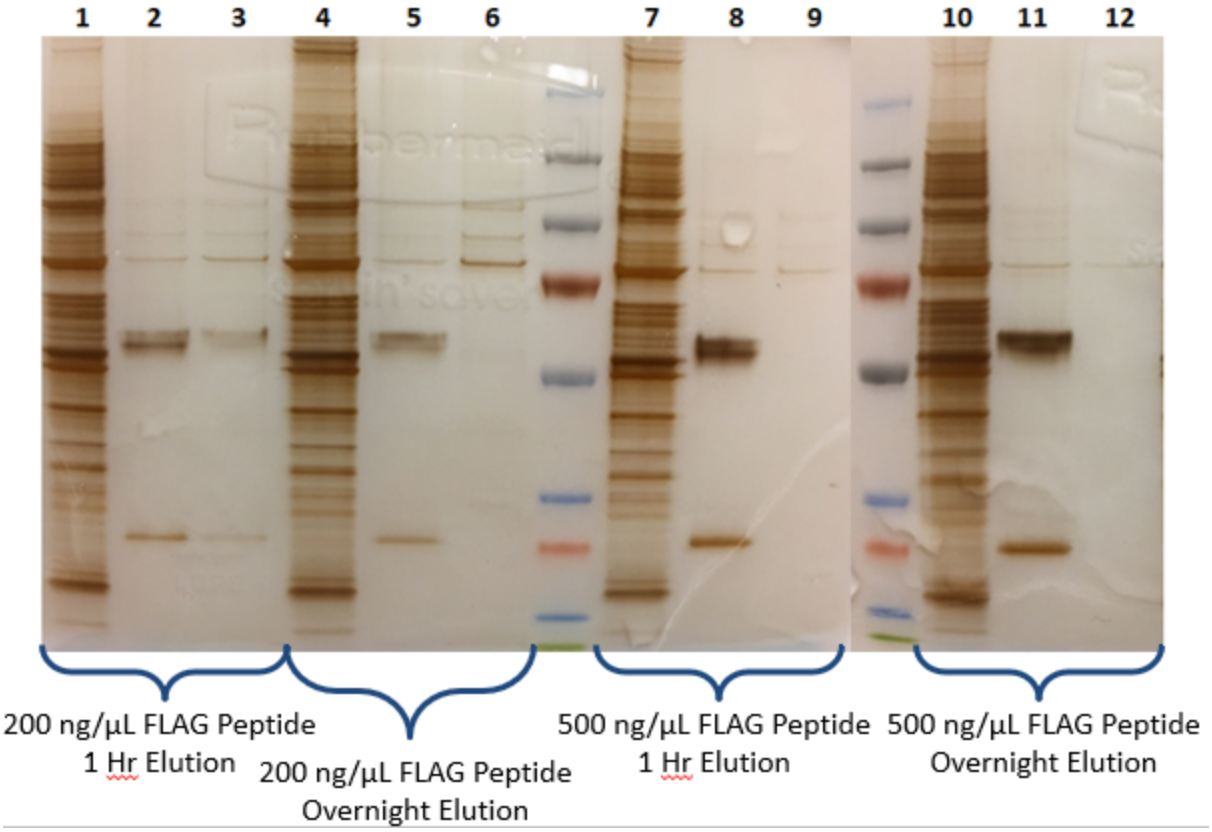

Figure 9. Effect of M2 Elution Condition on Elution Yield and Purity: SDS-PAGE silver stain analysis of different M2 elution conditions. Each set of three wells contains the resin flow-through in the left-most lane, the eluted M2 resin in the middle lane, and the eluent fraction in the right-most lane. Little to no protein was observed in the elution lanes under any elution condition. Bands in lane 3 are due to loading cross-contamination from lane 2.

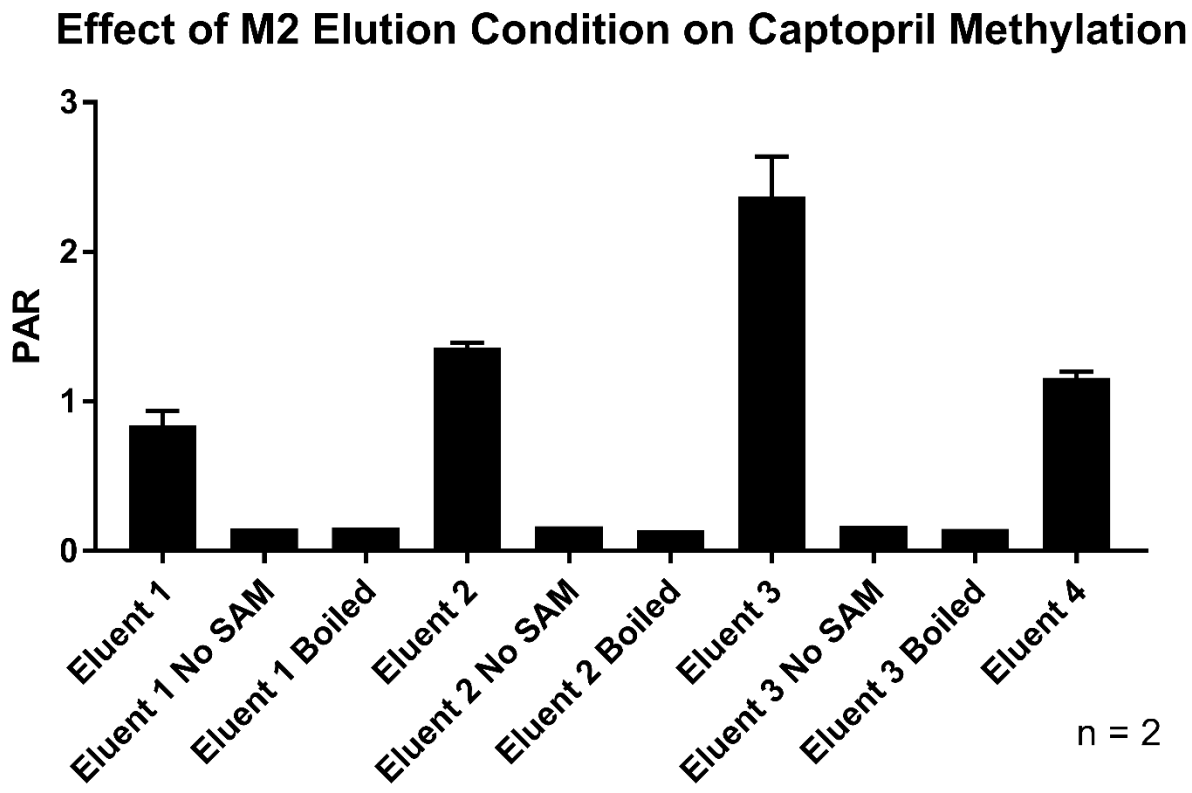

Figure 10. Effect of M2 Elution Condition on Eluent Captopril Methylation: Captopril methylation was measured in multiple eluent fractions collected under different elution conditions. Eluent 1 was eluted with 200 ng/µL FLAG peptide for 1 hour. Eluent 2 was eluted with 200 ng/µL FLAG peptide overnight. Eluent 3 was eluted with 500 ng/µL FLAG peptide for 1 hour. Eluent 4 was eluted with 500 ng/µL FLAG peptide overnight. Data are presented as mean ± standard deviation.

Bioinformatic analysis of the METTL7B primary sequence was conducted using the Solvent Accessibilities (SABLE) secondary structure and transmembrane propensity prediction engine developed by the Meller lab at the University of Cincinnati, College of Medicine. SABLE predicted that the N-terminus of the METTL7B protein forms a highly hydrophobic alpha helix and that the highlighted residues (positions 2-25) likely insert into plasma membranes. The graphical results of the structure prediction are shown below in Figure 11.

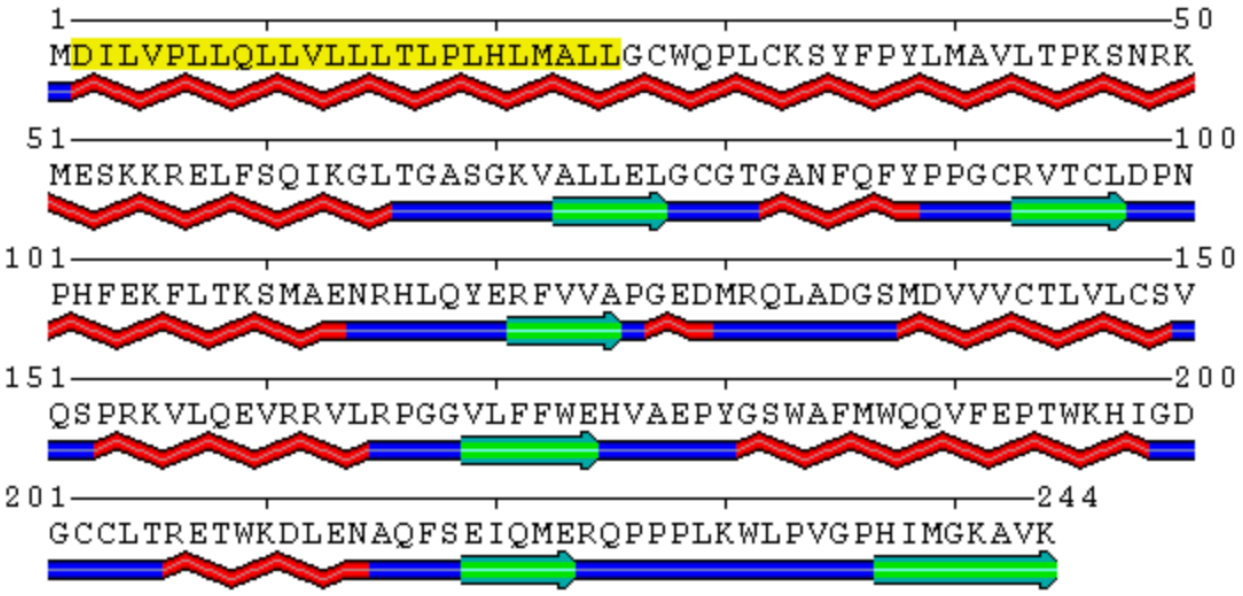

Figure 11. METTL7B Secondary Structure and Transmembrane Prediction: Secondary structure prediction, conducted by SABLE, identified a highly hydrophobic N-terminal alpha helical segment that will likely insert into plasma membranes. Red portions signify alpha helices, blue portions signify random coil, and green portions signify beta sheets.

Given that the recombinant METTL7B contains a very hydrophobic N-terminal alpha helix, we hypothesized that there could be strong non-specific binding between the METTL7B fusion protein and the agarose resin. The agarose beads used in the M2 affinity resin are 4% crosslinked. Increasing the crosslinking percentage should in theory decrease bead pore size and possibly reduce non-specific binding. It was difficult to find 6% crosslinked anti-FLAG resin however Pierce anti-c-Myc agarose uses 6% crosslinked agarose and was commercially available. This resin should work well for affinity purification because it binds the Myc portion of the METTL7B fusion protein dual affinity tag. Figures 12 and 13 show that METTL7B could be retained and eluted from Pierce anti-c-Myc affinity resin, which supports the hypothesis of non-specific binding to highly porous agarose beads. An alternative explanation is that cMyc-

tagged proteins are more easily eluted than FLAG-tagged proteins however the large number of publications reporting successful purification of FLAG-tagged proteins suggests otherwise.

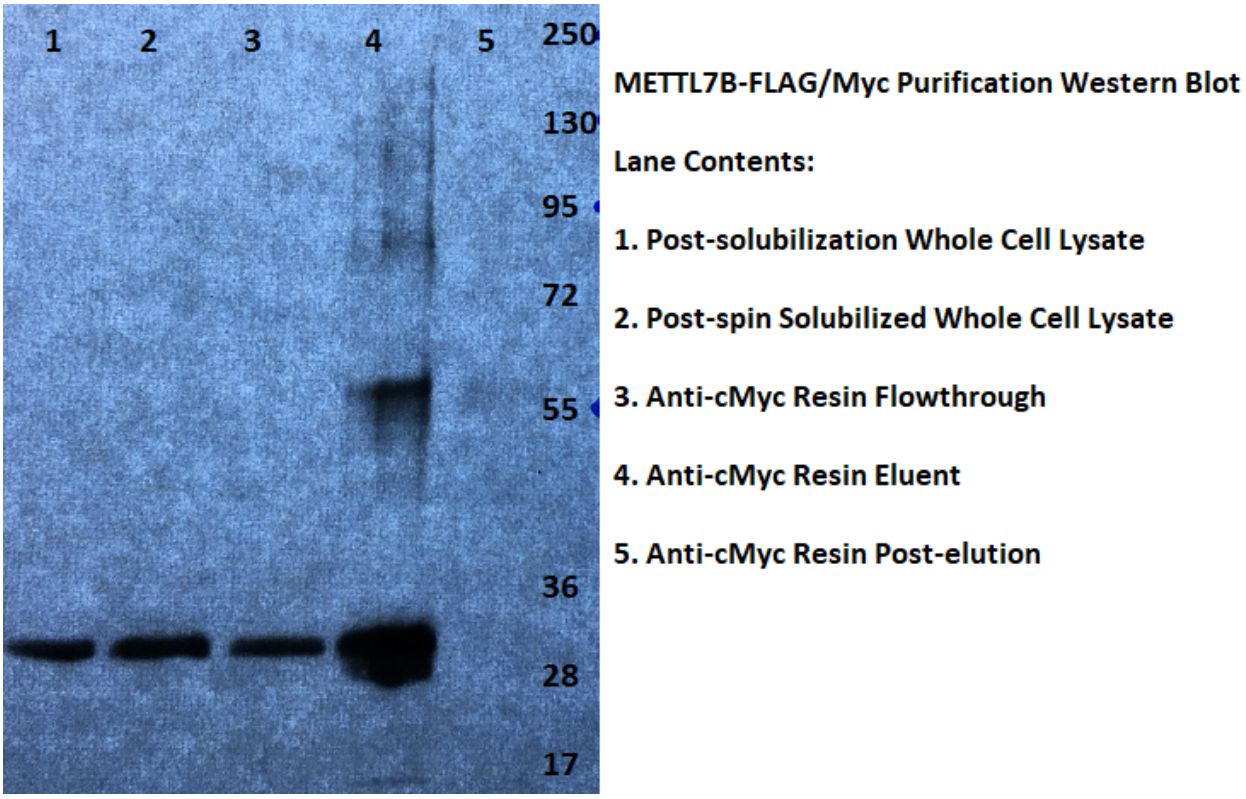

Figure 12. Example METTL7B cMyc Purification Western Blot: Protein-normalized samples were analyzed using an anti-METTL7B primary antibody. A distinct 31 kDa band is present in all samples except for the eluted anti-cMyc resin sample. The eluent fraction contains a relatively intense band compared to other samples.

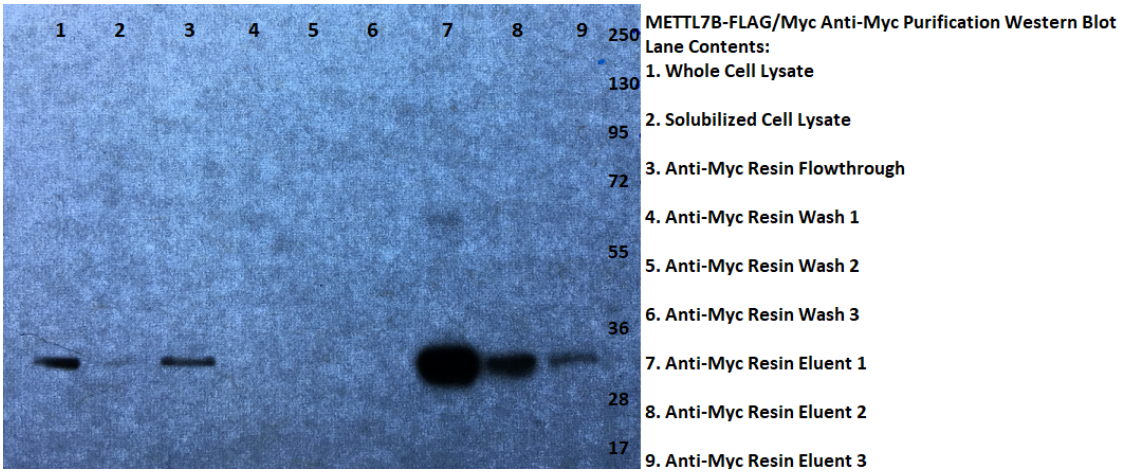

Figure 13. METTL7B Non-specific Binding in cMyc Affinity Purification: A 31 kDa METTL7B band was observed in whole cell lysate, solubilized cell lysate, resin loading flow-through, and all elution fractions. No bands were detected in the resin wash fractions. Elution band intensity decreased upon subsequent incubations with elution buffer.

Sequential rounds of elution from the same anti-cMyc resin produced decreasing amounts of METTL7B and captopril methylation. The METTL7B band intensity pattern in lanes 7-9 of Figure 12 directly correlates to the observed thiol methyltransferase activity displayed in Figure 14. All active protein was eluted after three sequential incubations in elution buffer and very little activity was observed associated with eluted resin. This again supports the hypothesis that the hydrophobic N-terminus of the METTL7B fusion protein was interacting with the agarose beads which was minimized by using a more crosslinked resin, namely 6% agarose rather than 4% agarose.

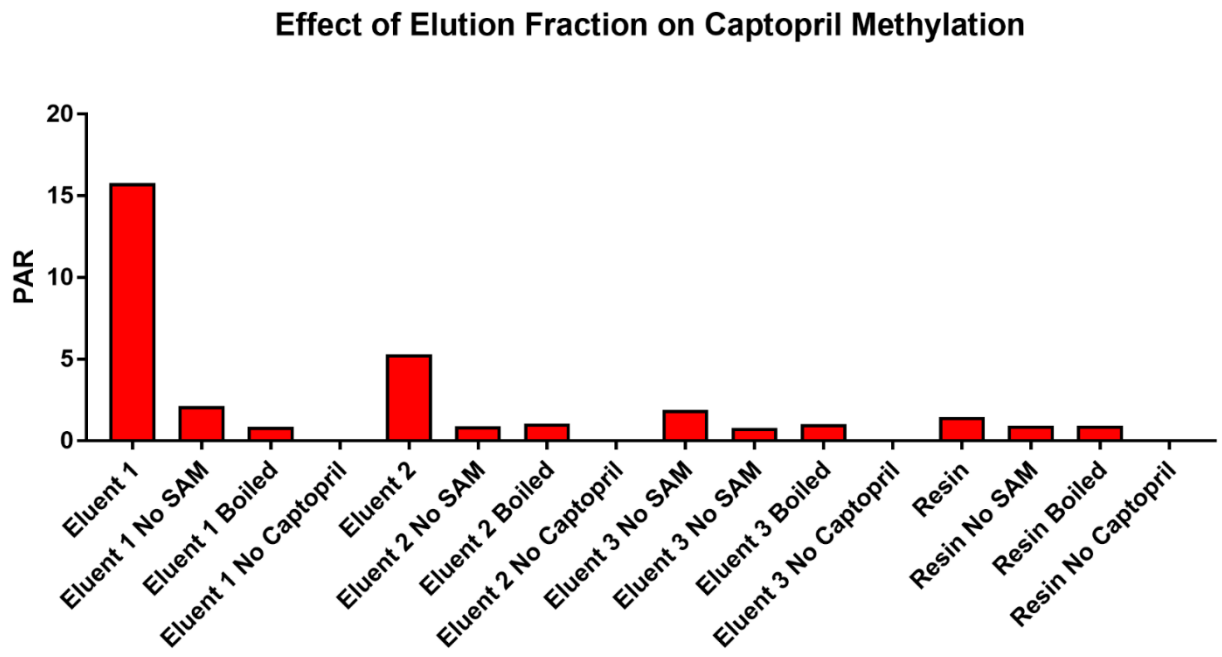

Figure 14. Captopril Methylation in Subsequent Anti-cMyc Elution Fractions: Captopril methylation activity measured in each anti-cMyc elution fraction. Captopril methylation decreased with increasing rounds of elution. Little to no activity was observed in the eluted resin fraction or in any negative control samples.

The purity and yield of anti-cMyc purification of tagged METTL7B was determined by silver stain, shown in Figure 15. Lanes 7 and 8 do not contain a distinct band in the lower half of the gel, where one would expect recombinant METTL7B, despite knowing that elution efficacy

is not problematic. Higher molecular weight contaminants are present in much greater abundance than any potential METTL7B protein despite observing captopril methylation activity. Therefore, it is likely that the overall yield of recombinant METTL7B is extremely low. Despite having solved the non-specific binding issue, purification from mammalian cells does not appear to have a high enough yield to be a viable purification strategy going forward, even upon scaling up suspension culture volumes.

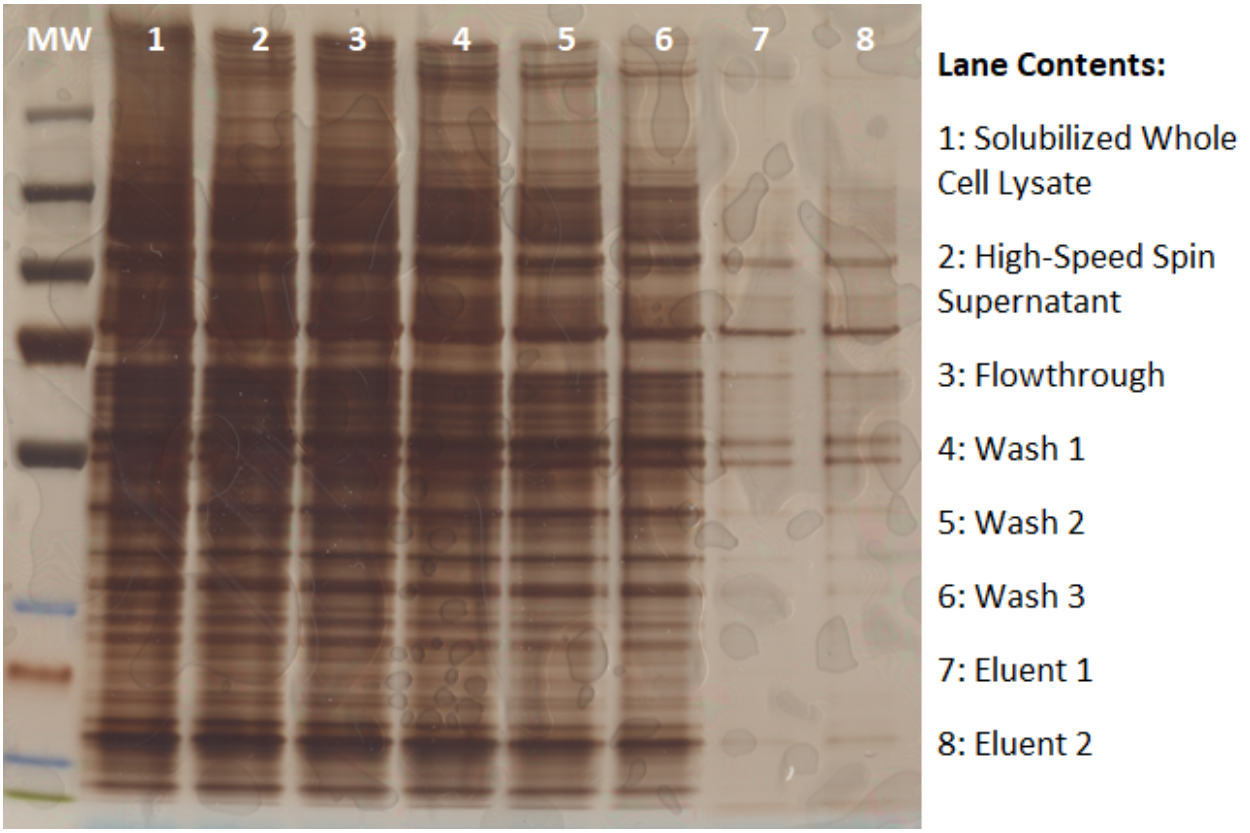

Figure 15. Example anti-cMyc Purification SDS-PAGE Silver Stain: Multiple purification fractions were analyzed from an anti-cMyc purification of tagged METTL7B. Similar contaminating band patterns were observed between elution and wash fractions. No METTL7B band was apparent in either eluent lane.

Pitfalls and Potential Fixes:

As shown in the prior results, purification of METTL7B is complicated by the fact that the N-terminal alpha helix is extremely hydrophobic which likely caused non-specific binding to some agarose resins. This non-specific binding can be reduced by selecting highly crosslinked

agarose supports. Unfortunately, overall yield of recombinant protein remained very low even under optimal purification conditions. This is a known drawback of recombinant protein expression in mammalian cells compared to other microorganisms such as yeast or *E. coli*.

Mammalian cell culture can be scaled up through the use of suspension culture yet the growth rates will not be comparable to *E. coli,* which can have replication times of around 20 minutes. If recombinant protein must be produced in mammalian cells and high yield is required, I suggest transfecting suspension-cultured cells, possibly pooling many samples prior to purification, or growing stable-expressing cells in a bioreactor. Otherwise, recombinant expression of the protein of interest in *E. coli* is highly preferred.

Second Purification Attempt: C-terminal His Tag

Set-Up and Choice of Method:

The second purification approach used was a pEX-C-His bacterial expression vector to express METTL7A or METTL7B protein as shown below in Figure 16. This method was chosen because it would allow the protein of interest to be expressed in *E. coli* which allows much higher amounts of total expressed protein, solving the main issue observed with purification from overexpressed mammalian cells.

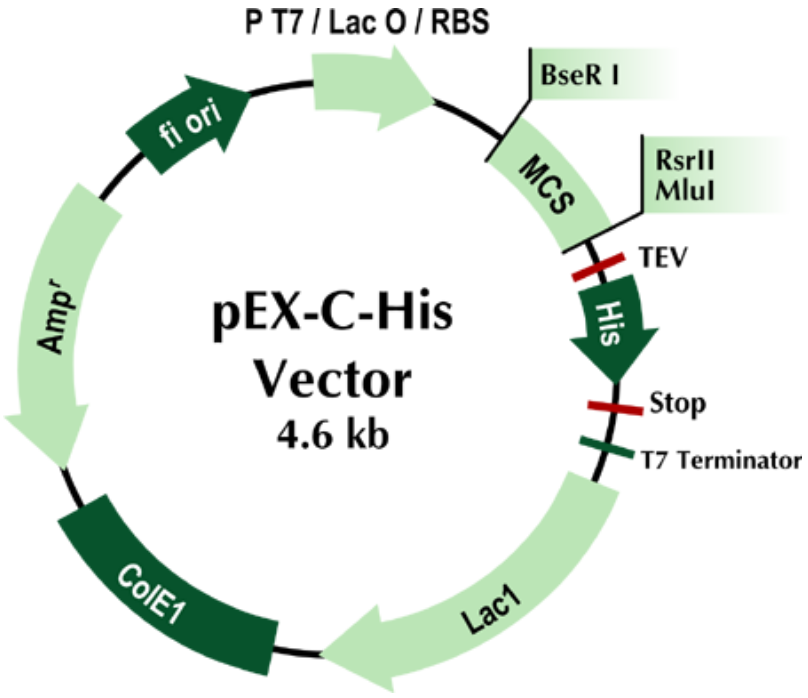

Figure 16. pEX-C-His Expression Vector Plasmid Map: Expression of the gene of interest is placed under control of the lac operon. Therefore, protein synthesis is triggered by addition of IPTG. The recombinant protein has a histidine affinity tag added to the C-terminus. The plasmid map is courtesy of Origene.

Unlike mammalian cell culture, *E. coli* can be grown at a wide range of temperatures and under normal atmospheric conditions. The main requirement prior to expressing recombinant protein in *E. coli* is the generation of transformed cell stock. This can be completed using commercially competent BL21(DE3) cells, the plasmid of choice, the manufacturer or Cold Spring Harbor heat shock protocol, and selective growth media. This process will take 2-3 days depending on the rate of formation of transformed colonies. Additionally, all growth media must be made fresh and antibiotics must be added directly prior to inoculation. All *E. coli* growth presented below was performed using the shaker incubators present in the Atkins lab.

Experimental Results:

The first experiment conducted using a new expression plasmid or host organism is a protein expression time course. This experiment was performed by varying the time following IPTG addition to the expression media prior harvesting. Since the pEX-C-His plasmid places expression of *METTL7A* and *METTL7B* under control of the lac operon, recombinant protein will

only be produced after adding the IPTG inducer. Expression of His-tagged METTL7B was determined by western blot at multiple time points after induction, shown in Figure 17. METTL7B expression was not visible at 2 hours post-induction but increased with time, with maximal expression occurring at 24 hours post-induction. This induction time period was used for all *E. coli* expression of His-tagged METTL7B using the pEX-C-His plasmid.

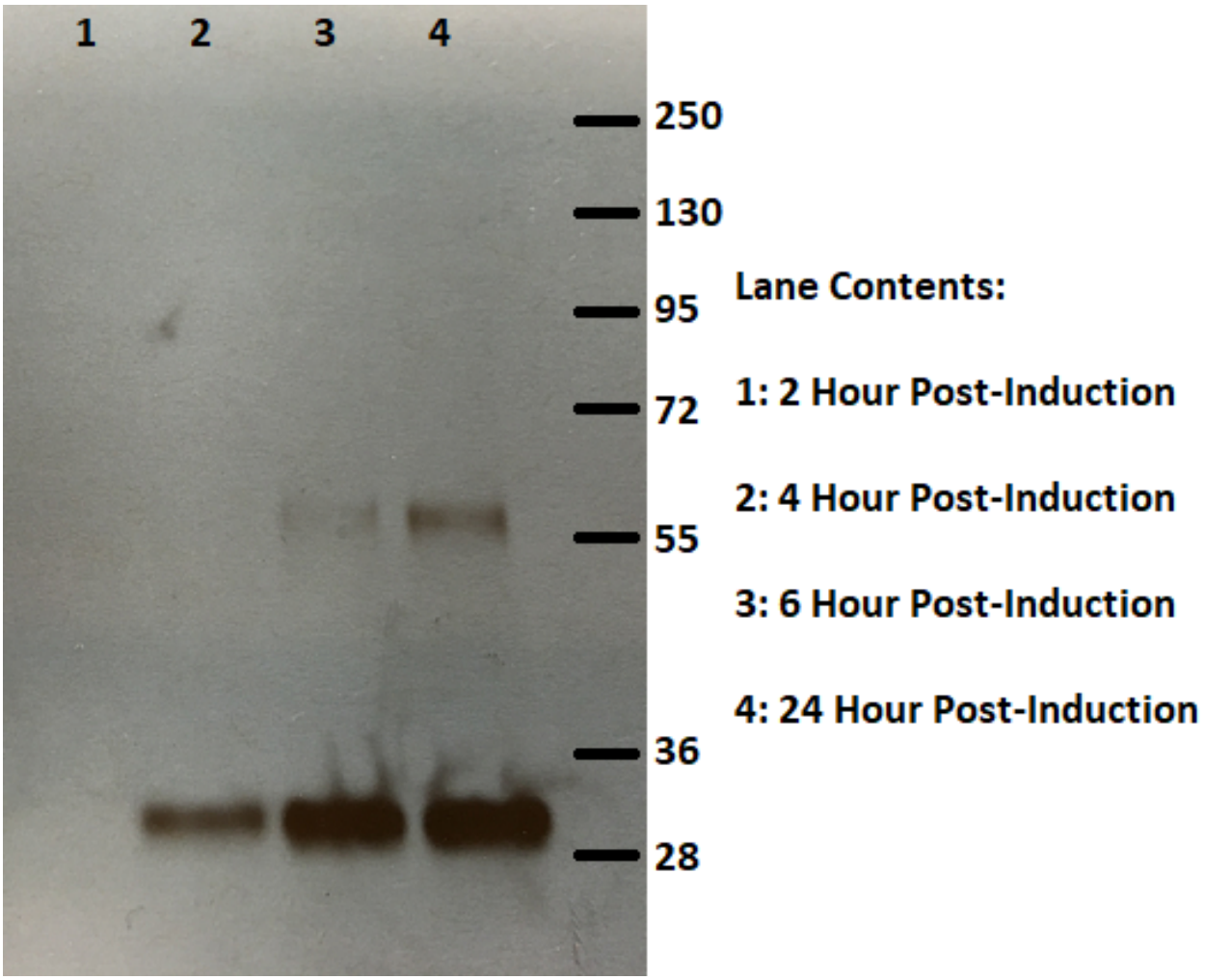

Figure 17. His-tagged METTL7B Expression Time Course Western Blot: METTL7B expression was measured in *E. coli* whole cell lysate at 2, 4, 6, and 24 hours post-induction with IPTG. The METTL7B band was not present at 2 hours but was extremely evident at all other time points. The greatest expression was observed at 24 hours post-induction.

Initial purification attempts using NiNTA affinity resin displayed significant numbers of contaminating proteins in the eluent fractions. Fortunately, there was also a strong band observed near the predicted fusion protein molecular weight of 28 kDa, shown in Figure 18. Interestingly, no captopril methylation was observed in these eluent fractions.

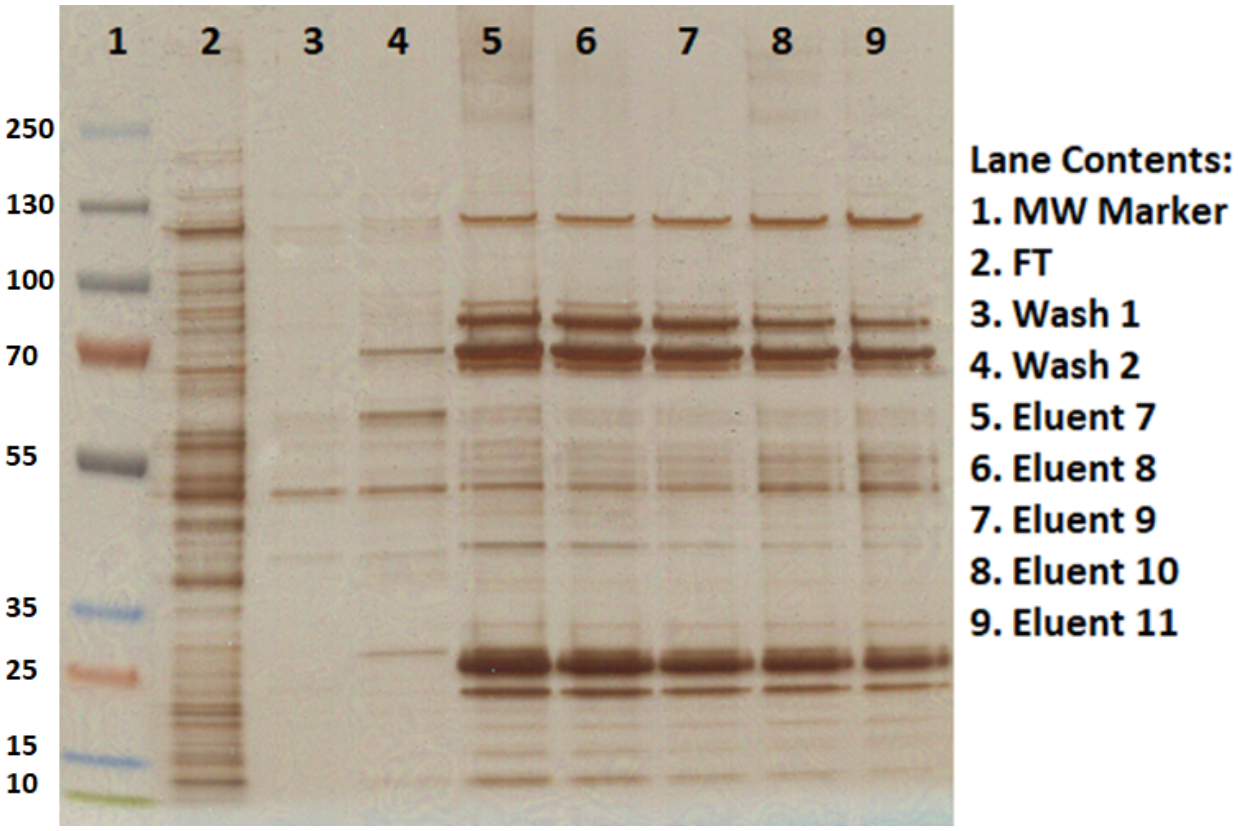

Figure 18. SDS-PAGE Silver Stain of Initial NiNTA Purification of His-tagged METTL7B: Purification fractions from an initial NiNTA purification of His-tagged METTL7B were analyzed by SDS-PAGE silver stain. Sequential elution fractions in lanes 5-9 exhibit a very distinct band around 28 kDa. Many other contaminating proteins are present in the elution fractions.

No captopril methylation was present in any purification elution fractions using NiNTA and METTL7B expressed using the pEX-C-His expression vector. To confirm purification of METTL7B, NiNTA elution fractions were analyzed by Native PAGE and the major bands were excised and subjected to in-gel tryptic digest, shown in Figure 19. Proteomic analysis determined that the major bands were composed of the *E. coli* proteins, SlyD and ArnA, and that METTL7B was not present. Both proteins naturally bind nickel residues and are known

contaminants during purification of His-tagged proteins expressed in *E. coli*. Given that the molecular weight of SlyD is slightly above 20 kDa and that ArnA is around 75 kDa, it is probable that the NiNTA elution fractions were almost entirely composed of these two proteins rather than METTL7B.

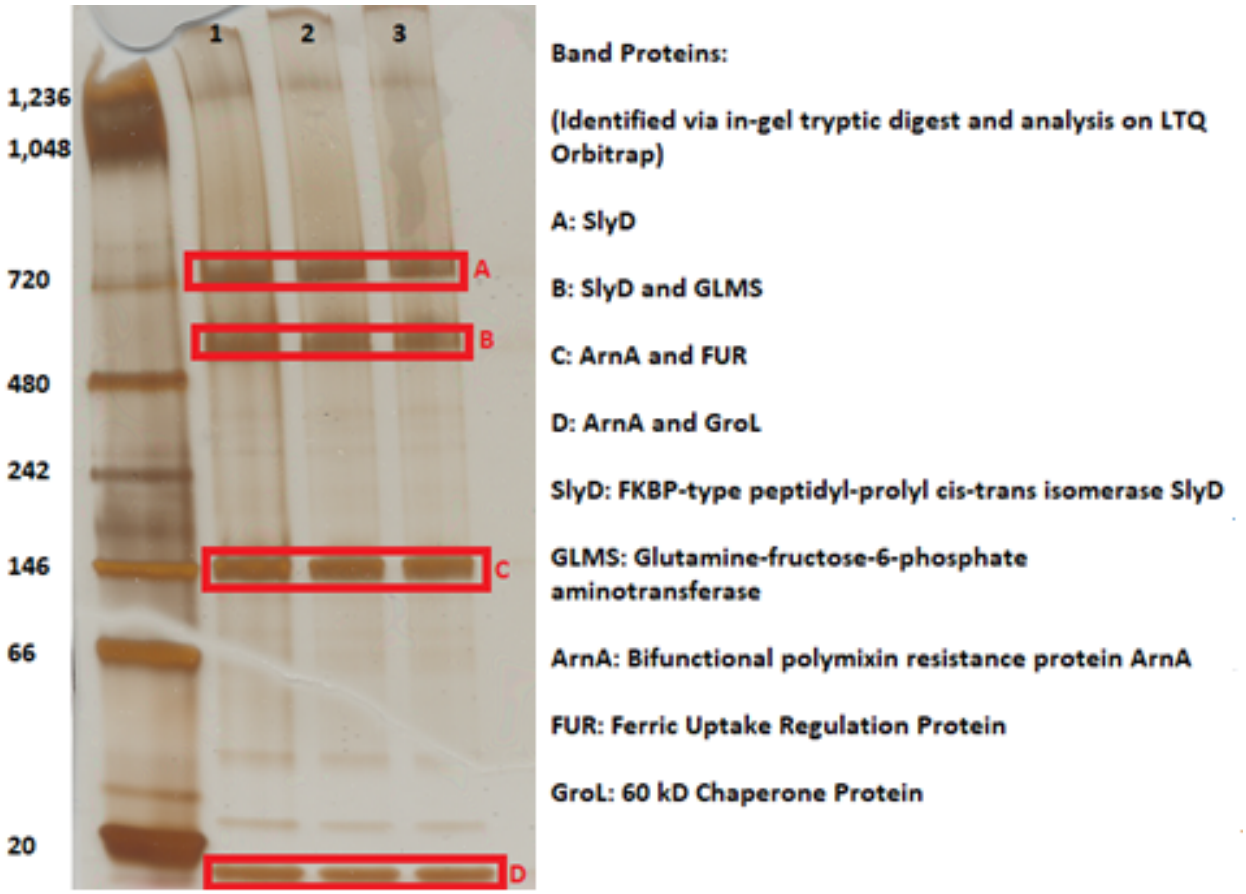

Figure 19. Native PAGE Silver Stain of NiNTA Purification Eluent: An eluent fraction from a NiNTA purification of METTL7B from *E. coli* was analyzed by Native PAGE and visualized by silver staining. The bands in the red boxes were excised, digested with trypsin, and analyzed using shotgun proteomics. The major proteins present in each band are listed on the right and consist of known endogenous *E. coli* proteins that will bind nickel ions.

One potential hypothesis for the poor METTL7B yield was that the solubilization procedure used in this purification was not applicable for *E. coli* purifications given that it was optimized for mammalian cell-based purifications. Therefore, the solubilization of His-tagged METTL7B from *E. coli* membranes was investigated using a range of CHAPS concentrations as

well as 2% (w/v) SDS as the positive control. After incubation in each solubilization buffer, the *E. coli* lysates were centrifuged at high speed to pellet the membranes. The presence of METTL7B in the supernatant and the pre-spin cell lysates was analyzed by anti-METTL7B western blot as shown in Figure 20. METTL7B was absent from all centrifugation supernatants under all conditions tested, including the proposed positive control. This signifies that overexpressed METTL7B in *E. coli* is extremely difficult to remove from the cellular membrane and also explains why prior NiNTA purifications had failed to yield recombinant METTL7B.

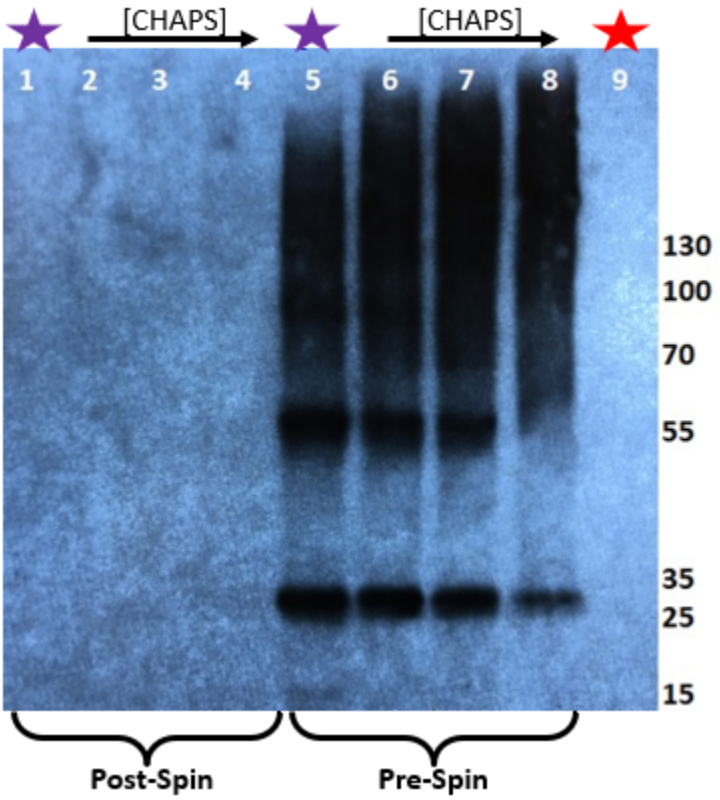

Figure 20. Anti-METTL7B Western Blot of *E. coli* Membrane Solubilization Conditions: Cell lysates were treated with 0.1, 1, 10 or 100 mM CHAPS in lysis buffer, rotated end-over-end for an hour at 4 °C, and centrifuged at 100,000 x g for 1 hour.

Pitfalls and Potential Fixes:

As shown in the data above, purification of His-tagged METTL7B was impaired by difficulties removing the hydrophobic N-terminus from the *E. coli* membranes. Initial solubilization conditions were assumed to be sufficient based off prior purification work in

mammalian systems as well as the presence of a band near 28 kDa in NiNTA purification eluents. Unfortunately, the promising band in the eluent likely belonged to the endogenous *E. coli* protein, SlyD, which naturally binds nickel ions.

Western blotting results showed that the His-tagged METTL7B was not solubilized even after incubation with 2% (w/v) SDS. Therefore, it is unlikely that suitable solubilization conditions can be found that would adequately remove the recombinant protein from the membrane while also maintaining enzymatic activity.

Compounded with the SlyD and ArnA contamination issues, a different affinity tag including a GST tag was engineered onto the METTL7B protein sequence for future purifications. This tag allows affinity purification that is not dependent upon heavy metal binding and also helps increase the solubility of the protein of interest.

Third Purification Attempt: N-terminal GST Tag on Full Length and Truncated Protein

Set-Up and Method of Choice:

The third purification attempt utilized a pGEX-3X vector which allows expression in *E. coli* and places an N-terminal glutathione S-transferase (GST) tag onto the protein of interest. A plasmid map is shown below in Figure 21. As previously discussed, the expression in *E. coli* enables easy scale up of protein expression for increasing future purification yields. The N-terminal GST tag not only acts as an affinity tag but also should increase the solubility of the overall fusion protein. Therefore, this third attempt built on the lessons learned in the prior two expression attempts and should enable purification of significant amounts of soluble fusion protein without significant contamination from endogenous *E. coli* proteins.

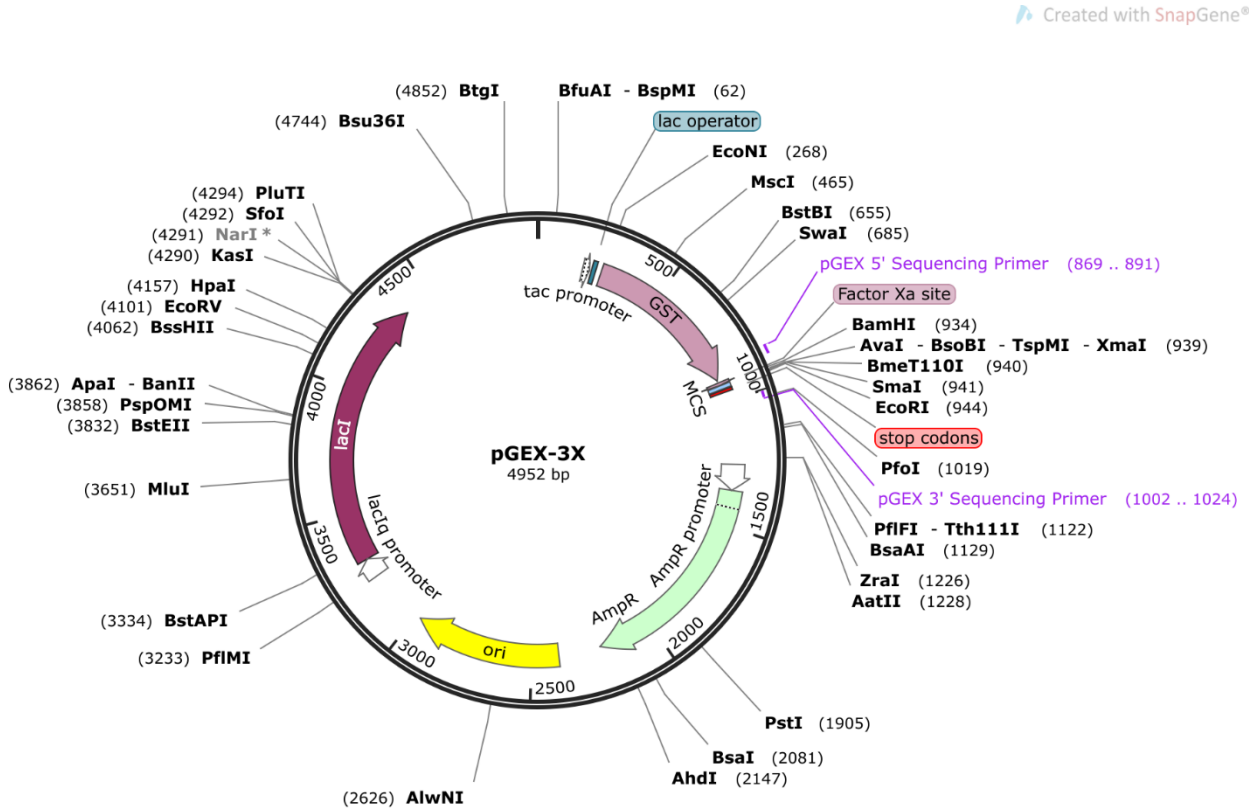

Figure 21. Plasmid Map of the pGEX-3X Expression Vector: The pGEX-3X plasmid confers ampicillin resistance to transformed *E. coli* and places expression of the gene of interest under control of the lac operon. A GST fusion tag is placed directly upstream of the multiple cloning site, placing it on the N-terminal end of the expressed fusion protein. There is also a Factor Xa protease recognition site between the GST tag and the protein of interest for potential removal of the affinity tag. The plasmid map is courtesy of SnapGene.

The set-up requirements for this round of purification are similar to those observed in the second purification attempt. The major difference in set-up between the second and third purification attempts, is the creation of multiple expression plasmids. Due to the difficulty caused by the N-terminal hydrophobic alpha helix, truncated forms of METTL7A and METTL7B were inserted into the pGEX-3X expression vectors. These truncations removed the first 23 amino acids of each sequence, which encompasses the entirety of the predicted hydrophobic N-terminal alpha helix. While many of the plasmid creation experiments can be conducted in parallel, adding truncations does increase the set-up workload.

Experimental Results:

Several transformed *E. coli* colonies were tested for captopril methylation activity in whole cell lysates after a 24-hour induction period with IPTG. The resulting activities, shown in Figures 22 and 23, were relatively variable between individual colonies. This could result from different copy numbers of each expression plasmid between colonies however further testing would be required to confirm. Overall, full-length METTL7B exhibited the highest activity under the conditions tested. Comparatively, full-length METTL7A has much lower activity but was above baseline levels. For both METTL7A and METTL7B, truncation of the N-terminal alpha helix significantly decreased the captopril methylation activity in *E. coli* whole cell lysate. Truncation of METTL7B decreased activity by about 20-fold whereas truncated METTL7A colonies were devoid of any captopril methylation activity above background levels.

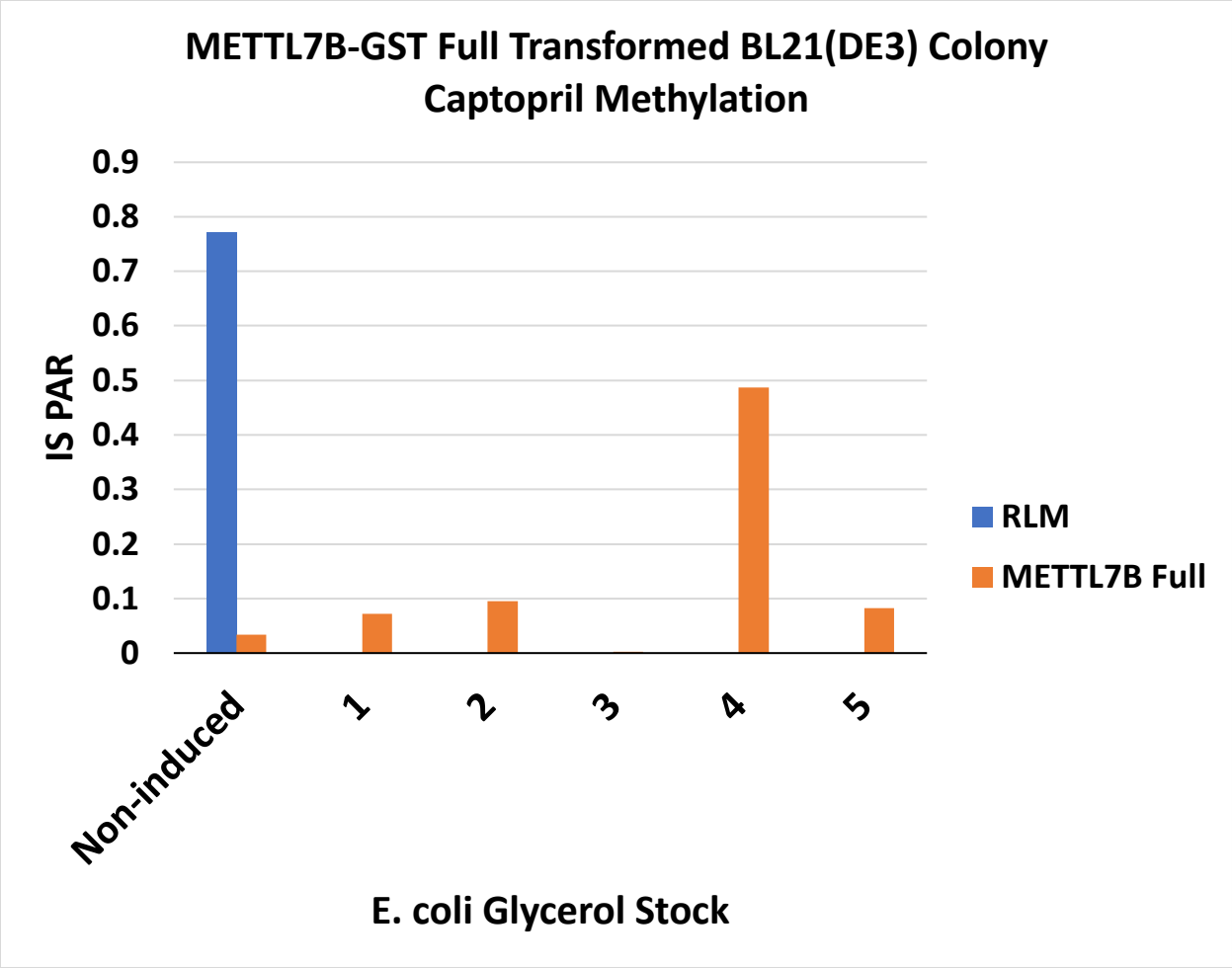

Figure 22. Captopril Methylation in pGEX-3X Full-length METTL7B *E. coli* Colonies: Captopril methylation in *E. coli* whole cell lysates containing full-length METTL7B was highly variable. At least one colony did not exhibit any activity despite being ampicillin resistant. All other colonies showed activity above non-induced background values.

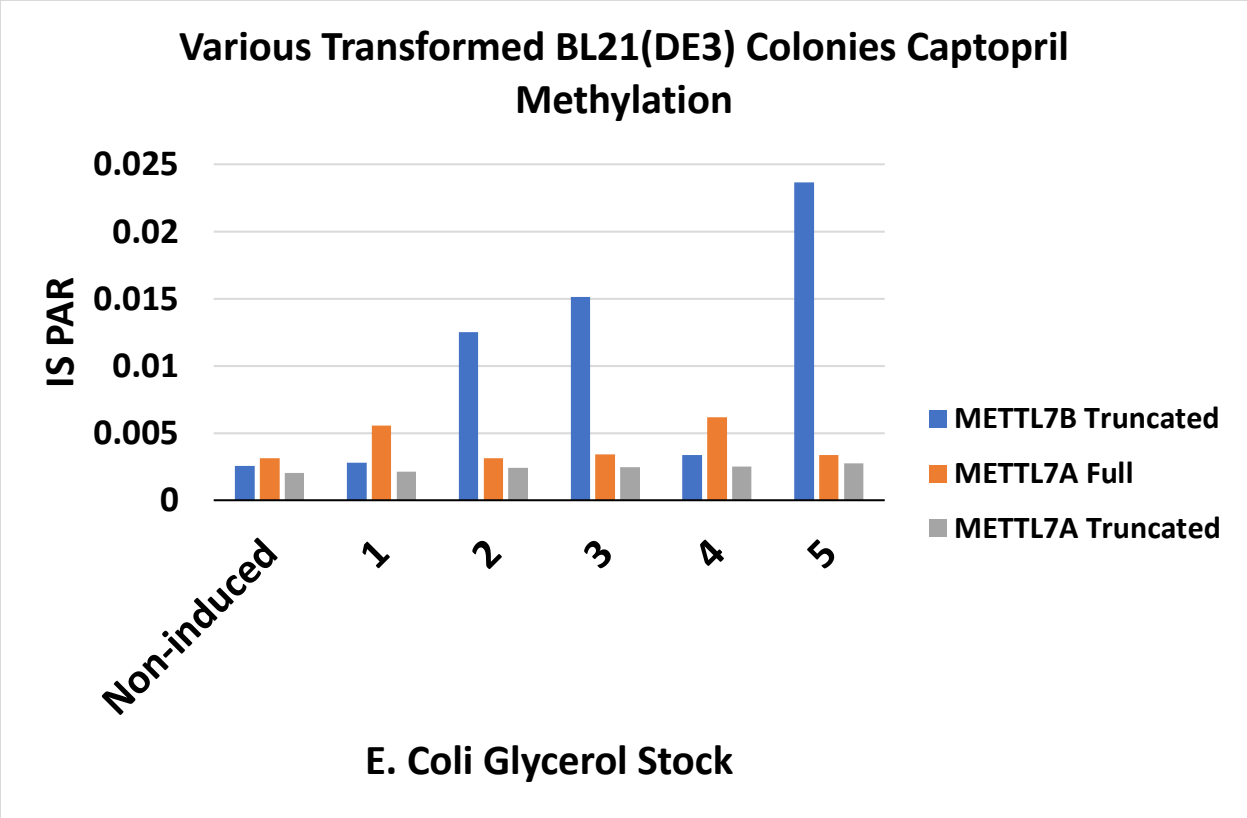

Figure 23. Captopril Methylation in Various pGEX-3X *E. coli* Colonies: Captopril methylation in *E. coli* whole cell lysates containing truncated METTL7B, and both full-length and truncated METTL7A was highly variable as well. Generally, truncated METTL7B activity was significantly impaired compared to full-length METTL7B (Figure 22). Full-length METTL7A activity was much lower than full-length METTL7B activity. Truncated METTL7A activity was roughly similar to background levels observed in non-induced cell lysates.

It is possible that the truncated METTL7A and METTL7B proteins were not well expressed compared to the full-length proteins because captopril activity assays give no indication about protein quantity. Decreased protein expression of the truncated proteins could explain the large decrease in captopril methylation observed in *E. coli* whole cell lysates. Therefore, expressed *E. coli* lysates containing truncated METTL7A and METTL7B were solubilized using the mammalian protocol and centrifuged. As shown in Figure 24, subcellular fractions analyzed by western blot show that both truncated METTL7A and METTL7B are adequately expressed. The western blot results also indicate that truncated METTL7A and

METTL7B are easily solubilized due to the intense bands present in the high-speed centrifugation supernatant fraction. This supports the fact that the GST fusion tag and N-terminal truncation help to solubilize the fusion proteins from the *E. coli* membranes, however at a significant loss of activity.

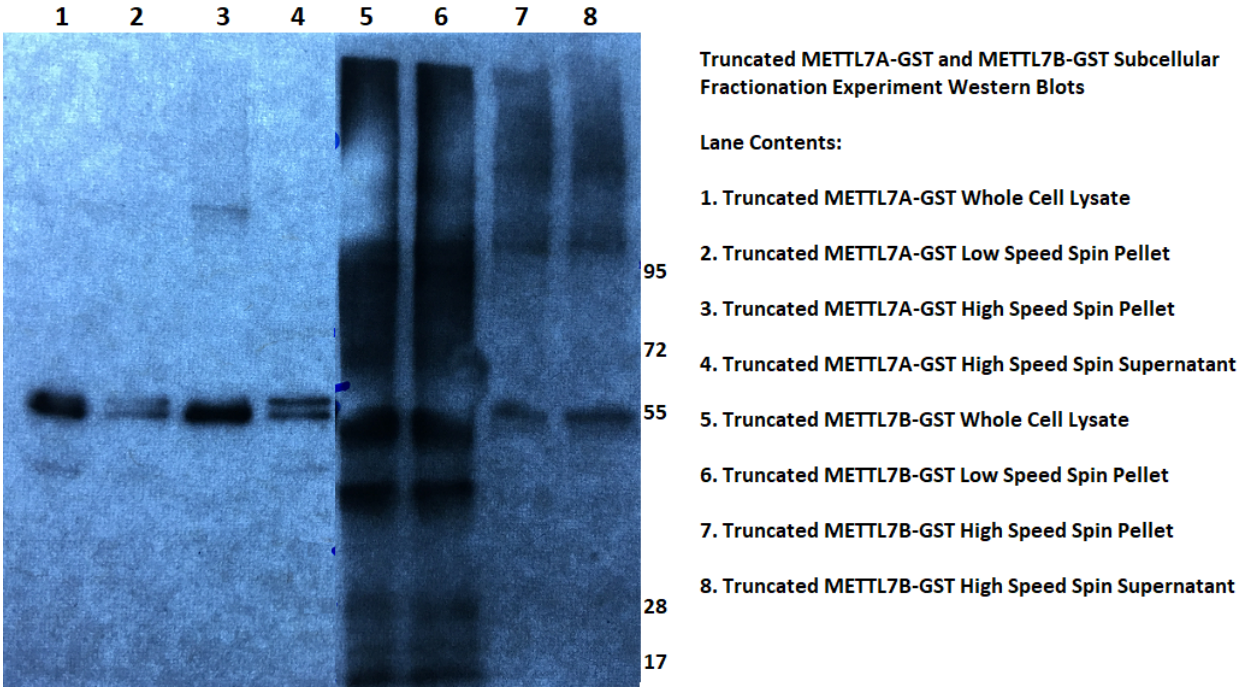

Figure 24. Western Blot Analysis of Expressed *E. coli* Subcellular Fractions: Distinct fusion protein bands were visible near the 55 kDa molecular weight marker in all subcellular fractions from *E. coli* expressing truncated METTL7A or METTL7B. Therefore, some amount of each fusion protein can be solubilized from *E. coli* membranes using the current methodology.

Truncated METTL7A and METTL7B were adequately expressed in cell lysates yet still exhibited very low captopril methylation activity. Therefore, further purification of the truncated forms was halted and focus was shifted entirely to the full-length GST-tagged fusion proteins. Future expression experiments used glycerol stock #4 for both full-length METTL7A and METTL7B because they contained the highest captopril methylation activity. Initial experiments used a 24-hour expression period at 37 ^{o}C. Before shifting to large scale expressions, induction

time courses at multiple temperatures were conducted to ensure the optimal expression conditions. As shown in Figures 25 and 26, expression at lower temperatures tended to increase the expression of active protein and that induction should continue for 10-24 hours before harvesting.

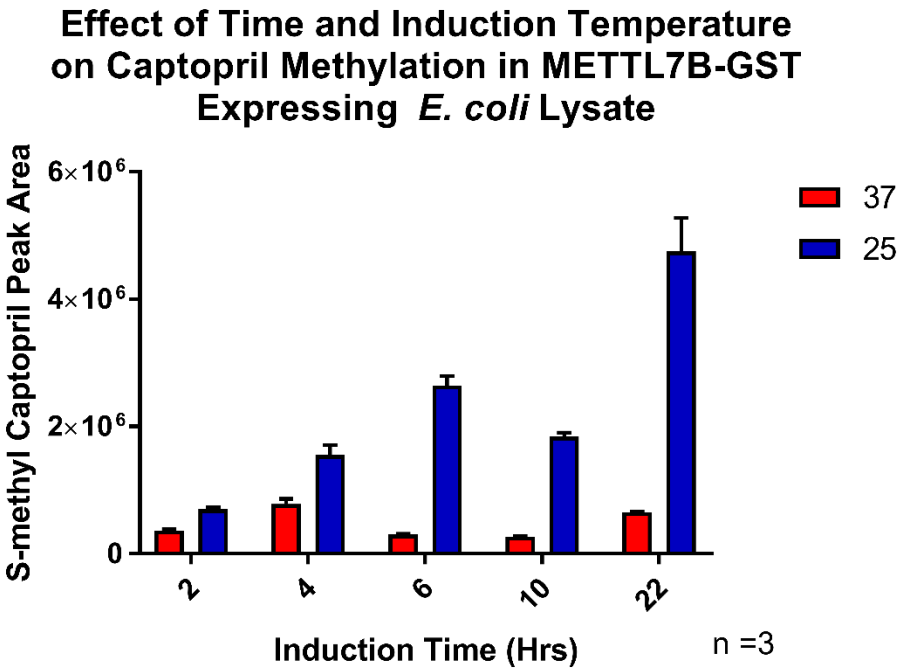

Figure 25. Effect of Induction Time and Temperature on METTL7B Activity in Whole Cell Lysate: Greater amounts of active METTL7B were produced in *E. coli* grown at 25 ºC compared to cells grown at 37 ºC. Expression increased with induction time for the first six hours, dropped at 10 hours, but was the highest at 22 hours post-induction. Protein-normalized fractions were tested for captopril methylation in triplicate. Data are presented as the mean ± standard deviation.

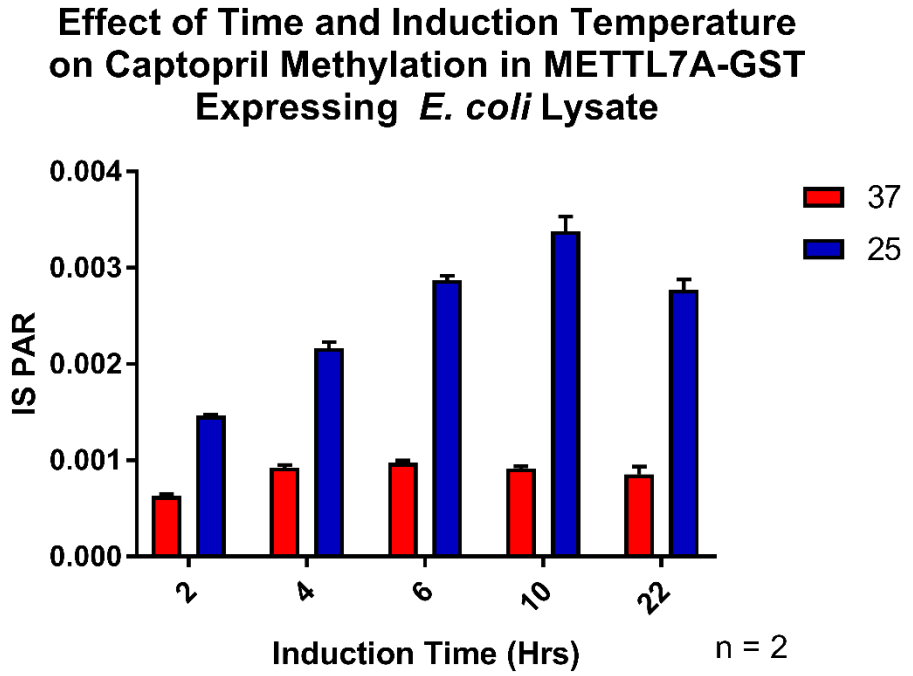

Figure 26. Effect of Induction Time and Temperature on METTL7A Activity in Whole Cell Lysate: Expression of active METTL7A increased with induction time and was highest at 10 hours post-induction. Activity decreased at the further time point. Greater amounts of activity were measured in cells grown at lower temperatures, similar to METTL7B. Protein-normalized fractions were tested for captopril methylation in triplicate. Data are presented as the mean ± standard deviation.

The increase in activity associated with reduced incubation temperatures was interesting. This trend was further studied by conducting an extended temperature variation experiment as shown in Figure 27. Expression of active protein continued to increase with decreasing incubation temperatures. It is important to note that the reported activities are intrinsic specific activities due to protein normalization. Therefore, it is possible that larger total amounts of active protein could be obtained from warmer culture temperatures however the overall protein quality is higher when expressed at lower temperatures. For future expression experiments, the conditions were set at15 ^{o}C for METTL7B for 24 h induction period

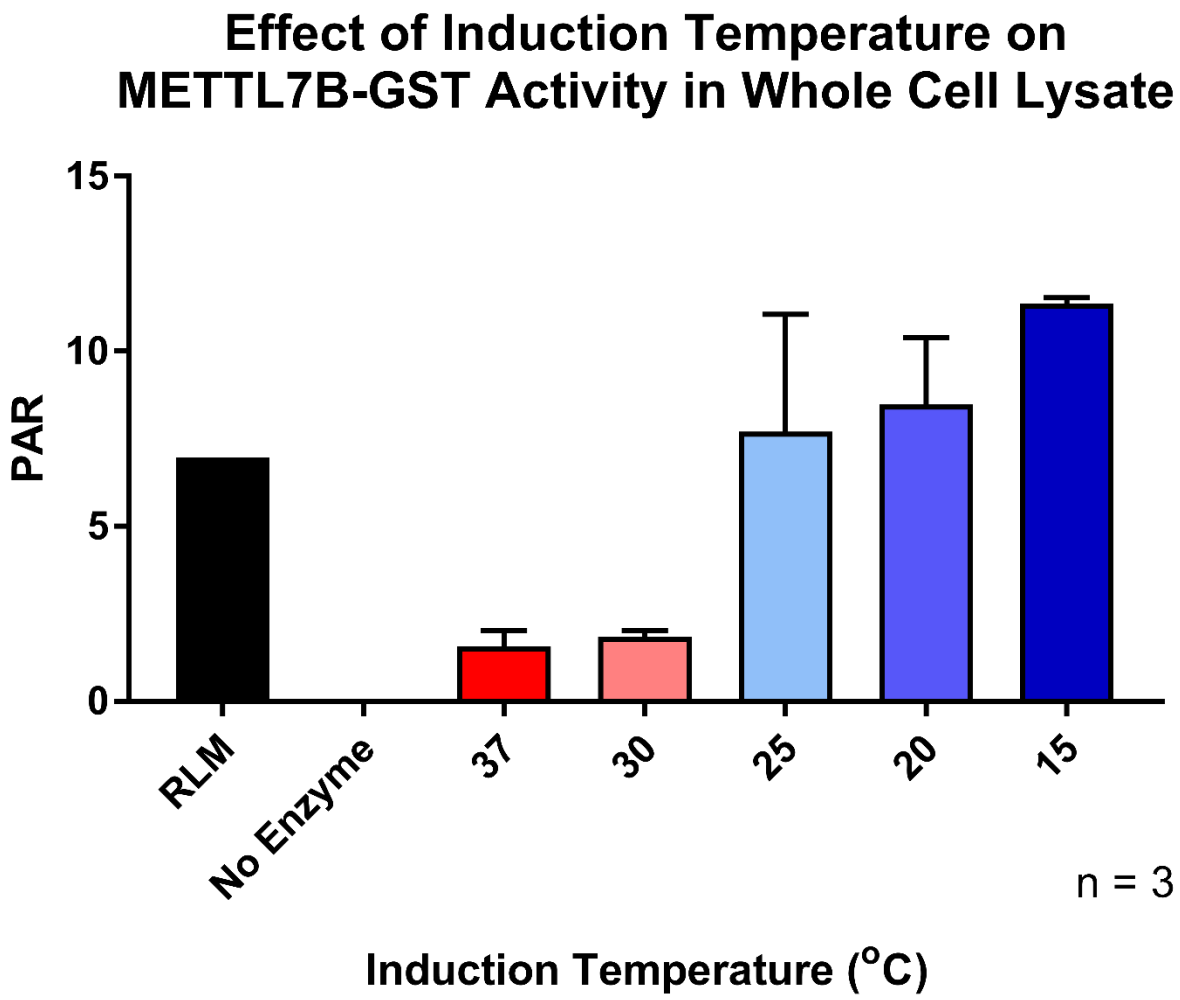

Figure 27. Effect of Induction Temperature on METTL7B Captopril Methylation in Whole Cell Lysates: Lower induction temperatures increased the specific activity in METTL7B-expressing *E. coli* cell lysates. The highest specific activity was observed at 15 °C. Protein-normalized fractions were tested for captopril methylation in triplicate. Data are presented as the mean ± standard deviation.

At this point, much of the METTL7A purification work was halted because these experiments could not be conducted in parallel. We focused on METTL7B for future purification efforts because the observed captopril methylation in cell lysates was much higher, easier to measure and the enzyme seemed more stable.

As previously mentioned, the GST fusion tag acts to both solubilize the overall fusion protein and can be used as a handle for affinity purification via its interaction with glutathione. Solubilized *E. coli* lysates containing GST-METTL7B fusion protein were flowed over affinity resin decorated with immobilized glutathione, namely GSTrapFF resin (GE Healthcare). After subsequent washing with purification buffer (50 mM KPi pH 7.0, 20% (v/v) glycerol, 150 mM NaCl, 10 mM CHAPS), bound protein was eluted in purification buffer adjusted to pH 8.0 and containing 10 mM free glutathione which competitively binds to the GST affinity tag. The relative yield and purity of initial expression experiments are shown below in Figure 28. Elution efficiency was improved by increasing the elution buffer to pH which helps to increase the amount of charged glutathione present in solution. Overall, the yield and purity were very high compared to prior purification attempts. The presence of METTL7B was additionally confirmed by in-gel proteomic analysis to avoid potential mis-identification of SDS-PAGE bands again.

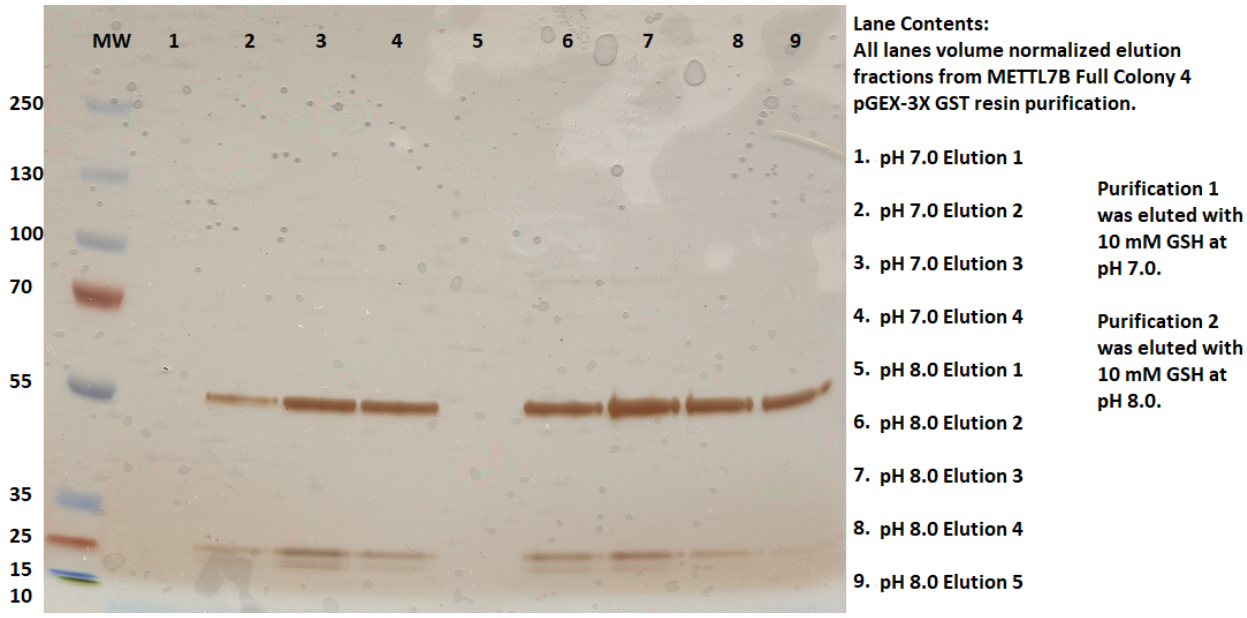

Figure 28. Effect of pH on GST Fusion Protein Elution: GST-METTL7B fusion protein was purified using GSH affinity resin and eluted at either pH 7.0 or pH 8.0. The overall yield was very good and there were few contaminating proteins as determined by SDS-PAGE silver stain. Elution efficiency was increased when eluting in a higher pH buffer.

At this point, recombinant GST-METTL7B fusion protein could be purified from solubilized *E. coli* whole cell lysates with high yield and purity using GSH affinity resin. The few contaminating bands likely belonged to chaperone proteins and GST-tag aborted synthesis products. The purified protein methylated captopril in a SAM-dependent manner and product formation was linear with respect to time and protein concentration, as shown in Chapter 3.

The only major consideration prior to biochemical characterization was the potential impact of the fusion tag on the enzymatic activity. It is entirely possible that the presence of the GST tag could impact the folding, substrate specificity, or turnover kinetics of METTL7B given that they are almost equivalent in size. The pGEX-3X expression plasmid contains a Factor Xa cleavage site between the GST tag and the protein of interest. Therefore, we attempted to cleave the METTL7B fusion protein with commercial Factor Xa protease. Multiple cleavage incubation times were tested as well as the presence of liposomes to help maintain enzyme activity post-cleavage. The results, shown in Figure 29, showed that the GST-METTL7B fusion protein was stable to proteolytic analysis for up to 48 hours.

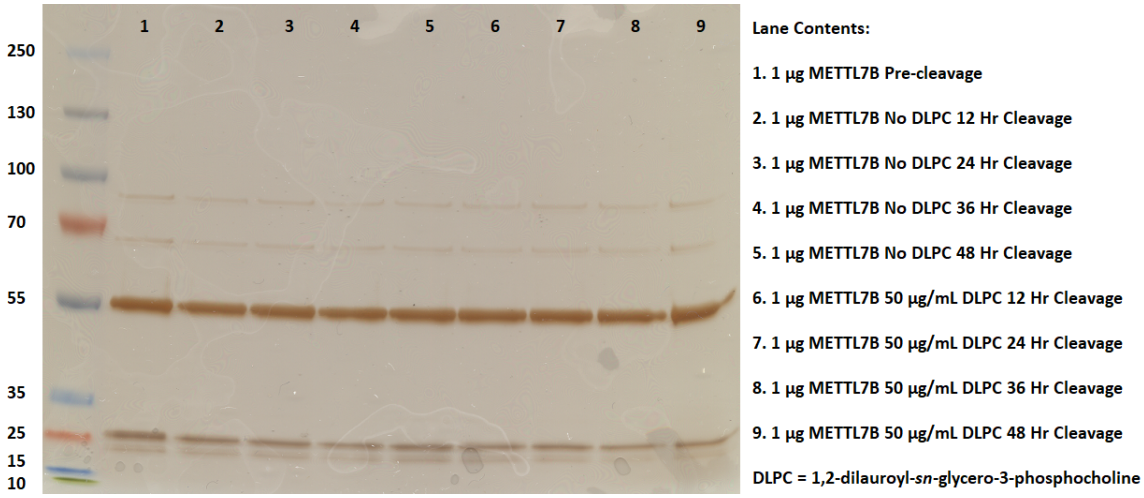

Figure 29. Factor Xa Cleavage Time Course of Purified GST-METTL7B: The GST-METTL7B fusion protein was not digested by Factor Xa even after a 48-hour incubation. Additionally, the presence of DLP liposomes did not improve digestion efficiency. The fusion protein band at 55 kDa did not decrease in intensity compared to the negative control present in lane 1.

Since the GST-METTL7B fusion protein was not cleavable by Factor Xa despite the presence of a recognition site, three new plasmid constructs were created. Two constructs contained additional protease cleavage recognition sequences and one contained a hydrophilic linker. These sequences were inserted prior to the N-terminus of the METTL7B gene sequence using overhang PCR (see Appendix I). One construct encoded a tobacco etch virus (TEV) protease site, another encoded a human rhinovirus 3C (HRV3C) protease site, and the hydrophilic linker was composed of Gly-Ser-Thr-Gly-Gly.

Ideally, the new proteases could cleave the GST fusion tag where Factor Xa had failed. TEV and HRV3C proteases are also active at 4 °C whereas Factor Xa requires room temperature for activity. The lower incubation temperature should help prevent thermal degradation of METTL7B during cleavage. The three new constructs were expressed, purified, and exposed to their respective proteases as shown below in Figures 30 and 31.

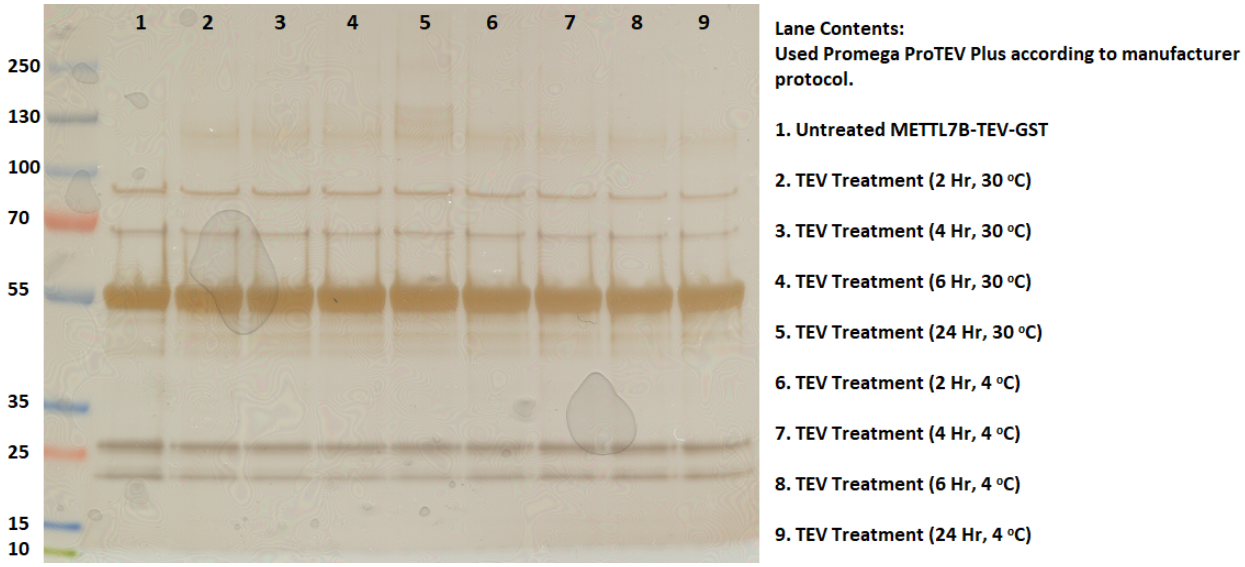

Figure 30. TEV Temperature Variation and Cleavage Time Course of GST-TEV-METTL7B: METTL7B fusion protein was not digested by TEV protease after 24-hour incubations at either 4 °C or 30 °C. The 55 kDa fusion protein band did not decrease in intensity compared to the untreated control in lane 1.

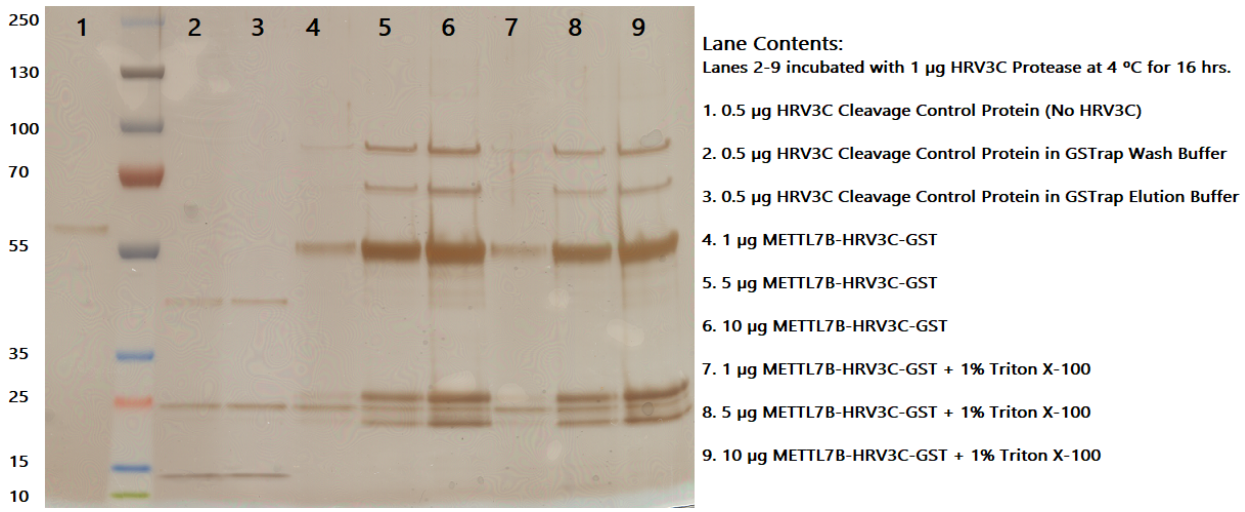

Figure 31. HRV3C Incubation with GST-HRV3C-METTL7B: The HRV3C positive control peptide was efficiently cleaved in the buffer conditions tested. The METTL7B fusion protein was not digested by HRV3C protease at any of the tested protein:protease ratios or in the presence of Triton X-100.

Neither HRV3C nor TEV cleaved the new METTL7B fusion proteins at any temperature, incubation time, or protein:protease ratio tested. We believe that the hydrophobic N-terminus of the full-length METTL7B protein tightly associated with the neighboring protease sites and prevented efficient cleavage. To test this hypothesis, the new fusion proteins were incubated with Factor Xa because the addition of the linker structures placed the Factor Xa recognition site further from the METTL7B N-terminus. Slight proteolytic cleavage was observed when incubating the GST-HRV3C-METTL7B and GST-GSTGG-METTL7B fusion proteins with Factor Xa as evidenced by the appearance of bands around 31 kDa in lanes 4, 5, 7, and 8 in Figure 32.

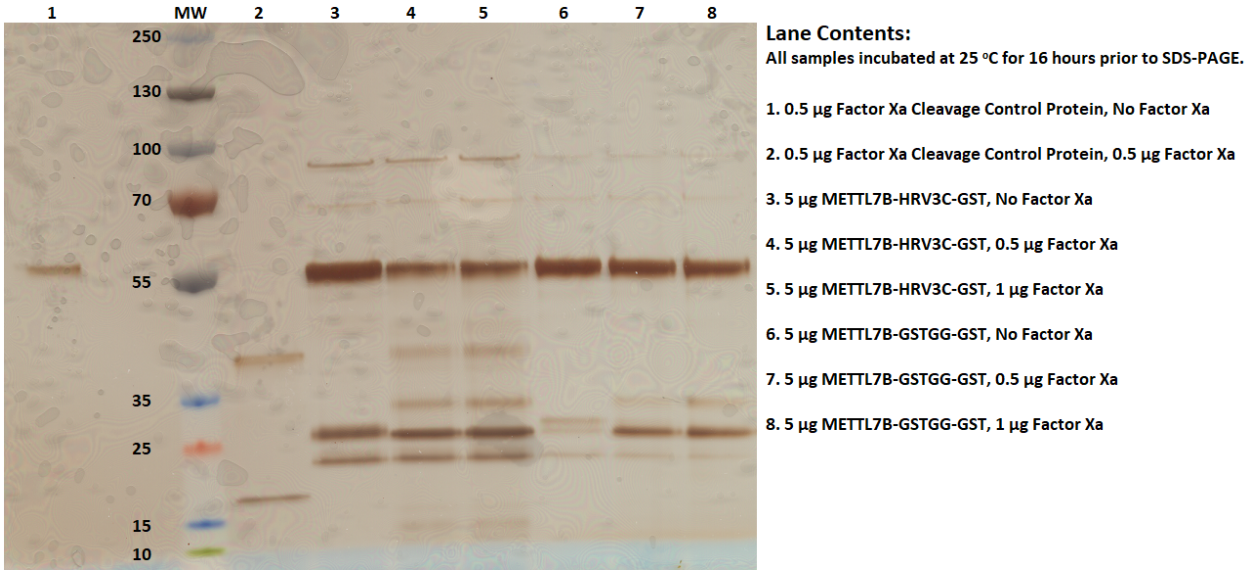

Figure 32. Factor Xa Incubation with GST-HRV3C-METTL7B and GST-GSTGG-METTL7B: The positive control peptide was efficiently cleaved by Factor Xa after a 16-hour incubation at room temperature. Both METTL7B fusion proteins, containing a hydrophilic linker or a HRV3C protease site, also exhibited small amounts of cleavage in the presence of Factor Xa.

Higher cleavage efficiency was observed with the GST-HRV3C-METTL7B fusion protein than the GST-GSTGG-METTL7B fusion protein which directly correlates to the length of the added linker sequence in each fusion protein. We believe that the longer HRV3C linker placed the Factor Xa recognition site further away from the METTL7B N-terminus compared to the GSTGG linker and allowed proteolysis to occur more readily.

Pitfalls and Potential Fixes:

Addition of a N-terminal GST tag enabled efficient solubilization of METTL7A and METTL7B fusion proteins from *E. coli* membranes. Purification with immobilized glutathione affinity resin resulted in high yield and low contamination. The major issue associated with this purification attempt was the inability to remove the N-terminal GST tag from the fusion protein. Despite the presence of a Factor Xa protease site, cleavage was inhibited by close proximity to the hydrophobic METTL7B N-terminal alpha helix. Alternative proteases sites were inserted

into the fusion protein sequence but also failed to cleave the GST tag. Interestingly, Factor Xa cleavage was observed in the new fusion proteins and cleavage efficiency correlated with increased distance between the Factor Xa recognition site and the METTL7B N-terminus. The final purification attempt, discussed in Chapter 3, utilizes an inflexible linker to increase the distance between the METTL7B N-terminus and the protease recognition site to further increase cleavage efficiency.